UNIVERSITAT POLITÈCNICA DE CATALUNYA BARCELONATECH

# *Development of novel techniques of advanced transport characterization of membranes*

**Marc Fernández de Labastida Ventura**


PhD program in Chemical Process Engineering

# Development of novel techniques of advanced transport characterization of membranes

**Doctoral thesis by:**

Marc Fernández de Labastida Ventura

**Thesis advisor:**

Andriy Yaroshchuk

Chemical Engineering Department

Barcelona, February 2020

**Article-based Thesis presented to obtain the qualification of Doctor awarded by the Universitat Politècnica de Catalunya**

*A la meva mare*

*For the wretched of the earth, there is a flame that never dies.*

*Even the darkest night will end and the sun will rise.*

Victor Hugo, Les misérables

# Acknowledgments

Once I finished my chemical engineering degree, I was not sure what I wanted to do after that. Then, I had the chance to work in the chemical engineering department, and after three years, I was offered to do a PhD. I had never considered it, but I finally decided to go for it, and here I am. I want to express my gratitude to all the people who have helped and supported me during this period.

This thesis has been performed within the scope of the RED-Heat-to-Power project (Conversion of Low Grade Heat to Power through closed loop Reverse Electro- Dialysis), Horizon 2020 Programme, Grant Agreement n. 640667 under the "supervision" of Andriy Yaroshchuk. Moreover, it received support from the project Waste2Product (CTM2014-57302-R) financed by the "Ministerio de Economía y Competitividad" and the Catalan Government (SGR2014-50-SETRI), Spain. Also, I want to acknowledge the Dow Chemical and Fujifilm manufacturers for the membranes supplied.

I want to acknowledge the contribution of Edxon Licon and Mykola Bondarenko in papers preparation, A.J. Karabelas for the numerical data provided, and Theo Putts and Stanislaw Koter for welcoming me in their departments. Moreover, I want to thank Rafa Bermudez and Jose Manuel Guerrero from mechanical workshop in ETSEIB. They always were ready to help when I asked for it and contributed notably in some of the setups that made this work possible.

The people with whom I shared so many moments every day all this time are fundamental for me. Mònica, Julio and Xanel were my greatest support along these years. They have been there helping and supporting me even in the worst times. I will never forget it. Mònica, you were there right from the start. I know I am not so talkative, but still, I like to think that this has not been a big impediment, and we shared many good moments anyway. Julio arrived six months after starting my PhD. I sometimes remember the first week we spent together in the lab, facing each other and barely talking. After that week we got along, fortunately, since we have shared office the last three years. Just imagine all this time, sitting next to each other without speaking. That same year Xanel arrived, and I started improving my Galician: *Xanel, tes moita leria e iso gústanos, é imposíbel non pasalo ben contigo*. Over the last years in EEBE, I have also shared office with Karina and Sonia. I see Karina is very busy counting nanoparticles, but she always has time to listen and to give good advice. Sonia had to come from Palencia (written with P, do not mix up with Valencia) so that I finally understood what the group of nucelar waste characterization does (yes, the word is nu-ce-lar). Meeting new people is always challenging for me and takes me a long time, but after so many breakfasts, meals and moments in the office, you became very important as well.

The last ones to join our group were Mahdi and Miguel; it was nice to meet you too. Thanks to all the professors in our group for your help when I needed it. Especially, I want to acknowledge Jose Luis Cortina for his support the last year, which I consider essential for the completion of this thesis.

Over the years, people come and people go. I also keep in mind those who are no longer working in our department. Mehrez was like a brother, and I have such good memories, in particular Fridays afternoon, “fixing the world” along with Julio. Julio Bastos always had a kind word for everybody and something funny to share. Besides, he was the founder of our “Run Club” with Julio and Mehrez, so I owe him my hobby for running. Sina and Brij were always in a good mood, and a great atmosphere was assured when one was with them. I also remember people with whom I only spent a short time, but I am glad to have met them anyway, such as Diana and Josep.

Finally, I want to acknowledge my parents for their support and the opportunities I have had in my life. This thesis is dedicated to my mother, who always was there, listening to my problems, advising and encouraging me. I admire so much her nature extroverted and optimistic and the way she faced life, that she always will be a reference for me.

Now that I am facing the final steps, I want to focus on the bright side of this experience and left out bad times. I always think in The Shawshank Redemption, when Andy wrote: *hope is a good thing, maybe the best of things, and no good thing ever dies*. I will remember. After all this time, I realized that sometimes, when one starts a new path, the destination and the place that one reaches are different places. However, one way is not necessarily better than the other. This thesis is where I have been able to reach and now, above anything else, I feel grateful to everyone who helped me. Thank you very much to all.

# Abstract

Optimization of membrane separation processes rely on the accurate determination of some parameters related to membrane structure, chemistry, morphology or transport mechanism. Therefore, membrane characterization is fundamental in membrane research and development. This thesis addresses two specific issues of membrane separation processes: the distribution of extent of concentration polarization (CP) over the membrane surface in test cells for pressure-driven membrane processes and the separate information of equilibrium (partitioning) and kinetic (diffusivity) properties of ion-exchange membranes for a better-understanding of ion-transport mechanisms.

The implications of CP inhomogeneity for the interpretation of measurements of solute rejection were qualitatively illustrated using a simple model of locally-1D CP combined with a postulated probability distribution of unstirred-layer thickness over the membrane thickness. Disregarding the CP distribution under-estimates the CP of strongly positively-rejected solutes and over-estimates the CP for the negatively-rejected ones. This is especially important in nanofiltration where strong positive and pronounced negative rejections can occur simultaneously for solutes of different charges. Therefore, it is desirable to reduce the inhomogeneity of CP distribution to a minimum in membrane-testing devices.

A novel test cell design was developed based on the classical configuration of rotating disk combined with the possibility of setting an operating pressure up to 20 bar. CFD simulations showed that CP was homogeneous over the major part of the membrane surface whereas there were some expectable deviations close to the membrane edge. The approach was also validated experimentally via studying the dependence of observed rejection on the rotation speed and demonstrating that intrinsic rejection was practically independent of it. Then, the cell utility was proved performing different ion rejection studies for several dominant salts (NaCl, $MgCl_2$, $Na_2SO_4$ and $MgSO_4$) plus trace ions ($Na^+$, $NH_4^+$, $Cl^-$ and $NO_3^-$) and for electrolyte mixtures of NaCl and $MgCl_2$. The solution-diffusion-electro-migration model was used to obtain ionic membrane permeances from the experimental data.

Besides, experiments performed with a cross-flow test cell demonstrated that there was filtration along the membrane porous support even if the membrane is supported by an impermeable surface. This occurs in the peripheral parts of the membrane due to membrane sealing and contribute to CP inhomogeneity.

Finally, a novel method based on non-stationary-diffusion of relatively small concentration differences was developed to determine salt diffusion and partitioning coefficients in addition to the ion perm-selectivity, which is the only parameter available from the conventional measurements of stationary membrane potential. An ion-exchange membrane supported by a relatively thick coarse-porous support (glass frit) is placed in a two-compartment stirred cell. The salt concentration in one compartment is kept stationary during the measurement whereas in the other compartment, the initial solution is rapidly replaced by a solution of different concentration. Thus, there is a time-dependent electrical response due to a progressive redistribution of applied concentration difference between the membrane and the porous support and the different ion perm-selectivities of those media. Experimental data was fitted to a mathematical model that describes transient transport phenomena including osmosis, which was found to contribute notably on the measurements. The osmotic permeability was determined in separate measurements. The rate of signal relaxation is primarily controlled by the diffusion permeability of the membrane but is also affected by the salt partitioning. The results were validated by comparison with the literature data and using conventional techniques. Systematic studies were also carried out under different conditions

# Resum

L'optimització dels processos de separació amb membranes depèn d'una combinació de factors relacionats amb les propietats fisicoquímiques, l'estructura o la morfologia. Per tant, una caracterització acurada és fonamental en la investigació i desenvolupament de membranes. Aquesta tesi aborda dos problemes específics dels processos de separació amb membranes: la distribució de l'abast de la polarització per concentració (PC) sobre la superfície de la membrana als mòduls de membrana on la força impulsora és la pressió i l'obtenció d'informació diferenciada de les propietats cinètiques i d'equilibri en membranes de bescanvi iònic per a una millor comprensió dels mecanismes de transport d'ions.

Les conseqüències de la inhomogeneïtat de la PC a l'hora d'interpretar les mesures del rebuig del solut es van il·lustrar qualitativament mitjançant un senzill model que descriu la PC localment en 1D combinat amb una distribució de probabilitats pel gruix de la capa límit. Ignorar la distribució a la PC subestima la PC dels soluts rebutjats positivament i sobreestima la PC per als rebutjats negativament. Aquest fet és especialment important en la nanofiltració, on es poden produir simultàniament rebuigs positius i negatius pronunciats per a soluts de diferents càrregues. Per tant, és desitjable reduir al màxim la inhomogeneïtat de la distribució de la PC als mòduls de membrana.

Es va desenvolupar un nou disseny de mòdul per membranes basat en la clàssica configuració de disc rotatiu. Simulacions de dinàmics de fluids van demostrar que la PC es homogènia a la major part de la superfície de la membrana mentre que es van obtenir algunes desviacions esperables a prop de la vora de la membrana. A més, es va validar experimentalment estudiant la dependència del rebuig observat amb la velocitat de rotació i demostrant que el rebuig intrínsec es pràcticament independent. Posteriorment, es van obtenir les permeances iòniques mitjançant el model "Solution-diffusion-electro-migration" realitzant diferents estudis amb salts dominants (NaCl, $MgCl_2$, $Na_2SO_4$ i $MgSO_4$) més ions traça ($Na^+$, $NH_4^+$, $Cl^-$ i $NO_3^-$) i amb mescles binàries de NaCl i $MgCl_2$.

D'altra banda, alguns experiments amb una cel·la de flux tangencial van demostrar que hi ha una filtració al llarg del suport porós de la membrana, fins i tot si aquesta esta recolzada per una superfície impermeable. Això es produeix a les zones perifèriques de la membrana, a causa de la pressurització del mòdul i contribueix a la inhomogeneïtat de la PC.

Finalment, es va desenvolupar un nou mètode basat en la difusió no estacionària en condicions de diferències de concentració relativament petites per determinar la difusió i els coeficients de partició, a més de la permselectivitat iònica, que és l'únic paràmetre disponible a partir de les mesures convencionals del potencial de membrana en estat estacionari. Una membrana de bescanvi iònic recolzada per un suport relativament gruixut i porós es col·loca en una cel·la agitada de dos compartiments. La concentració de sal en un compartiment es manté estacionària durant l'experiment mentre que a l'altre compartiment, la solució inicial és substitueix ràpidament per una solució de concentració diferent. Així, hi ha una resposta elèctrica depenent de temps a causa d'una redistribució progressiva de la diferència de concentració aplicada entre la membrana i el suport porós degut a les diferents selectivitats iòniques entre ambdós medis. Les dades experimentals es van ajustar a un model matemàtic que descriu els fenòmens de transport en estat transitori, incloent la osmosis, ja que es va observar que contribueix significativament en les mesures. La permeabilitat osmòtica es va determinar paral·lelament. La velocitat de relaxació de la senyal obtinguda està controlada principalment per la difusió de la membrana, tot i que també es veu afectada pel coeficient de partició de la sal. Els resultats es van validar amb les dades de la literatura i mitjançant tècniques convencionals.

# Summary

# Glossary

AEM: Anion-exchange membrane

ATR-FTIR: Attenuated total reflection Fourier transform infrared spectroscopy

CEM: Cation-exchange membrane

CFD: Computational fluid dynamics

CP: Concentration polarization

DC: Direct current

EIS: Electrochemical impedance spectroscopy

MF: Microfiltration

NF: Nanofiltration

PFG-NMR: Pulsed-field gradient nuclear magnetic resonance

QCM: Quartz crystal microbalance

RBS: Rutherford backscattering spectrometry

RDM: Rotating disk-like membrane

RO: Reverse osmosis

SDEM: Solution-diffusion-electromigration model

UF: Ultrafiltration

# CHAPTER 1

# Introduction

# 1. Introduction

## 1.1 The role of membrane characterization in membrane development

Over the years, membrane technology has developed and advanced to such an extent that it has acquired an important role in chemistry engineering. It is fundamental in sustainable separation processes for water purification and wastewater reclamation and reuse [1–5]. Further on, membrane technology has also been widely used in a broad range of industrial applications such as chemical, pharmaceutical, food or biotechnological applications [6–8]. Membrane technology proved to be an effective, reliable separation process and economically competitive with conventional techniques due to several benefits including easy operation, flexibility, monitoring and maintenance, compact modular construction, high separation efficiency or low energy consumption. Moreover, membrane processes can be integrated with other separation processes which has been increasingly performed in many fields [9–13].

Membrane technologies contribute notably to the resource management and recovery of materials in industry, which is essential regarding the challenges involved in an ever-growing global society. Only increasing the efficiency of membrane processes can be satisfied the increase in the needs due to global expansion. Then, continuous research on new membranes development and enhancement of membrane processes lead to the emergence of new applications that provides a growth of the membrane industry.

Membrane characterization becomes essential for the technology development since improving membrane performance is only possible provided that the information obtained on membrane properties is reliable. The use of several techniques either individually or combined lead to a global understanding of the chemical, physical and mechanical membrane properties that can be used to develop novel membranes using new materials and manufacturing techniques. Accurate membrane characterization is important to identify improvement points and to assure the impact of a change in the manufacturing process on the resultant membrane property.

Optimization of membrane processes rely on several factors such as membrane chemistry, physical properties, surface characteristics, etc. [14,15] Some of these properties are known and even set to optimum desired value along the manufacturing process to meet a certain number of specification criteria (for instance, flux, rejection or molecular weight cut-off). However, additional information is always required in membrane development to address several aspects as for modelling. Moreover, chemical and physical properties may be modified because of membrane conditioning, fouling, cleaning, etc. Therefore, additional membrane characterization methods are required.

A complete membrane characterization is difficult due to the large number of independent parameters involved, especially regarding the complex structure that the membranes have at present. Moreover, obtaining some information is difficult due to technical limitations like for example properties that require measuring at atomic length scale.

Transport properties are fundamental within membrane characterization since they provide important knowledge about separation mechanism and allow describing them. In this case is especially important obtaining independently measured characteristics in addition to the conventional performance tests. Transport properties are also intimately related to modelling development that is extremely useful for membrane performance prediction and processes optimization. Over the last decades, a lot of effort has been devoted to membrane modelling development.

The different transport mechanism occurring across the membrane depend on the type of membrane and the driving force [14,16–18]. Usually, the driving force is pressure, concentration or electric potential difference through the membrane. This thesis has been devoted to developing methods for transport characterization of membranes in the cases of pressure-driven membrane processes and ion exchange membranes.

## 1.2 Membrane transport phenomena in pressure-driven processes

Pressure-driven membrane processes constitute essential and mature technology with numerous applications in water treatment and drinking water production.

The driving force in these processes is a pressure difference applied to a solution in contact with a semi-permeable membrane. The membrane rejects selectively some components depending on the type of membrane. The principal processes are microfiltration (MF), ultrafiltration (UF), nanofiltration (NF) and reverse osmosis (RO). All of them work under the same principle, although the difference in pore diameter makes big difference in each membrane process application [18].

MF is mainly applied to remove particles, colloids and bacteria whereas UF can even reject virus and macromolecules due to the smaller pore size. NF has been typically used to remove divalent ions and small organic compounds while allowing some monovalent salts to pass through. Recently, it has been also applied to applications such as removal of Arsenic, persistent organic pollutants, pharmaceutical organic compounds or hormones [19]. RO membranes are even tighter than NF membranes, so they are able to reject all monovalent ions while allowing water molecules to pass through in aqueous solutions. RO has been widely applied to seawater desalination and it has also proved useful in selective separation, purification and concentration for example in food industry or water treatment [20].

### 1.2.1 Concentration polarization

Rejection of solutes by the membrane leads to their accumulation at the membrane vicinity, so there is a concentration rise near the membrane surface as illustrated in Fig. 1. This phenomenon is known as concentration polarization (CP) and strongly influences the membrane performance.

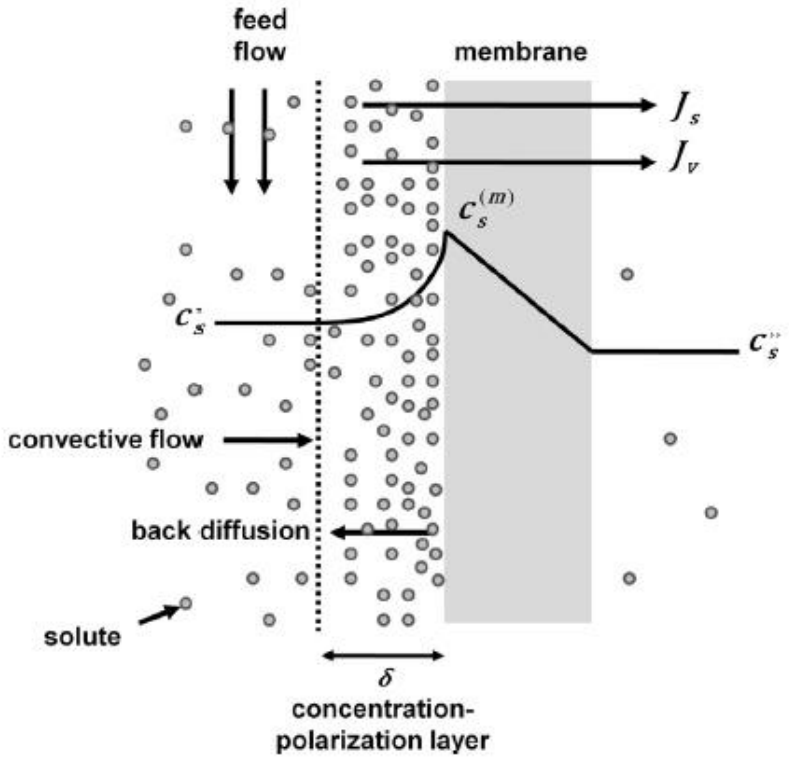


**Fig. 1** Schematic description of ion transport processes through both concentration polarization and membrane layers. $J_s$ is the trans-membrane solute flux, $J_v$ is the trans-membrane volume flux, $c_s'$ is the solute concentration in the feed solution, $c_s^m$ is the solute concentration at the membrane surface, $c_s''$ is the solute concentration in the permeate and δ is the concentration polarization layer thickness [21]

Due to increase in osmotic-pressure difference, CP reduces the driving force across the membrane, thereby reducing permeate flux and the membrane selectivity. CP development in a membrane channel depends on several factors such as local hydrodynamic conditions, mass transfer, operation conditions, feed solution, membrane process, etc. Therefore, its influence on the membrane process depends on the exact application.

Correct description of CP is important for the interpretation of experimental data with the purpose of obtaining accurate information on the membrane properties and predicting properly the performance of pressure-driven processes. CP needs to be accounted to determine the intrinsic rejection of the membrane from the concentration at the membrane surface instead of the observed rejection based on the feed concentration.

The classical approach to quantify CP is based on the so-called Nernst model [22–26], which postulates the existence of a diffusion boundary layer sharply separated from a perfectly-stirred core-flow zone. Assuming uniform CP layer with constant permeate flux along the filtration channel does not consider the complex fluid hydrodynamics occurring in membrane modules, but it can be used to explain most of the experimental data [27].

A different procedure relies on the dimensional analysis applied to solve heat transfer problems. Correlations deduced from heat and mass transfer (typically kinetics of dissolution) experiments are frequently used to estimate the thickness of boundary layer. The experimental output of such studies is the dependences of dissolution rate on the cross-flow velocity, diffusion coefficient of the solute (or thermal conductivity in the heat-transfer studies) as well as on the flow-channel geometry. Evidently, this can provide information only on mass- or heat-transfer characteristics averaged along the channel. Moreover, the obtained correlations have a restricted range of applicability and do not provide information on the dependence of CP on membrane properties.

Apart from these theoretical approaches that depend on measurement of indirect macroscopic parameters such as permeation flux, rejection and pressure drop, CP has been also addressed developing techniques for in-situ monitoring of membrane filtration process by measuring microscopic properties [28]. These techniques are meant to provide valuable information to understand the mechanisms governing the development of CP layer near the membrane surface and to allow testing theoretical models. In principle, direct and rigorous observation of changes in CP layer is possible by means of these monitoring techniques. However, the available studies on in situ monitoring techniques only provide qualitative or semi-quantitative information on CP. Some of these techniques would need an improvement on accuracy and resolution.

Due to the complexity of the phenomena and their experimental observation, computational fluid dynamics (CFD) has recently become a technique of choice for the calculation of flow and concentration fields inside feed membrane channels. Thus for instance some studies simulated the flow and CP in narrow rectangular channels with spacers [29–34]. Their results show inhomogeneous CP distribution strongly dependent on the spacer configuration and reveal up to an order of magnitude variation in the local mass-transfer coefficient depending on the position along the membrane surface (Fig. 2) [33,35–37].

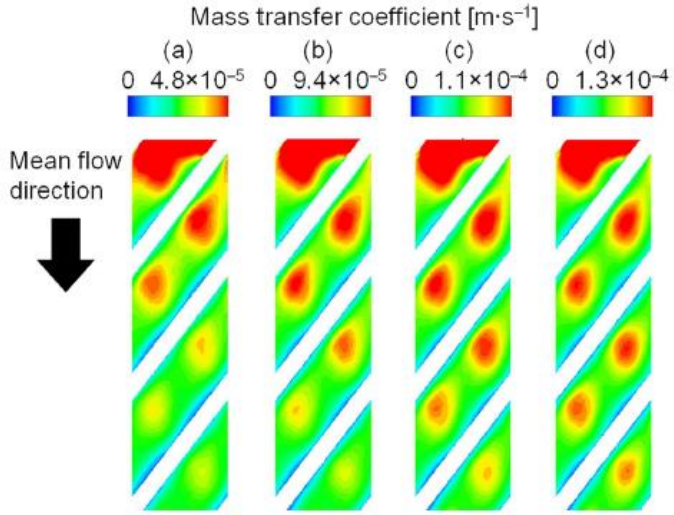


**Fig. 2** Contours of mass transfer coefficient on membrane surface for different Reynolds numbers [36]

Despite this pronounced inhomogeneity, the results of CFD simulations are often reported as Sherwood number (or mass-transfer coefficient) averaged over the membrane surface. Sherwood number is defined as a ratio of a characteristic length (for example, channel height) and the unstirred-layer thickness. Some authors made reference to the error associated with an inaccurate description in the CP boundary layer in determining the intrinsic rejection and the membrane transport parameters [38]. However, these estimates related only to the specific experimental conditions of those studies. More systematically, [39] simulated numerically the distribution of solute concentration at the membrane surface in infinitely-broad slit-like channels with developed laminar flow and the membrane exhibiting constant rejection (independent of either solute concentration or trans-membrane volume flow). The results were interpreted in terms of dependence of average extent of CP on the trans-membrane mass-transfer rate. Mostly, empirical correlations were considered but some comparison with the film (Nernst) model was also performed. It was found that at weak CPs the film model reproduced the results of numerical simulations quite well but at moderate to strong CPs there were considerable deviations. The authors ascribed them to the effect of "suction" due to the non-zero trans-membrane volume flow, which is often disregarded. However, we believe that actually a major part of those deviations occurred due to the inhomogeneity of distribution of CP along the channel. Unfortunately, only the case of 100% solute rejection was considered in the context of comparison with the film model.

In a number of cases instead of the rejecting-membrane boundary condition, the authors used the impermeable dissolving wall condition, which sets a constant solute concentration and zero normal fluid velocity at the wall [35,40,41]. In this case, the contribution of more stagnant zones to the average mass-transfer (dissolution) rate is under-proportional to their surface fraction since the local Sherwood number is smaller in those regions. In the more realistic case of membrane boundary condition, this contribution is over-proportional at positive rejections due to the stronger solute accumulation. In any case, the use of dissolving-wall boundary condition does not allow for an analysis of dependence of averaged mass transfer on the solute rejection. This dependence can be essential as we will see below. In addition, even in the studies where the membrane boundary condition was used [30–33,36,37,42,43], reporting the results in terms of averaged Sherwood number (instead of reciprocal one) makes difficult drawing conclusions on the correlation between the averaged mass transfer and solute diffusion coefficient (especially when the CP is not weak). In turn, a previous study characterized shear stresses and mass transfer coefficients at the membrane surface of a high pressure stirred filtration cell at different conditions [44]. The authors observed a considerable variation of local values of shear stress at relatively low rotation speeds, with its averaged standard deviation decreasing with increasing Reynolds number. As for the mass-transfer coefficient, the radial distribution is qualitatively similar but more uniform than shear stress, although there is still a variation around 50% in the time averaged Sherwood number.

Fluid-dynamics simulations are quite complex mathematically and can be performed only numerically. In this thesis, an alternative approach is adopted to obtain transparent analytical results (Publication 1): assume a distribution of unstirred-layer thickness over the membrane surface and use a simple locally-1D description of CP. Its simplicity enables to use the membrane boundary condition with various intrinsic solute rejections (including negative ones). In this way, one can obtain the local permeate concentration as a function of trans-membrane volume flux and solute diffusion coefficient. Then, the observable rejection is calculated via averaging this concentration over the membrane surface by using the postulated probability-density function for the distribution of unstirred-layer thickness.

Of course, this approach is approximate primarily because it disregards lateral solute flows (both convective and diffusive). However, if the unstirred-layer thickness is much smaller than the characteristic scale of inhomogeneity of its distribution along the membrane surface the local 1D approach can be sufficiently accurate. This condition can be met for typical feed spacers with the characteristic mesh sizes of a couple of millimetres, while the typical

unstirred-layer thickness in laminar flows is around 100 μm. Some of the results obtained below do not depend on the exact form of distribution function. For more quantitative illustrations, a simple log normal distribution is used in the first instance. Later, this approach is also tested in the case of a distribution function obtained from CFD simulations [41].

### 1.2.2 Modelling in nanofiltration

Among the different pressure-driven membrane processes, CP inhomogeneity is especially problematic for NF. In the case of low-pressure driven processes such as MF or UF, some mechanistic models allow prediction of membrane operation using membrane parameters such as the membrane pore size or hydraulic resistance that are easily measurable for those kinds of membranes. However, the complexity of transport mechanisms of NF makes difficult establishing predictive models, especially in the case of multi-electrolyte solutions containing both mono and divalent ions. A considerable effort has been devoted to NF modelling and several approaches can be found in the literature [19,45–50].

In general, there are two kinds of transport models in NF: mechanistic models and irreversible thermodynamics descriptions [45]. The former assume nanoporous materials in which ion exclusion (steric, electric and dielectric) and hindered diffusion and convection occur [46,49]. These models based on macroscopic approaches intended for ultrafiltration description, depend on chemical and physical characterization of the membrane that are challenging due to the technical limitations related to the need of measuring at near atomic scale. Therefore, rigorous physical description is limited by the lack of knowledge of the physical structure and electrical properties of NF membranes. This kind of models are problematic unless the membrane characterization techniques improve to such extent that the required membrane parameters can be correctly determined.

On the other hand, irreversible thermodynamics uses only phenomenological coefficients (ion permeabilities and transmission coefficients) to describe ion flux in terms of gradients of ion electrochemical potentials and trans-membrane volume flows. This treatment combined with some assumptions lead to simpler models such as Spiegler-Kedem [48,50], solution-diffusion [51] or solution-diffusion-electromigration [52].

Despite the fact that irreversible thermodynamics approach does not specify physico-chemical mechanisms, advanced engineering models based on irreversible thermodynamics seem to be the choice for practical NF modelling [45]. Nanopore models may provide qualitative knowledge of transport phenomena, but they depend on the determination of several membrane parameters that are challenging to determine experimentally due to the complexity in chemical and pore structure of NF [46]. Besides, the essentially macroscopic description used up to date is also problematic at the nanoscale.

Even though advanced engineering models do not assume any physical ion exclusion and hindrance mechanisms, they should capture principal transport phenomena using a limited number of fitting parameters obtained from a well-defined set of experiments. For instance, solution-diffusion-electromigration model (SDEM) describes ion transport accounting for spontaneously arising trans-membrane electric fields in NF due to different permeances to cations and anions using ionic permeances as phenomenological coefficients [52]. This approach has been widely used [53–57] and explains several observed experimental trends using a limited number of adjustable parameters.

Including convective ion transport to the SDEM ion transport mechanisms would extend the applicability scope of the engineering model. However, this would double the number of adjustable parameters since transmission coefficients would be added to the ionic permeances for each ion. Unambiguous determination of this increased number of model parameters relies on the accuracy of obtained information from experimental data to guarantee a good input for modelling. Therefore, it is important to control CP in membrane test cells to improve the quality of the experimental data, which may be considerably impaired due to the CP inhomogeneity (especially in the case of very different simultaneous rejections in multi-ion solutions). It was demonstrated that disregarding the CP distribution can under-estimate the CP of strongly positively-rejected solutes and over-estimate the CP for negatively-rejected ones, leading to a several-times difference in the effective unstirred-layer thicknesses estimated for such solutes by using standard Nernst model [58]. Therefore, it is desirable to reduce CP inhomogeneity to a minimum in membrane test-cells for pressure-driven processes.

### 1.2.3 Test cell membrane design to address concentration polarization problem

In membrane modules, the membrane transport properties manifest themselves against the background of complicated flow-distribution and external-mass-transfer phenomena. Therefore, these properties (such as solute rejection and volume flux) are often studied in dedicated test cells, where attempts are made to reduce those complications to a minimum.

In the case of CP, membrane test cells are designed to reduce the effect of this phenomenon by modifying membrane module hydrodynamics. The purpose is to promote turbulence creating flow instabilities and secondary flows to disrupt the boundary layer. Increasing the local mixing enhances the mass transfer, thereby reducing the concentration at the membrane surface.

There are several ways to achieve this such as increasing the cross-flow velocity or including turbulence promoters into the feed channel. Spacers are frequently used as turbulence promoters in addition to being a mechanical support for the membrane channel, so many research has been performed on spacer configuration optimization.

Despite this effort devoted to cell design optimization, there is inevitably some distribution of extent of CP over the membrane surface in test cells for pressure-driven membrane processes. Actually, CFD studies have demonstrated that this inhomogeneity of CP is especially pronounced in test cells with spacer-filled channels [29–34], where one order of magnitude variation can be found in the local mass-transfer coefficient depending on the position along the membrane surface [33,35–37]. The existing test cell designs are focused on minimizing the impact of CP disregarding the fact that there is an inhomogeneous distribution.

In view of the complexity of mechanisms of NF [19,59], it is highly desirable to decouple internal and external mass-transfer problems because coupled models involve too many adjustable parameters and uncertainties. Such a decoupling can easily be achieved provided that the extent of CP is the same over the whole membrane surface. In this thesis, this is implemented experimentally in a novel test cell using rotating disk-like membrane (RDM) (Publication 2).

Feron et at [60] developed a test cell for the characterization of high flux flat sheet gas separation membranes with uniform mass-transfer and constant permeate concentration over the whole membrane surface. Other publications also investigated experimental systems using rotating elements, in particular, rotating disk-like bodies with membranes fixed to them [61,62,71,63–70]. However, the principal purpose of those studies was the enhancement of shear rate at the membrane surface in view of applications with high-viscosity fluids. The geometry of these systems was quite different from infinite rotating disk and didn´t give rise to homogeneous distribution of CP. At the same time, the hydrodynamic and convection-diffusion equations for the system of interest have been extensively studied in electrochemistry in the context of rotating disk electrodes [72–74]. Those are experimental systems of choice for a quantitative control of mass-transfer limitations in the studies of electrode kinetics.

Besides, a previous study employed electrochemical techniques to characterize shear stress and mass transfer coefficient at the membrane surface in a high-pressure stirred filtration cell [44]. The authors observed a considerable variation of local values of shear stress at relatively low rotation speeds, with its time-averaged standard deviation decreasing with increasing Reynolds number. As for the mass-transfer coefficient, the radial distribution is qualitatively similar but more uniform than that of shear stress, although there is still a variation around 50% in the time averaged Sherwood number. Thus, the equal accessibility could not be achieved.

This thesis presents a novel design of membrane test cell with equally-accessible surface of a flat-sheet membrane (Publication 2). First, this design is studied via numerical CFD simulations and the results confirm that despite some deviations from the ideal geometry a major part of the membrane surface is, indeed, equally accessible. Moreover, the unstirred-layer thickness obtained in the simulations is in good agreement with the well-known Levich formula [75]. The simulations become unstable at higher rotation speeds, so the system is additionally validated experimentally via measurements of dependence of observed rejection of a single salt on the rotation speed. By using Levich formula for the unstirred-layer thickness in the CP-correction procedure it is demonstrated that the intrinsic rejection is practically independent of the rotation speed as it should be. Further on, the cell utility is demonstrated by CP-correcting of a number of experimental data obtained with a commercial NF membrane and several single-salt and mixed-electrolyte solutions. Ion rejection dependence on trans-membrane flux obtained for dominant salts and trace ions is fitted using SDEM model to

determine ion permeances (Publication 5). Besides, ion rejection is studied in the case of binary mixtures of NaCl and $MgCl_2$ (Publication 6). This new experimental setup can be useful for obtaining systematic information on the intrinsic rejections of various solutes by NF membranes.

Another aspect of test-cells design that may influence the quality of membrane characterization is the membrane sealing. This thesis shows that there is filtration along membrane supports in the peripheral zones of the membrane supported by impermeable cell body (Publication 3). In such zones, mass transfer conditions may be non-reproducible and worse than in the feed channel, so CP can become very strong. If not properly addressed this can affect drastically membrane performance.

## 1.3 Transport phenomena in ion-exchange membranes

Ion-exchange membranes are central elements of well-established electro-membrane processes such as electrodialysis, diffusion dialysis and electrolysis. [12,76–81]. In the last years, there has been an increasing interest in development of environmentally friendly ("clean") energy processes using ion exchange membranes. As a consequence, some new applications for them have emerged [76,82] such as capacitive deionization [83], polymer electrolyte membrane fuel cells [84], redox flow batteries [85], reverse electrodialysis cells [86] or water electrolysis [87].

Ion-exchange membrane are a kind of dense polymeric membranes that contain fixed charges in the polymer matrix so that they allow the passage of oppositely charged ions (counter-ions) while restricting similarly charged ions (co-ions). Ideally, only counter-ions pass through the membrane, but in practical application there is also some transport of co-ions and water through the membranes which affects the ion exchange membrane performance (decreasing purity in separation processes or reducing efficiency in energy-conversion applications). The efficiency of technologies based on ion exchange membranes depends critically on the permselectivity of the membrane, namely the ability of the membrane to exclude co-ions while permitting the transport of counter-ions. Therefore, a better understanding of transport mechanisms is needed to improve ion exchange membrane performance.

Transport across ion exchange membrane occurs principally under concentration or electric potential difference as a driving force. There are several transport mechanism acting simultaneously (convection, diffusion and electromigration) which makes complex the transport phenomena description. The contribution of each transport mechanism depends on the relative difference between the concentration difference and the magnitude of applied electric field [76].

Ion transport through ion exchange membranes can be phenomenologically addressed to overcome the complexity of the transport mechanisms. The most applied approach in the literature is based on the extended Nernst-Planck equation which describes ionic flux as a sum of three terms that reflect the contribution of each transport mechanism. Only one diffusion coefficient per ionic specie is needed in the Nernst-Planck equation, so it can be easily coupled with other equations to describe hydrodynamics, ion transport, boundary conditions, etc. Therefore, it has been widely applied as basis for quantitative treatment [76]. However, there are some restrictions that reduce the application of this equation as for example that it is only valid for isothermal systems, it assumes ion transport through homogeneous media or that the diffusion term is limited in describing the diffusion of multicomponent systems. Alternatively, one can use Stefan-Maxwell frictional treatment which is more general and suitable in the diffusion of multi-components systems [76].

A different more fundamental approach is based on the principles of irreversible thermodynamics which describe membrane phenomena by coupling driving forces with resultant permeation fluxes of species through the membrane using phenomenological equations derived from dissipation function [88]. Irreversible Thermodynamics does not postulate any mechanistic model of membrane transport. Interactions among different ions and solvent are considered in irreversible thermodynamics whereas the Nernst-Planck equation assumes that cations and anions independently migrate in the solution and membrane matrix. Therefore, irreversible thermodynamics is more realistic and rigorous.

There are six independent transport parameters that allow a complete characterization of ion exchange membrane transport processes in solutions of single salts: electrical conductivity, transport number of the counter-ion, diffusion permeability, water transport number or electro-osmotic permeability, hydraulic permeability and salt reflection coefficient [89]. These parameters allow to model fluxes of electrolyte ions, and solvent through ion exchange membranes according to the irreversible thermodynamics equations. However,

phenomenological coefficients have to be obtained from independent experiments. Phenomenological coefficients depend on the chosen frame of reference, so relative velocity difference of the species is used to develop frictional forces between species. A complete characterization of membrane transport properties in terms of irreversible thermodynamics is a laborious process implemented just for a couple of membranes and electrolytes in the whole history of membrane science. Therefore, correct selection of simplified models (and corresponding reduced set of experimental measurements) is an important issue. There are two possible ways to proceed: neglecting some parameters or finding relations between them that allow to evaluate one parameter as a function of a known one. Although it is not possible to find exact relations which could reduce the number of independent transport parameters, it may be possible to establish sufficiently accurate approximate relations [89].

Ion exchange membrane properties are controlled primarily by the amount of fixed charge in the membrane (ion exchange capacity), nature of the charged groups and their distribution in the membrane and the amount of water molecules adsorbed in the membrane. The principal properties that should be considered depend strongly on the application. In any case, a better understanding of ion-transport mechanisms requires detailed information on the transport and equilibrium properties of ion-exchange membranes, in particular, separate information on the equilibrium (partitioning) and kinetic (diffusivity) properties of the membranes with respect to ions. The partition coefficient of an ion refers to its distribution between the membrane and the solution whereas the diffusivity coefficient is related to the ion mobility in the membrane [90].

Stationary techniques of membrane characterization such as membrane potential or DC electrical resistance provide only information on ionic permeabilities, which are products of partitioning and diffusion coefficients [15]. Thus, stationary techniques require additional measurements to determine either partition or diffusion coefficients. Once the steady state permeability is known, one can determine separately partition and estimate diffusion or vice versa [91].

Equilibrium salt sorption can be measured via salt desorption using standard methods or advanced techniques such as attenuated total reflection Fourier transform infrared spectroscopy (ATR-FTIR) [92–95], Rutherford backscattering spectrometry (RBS) [96,97] or quartz crystal microbalance (QCM) sensors [98]. On the other hand, diffusivity may be measured using tracer-based techniques such as pulsed-field gradient nuclear magnetic

resonance (PFG-NMR) [99,100]. Moreover, electrochemical impedance spectroscopy (EIS) has been used to determine both partitioning and diffusivity coefficients in the case of electroactive solutes [101].

Non-stationary diffusion in principle allows for separate determination of those properties for a diffusing species from interpretation of a single time-resolved measurement [102]. However, the typical use of pure solvent in the receiving compartment (needed to reliably detect initially small concentration changes) [103] implies large trans-membrane salt-concentration differences and strongly non-linear diffusion that would complicate the interpretation in the case of ion-exchange membranes whose diffusion permeability is a strong function of salt concentration [104]. Non-stationary diffusion of radiotracer ions [90,105] can provide information on the ion diffusivity and partitioning from which the salt-related properties can be calculated. However, the use of radiotracers is possible only in certified laboratories. Besides, suitable radiotracers are available only for some ions.

A different approach based on time-resolved measurements consists in measuring the electrical response to a sudden change in the electrolyte concentration at one of the membrane sides [106–108]. Sørensen and Compañ developed a method to determine ion transport numbers within a surface layer of a membrane by measuring initial-time membrane potential. Once the membrane was equilibrated with an equilibrium solution, one of the membrane faces was exposed to a non-equilibrium solution and the membrane potential was measured immediately. Initially, the concentration gradient remained localized within a surface layer of the membrane. Therefore, the electrical response was controlled by the ion transport numbers within a narrow surface zone and could be estimated for each face of the membrane. The initial time method was used to evaluate the asymmetry between the two faces of a membrane and conclude if it was homogeneous or not.

Later, refs.[109,110] pointed out a problem related to the solution replacement technique (as implemented in [106–108]), which is the presence of an unstirred layer at the membrane surface that does not allow for a change in the electrolyte concentration directly at the membrane surface but only at the external surface of a boundary layer. For nanofiltration membranes studied in [109,110] the characteristic relaxation time of the initial signal could be as short as a couple of milliseconds, so in the presence of an unstirred layer it was impossible to measure the initial membrane-potential values. Therefore, refs.[109,110]

introduced an alternative approach to the rapid concentration change at the membrane surface (touching the membrane surface with a pendant drop).

However, in the case of ion-exchange membranes, the relaxation of initial signal takes tens of seconds since these membranes are relatively thick compared with the active layers of nanofiltration membranes. Therefore, the solution replacement can be implemented simply via evacuating an equilibrium solution and replacing it with a non-equilibrium one.

This thesis presents a novel non-stationary-diffusion method to determine salt diffusion and partitioning coefficients under (quasi)-linear conditions of relatively small concentration differences (Publication 4). The electrical response is measured for a membrane supported by a relatively coarse-porous material. The different ion perm-selectivities of the membrane (thin and relatively dense) and porous support (thicker and much more porous than the membrane) make the response time-dependent due to the progressive redistribution of applied concentration difference between those two media. The porous support was characterized in separate measurements in terms of porosity and effective salt diffusivity needed for the interpretation of the results. Experimental data is fitted to a mathematical model that describes transient transport phenomena including osmosis, which has noticeable impact on the measurements.

First, the new procedure is applied to a membrane (Nafion 120) that has been previously extensively characterized by using well-established conventional techniques. The results have been compared with the literature to validate the new method. Further on, the method has been implemented for a range of NaCl concentrations to obtain information on concentration dependences of properties of a novel ion-exchange membrane (Type 10, Fujifilm NL). In this case, conventional techniques have been used in order to validate the new method because the corresponding results are not, yet, available in the literature for those membranes. Afterward, the new approach is used to investigate the effect of different electrolyte solutions (LiCl and KOAc) and also the effect of temperature for NaCl (Publication 7).

## 1.4 References

[1] M.R. Esfahani, S.A. Aktij, Z. Dabaghian, M.D. Firouzjaei, A. Rahimpour, J. Eke, I.C. Escobar, M. Abolhassani, L.F. Greenlee, A.R. Esfahani, A. Sadmani, N. Koutahzadeh, Nanocomposite membranes for water separation and purification: Fabrication, modification, and applications, Sep. Purif. Technol. 213 (2019) 465–499. doi:10.1016/j.seppur.2018.12.050.

[2] A. Figoli, A. Criscuoli, Sustainable Membrane Technology for Water and Wastewater Treatment, Springler, 2017. doi:10.1007/978-981-10-5623-9.

[3] N.P. Hankins, R. Singh, Emerging membrane technology for sustainable water treatment, 2016. http://mendeley.csuc.cat/fitxers/951ae526dea5f7c00eb9daafdb49b6df (accessed August 29, 2019).

[4] R. Singh, Membrane technology and engineering for water purification : application, systems design and operation, Second Edi, Elsevier Inc., 2014. doi:10.1016/C2013-0-15275-0.

[5] K.V. Peinemann, S.P. Nunes, Membrane technology, Membranes for water treatment, vol. 4, Weinheim Wiley-VCH, 2010.

[6] A.K. Pabby, A.M. Sastre, S.S.H. Rizvi, Handbook of membrane separations : chemical, pharmaceutical, and biotechnological applications, Second edition, Taylor&Francis group, 2015.

[7] S.P. Nunes, K.V. Peinemann, Membrane technology in the chemical industry, Wiley, 2006.

[8] C. Abels, F. Carstensen, M. Wessling, Membrane processes in biorefinery applications, J. Memb. Sci. 444 (2013) 285–317. doi:10.1016/j.memsci.2013.05.030.

[9] M. Reig, X. Vecino, M. Hermassi, C. Valderrama, O. Gibert, J.L. Cortina, Integration of selectrodialysis and solvent-impregnated resins for Zn(II) and Cu(II) recovery from hydrometallurgy effluents containing As(V), Sep. Purif. Technol. 229 (2019) 115818. doi:10.1016/j.seppur.2019.115818.

[10] J. López, M. Reig, O. Gibert, J.L.L. Cortina, Increasing sustainability on the metallurgical industry by integration of membrane nanofiltration processes: Acid recovery, Sep. Purif. Technol. 226 (2019) 267–277. doi:10.1016/j.seppur.2019.05.100.

[11] J. López, M. Reig, O. Gibert, J.L.L. Cortina, Integration of nanofiltration membranes in recovery options of rare earth elements from acidic mine waters, J. Clean. Prod. 210 (2019) 1249–1260. doi:10.1016/j.jclepro.2018.11.096.

[12] M. Reig, S. Casas, C. Valderrama, O. Gibert, J.L.L. Cortina, Integration of monopolar and bipolar electrodialysis for valorization of seawater reverse osmosis desalination brines: Production of strong acid and base, Desalination. 398 (2016) 87–97. doi:10.1016/j.desal.2016.07.024.

[13] C.H. Neoh, Z.Z. Noor, N.S.A. Mutamim, C.K. Lim, Green technology in wastewater treatment technologies: Integration of membrane bioreactor with various wastewater treatment systems, Chem. Eng. J. 283 (2016) 582–594. doi:10.1016/j.cej.2015.07.060.

[14] N. Hilal, A.F. Ismail, T. Matsuura, D. Oatley-Radcliffe, Membrane Characterization, 2017.

[15] R. Bernstein, Y. Kaufman, V. Freger, Membrane Characterization, Encycl. Membr. Sci. Technol. (2013) 1–41. doi:10.1002/9781118522318.emst063.

[16] E. Drioli, L. Giorno, Comprehensive membrane science and engineering, Elsevier Science, 2010.

[17] R. Singh, Introduction to membrane technology, Hybrid Membr. Syst. Water Purif. (2005) 1–56. doi:10.1016/b978-185617442-8/50002-6.

[18] R.W. Baker, Membrane Technology and Applications, 2004. doi:10.1002/0470020393.

[19] A.W. Mohammad, Y.H. Teow, W.L. Ang, Y.T. Chung, D.L. Oatley-Radcliffe, N. Hilal, Nanofiltration membranes review: Recent advances and future prospects, Desalination. 356 (2015) 226–254. doi:10.1016/j.desal.2014.10.043.

[20] I.G. Wenten, Khoiruddin, Reverse osmosis applications: Prospect and challenges, Desalination. 391 (2016) 112–125. doi:10.1016/j.desal.2015.12.011.

[21] N. Pages, A. Yaroshchuk, O. Gibert, J.L. Cortina, Rejection of trace ionic solutes in nanofiltration : Influence of aqueous phase composition, 104 (2013) 1107–1115. doi:10.1016/j.ces.2013.09.042.

[22] S. Bhattacharjee, J.C. Chen, M. Elimelech, Coupled model of concentration polarization and pore transport in crossflow nanofiltration, AIChE J. 47 (2001) 2733–2745. doi:10.1002/aic.690471213.

[23] S. Bouranene, P. Fievet, A. Szymczyk, M. El-Hadi Samar, A. Vidonne, Influence of operating conditions on the rejection of cobalt and lead ions in aqueous solutions by a nanofiltration polyamide membrane, J. Memb. Sci. 325 (2008) 150–157. doi:10.1016/j.memsci.2008.07.018.

[24] W.R. Bowen, B. Cassey, P. Jones, D.L. Oatley, Modelling the performance of membrane nanofiltration - Application to an industrially relevant separation, J. Memb. Sci. 242 (2004) 211–220. doi:10.1016/j.memsci.2004.04.028.

[25] V. Geraldes, M.D. Afonso, Prediction of the concentration polarization in the nanofiltration/reverse osmosis of dilute multi-ionic solutions, J. Memb. Sci. 300 (2007) 20–27. doi:10.1016/j.memsci.2007.04.025.

[26] T.Y. Qiu, P.A. Davies, Concentration polarization model of spiral-wound membrane modules with application to batch-mode RO desalination of brackish water, Desalination. 368 (2015) 36–47. doi:10.1016/j.desal.2014.12.048.

[27] W. Li, X. Su, A. Palazzolo, S. Ahmed, Numerical modeling of concentration polarization and inorganic fouling growth in the pressure-driven membrane filtration process, J. Memb. Sci. 569 (2019) 71–82. doi:10.1016/j.memsci.2018.10.007.

[28] J.C. Chen, Q. Li, M. Elimelech, In situ monitoring techniques for concentration polarization and fouling phenomena in membrane filtration, Adv. Colloid Interface Sci. 107 (2004) 83–108. doi:10.1016/j.cis.2003.10.018.

[29] V. Geraldes, V. Semião, M.N. de Pinho, Flow management in nanofiltration spiral wound modules with ladder-type spacers, J. Memb. Sci. 203 (2002) 87–102. doi:10.1016/S0376-7388(01)00753-0.

[30] V. Geraldes, V. Semião, M.N. de Pinho, The effect of the ladder-type spacers configuration in NF spiral-wound modules on the concentration boundary layers disruption, Desalination. 146 (2002) 187–194. doi:10.1016/S0011-9164(02)00467-8.

[31] V. Geraldes, V. Semiao, M. Norberta de Pinho, Concentration polarisation and flow structure within nanofiltration spiral-wound modules with ladder-type spacers, Comput. Struct. 82 (2004) 1561–1568. doi:10.1016/j.compstruc.2004.03.052.

[32] L. Song, S. Ma, Numerical studies of the impact of spacer geometry on concentration polarization in spiral wound membrane modules, Ind. Eng. Chem. Res. 44 (2005) 7638–7645. doi:10.1021/ie048795w.

[33] M. Amokrane, D. Sadaoui, M. Dudeck, C.P. Koutsou, New spacer designs for the performance improvement of the zigzag spacer configuration in spiral-wound membrane modules, Desalin. Water Treat. 3994 (2015) 1–9. doi:10.1080/19443994.2015.1022003.

[34] M. Paipuri, S.H. Kim, O. Hassan, N. Hilal, K. Morgan, Numerical modelling of concentration polarisation and cake formation in membrane filtration processes, Desalination. 365 (2015) 151–159. doi:10.1016/j.desal.2015.02.022.

[35] J. Schwinge, D.E. Wiley, D.F. Fletcher, Simulation of the flow around spacer filaments between channel walls. 2. Mass-transfer enhancement, Ind. Eng. Chem. Res. 41 (2002) 4879–4888. http://www.scopus.com/inward/record.url?eid=2-s2.0-0037130790&partnerID=tZOtx3y1.

[36] T. Ishigami, H. Matsuyama, Numerical Modeling of Concentration Polarization in Spacer-filled Channel with Permeation across Reverse Osmosis Membrane, Ind. Eng. Chem. Res. 54 (2015) 1665–1674. doi:10.1021/ie5039665.

[37] M. Amokrane, D. Sadaoui, C.P. Koutsou, A.J. Karabelas, M. Dudeck, A study of flow field and concentration polarization evolution in membrane channels with two-dimensional spacers during water desalination, J. Memb. Sci. 477 (2015) 139–150. doi:10.1016/j.memsci.2014.11.029.

[38] S. Bason, V. Freger, Phenomenological analysis of transport of mono- and divalent ions in nanofiltration, J. Memb. Sci. 360 (2010) 389–396. doi:10.1016/j.memsci.2010.05.037.

[39] V. Geraldes, M.D. Afonso, Generalized mass-transfer correction factor for nanofiltration and reverse osmosis, AIChE J. 52 (2006) 3353–3362. doi:10.1002/aic.10968.

[40] J.L.C. Santos, V. Geraldes, S. Velizarov, J.G. Crespo, Investigation of flow patterns and mass transfer in membrane module channels filled with flow-aligned spacers using computational fluid dynamics (CFD), J. Memb. Sci. 305 (2007) 103–117. doi:10.1016/j.memsci.2007.07.036.

[41] C.P. Koutsou, S.G. Yiantsios, a. J. Karabelas, A numerical and experimental study of mass transfer in spacer-filled channels: Effects of spacer geometrical characteristics and Schmidt number, J. Memb. Sci. 326 (2009) 234–251. doi:10.1016/j.memsci.2008.10.007.

[42] J.M. Miranda, J.B.L.M. Campos, Mass transfer in the vicinity of a separation membrane - The applicability of the stagnant film theory, J. Memb. Sci. 202 (2002) 137–150. doi:10.1016/S0376-7388(01)00747-5.

[43] V. Geraldes, V. Semião, M. Norberta Pinho, Hydrodynamics and concentration polarization in NF/RO spiral-wound modules with ladder-type spacers, Desalination. 157 (2003) 395–402. doi:10.1016/S0011-9164(03)00422-3.

[44] C.P. Koutsou, A.J. Karabelas, Shear stresses and mass transfer at the base of a stirred filtration cell and corresponding conditions in narrow channels with spacers, J. Memb. Sci. 399–400 (2012) 60–72. doi:10.1016/j.memsci.2012.01.029.

[45] A. Yaroshchuk, M.L.M.L. Bruening, E. Zholkovskiy, Modelling nanofiltration of electrolyte solutions, Adv. Colloid Interface Sci. 268 (2019) 39–63. doi:10.1016/j.cis.2019.03.004.

[46] P. Ortiz-albo, R. Ibañez, A. Urtiaga, I. Ortiz, Phenomenological prediction of desalination brines nanofiltration through the indirect determination of zeta potential, Sep. Purif. Technol. (2018). doi:10.1016/j.seppur.2018.08.066.

[47] N. Fridman-bishop, K.A. Tankus, V. Freger, Permeation mechanism and interplay between ions in nano fi ltration, J. Memb. Sci. 548 (2018) 449–458. doi:10.1016/j.memsci.2017.11.050.

[48] S.S. Wadekar, R.D. Vidic, Insights into the rejection of barium and strontium by nanofiltration membrane from experimental and modeling analysis, J. Memb. Sci. 564 (2018) 742–752. doi:10.1016/j.memsci.2018.07.060.

[49] K. Thibault, H. Zhu, A. Szymczyk, G. Li, The averaged potential gradient approach to model the rejection of electrolyte solutions using nanofiltration: Model development and assessment for highly concentrated feed solutions, Sep. Purif. Technol. 153 (2015) 126–137. doi:10.1016/j.seppur.2015.08.041.

[50] S. Anisah, M. Kanezashi, H. Nagasawa, T. Tsuru, Hydrothermal stability and permeation properties of TiO2-ZrO2 (5/5) nanofiltration membranes at high temperatures, Sep. Purif. Technol. 212 (2019) 1001–1002. doi:10.1016/j.seppur.2018.12.006.

[51] A. Yaroshchuk, X. Martínez-Lladó, L. Llenas, M. Rovira, J. de Pablo, Solution-diffusion-film model for the description of pressure-driven trans-membrane transfer of electrolyte mixtures: One dominant salt and trace ions, J. Memb. Sci. 368 (2011) 192–201. doi:10.1016/j.memsci.2010.11.037.

[52] A. Yaroshchuk, M.L. Bruening, E. Eduardo, L. Bernal, Solution-Diffusion – Electro-Migration model and its uses for analysis of nano fi ltration , pressure-retarded osmosis and forward osmosis in multi-ionic solutions, J. Memb. Sci. 447 (2013) 463–476. doi:10.1016/j.memsci.2013.07.047.

[53] J. Lopez, M. Reig, O. Gibert, C. Valderrama, J.L. Cortina, Evaluation of NF membranes as treatment technology of acid mine drainage: metals and sulfate removal, Desalination. 440 (2018) 122–134. doi:10.1016/j.desal.2018.03.030.

[54] J. López, M. Reig, A. Yaroshchuk, E. Licon, O. Gibert, J.L. Cortina, Experimental and theoretical study of nanofiltration of weak electrolytes: SO42–/HSO4–/H+ system, J. Memb. Sci. 550 (2018) 389–398. doi:10.1016/j.memsci.2018.01.002.

[55] A. Yaroshchuk, M.L. Bruening, An analytical solution of the solution-diffusion-electromigration equations reproduces trends in ion rejections during nanofiltration of mixed electrolytes, J. Memb. Sci. 523 (2017) 361–372. doi:10.1016/j.memsci.2016.09.046.

[56] N. Pagès, M. Reig, O. Gibert, J.L. Cortina, Trace ions rejection tunning in NF by selecting solution composition: Ion permeances estimation, Chem. Eng. J. 308 (2017) 126–134. doi:10.1016/j.cej.2016.09.037.

[57] M. Reig, E. Licon, O. Gibert, A. Yaroshchuk, J.L. Cortina, Rejection of ammonium and nitrate from sodium chloride solutions by nanofiltration: Effect of dominant-salt concentration on the trace-ion rejection, Chem. Eng. J. 303 (2016) 401–408. doi:10.1016/j.cej.2016.06.025.

[58] M. Fernández de Labastida, E.E. Licon Bernal, A. Yaroshchuk, Implications of inhomogeneous distribution of concentration polarization for interpretation of pressure-driven membrane measurements, J. Memb. Sci. 520 (2016) 693–698. doi:10.1016/j.memsci.2016.08.040.

[59] N. Hilal, N.A. Darwish, A.W. Mohammad, M.A. Arabi, A comprehensive review of nanofiltration membranes : Treatment , pretreatment , modelling , and atomic force microscopy, 170 (2004) 281–308. doi:10.1016/j.desal.2004.01.007.

[60] P. Feron, J.W. Van Heuven, J.J. Akkerhuis, R. Van Der Welle, Design and development of a membrane testcell with uniform mass transfer : Application to characterisation of high flux gas separation membranes *, 80 (1993) 157–164.

[61] M.Y. Jaffrin, Dynamic shear-enhanced membrane filtration : A review of rotating disks , rotating membranes and vibrating systems, 324 (2008) 7–25. doi:10.1016/j.memsci.2008.06.050.

[62] R. Bouzerar, M.Y. Jaffrin, L. Ding, P. Paullier, Influence of Geometry and Angular Velocity on Performance of a Rotating Disk Filter, 46 (2000) 257–265.

[63] R. Bouzerar, L. Ding, M.Y. Jaffrin, Local permeate flux – shear – pressure relationships in a rotating disk microfiltration module : implications for global performance, 170 (2000) 127–141.

[64] C. Torras, J. Pallares, R. Garcia-valls, M.Y. Jaffrin, Numerical simulation of the flow in a rotating disk filtration module, DES. 235 (2009) 122–138. doi:10.1016/j.desal.2008.02.006.

[65] A. Brou, L. Ding, P. Boulnois, M.Y. Jaffrin, Dynamic microfiltration of yeast suspensions using rotating disks equipped with vanes, 197 (2002) 269–282.

[66] M.Y. Jaffrin, L. Ding, O. Akoum, A. Brou, A hydrodynamic comparison between rotating disk and vibratory dynamic filtration systems, 242 (2004) 155–167. doi:10.1016/j.memsci.2003.07.029.

[67] M. Frappart, O. Akoum, L.H. Ding, M.Y. Jaffrin, Treatment of dairy process waters modelled by diluted milk using dynamic nanofiltration with a rotating disk module, 282 (2006) 465–472. doi:10.1016/j.memsci.2006.06.005.

[68] M. Frappart, M. Jaffrin, L.H. Ding, Reverse osmosis of diluted skim milk : Comparison of results obtained from vibratory and rotating disk modules, 60 (2008) 321–329. doi:10.1016/j.seppur.2007.09.007.

[69] R. Bouzerar, P. Paullier, M.Y. Jaffrin, using a rotating disk dynamic filtration module, 158 (2003) 79–85.

[70] J. Luo, L. Ding, Y. Wan, P. Paullier, M.Y. Jaffrin, Application of NF-RDM ( nanofiltration rotating disk membrane ) module under extreme hydraulic conditions for the treatment of dairy wastewater, Chem. Eng. J. 163 (2010) 307–316. doi:10.1016/j.cej.2010.08.007.

[71] J. Luo, L. Ding, Y. Wan, M.Y. Jaffrin, Flux decline control in nanofiltration of detergent wastewater by a shear-enhanced filtration system, Chem. Eng. J. 181–182 (2012) 397–406. doi:10.1016/j.cej.2011.11.101.

[72] A.J. Bard, L.R. Faulkner, E. Swain, C. Robey, Electrochemical methods: Fundamentals and Applications, 2nd edition, Wiley, 2010

[73] M.T. Crespo, A review of electrodeposition methods for the preparation of alpha-radiation sources, Appl. Radiat. Isot. 70 (2012) 210–215. doi:10.1016/j.apradiso.2011.09.010.

[74] S Treimer, A Tanga, DC Johnson, Consideration of the Application of Koutecky-Levich Plots in the Diagnoses of Charge-Transfer Mechanisms at Rotated Disk Electrodes, Electroanalysis. 14 (2002) 165–171.

[75] V.G. Levich, R.J. Seeger, Physicochemical Hydrodynamics, Am. J. Phys. 31 (1963). doi:10.1119/1.1969158.

[76] T. Luo, S. Abdu, M. Wessling, Selectivity of Ion Exchange Membranes: A Review, (2018). doi:10.1016/j.memsci.2018.03.051.

[77] M. Micari, M. Bevacqua, A. Cipollina, A. Tamburini, W. Van Baak, T. Putts, G. Micale, E ff ect of di ff erent aqueous solutions of pure salts and salt mixtures in reverse electrodialysis systems for closed-loop applications, J. Memb. Sci. 551 (2018) 315–325. doi:10.1016/j.memsci.2018.01.036.

[78] A. Tamburini, M. Tedesco, A. Cipollina, G. Micale, M. Ciofalo, M. Papapetrou, W. Van Baak, A. Piacentino, Reverse electrodialysis heat engine for sustainable power production, Appl. Energy. 206 (2017) 1334–1353. doi:10.1016/j.apenergy.2017.10.008.

[79] M. Reig, X. Vecino, C. Valderrama, O. Gibert, J.L. Cortina, Application of selectrodialysis for the removal of As from metallurgical process waters: Recovery of Cu and Zn, Sep. Purif. Technol. 195 (2018) 404–412. doi:10.1016/j.seppur.2017.12.040.

[80] T. Rijnaarts, N.T. Shenkute, A. Wood, W.M. De Vos, K. Nijmeijer, Divalent Cation Removal by Donnan Dialysis for Improved Reverse Electrodialysis, (2018). doi:10.1021/acssuschemeng.8b00879.

[81] C. Agarwal, R.W. Cattrall, S.D. Kolev, Donnan dialysis based separation of gold ( III ) from electronic waste solutions using an anion exchange pore- fi lled membrane, J. Memb. Sci. 514 (2016) 210–216. doi:10.1016/j.memsci.2016.04.033.

[82] J. Ran, L. Wu, Y. He, Z. Yang, Y. Wang, C. Jiang, L. Ge, E. Bakangura, T. Xu, Ion exchange membranes: New developments and applications, J. Memb. Sci. 522 (2017) 267–291. doi:10.1016/j.memsci.2016.09.033.

[83] W. Shi, X. Liu, C. Ye, X. Cao, C. Gao, J. Shen, Efficient lithium extraction by membrane capacitive deionization incorporated with monovalent selective cation exchange membrane, Sep. Purif. Technol. 210 (2019) 885–890. doi:10.1016/j.seppur.2018.09.006.

[84] D. Saebea, C. Chaiburi, S. Authayanun, Model based evaluation of alkaline anion exchange membrane fuel cells with water management, Chem. Eng. J. 374 (2019) 721–729. doi:10.1016/j.cej.2019.05.200.

[85] T. Wang, S.J. Moon, D.S. Hwang, H. Park, J. Lee, S. Kim, Y.M. Lee, S. Kim, Selective ion transport for a vanadium redox flow battery (VRFB) in nano-crack regulated proton exchange membranes, J. Memb. Sci. 583 (2019) 16–22. doi:10.1016/j.memsci.2019.04.017.

[86] S. Mehdizadeh, M. Yasukawa, M. Kuno, Y. Kawabata, M. Higa, Evaluation of energy harvesting from discharged solutions in a salt production plant by reverse electrodialysis (RED), Desalination. 467 (2019) 95–102. doi:10.1016/j.desal.2019.04.007.

[87] D.D. Tham, D. Kim, C2 and N3 substituted imidazolium functionalized poly(arylene ether ketone) anion exchange membrane for water electrolysis with improved chemical stability, J. Memb. Sci. 581 (2019) 139–149. doi:10.1016/j.memsci.2019.03.060.

[88] Y. Tanaka, Ion exchange membranes : fundamentals and applications: Second edition, Elsevier, 2015. https://doi.org/10.1016/C2013-0-12870-X

[89] B. Auclair, V. Nikonenko, C. Larchet, M. Métayer, L. Dammak, Correlation between transport parameters of ion-exchange membranes, J. Memb. Sci. 195 (2002) 89–102.

[90] A.N. Naik, C. Agarwal, S. Chaudhury, A. Goswami, Non-stationary radiotracer method for diffusion coefficients of Cs , Ba , Eu tracers in Nafion-117 membrane, Sep. Sci. Technol. 52 (2017) 2379-2384. doi:10.1080/01496395.2016.1256324.

[91] G.M. Geise, B.D. Freeman, D.R. Paul, Sodium chloride diffusion in sulfonated polymers for membrane applications, J. Memb. Sci. 427 (2013) 186–196. doi:10.1016/j.memsci.2012.09.029.

[92] V. Freger, A. Ben-David, Use of attenuated total reflection infrared spectroscopy for analysis of partitioning of solutes between thin films and solution, Anal. Chem. 77 (2005) 6019–6025. doi:10.1021/ac050689w.

[93] A. Ben-David, Y. Oren, V. Freger, Thermodynamic factors in partitioning and rejection of organic compounds by polyamide composite membranes, Environ. Sci. Technol. 40 (2006) 7023–7028. doi:10.1021/es0609912.

[94] A. Ben-David, S. Bason, J. Jopp, Y. Oren, V. Freger, Partitioning of organic solutes between water and polyamide layer of RO and NF membranes: Correlation to rejection, J. Memb. Sci. 281 (2006) 480–490. doi:10.1016/j.memsci.2006.04.017.

[95] A. Ghoufi, E. Dražević, A. Szymczyk, Interactions of Organics within Hydrated Selective Layer of Reverse Osmosis Desalination Membrane: A Combined Experimental and Computational Study, Environ. Sci. Technol. 51 (2017) 2714–2719. doi:10.1021/acs.est.6b05153.

[96] X. Zhang, D.G. Cahill, O. Coronell, B.J. Mariñas, Partitioning of salt ions in FT30 reverse osmosis membranes, Appl. Phys. Lett. 91 (2007). doi:10.1063/1.2802562.

[97] B. Mi, B.J. Mariñas, D.G. Cahill, RBS characterization of arsenic(III) partitioning from aqueous phase into the active layers of thin-film composite NF/RO membranes, Environ. Sci. Technol. 41 (2007) 3290–3295. doi:10.1021/es062292v.

[98] J. Wang, R.S. Kingsbury, L.A. Perry, O. Coronell, Partitioning of Alkali Metal Salts and Boric Acid from Aqueous Phase into the Polyamide Active Layers of Reverse Osmosis Membranes, Environ. Sci. Technol. 51 (2017) 2295–2303. doi:10.1021/acs.est.6b04323.

[99] I. Nicotera, C. Simari, L.G. Boutsika, L. Coppola, K. Spyrou, A. Enotiadis, NMR investigation on nanocomposite membranes based on organosilica layered materials bearing different functional groups for PEMFCs, Int. J. Hydrogen Energy. 42 (2017) 27940–27949. doi:10.1016/j.ijhydene.2017.05.014.

[100] R. Mueller, V. Hariharan, C. Zhang, R. Lively, S. Vasenkov, Relationship between mixed and pure gas self-diffusion for ethane and ethene in ZIF-8/6FDA-DAM mixed-matrix membrane by pulsed field gradient NMR, J. Memb. Sci. 499 (2016) 12–19. doi:10.1016/j.memsci.2015.10.036.

[101] E. Drazevic, S. Bason, K. Kosutic, V. Freger, Enhanced partitioning and transport of phenolic micropollutants within polyamide composite membranes, Environ. Sci. Technol. 46 (2012) 3377–3383. doi:10.1021/es204188j.

[102] J. Kamcev, D.R. Paul, G.S. Manning, B.D. Freeman, Accounting for frame of reference and thermodynamic non-idealities when calculating salt diffusion coefficients in ion exchange membranes, J. Memb. Sci. 537 (2017) 396–406. doi:10.1016/j.memsci.2017.05.034.

[103] A. Cañas, M.J. Ariza, J. Benavente, Characterization of active and porous sublayers of a composite reverse osmosis membrane by impedance spectroscopy , streaming and membrane potentials , salt diffusion and X-ray photoelectron spectroscopy measurements, J. Mem. Sci. 183 (2001) 135–146. https://doi.org/10.1016/S0376-7388(00)00583-4

[104] R.S. Kingsbury, S. Zhu, S. Flotron, O. Coronell, Microstructure Determines Water and Salt Permeation in Commercial Ion-Exchange Membranes, ACS Appl. Mater. Interfaces. 10 (2018) 39745–39756. doi:10.1021/acsami.8b14494.

[105] A. Goswami, A. Acharya, A.K. Pandey, Study of Self-Diffusion of Monovalent and Divalent Cations in Nafion-117, J. Phys. Chem. B., 2001, 105, 38, 9196–9201. doi:10.1021/jp010529y.

[106] V. Compan, M.L. Lopez, T.S. Soerensen, J. Garrido, Transport Numbers in the Surface Layers of Asymmetric Membranes from Initial Time Measurements, J. Phys. Chem. 98 (1994) 9013–9021. doi:10.1021/j100087a033.

[107] V. Compañ, T.S. Sorensen, S.R. Rivera, Comparison of Initial Time and Stationary State Measurements of the Emf of Concentration Cells Using Phenolsulfonic Acid Membrane Separators, J. Phys. Chem., 1995, 99, 33, 12553–12558. doi.org/10.1021/j100033a030

[108] V. Compañ, T.S. Sorensen, A. Andrio, D. Abajo, Transport numbers from initial time and stationary state measurements of EMF in non-ionic polysulphonic membranes, J. Mem. Sci. 123 (1997) 293–302. https://doi.org/10.1016/S0376-7388(96)00228-1

[109] A. Yaroshchuk, Y. Boiko, A. Makovetskiy, Electrochemical perm-selectivity of active layers and diffusion permeability of supports of an asymmetric and a composite NF membrane studied by concentration-step method, Desalination. 245 (2009) 374–387. doi:10.1016/j.desal.2009.02.001.

[110] A.E. Yaroshchuk, A.L. Makovetskiy, Y.P. Boiko, E.W. Galinker, Non-steady-state membrane potential: Theory and measurements by a novel technique to determine the ion transport numbers in active layers of nanofiltration membranes, J. Memb. Sci. 172 (2000) 203–221.

# CHAPTER 2

# Objectives

# 2. Objectives

The main objective of the present PhD thesis is to develop new techniques for systematic transport characterization of membranes. In particular, addressing two specific issues concerning membrane separation in pressure-driven membrane processes and ion-exchange membranes.

## 2.1 Specific objectives

The specific objectives were related to the quantitative control of CP in pressure-driven membrane processes and to the possibility of having detailed information on the transport and equilibrium properties of ion exchange membranes for optimization of electro-membrane processes.

- To demonstrate the consequences of disregarding inhomogeneous CP distribution for the interpretation of experimental results.
- To develop a membrane test cell with equally-accessible membrane surface to reduce the inhomogeneity of CP over the membrane surface and to provide a procedure to correct for CP.
- To validate that the designed membrane test cell satisfies the condition of having homogeneous distribution of CP over the membrane surface.
- To employ the designed membrane test cell for systematic transport characterization of membranes in different conditions.
- To develop a new technique based on non-stationary diffusion that allow simultaneous determination of separate information on the partitioning and diffusivity properties of ion-exchange membranes.
- To validate the developed procedure by comparing the obtained results with conventional well-established techniques.

# CHAPTER 3

# Thesis overview

# 3. Thesis overview

This thesis presents new approaches in the field of membrane characterization, specifically for pressure-driven and electrically-driven membrane processes.

The first study pointed out the inhomogeneity of CP over the membrane surface in pressure-driven membrane test cells and shows the consequences of disregarding this fact in the interpretation of measurements of solute rejection in pressure-driven membrane processes **(Publication 1)**. Therefore, a novel design of test cell with equally-accessible membrane surface was developed based on the classical configuration of rotating disk-like membrane **(Publication 2)**. The equal accessibility condition allows for corrections for CP even for complex multi-ionic systems. This cell was used to study ion rejection of NF membranes in electrolyte mixtures consisting in several dominant salts and trace ions **(Publication 5)** and binary mixtures of NaCl-$MgCl_2$ **(Publication 6)**. Moreover, it was demonstrated the relevance of membrane sealing in a test cell to its performance **(Publication 3)**.

As for the electrically-driven processes, a novel non-stationary-diffusion method was developed to determine salt diffusion and partitioning coefficients under (quasi)-linear conditions of relatively small concentration differences **(Publication 4)**. The new method was used to study non-conventional electrolytes (LiCl and KOAc) and also to study the effect of temperature on ion transport in the case of NaCl **(Publication 7)**.

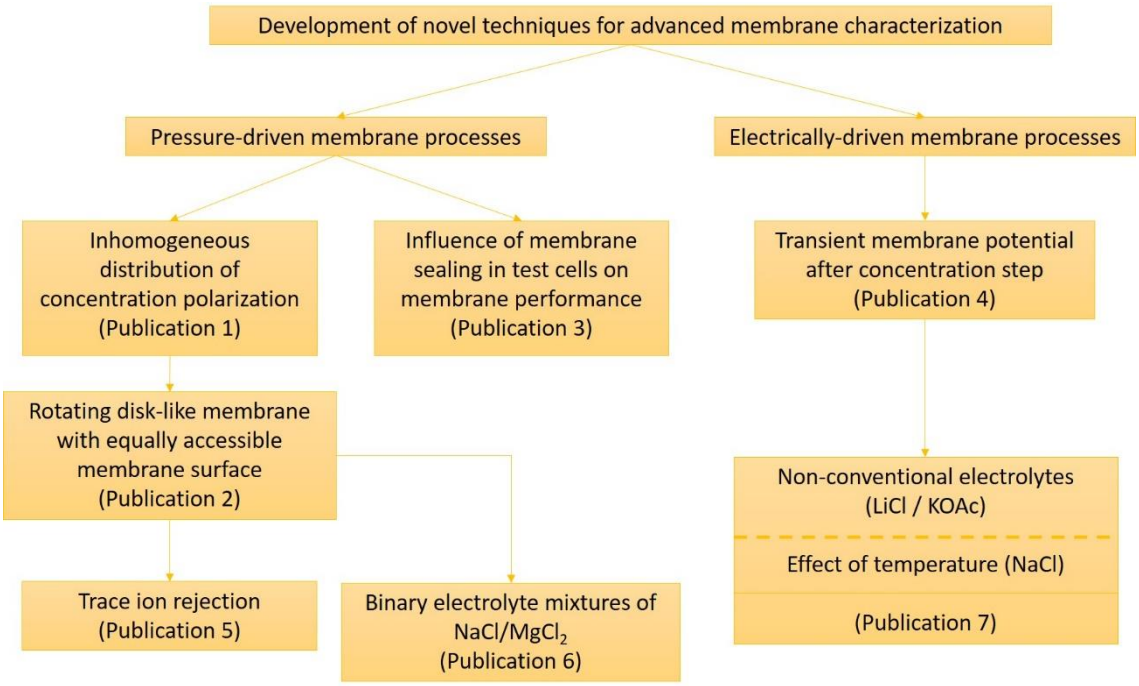


**Fig. 3** Thesis overview

**Publication 1:** M. Fernández de Labastida, E.E. Licon Bernal, A. Yaroshchuk. (2016). *Implications of inhomogeneous distribution of concentration polarization for interpretation of pressure-driven membrane measurements.* Journal of Membrane Science 520, (2016), 693 – 698.

**Publication 2:** M. Fernández de Labastida, E.E. Licón, M. Bondarenko, A. Yaroshchuk. *Rotating disk-like membrane cell for pressure-driven measurements with equally-accessible membrane surface: Numerical simulation and experimental validation.* Journal of Membrane Science 550, (2018) 492–501.

**Publication 3:** M. Fernández de Labastida, A. Yaroshchuk. *Influence of Membrane Sealing in Pressure-Driven Test Cells on Their Performance.* Journal of Membrane Science & Research 5, (2019), 240–243.

**Publication 4:** M. Fernández de Labastida, A. Yaroshchuk. *Transient membrane potential after concentration step: A new method for advanced characterization of ion-exchange membranes.* Journal of Membrane Science 585, (2019), 271–281.

# CHAPTER 4

# Publication 1

*"Implications of inhomogeneous distribution of concentration polarization for interpretation of pressure-driven membrane measurements"*

Journal of Membrane Science 520 (2016) 693–698

Contents lists available at ScienceDirect

Journal of Membrane Science

journal homepage: www.elsevier.com/locate/memsci

# Implications of inhomogeneous distribution of concentration polarization for interpretation of pressure-driven membrane measurements

Marc Fernández de Labastida [a,*], Edxon E. Licon Bernal [a], Andriy Yaroshchuk [a,b]

[a] Dept of Chemical Engineering, Polytechnic University of Catalonia – BarcelonaTech, av. Diagonal 647, 08028 Barcelona, Spain
[b] ICREA, Passeig Lluís Companys 23, Barcelona, Spain

ARTICLE INFO

*Article history:*
Received 28 April 2016
Received in revised form
29 July 2016
Accepted 22 August 2016
Available online 24 August 2016

*Keywords:*
Concentration polarization
Inhomogeneous distribution
Unstirred-layer thickness
Pressure-driven
Spacer-filled feed cannel

ABSTRACT

A number of CFD studies have demonstrated that there is a considerable inhomogeneity of extent of Concentration Polarization (CP) over the membrane surface especially in spacer-filled feed channels. However, the consequences of this inhomogeneity for the interpretation of measurements of solute rejection in pressure-driven membrane processes have received little attention.

This study uses a simple model of locally-1D CP combined with a postulated probability distribution of unstirred-layer thickness over the membrane thickness. In this way, we obtain transparent analytical results and can consider qualitative consequences of inhomogeneous distribution of CP over membrane surface. Our analysis shows that disregarding the CP distribution under-estimates the CP of strongly positively-rejected solutes and over-estimates the CP for the negatively-rejected ones. This observation is especially important for the interpretation of ion rejection from multi-ion solutions in nanofiltration where strong positive and pronounced negative rejections can occur simultaneously for solutes of different charges.

We conclude that for reliable interpretation of pressure-driven membrane measurements it is desirable to reduce the inhomogeneity of CP distribution to a minimum in membrane-testing devices.



## 1. Introduction

Correct description of concentration polarization (CP) is important for the interpretation of experimental data with the purpose of obtaining accurate information on the membrane properties and predicting properly the performance of pressure-driven processes. The classical approach to quantify CP is based on the so-called Nernst model [1–5], which postulates the existence of a diffusion boundary layer sharply separated from a perfectly-stirred core-flow zone. Correlations deduced from heat and mass transfer (typically kinetics of dissolution) experiments are frequently used to estimate the thickness of boundary layer. The experimental output of such studies is the dependences of dissolution rate on the cross-flow velocity, diffusion coefficient of the solute (or thermal conductivity in the heat-transfer studies) as well as on the flow-channel geometry. Evidently, this can provide information only on mass- or heat-transfer characteristics averaged along the channel.

Due to the complexity of the phenomena, computational fluid dynamics (CFD) has recently become a technique of choice for the calculation of flow and concentration fields inside feed membrane channels. Thus for instance some studies simulated the flow and CP in narrow rectangular channels with spacers [6–11]. Their results show inhomogeneous CP distribution strongly dependent on the spacer configuration and reveal up to an order of magnitude variation in the local mass-transfer coefficient depending on the position along the membrane surface [10,12–14].

Despite this pronounced inhomogeneity, the results of CFD simulations are often reported as Sherwood number (or mass-transfer coefficient) averaged over the membrane surface. Sherwood number is defined as a ratio of a characteristic length (for example, channel height) and the unstirred-layer thickness. Some authors made reference to the error associated with an inaccurate description in the CP boundary layer in determining the intrinsic rejection and the membrane transport parameters [15]. However, these estimates related only to the specific experimental conditions of those studies. More systematically, [16] simulated numerically the distribution of solute concentration at the membrane surface in infinitely-broad slit-like channels with developed laminar flow and the membrane exhibiting constant rejection

* Corresponding author.

http://dx.doi.org/10.1016/j.memsci.2016.08.040
0376-7388/

(independent of either solute concentration or trans-membrane volume flow). The results were interpreted in terms of dependence of average extent of CP on the trans-membrane mass-transfer rate. Mostly, empirical correlations were considered but some comparison with the film (Nernst) model was also performed. It was found that at weak CPs the film model reproduced the results of numerical simulations quite well but at moderate to strong CPs there were considerable deviations. The authors ascribed them to the effect of "suction" due to the non-zero trans-membrane volume flow, which is often disregarded. However, we believe that actually a major part of those deviations occurred due to the inhomogeneity of distribution of CP along the channel. Unfortunately, only the case of 100% solute rejection was considered in the context of comparison with the film model.

In a number of cases instead of the rejecting-membrane boundary condition, the authors used the impermeable dissolving wall condition, which sets a constant solute concentration and zero normal fluid velocity at the wall [12,17,18]. In this case, the contribution of more stagnant zones to the average mass-transfer (dissolution) rate is under-proportional to their surface fraction since the local Sherwood number is smaller in those regions. In the more realistic case of membrane boundary condition, this contribution is over-proportional at positive rejections due to the stronger solute accumulation. In any case, the use of dissolving-wall boundary condition does not allow for an analysis of dependence of averaged mass transfer on the solute rejection. This dependence can be essential as we will see below. In addition, even in the studies where the membrane boundary condition was used [7–10,13,14,19,20], reporting the results in terms of averaged Sherwood number (instead of reciprocal one) makes difficult drawing conclusions on the correlation between the averaged mass transfer and solute diffusion coefficient (especially when the CP is not weak). In turn, a previous study characterized shear stresses and mass transfer coefficients at the membrane surface of a high pressure stirred filtration cell at different conditions [21]. The authors observed a considerable variation of local values of shear stress at relatively low rotation speeds, with its averaged standard deviation decreasing with increasing Reynolds number. As for the mass-transfer coefficient, the radial distribution is qualitatively similar but more uniform than shear stress, although there is still a variation around 50% in the time averaged Sherwood number.

Fluid-dynamics simulations are quite complex mathematically and can be performed only numerically. In order to obtain transparent analytical results, in this study we adopt an alternative approach: we postulate a distribution of unstirred-layer thickness over the membrane surface and use a simple locally-1D description of CP. Its simplicity enables us to use the membrane boundary condition with various intrinsic solute rejections (including negative ones). In this way, we obtain local permeate concentration as a function of trans-membrane volume flux and solute diffusion coefficient. Then, the observable rejection is calculated via averaging this concentration over the membrane surface by using the postulated probability-density function for the distribution of unstirred-layer thickness.

Of course, this approach is approximate primarily because it disregards lateral solute flows (both convective and diffusive). However, if the unstirred-layer thickness is much smaller than the characteristic scale of inhomogeneity of its distribution along the membrane surface the local 1D approach can be sufficiently accurate. This condition can be met for typical feed spacers with the characteristic mesh sizes of a couple of millimeters, while the typical unstirred-layer thickness in laminar flows is around 100 μm. Some of the results obtained below do not depend on the exact form of distribution function. For more quantitative illustrations in the first instance, we will use a simple log normal distribution. We will also test our approach in the case of a distribution function obtained from CFD simulations [18].

## 2. Theory

First, we define the classical convection-diffusion equation in the unstirred layer for the 1D description of local CP:

$$J_s = -D\frac{dc}{dx} + J_v c \tag{1}$$

where $J_s$ is the trans-membrane solute flux, $D$ is the solute diffusion coefficient, $c$ is the solute concentration, $x$ is the coordinate across the unstirred layer, $J_v$ is the trans-membrane volume flux. The boundary condition is a given solute concentration, $c_f$, at the external boundary of unstirred layer (local Nernst model).

Further, it is assumed that there is a distribution of thickness of unstirred layer over the membrane surface. Taking into account that there is a most probable value of this thickness, $\delta$, and defining the ratio of actual local unstirred-layer thickness to the most probable one as the parameter $\alpha$, Eq. (1) can be rewritten in this way:

$$\alpha\cdot\tilde{J}_s = -\frac{dc}{d\xi} + \alpha\cdot Pe\cdot c \tag{2}$$

where

$$\tilde{J}_s \equiv \frac{J_s\delta}{D} \tag{3}$$

$$Pe \equiv \frac{J_v\delta}{D} \tag{4}$$

$$\xi \equiv x/\delta \tag{5}$$

By assuming that the solute rejection is a constant independent of solute concentration and trans-membrane volume flow, Eq. (2) can be easily integrated to yield the solute concentration at the membrane surface, $c_m$:

$$c_m = \frac{c_f}{1-R + R\cdot exp(-\alpha\cdot Pe)} \tag{6}$$

where $c_f$ is the feed concentration and $R$ is the solute rejection defined as $\frac{(c_m - c_p)}{c_m}$. Therefore for the local permeate concentration, $c_p$, we obtain

$$c_p = (1-R)\cdot c_m \equiv \frac{(1-R)\cdot c_f}{1-R + R\cdot exp(-\alpha\cdot Pe)} \tag{7}$$

The averaged permeate concentration is:

$$\bar{c}_p = (1-R)\cdot c_f\cdot \int_0^\infty \frac{f(\alpha)d\alpha}{1-R + R\cdot exp(-\alpha\cdot Pe)} \tag{8}$$

where $f(\alpha)$ is the probability-density function for the distribution of relative unstirred-layer thickness (scaled on its most probable value, $\delta$) over the membrane surface. By definition,

$$\int_0^\infty f(\alpha)d\alpha \equiv 1 \tag{9}$$

One can also use Eq. (7) to define an effective value of parameter $\alpha$ that would correspond to the average permeate concentration if the inhomogeneous distribution of unstirred-layer thickness over the membrane surface were disregarded:

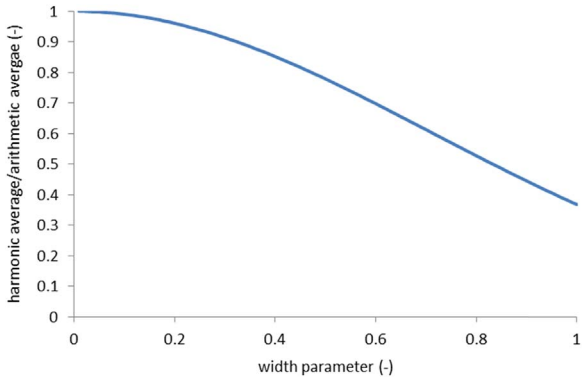


**Fig. 1.** Ratio of harmonic average to the arithmetic average as a function of the width parameter of the log-normal distribution.

$$\overline{c}_p = \frac{(1-R)\cdot c_f}{1-R+R\cdot exp\left(-\alpha_{eff}\cdot Pe\right)} \tag{10}$$

Such procedure corresponds to neglecting the distribution of extent of CP over the membrane surface and describing CP by using a single value of an effective unstirred-layer thickness (or mass-transfer coefficient).

Finally, by using Eq. (8), for $\alpha_{eff}$ we obtain

$$\alpha_{eff}=-\frac{1}{Pe}\cdot ln\left[1+\frac{1}{R}\cdot\left(\frac{1}{\int_0^\infty \frac{f(\alpha)d\alpha}{1-R+R\cdot exp(-\alpha\cdot Pe)}}-1\right)\right] \tag{11}$$

Expectedly, such effective value turns out a function of solute rejection, Péclet number ($Pe$), and distribution function. Below, we will investigate these dependences for a model probability-distribution function and demonstrate that neglecting the distribution of CP extent over the membrane surface can lead to considerable errors in the interpretation of experimental data, especially in the case of mixed solutions containing components with essentially different rejections (e.g., ions of different charge magnitude in nanofiltration).

## 3. Results and discussion

First of all, let us consider the limiting case of weak CP. By using Eq. (11) one can show that at $Pe \to 0$ (weak CP)

$$\alpha_{eff} \underset{Pe\to 0}{\to} \alpha_m \equiv \int_0^\infty \alpha\cdot f(\alpha)d\alpha \tag{12}$$

which is just the definition of average value of parameter $\alpha$. This is expectable because the weak CP is linear in the Péclet number so the surface concentration is controlled just by the average unstirred-layer thickness over the membrane surface.

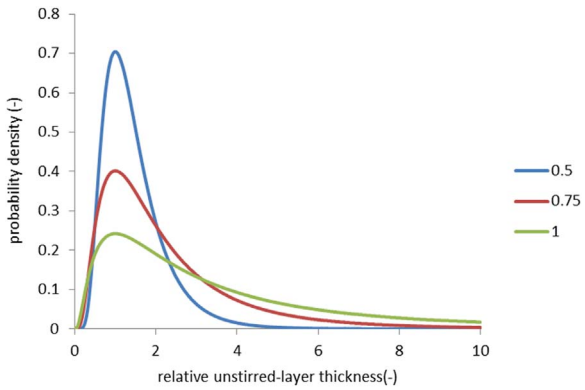


**Fig. 2.** The probability-density distribution functions used for the sample calculations below; the legend gives the values of width parameter.

Notably, in the academic literature it is customary to report the results of CFD simulations of mass transfer (e.g., in spacer-filled channels) in terms of average Sherwood number [17,18,22]. The latter is inversely proportional to the unstirred-layer thickness. In our terms, this would correspond to the averaging of reciprocal parameter $\alpha$ that is to the calculation of its harmonic average according to:

$$\alpha_{ha} \equiv \frac{1}{\int_0^\infty \frac{f(\alpha)}{\alpha}d\alpha} \tag{13}$$

According to Eq. (12), the correct asymptotics at weak CP corresponds to the arithmetic average of relative unstirred-layer thickness. Fig. 1 shows the ratio of harmonic average to the arithmetic average as a function of the width parameter of the log-normal distribution used below for the sample calculations.

Expectedly, this ratio tends to unity when the width parameter goes to zero. However, at any finite width the harmonic average is smaller than the arithmetic one. This means that the averaging of Sherwood number underestimates the average impact of even weak inhomogeneous CP. The harmonic average unduly amplifies the contribution of zones with the weakest CP. One can see that at the width parameter equal to one (relatively broad but still rather compact distribution, see Fig. 2), the averaging of Sherwood number underestimates the extent of weak CP by a factor of almost 3.

The ratio plotted in Fig. 1 was obtained by using a specific probability-density function. By assuming a sufficiently narrow distribution we will show that this ratio is always smaller than one even for an arbitrary distribution function. Indeed, one can always represent parameter $\alpha$ as the sum of its arithmetic average and deviation from it

$$\alpha \equiv \alpha_m + \delta\alpha \tag{14}$$

By substituting Eq. (14) into the definition of harmonic average of Eq. (13), taking into account that $\int_0^\infty \delta\alpha\cdot f(\alpha)d\alpha = 0$ (by definition) and $\delta\alpha/\alpha_m \ll 1$ (narrow distribution), one can show that

$$\alpha_{ha} \approx \alpha_m - \frac{1}{\alpha_m}\cdot\int_0^\infty (\delta\alpha)^2\cdot f(\alpha)d\alpha \tag{15}$$

The integral in the right-hand side of Eq. (15) is always positive so $\alpha_{ha} < \alpha_m$.

At finite Péclet numbers even the arithmetic averaging is incorrect. We will illustrate this for a model distribution of unstirred-layer thickness. Let us use a particular case of log-normal distribution given by this equation

$$f(\alpha) \equiv \frac{1}{\alpha\cdot\sigma\sqrt{2\pi}}\cdot exp\left[-\frac{\left(ln(\alpha)-\sigma^2\right)^2}{2\sigma^2}\right] \tag{16}$$

where $\sigma$ is the width parameter. With this version of log-normal distribution the maximum probability density always occurs at $\alpha = 1$. This is illustrated by Fig. 2, which also shows that the dependence of function shape on the width parameter is quite strong. Thus for instance, at $\sigma = 1$ the distribution is much broader than at $\sigma = 0.5$. Nonetheless, even in the former case the fraction of zones where the unstirred-layer thickness is ca.10 times larger than the most probable value is about 7%. For $\sigma = 0.75$ this fraction is below 1%, which seems to correspond (by the order of magnitude) to the color maps published in [23]. Interestingly, the function of Eq. (16) generates exactly the same distribution of the reciprocal parameter $\alpha$ (proportional to the Sherwood number, see

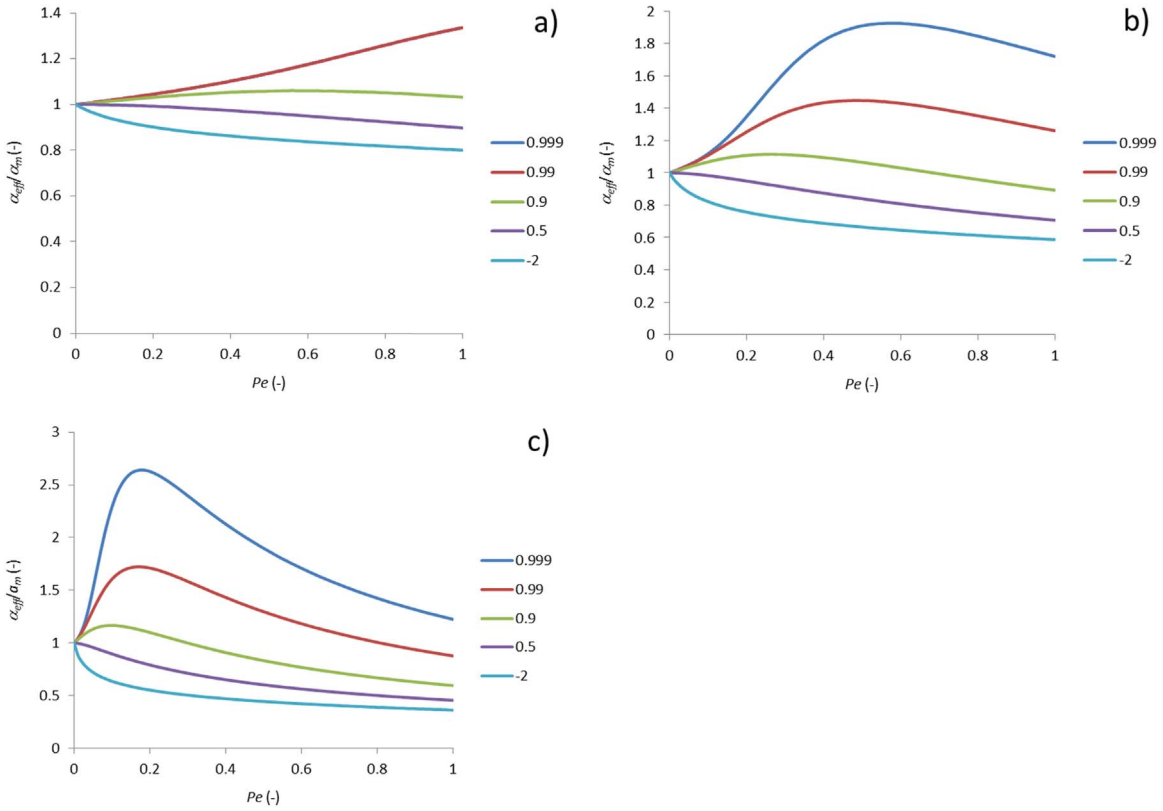


**Fig. 3.** Ratio of effective to the average unstirred-layer thickness vs. Péclet number for various intrinsic rejections and width parameters: (a) $\sigma=0.5$; (b) $\sigma=0.75$ and (c) $\sigma=1$.

above). Therefore, the graphs from Fig. 2 can be directly compared with the CFD-generated probability-density distributions of local Sherwood number shown in Fig. 9 of [18] which look qualitatively similar (especially for the larger Schmidt numbers).

Fig. 3 shows the dependences of the ratio of effective relative unstirred-layer thickness defined by Eq. (11) and the average one defined by Eq. (12) on the Péclet number (extent of CP). The deviation of this ratio from unity is a measure of error introduced due to neglecting the CP distribution over the membrane surface. As discussed above, all the curves converge to one at $Pe \to 0$ (weak CP), which means that the procedure of averaging the unstirred-layer thickness (but not of Sherwood number) is correct in this limiting case. At finite Péclet numbers, there are considerable deviations from unity. Remarkably, they strongly depend on the solute rejection and the Péclet number (and through the latter on the solute diffusivity). Most interestingly, the ratio is larger than one for high positive rejections whereas it is smaller than one for the negative rejections. This can be explained by the fact that (due to the exponential nature of CP) the strongly-rejected solutes over-proportionally accumulate within poorly-stirred zones (larger unstirred-layer thicknesses) so their average concentration at the membrane surface turns out larger than predicted with the average unstirred-layer thickness. At the same time, the concentration of negatively-rejected solutes at the membrane surface is reduced and tends to zero at very strong CP. Therefore, poorly-stirred zones make under-proportional contribution to the trans-membrane flux of such solutes. To sum up, our analysis shows that disregarding CP distribution over the membrane surface under-estimates the CP of strongly positively-rejected solutes and over-estimates the CP for the negatively-rejected ones. Fig. 3 shows that the difference in the effective thicknesses of unstirred layer between the highest positive and the negative rejections can be as large as four to six times for the broader distributions. It is also important to note the considerable dependence on the Péclet number, which depends on

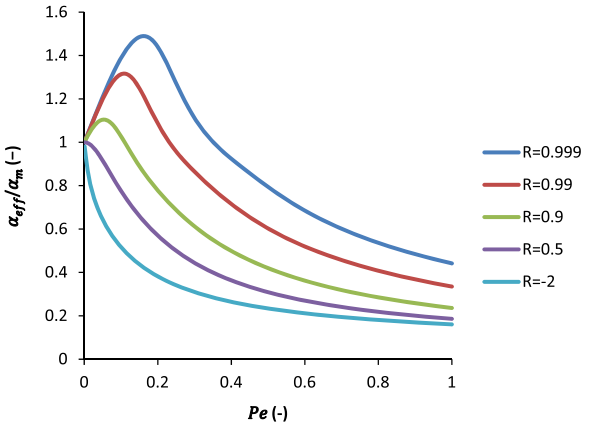


**Fig. 4.** Ratio of effective to the average unstirred-layer thickness vs. Péclet number for various intrinsic rejections for the case of CFD-generated distribution function.

the trans-membrane volume flow and the solute diffusion coefficient.

Even with a single solute this is a problem because one cannot quantitatively fit the dependence of rejection on the trans-membrane volume flow by using a single value of unstirred-layer thickness (or mass-transfer coefficient). However, the situation gets even more problematic with several solutes experiencing very different intrinsic rejections. A relevant example is the nanofiltration of multi-ionic solutions containing, for example, sulfates and chlorides. The intrinsic rejection of sulfates in NF is typically above 99% whereas chloride ions in the presence of sulfates often experience pronounced negative rejections. According to our analysis, with inhomogeneous CP, one cannot use the same effective thickness of unstirred layer for these two solutes even approximately. In [24] a procedure was suggested of fitting the unstirred-layer thickness to the dependence of rejection of

dominant salt on the trans-membrane volume flow and using this thickness to make the CP corrections for the trace ions. The present analysis reveals that this procedure may well be incorrect in the case of strongly-rejected dominant salts and negatively-rejected trace ions especially if the measurements are done in test cells with spacer-filled feed channels as it was the case in [24]. Besides, our results probably can explain the dependence of estimated thickness of unstirred layer on the type of dominant salt observed in [24]. The fitted thickness was larger for salts with lower diffusion coefficients, which would correspond to the dependence of Péclet number on the solute diffusion coefficient to the left from the maxima seen in Fig. 3. Additionally, the dependence of effective unstirred-layer thickness on the intrinsic solute rejection could also contribute because salts with lower diffusion coefficients had higher intrinsic rejections.

Now we will use one of the CFD-generated probability-density distributions of local Sherwood number shown in Fig. 16 of [18,25]. Notably, the largest Schmidt number in these simulations was 100, which is not representative of typical solutes in aqueous solutions (this low value of Schmidt number was probably used because of computational reasons; the realistic value is around 1000). Moreover, in this distribution there is a non-zero probability of Sherwood number is equal exactly to zero. Within the scope of our locally 1D model this rise to infinitely strong concentration polarization. Therefore, this point was discarded and the rest of distribution was rescaled to have all the probabilities to add up to 100%.

Fig. 4 shows the effective unstirred-layer thickness defined by Eq. (11) scaled on the average one defined by Eq. (12) as a function of Péclet number defined with the average thickness. Qualitatively the results are similar to those obtained for the broader log-normal distribution (Fig. 3c). However, the deviations from unity are even more pronounced in this case. The reason is that the CFD-generated distribution is still broader primarily due to the existence of a range of quite small Sherwood numbers occurring with roughly equal probability density of around 0.5%.

This shows that irrespective of the specific form of probability distribution function (if sufficiently broad) the concept of average unstirred-layer thickness becomes rather useless because it does not reflect the considerable dependence of overall concentration polarization on the intrinsic solute rejection, diffusion coefficient and trans-membrane volume flow.

## 4. Conclusions

A number of CFD studies have demonstrated that there is a considerable distribution of extent of CP over the membrane surface especially in spacer-filled feed channels. Despite the up to an order of magnitude variability in the simulated local Sherwood number, the impact of this distribution on the observable rejections received little attention in the previous studies.

This study elucidates qualitative consequences of inhomogeneous CP by using a locally 1D description of CP and postulated probability distributions of unstirred-layer thickness over the membrane surface. The principal conclusions of our analysis are:

1. In the limiting case of weak CP averaging local unstirred-layer thickness produces correct results. On the contrary, averaging local Sherwood number (inversely proportional to the unstirred-layer thickness) is incorrect even in this limiting case.
2. At moderate to strong CP, the whole description in terms of a single value of Nernst- layer thickness fails because the effective unstirred-layer thickness turns out a noticeable function of intrinsic rejection, trans-membrane volume flow and solute diffusion coefficient.
3. Disregarding the CP distribution under-estimates the CP of strongly positively-rejected solutes and over-estimates the CP for the negatively-rejected ones; the difference in the effective unstirred-layer thicknesses calculated for such solutes can be several times.
4. Inhomogeneous CP complicates considerably the task of obtaining reliable information on the membrane transport properties from experimental data. Therefore, in membrane-testing devices it is desirable to reduce this inhomogeneity to a minimum.

## Acknowledgments

The authors gratefully appreciate the numerical data provided by A.J. Karabelas and acknowledge support from the project "Valorization of by-product from industrial effluents: integration of membrane technologies in the separation, concentration and purification steps" (Waste2Product, CTM2014-57302-R) funded by the Ministry of Science and Innovation (MINECO, Spain) and the Catalan government (project ref. 2014SGR050).

### Nomenclature

| | |
|---|---|
| $c$ | solute concentration |
| $c_f$ | feed solute concentration (external boundary of unstirred layer) |
| $c_m$ | solute concentration at the membrane surface |
| $c_p$ | local permeate concentration |
| $\bar{c}_p$ | average permeate concentration |
| $D$ | solute diffusion coefficient |
| $f(\alpha)$ | probability-density function of the distribution of relative unstirred-layer thickness (scaled on its most probable value, $\delta$) |
| $J_s$ | trans-membrane solute flow |
| $J_v$ | trans-membrane volume flux |
| $Pe$ | Péclet number |
| $R$ | solute intrinsic rejection |
| $x$ | coordinate across the unstirred layer |

*Greek letters*

| | |
|---|---|
| $\alpha$ | ratio of actual local unstirred-layer thickness to the most probable one |
| $\alpha_{eff}$ | effective value of parameter α |
| $\alpha_{ha}$ | harmonic average of parameter α |
| $\alpha_m$ | arithmetic average of parameter α |
| $\delta$ | most probable thickness of unstirred layer |
| $\delta\alpha$ | deviation of parameter α |
| $\xi$ | coordinate normalized by the local unstirred layer thickness |
| $\sigma$ | width parameter |

## References

[1] S. Bhattacharjee, J.C. Chen, M. Elimelech, Coupled model of concentration polarization and pore transport in crossflow nanofiltration, AIChE J. 47 (2001) 2733–2745, http://dx.doi.org/10.1002/aic.690471213.
[2] S. Bouranene, P. Fievet, A. Szymczyk, M. El-Hadi Samar, A. Vidonne, Influence of operating conditions on the rejection of cobalt and lead ions in aqueous solutions by

a nanofiltration polyamide membrane, J. Memb. Sci. 325 (2008) 150–157, http://dx.doi.org/10.1016/j.memsci.2008.07.018.
[3] W.R. Bowen, B. Cassey, P. Jones, D.L. Oatley, Modelling the performance of membrane nanofiltration – application to an industrially relevant separation, J. Memb. Sci. 242 (2004) 211–220, http://dx.doi.org/10.1016/j.memsci.2004.04.028.
[4] V. Geraldes, M.D. Afonso, Prediction of the concentration polarization in the nanofiltration/reverse osmosis of dilute multi-ionic solutions, J. Memb. Sci. 300 (2007) 20–27, http://dx.doi.org/10.1016/j.memsci.2007.04.025.
[5] T.Y. Qiu, P.A. Davies, Concentration polarization model of spiral-wound membrane modules with application to batch-mode RO desalination of brackish water, Desalination 368 (2015) 36–47, http://dx.doi.org/10.1016/j.desal.2014.12.048.
[6] V. Geraldes, V. Semião, M.N. de Pinho, Flow management in nanofiltration spiral wound modules with ladder-type spacers, J. Memb. Sci. 203 (2002) 87–102, http://dx.doi.org/10.1016/S0376-7388(01)00753-0.
[7] V. Geraldes, V. Semião, M.N. de Pinho, The effect of the ladder-type spacers configuration in NF spiral-wound modules on the concentration boundary layers disruption, Desalination 146 (2002) 187–194, http://dx.doi.org/10.1016/S0011-9164(02)00467-8.
[8] V. Geraldes, V. Semiao, M. Norberta de Pinho, Concentration polarisation and flow structure within nanofiltration spiral-wound modules with ladder-type spacers, Comput. Struct. 82 (2004) 1561–1568, http://dx.doi.org/10.1016/j.compstruc.2004.03.052.
[9] L. Song, S. Ma, Numerical studies of the impact of spacer geometry on concentration polarization in spiral wound membrane modules, Ind. Eng. Chem. Res. 44 (2005) 7638–7645, http://dx.doi.org/10.1021/ie048795w.
[10] M. Amokrane, D. Sadaoui, M. Dudeck, C.P. Koutsou, New spacer designs for the performance improvement of the zigzag spacer configuration in spiral-wound membrane modules, Desalin. Water Treat. 3994 (2015) 1–9, http://dx.doi.org/10.1080/19443994.2015.1022003.
[11] M. Paipuri, S.H. Kim, O. Hassan, N. Hilal, K. Morgan, Numerical modelling of concentration polarisation and cake formation in membrane filtration processes, Desalination 365 (2015) 151–159, http://dx.doi.org/10.1016/j.desal.2015.02.022.
[12] J. Schwinge, D.E. Wiley, D.F. Fletcher, Simulation of the flow around spacer filaments between channel walls. 2. Mass-transfer enhancement, Ind. Eng. Chem. Res. 41 (2002) 4879–4888 ⟨http://www.scopus.com/inward/record.url?eid=2-s2.0-0037130790&partnerID=tZOtx3y1⟩.
[13] T. Ishigami, H. Matsuyama, Numerical modeling of concentration polarization in spacer-filled channel with permeation across reverse osmosis membrane, Ind. Eng. Chem. Res. 54 (2015) 1665–1674, http://dx.doi.org/10.1021/ie5039665.
[14] M. Amokrane, D. Sadaoui, C.P. Koutsou, A.J. Karabelas, M. Dudeck, A study of flow field and concentration polarization evolution in membrane channels with two-dimensional spacers during water desalination, J. Memb. Sci. 477 (2015) 139–150, http://dx.doi.org/10.1016/j.memsci.2014.11.029.
[15] S. Bason, V. Freger, Phenomenological analysis of transport of mono- and divalent ions in nanofiltration, J. Memb. Sci. 360 (2010) 389–396, http://dx.doi.org/10.1016/j.memsci.2010.05.037.
[16] V. Geraldes, M.D. Afonso, Generalized mass-transfer correction factor for nanofiltration and reverse osmosis, AIChE J. 52 (2006) 3353–3362, http://dx.doi.org/10.1002/aic.10968.
[17] J.L.C. Santos, V. Geraldes, S. Velizarov, J.G. Crespo, Investigation of flow patterns and mass transfer in membrane module channels filled with flow-aligned spacers using computational fluid dynamics (CFD), J. Memb. Sci. 305 (2007) 103–117, http://dx.doi.org/10.1016/j.memsci.2007.07.036.
[18] C.P. Koutsou, S.G. Yiantsios, a J. Karabelas, A numerical and experimental study of mass transfer in spacer-filled channels: effects of spacer geometrical characteristics and Schmidt number, J. Memb. Sci. 326 (2009) 234–251, http://dx.doi.org/10.1016/j.memsci.2008.10.007.
[19] J.M. Miranda, J.B.L.M. Campos, Mass transfer in the vicinity of a separation membrane – the applicability of the stagnant film theory, J. Memb. Sci. 202 (2002) 137–150, http://dx.doi.org/10.1016/S0376-7388(01)00747-5.
[20] V. Geraldes, V. Semião, M. Norberta Pinho, Hydrodynamics and concentration polarization in NF/RO spiral-wound modules with ladder-type spacers, Desalination 157 (2003) 395–402, http://dx.doi.org/10.1016/S0011-9164(03)00422-3.
[21] C.P. Koutsou, A.J. Karabelas, Shear stresses and mass transfer at the base of a stirred filtration cell and corresponding conditions in narrow channels with spacers, J. Memb. Sci. 399–400 (2012) 60–72, http://dx.doi.org/10.1016/j.memsci.2012.01.029.
[22] E. Lyster, Y. Cohen, Numerical study of concentration polarization in a rectangular reverse osmosis membrane channel: permeate flux variation and hydrodynamic end effects, J. Memb. Sci. 303 (2007) 140–153, http://dx.doi.org/10.1016/j.memsci.2007.07.003.
[23] J.L.C. Santos, J.G. Crespo, V. Geraldes, OpenFOAM simulation of mass transfer in spacer-filled channels, Eur. Conf. Comput. Fluid Dyn. (2010) 14–17 ⟨http://web.univ-ubs.fr/limatb/EG2M/Disc_Seminaire/ECCOMAS-CFD2010/papers/01454.pdf⟩.
[24] A. Yaroshchuk, X. Martínez-Lladó, L. Llenas, M. Rovira, J. de Pablo, Solution-diffusion-film model for the description of pressure-driven trans-membrane transfer of electrolyte mixtures: one dominant salt and trace ions, J. Memb. Sci. 368 (2011) 192–201, http://dx.doi.org/10.1016/j.memsci.2010.11.037.
[25] A. J. Karabelas, personal communication, 2015.

# CHAPTER 5

# Publication 2

*"Rotating disk-like membrane cell for pressure-driven measurements with equally-accessible membrane surface: Numerical simulation and experimental validation"*

Journal of Membrane Science 550 (2018) 492–501

Contents lists available at ScienceDirect

Journal of Membrane Science

journal homepage: www.elsevier.com/locate/memsci

# Rotating disk-like membrane cell for pressure-driven measurements with equally-accessible membrane surface: Numerical simulation and experimental validation

Marc Fernández de Labastida[a,b], Edxon E. Licón[c], Mykola Bondarenko[d], Andriy Yaroshchuk[c,e]

[a] Department of Chemical Engineering, Polytechnic University of Catalonia – BarcelonaTech, C/ Eduard Maristany 10-14 (Campus Diagonal-Besòs), 08930, Barcelona, Spain
[b] Barcelona Research Center in Multiscale Science and Engineering, C/ Eduard Maristany, 10-14 (Campus Diagonal-Besòs), 08930, Barcelona, Spain
[c] Department of Chemical Engineering, Polytechnic University of Catalonia – BarcelonaTech, av. Diagonal 647, 08028 Barcelona, Spain
[d] Institute of Bio-Colloid Chemistry, National Academy of Sciences of Ukraine, 42 Vernadskiy av., 03142 Kyiv, Ukraine
[e] ICREA, Passeig Lluís Companys 23, Barcelona, Spain

ARTICLE INFO

*Keywords:*
Concentration polarization
Equally-accessible surface
Unstirred-layer thickness
Rotating disk
Nanofiltration

ABSTRACT

This work presents a new approach to correcting for concentration polarization (CP) in pressure-driven membrane measurements. In the existing test cells (both cross-flow and stirred-batch) there are distributions of extent of CP over membrane surface. This complicates the interpretation of experimental data.

A novel design of test cell with equally-accessible membrane surface has been developed based on the classical configuration of rotating disk combined with the possibility of applying trans-membrane hydrostatic pressure differences of up to 20 bar. Due to the equal accessibility, corrections for CP can easily be made even in multi-ionic systems, which would be much more difficult with other membrane test cells.

Since the membrane has to be sealed at the edge the geometry somewhat deviates from the ideal case of infinite disk. The impact of these deviations has been quantified via CFD simulations. A major part of the membrane surface is shown to be equally accessible while there are some expectable deviations close to the sealed membrane edge. This zone could be "screened" in the experiments. The approach could also be validated experimentally via studying the dependence of observed rejection on the rotation speed and demonstrating that intrinsic rejection was practically independent of it.

Finally, to demonstrate the cell utility, we performed and interpreted a number of experiments using commercial NF270 membrane and various feed solutions (single salts and electrolyte mixtures). We conclude that this cell can be employed for systematic transport characterization of membranes and the obtained information can be used as input in the CFD modelling of membrane modules.

## 1. Introduction

In test cells for pressure-driven membrane processes (both cross-flow and batch [1]) there is some distribution of extent of concentration polarization (CP) over membrane surface. A number of CFD studies have demonstrated this inhomogeneity of CP, which is especially pronounced in test cells with spacer-filled feed channels [2–7], and revealed up to one order of magnitude variation in the local mass-transfer coefficient depending on the position along the membrane surface [6,8–10]. However, this fact has been usually ignored and average values of mass transfer coefficient were reported [3–6,9–12].

A previous theoretical study [13] illustrated the implications of inhomogeneous CP distribution for the interpretation of membrane-transport measurements. It was demonstrated that disregarding the CP distribution can under-estimate the CP of strongly positively-rejected solutes and over-estimate the CP for negatively-rejected ones, leading to a several-times difference in the effective unstirred-layer thicknesses estimated for such solutes by using standard Nernst model. Therefore, the CP inhomogeneity makes difficult obtaining accurate information on the membrane transport properties from experimental data especially in the case of multi-ion solutions. Given the complexity of mechanisms of nanofiltration (NF) [14,15], this makes highly desirable decoupling of internal and external mass-transfer problems because coupled models involve too many adjustable parameters and uncertainties. Such a decoupling can easily be performed provided that the extent of CP is the same over the whole membrane surface. In this study, we achieve this experimentally in a novel test cell using rotating disk-like membrane (RDM).

Feron et at [16] developed a test cell for the characterization of high flux flat sheet gas separation membranes with uniform mass-transfer and constant permeate concentration over the whole membrane surface. Other publications also investigated experimental systems using

http://dx.doi.org/10.1016/j.memsci.2017.10.057
Received 3 July 2017; Received in revised form 26 October 2017; Accepted 27 October 2017
Available online 28 October 2017
0376-7388/ 

**Nomenclature**

| | |
|---|---|
| $c_i$ | ionic concentration |
| | bulk concentration |
| $c_m$ | surface membrane concentration |
| $c_{ip}$ | ionic permeate concentration |
| $D$ | diffusion coefficient of the salt |
| $D_i$ | ionic diffusion coefficient |
| $F$ | Faraday constant |
| J | solute flux |
| $J_V$ | trans-membrane flux |
| $k$ | mass-transfer coefficient |
| $p$ | hydrostatic pressure |
| $N$ | rotation speed (rpm) |
| $Pe_i$ | ionic Péclet number |
| $Pe_s$ | Péclet number of the salt |
| $R$ | ideal gas constant |
| $R_s^{(obs)}$ | observed rejection of the salt |
| $R_s^{(int)}$ | intrinsic rejection of the salt |
| $T$ | temperature |
| $u$ | radial component of the fluid velocity |
| $\vec{u}$ | velocity vector |
| $v$ | angular component of the fluid velocity |
| $V$ | velocity magnitude |
| $w$ | axial component of the fluid velocity |
| $x$ | coordinate across the unstirred layer |
| $Z_i$ | charge of ion |

*Greek letters*

| | |
|---|---|
| $\delta$ | thickness of concentration polarization layer |
| $\xi$ | coordinate normalized by the local unstirred layer thickness |
| $\mu$ | dynamic viscosity |
| $\nu$ | kinematic viscosity |
| $\rho$ | density |
| $\varphi$ | electrostatic potential |
| $\omega$ | angular velocity |

rotating elements, in particular, rotating disk-like bodies with membranes fixed to them [17–27]. However, the principal purpose of those studies was the enhancement of shear rate at the membrane surface in view of applications with high-viscosity fluids. The geometry of these systems was quite different from infinite rotating disk and didn´t give rise to homogeneous distribution of CP. At the same time, the hydrodynamic and convection-diffusion equations for the system of interest have been extensively studied in electrochemistry in the context of rotating disk electrodes [28–30]. Those are experimental systems of choice for a quantitative control of mass-transfer limitations in the studies of electrode kinetics.

Besides, a previous study employed electrochemical techniques to characterize shear stress and mass transfer coefficient at the membrane surface in a high-pressure stirred filtration cell [1]. The authors observed a considerable variation of local values of shear stress at relatively low rotation speeds, with its time-averaged standard deviation decreasing with increasing Reynolds number. As for the mass-transfer coefficient, the radial distribution is qualitatively similar but more uniform than that of shear stress, although there is still a variation around 50% in the time averaged Sherwood number. Thus, the equal accessibility could not be achieved.

This study presents a novel design of membrane test cell with

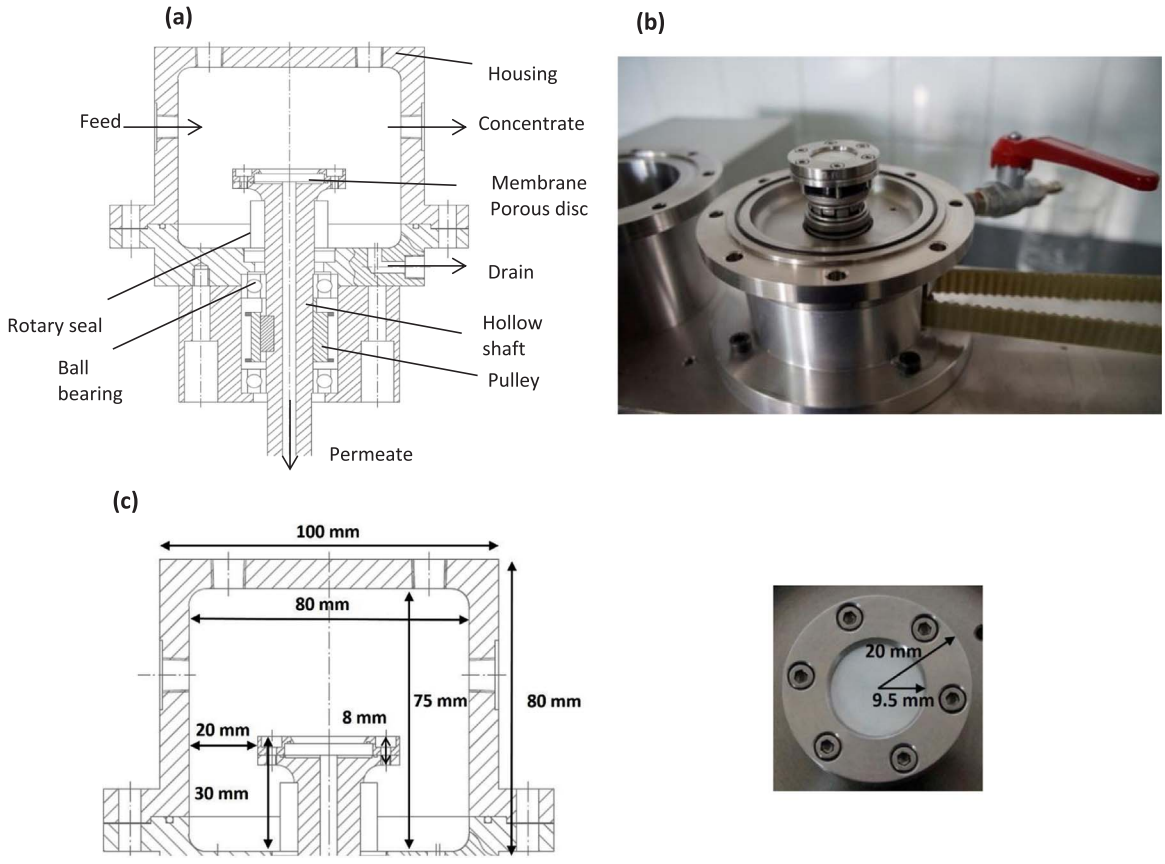


**Fig. 1.** (a) Schematic diagram, (b) photo of RDM cell and (c) cell dimensions.

**Table 1**
Concentration experimental design.

| Experiment group | Dominant salt | Trace salt | Feed concentration (mol/L) | |
|---|---|---|---|---|
| | | | Dominant salt | Trace salt |
| Single salts | NaCl | – | 0.01 | – |
| | $MgCl_2$ | – | | |
| | $Na_2SO_4$ | – | | |
| | $MgSO_4$ | – | | |
| Dominant salt + Trace ions | NaCl | $NH_4Cl$ + $NaNO_3$ | 0.01 | $2{\cdot}10^{-4}$ |
| | $MgCl_2$ | | | |
| | $Na_2SO_4$ | | | |
| | $MgSO_4$ | | | |

equally-accessible surface of a flat-sheet membrane. First, we explore this design via numerical computational fluid dynamics (CFD) simulations and conclude that despite some deviations from the ideal geometry a major part of the membrane surface is, indeed, equally accessible. Moreover, the unstirred-layer thickness obtained in the simulations is in good agreement with the well-known Levich formula [31]. The simulations become unstable at higher rotation speeds, so we additionally validate the system experimentally via measurements of dependence of observed rejection of a single salt on the rotation speed. By using Levich formula for the unstirred-layer thickness in the CP-correction procedure we demonstrate that the intrinsic rejection is practically independent of the rotation speed as it should be. Further on, we demonstrate the cell utility via CP-correcting of a number of experimental data obtained with a commercial NF membrane and several single-salt and mixed-electrolyte solutions.

We expect this new experimental setup to be useful for obtaining systematic information on the intrinsic rejections of various solutes by NF membranes.

## 2. Experimental materials and methods

### 2.1. Materials

Experimental data have been obtained with polyamide thin-film composite NF membrane NF-270 supplied by Dow Chemical Company (EE.UU). Membranes were mechanically supported by porous discs of 25 mm in diameter made from sintered stainless steel (average pore size 40 μm) kindly provided by GKN Sintered Metals (Germany). The chemical reagents used to prepare feed aqueous solutions in the experiments were of analysis grade.

### 2.2. Experimental set-up

The RDM test cell has been developed in-house. The experimental set-up consists in the membrane test cell (Fig. 1) with a motor and a variable frequency drive to control the RDM rotation speed up to 1000 rpm. Digital tachometer was used to measure the rotation speed of the membrane. Feed solution was refrigerated in a tank (10 L) to keep the temperature constant along the experiments around 20 °C ± 1 °C. Feed solution is pumped into the membrane test cell by a volumetric diaphragm pump (Hydracell G-21, EE.UU) and the trans-membrane pressure is adjusted through a needle valve. A high-pressure rotary seal allows operating the cell up to 20 bar. The set-up runs in a continuous mode with constant feed composition at a circulation rate of 1.5 L/min. The set-up also includes a pre-filter cartridge (100 μm, thermofischer) and housing made in stainless-steel suitable to withstand high pressures (Thermofischer scientific). The flat disk membrane has a diameter of 25 mm and a narrow external plastic ring is placed at the edge of the membrane to exclude membrane filtration in this zone, thus the exposed membrane diameter is 19 mm (see below about the "screening" of the peripheral membrane part).

### 2.3. Operation procedure

A new membrane was used for each experiment in order to have the same initial conditions in all the cases. The membranes were soaked in ultrapure water overnight. As a first step before any experiment, the membrane was compacted with deionized water at pressure of 15 bar during approximately 1 h in order to reach a steady state and prevent any changes of the membrane hydraulic resistance during the measurements. The pure water flux was measured to calculate water permeability and once it became steady, the compaction was finished. Thereafter, the same compaction procedure was used with the feed solutions used in the experiments. Experiments were performed at a constant pump flow rate of 1.5 L/min and the trans-membrane pressure was increased from 2 to 14 bar. Permeate samples were collected at each trans-membrane pressure after some stabilization time, which was checked by measuring the permeate conductivity. Feed samples were taken at the beginning and after finishing the experiment to make sure that feed composition was constant over the experiment.

### 2.4. Analytical techniques

The conductivity was measured by a conductivity meter (GLP31, Crison) to have a rough estimate of ion rejection. Afterwards, the samples were analyzed by ionic chromatography (DIONEX ICS-1000 / ICS-1100) using two different columns, IONPAC® CS16 and IONPAC® AS23 (Dionex), to analyze cations and anions respectively.

### 2.5. Experimental design

First, it was studied the rotation speed effect on the unstirred layer thickness and ion rejection in the particular case of 10 mM $MgCl_2$. After that, some filtration experiments were carried out and corrected for the CP in the case of 1) single salt and 2) electrolyte mixture consisting on a dominant salt plus trace ions. Table 1 shows the feed concentration of salts in each experiment. Experimental measurements were repeated to check reproducibility.

## 3. Theory

### 3.1. Modelling assumptions

In the simulations, we considered an incompressible fluid with constant physical characteristics being those of pure water (density $\rho$ = 1000 kg/m$^3$, dynamic viscosity $\mu$ = 0.001 Pa·s, kinematic viscosity $\nu$ = $10^{-6}$ m$^2$/s). In dilute solutions used in the experiments, deviations from these values are very limited.

The hydrodynamic and mass-transfer problems in the cell were solved assuming stationary and 2D-axisymmetric conditions, which is the simplest way to describe the basic transport features in systems with axisymmetric rotating bodies.

Despite the presence of liquid flows from the cell inlet towards its outlet (creating a kind of cross flow in the cell) they are disregarded in order to keep the model relatively simple. The main purpose of the simulations is figuring out approximately to what an extent the deviations from the ideal geometry can compromise the equal accessibility of the membrane surface. Therefore, the simulations were focused on the effect of membrane sealing on the unstirred-layer thickness distribution. Besides, the inflow velocity was kept constant in all the experiments and was typically lower than the linear velocity due to the rotation.

On the rotating body, the normal velocity component is set to zero while the tangential velocity corresponds to the angular component (sliding wall condition). At the stationary internal surface of the reservoir the radial component of the velocity is zero due to symmetry on the rotation axis (no slip condition). A constant normal solute flux at the membrane surface is set.

### 3.2. Governing equations in hydrodynamics

The flow is described by Navier-Stokes and volume conservation equations assuming the fluid to be incompressible:

$$\rho\frac{\partial \vec{u}}{\partial t}+\rho(\vec{u}\cdot\nabla)\vec{u} = \mu\nabla^2\vec{u}-\nabla p\nabla\cdot\vec{u} = 0 \quad (1)$$

Here, $\vec{u}$ denotes the velocity vector (m/s), ρ is the density (1000 kg/m$^3$), μ is the dynamic viscosity (0.001 Pa·s), and p is the hydrostatic pressure (Pa). For stationary conditions and in cylindrical coordinates (2D axisymmetric) such system is reduced to this [32]:

$$\rho\left(u\frac{\partial u}{\partial r} - \frac{v^2}{r}+w\frac{\partial u}{\partial z}\right) + \frac{\partial p}{\partial r} = \mu\left[\frac{1}{r}\frac{\partial}{\partial r}\left(r\frac{\partial u}{\partial r}\right) - \frac{u}{r^2} + \frac{\partial^2 u}{\partial z^2}\right]$$
$$\rho\left(u\frac{\partial v}{\partial r} - \frac{uv}{r}+w\frac{\partial v}{\partial z}\right) = \mu\left[\frac{1}{r}\frac{\partial}{\partial r}\left(r\frac{\partial v}{\partial r}\right) - \frac{v}{r^2} + \frac{\partial^2 v}{\partial z^2}\right]$$
$$\rho\left(u\frac{\partial w}{\partial r}+w\frac{\partial w}{\partial z}\right) + \frac{\partial p}{\partial z} = \mu\left[\frac{1}{r}\frac{\partial}{\partial r}\left(r\frac{\partial w}{\partial r}\right) + \frac{\partial^2 w}{\partial z^2}\right] \quad (2)$$

where u, v, w are the radial, angular and axial components of the fluid velocity.

Fig. 2 shows the cell structure and how the boundary conditions were defined. On the rotating body, the sliding-wall boundary condition was used, defining the velocity component normal to the surface as zero, and the angular component equal to the product of angular speed (2π*frequency), ω (1/s), times the radius (blue and red lines):

$$v = r\omega \quad (3)$$

No-slip condition was used at the stationary internal surface of the reservoir. Due to the symmetry on the rotation axis the radial component is zero:

$$u(r, z)\,|_{r=0} = 0 \quad (4)$$

### 3.3. Governing equations in mass transport

Stationary convection-diffusion equation was solved in the domain in order to simulate the mass transport boundary layer:

$$\vec{\nabla}\cdot(-D\vec{\nabla}c) + \vec{u}\cdot\vec{\nabla}c = 0 \quad (5)$$

The boundary conditions were zero normal flux at almost all the boundaries

$$\vec{n}\cdot\vec{J} = 0 \quad (6)$$

where

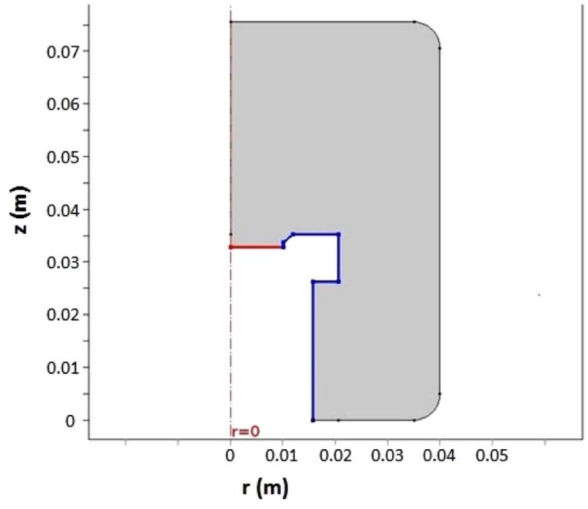


**Fig. 2.** Scheme of the computational domain (gray area).

$$\vec{J} = -D\vec{\nabla}c + \vec{u}\cdot c \quad (7)$$

except at the membrane surface (red line of Fig. 2) where we set a constant normal solute flux:

$$\vec{n}\cdot\vec{J} = \text{const} \quad (8)$$

It was shown that at relatively weak CP this is equivalent to the explicit consideration of solvent permeation through the membrane and solute rejection [33]. In agreement with the experimental procedure, within a narrow circular band (1 mm) at the external membrane edge the solute flux was declared equal to zero (to reduce the effect of perturbation of equal accessibility due to this zone with the largest deviations from the ideal geometry).

Assuming that the flux occurs due to diffusion through a layer with linear concentration profile, it can be written as:

$$J = -\frac{D}{\delta}\cdot(c_b - c_m) \quad (9)$$

Surface concentration at the membrane, $c_m$, bulk concentration, , and diffusion coefficient are known, so the unstirred-layer thickness can be directly obtained:

$$\delta = \frac{D}{J}\cdot(c_m - c_b) \quad (10)$$

### 3.4. Numerical methods

Hydrodynamics and mass transfer equations were solved using COMSOL version 5.0.1.276.

Hydrodynamic flow was simulated by means of Laminar Flow (spf) module (from the Single-Phase Flow section in Fluid Flow), selecting incompressible flow option in the physical model section. Besides, the mode of vortex flow (Swirl flow) was activated, which allows taking into account the azimuthal velocity component. The boundary conditions were set as the axial symmetry with respect to the cylinder axis and no slip on the stationary cell walls. On the surface of rotating block, the velocity field was set this way:

$$v_r = 0$$
$$v_\varphi = r\bullet\omega$$
$$v_z = 0$$

Then, the "Transport of Diluted Species" (chds) module from the "Chemical Species Transport" section was used to describe the solute transport. For simplicity, we considered the transfer of a one-component solution, a non-electrolyte, so only diffusion and convective transfer were taken into account. As for the boundary conditions in this case, on the cell axis the axial symmetry was set while on the membrane a constant flux $\vec{J}$ was set by using the condition "Flux". On the rest of the rotating assembly, the absence of solute flow was set by using the condition "No Flux". On the reservoir surface, a constant solute concentration, $c_0$, was set. Thus, we disregarded concentration changes far away from the membrane, but could solve the problem as stationary.

The problem was solved in two steps: first the hydrodynamic problem was solved, and second, the transfer of solute in the flow field obtained in the first step was modelled. In both steps an automatically constructed triangular grid mesh was used with the following parameters:

Maximum element size: $10^{-4}$ m
Minimum element size: $10^{-5}$ m
Maximum element growth rate: 1.05
Resolution curvature: 0.2
Resolution of narrow regions: 1

Taking into account that at higher rotation speeds the diffusion layer becomes quite thin, within a 1-mm thick layer immediately above the membrane (both active and passive parts) by using the "Free

Triangular" option, the element size is reduced by a factor of 2 along the radial axis (r), and by 4 times along axis z.

This mesh gave rise to visually smooth curves, and the results little changed with further reduction in the size of the element.

### 3.5. Rejection correction for CP

For infinite rotating disk, the thickness of the CP layer can be estimated by using Levich equation [31]:

$$\delta \approx 1.61 \cdot \left(\frac{D}{\nu}\right)^{1/3} \cdot \sqrt{\frac{\nu}{2\pi \cdot \left(\frac{N}{60}\right)}} \text{ (m)} \tag{11}$$

where

$\nu$: kinematic viscosity ($m^2/s$)
$D$: solute diffusion coefficient ($m^2/s$)
$N$: rotation speed (rpm)

Having defined the effective unstirred-layer thickness, further we adopt the so-called Nernst model, which postulates that within this layer one can consider only convection, diffusion and electromigration normal to the membrane surface while the solution composition is set at the external boundary of unstirred layer. The applicability of this approach in the case of rotating disk electrodes has been confirmed by numerous electrochemical studies [28–30].

Within the scope of Nernst model, the observed rejection obtained from the experiment is transformed to the intrinsic rejection by using this equation (in the case of single salts and non-electrolytes):

$$R_s^{(int)} = \frac{R_s^{(obs)} \cdot \exp(Pe_s)}{1 + R_s^{(obs)} \cdot (\exp(Pe_s) - 1)} \tag{12}$$

where

$$Pe_s \equiv \frac{J_V \delta}{D} \tag{13}$$

### 3.6. Concentration polarization in multi-ion solutions

First, we define the extended Nernst-Planck equation for the unstirred layer

$$c_{ip} J_v = -D_i \bullet \left(\frac{dc_i}{dx} + \frac{F}{RT} \bullet Z_i c_i \bullet \frac{d\varphi}{dx}\right) + c_i J_v \tag{14}$$

Scaling the coordinate $x$ on the unstirred-layer thickness, $\delta$, and dividing both sides by the ion diffusion coefficient, Eq. (14) can be rewritten as:

$$\frac{dc_i}{d\xi} + Z_i c_i \bullet \frac{d\widetilde{\varphi}}{d\xi} = (c_i - c_{ip}) \bullet Pe_i \tag{15}$$

where

$$Pe_i \equiv \frac{J_v \delta}{D_i} \tag{16}$$

$$\widetilde{\varphi} \equiv \frac{F\varphi}{RT} \tag{17}$$

Multiplying Eq. (15) by ionic charges, $Z_i$, and summing up over all the ions, the first term vanishes due to the solution electroneutrality and we obtain

$$\frac{d\widetilde{\varphi}}{d\xi} = \frac{\sum_j^n Z_j \bullet (c_j - c_{jp}) \bullet Pe_j}{\sum_j^n Z_j^2 c_j} \tag{18}$$

By substituting Eq. (18) to Eq. (15) we obtain a system of first-order ordinary differential equations resolved with respect to the derivatives

$$\frac{dc_i}{d\xi} = (c_i - c_{ip}) \bullet Pe_i - Z_i c_i \bullet \frac{\sum_j^n Z_j \bullet (c_j - c_{jp}) \bullet Pe_j}{\sum_j^n Z_j^2 c_j} \tag{19}$$

The permeate concentrations, $c_{ip}$, are known from experiment. If the thickness of unstirred layer, $\delta$, is assumed to be known, all the ionic Péclet numbers, $Pe_i$, are also know (since the trans-membrane volume flow is known from experiment and the ionic diffusion coefficients are known from the literature). Therefore, Eq. (19) can be easily solved numerically to yield the concentrations of all the ions at the membrane surface, $c_{im}$, which allows calculating the intrinsic rejection as:

$$R_s^{(int)} = 1 - \frac{C_{ip}}{C_{im}} \tag{20}$$

This approach automatically account for the coupling between the ion flows within the unstirred layers via spontaneously-arising electric fields.

It should be stressed that due to the equal accessibility of membrane surface, the permeate concentrations are the same over the whole (exposed, see below) membrane area. In other test cells, this is not the case and the permeate composition is a result of mixing of permeates having different compositions depending on the local extent of CP.

## 4. Results and discussion

### 4.1. Simulation of flow and CP

The principal feature of infinite rotating disk configuration is the same thickness of unstirred layer over the whole disk surface. In our experimental setup we could not fully implement this geometry. In the numerical simulations, we used a geometry that closely resembles that of the test cell at least, as far as the vicinity of membrane surface is concerned. The principal deviation from the infinite disk is the existence of a peripheral ring that is used to seal the membrane.

Fig. 3 shows a color map of the absolute value of fluid velocity as well as flow direction and magnitude (axial and radial, arrows) at angular velocity of 7 rad/s.

Fig. 4 shows the radial distribution of effective thickness of unstirred layer obtained from the radial distribution of solute concentration (solute diffusion coefficient equal to $10^{-9}$ $m^2/s$) at the membrane

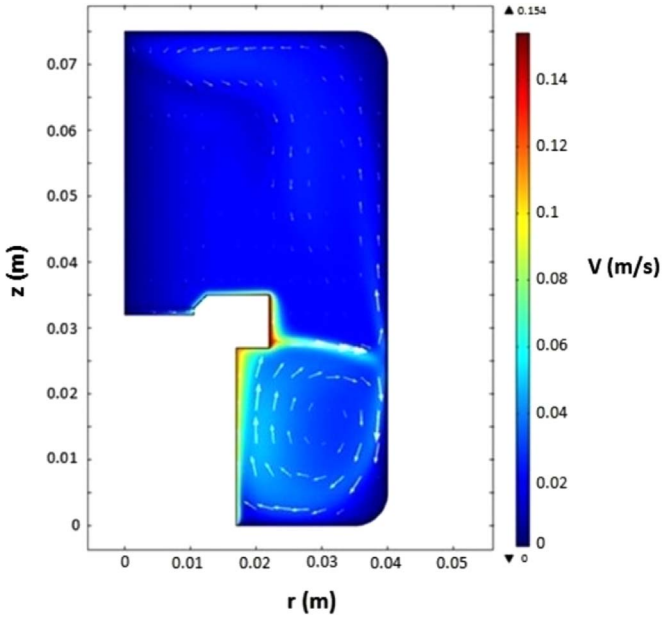


**Fig. 3.** Absolute value of fluid velocity (color) and velocity field (arrows). (For interpretation of the references to color in this figure legend, the reader is referred to the web version of this article.).

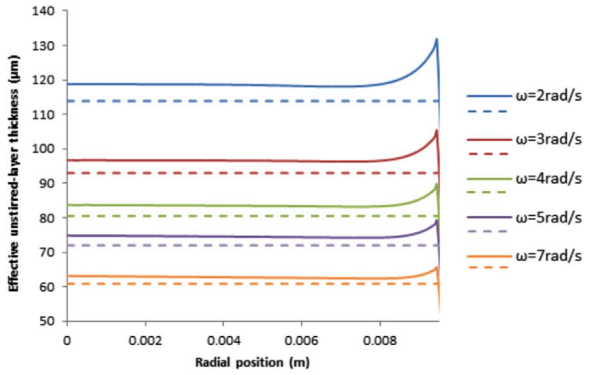


**Fig. 4.** Effective thickness of unstirred layer: numerics (solid lines) and prediction by Levich formula (dashed lines).

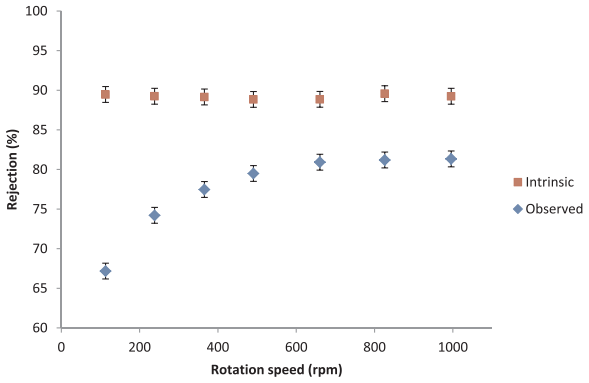


**Fig. 5.** Observed and intrinsic rejection of 0.01 M $MgCl_2$ vs. rotation speed.

surface by using Eq. (10).

The effective thickness remains practically constant up to the vicinity of the sealing ring where it increases. The latter could be expected because here the geometry and flow pattern deviate considerably from the ideal case. However, as discussed above, this part of the membrane could be "screened" in the experiments. Notably, there are some systematic deviations between the numerical results and the theoretical predictions (even in the zones where the effective thickness is practically constant). However, they are around or below 3–4% and may be related to different definitions of effective unstirred-layer thickness used in this study and the theoretical analysis by Levich.

At higher rotation speeds, the simulations became unstable. We speculate that this was occurring primarily in the parts of the test cell located far away from the membrane surface and did not affect directly the equal accessibility. Indeed, from Fig. 3 one can see that largest velocity gradients occur close to the external periphery of the rotating part while close to the (central part of) membrane they remain limited. To validate the purposeful test-cell operation at higher rotation speeds, we carried out an experimental study of rejection as a function of rotation speed.

### 4.2. Rejection dependence on rotation speed

Fig. 5 shows the dependence of observed rejection of 0.01 M $MgCl_2$ on the rotation speed at a fixed trans-membrane pressure of 14 bar. The rotation speed was initially set to the maximum (1000 rpm) and decreased progressively. For each rotation speed, we measured the trans-membrane volume flux and permeate conductivity. The thickness of unstirred layer was estimated by using Levich equation (Eq. (11)). The observed rejection was calculated from the permeate conductivity and intrinsic rejection was calculated by using Eq. (12).

Expectedly, the observed rejection increased with the rotation speed because at lower rotation speeds the CP is stronger since the unstirred layer thickness is larger. However, applying the correction for the CP (to estimate the intrinsic rejection) we find that the latter is practically constant (89.2 ± 0.3%).

**Table 2**
Unstirred-layer thickness at 1000 rpm, salt diffusion coefficients and mass transfer coefficients.

| Salt | δ (μm) | $D \cdot 10^{-9}$ ($m^2/s$) | $k \cdot 10^{-5}$ (m/s) |
|---|---|---|---|
| NaCl | 18.57 | 1.62 | 8.72 |
| $MgCl_2$ | 17.03 | 1.25 | 7.34 |
| $Na_2SO_4$ | 16.94 | 1.23 | 7.26 |
| $MgSO_4$ | 14.98 | 0.85 | 5.67 |

### 4.3. Rejection of single salts

This section explores the dependence of salt rejection on the trans-membrane volume flux for several salts at the maximum rotation speed (1000 rpm) kept constant in all the experiments. As seen in the previous section, the maximum rotation speed gives rise to a minimum unstirred layer thickness, so working at such rotation speed allows for a maximum reduction in the CP layer besides having it homogeneously distributed. Table 2 gives the thickness of unstirred layer at the rotation speed of 1000 rpm calculated with Eq. (11) for the salts employed in our experiments. Considering that the ratio of thickness to diffusion coefficient determines the extent of CP, it is clear that the effect of CP on the rejection is strongest for $MgSO_4$ due to the low diffusion coefficient compared with the other salts. On the contrary, CP is weakest for NaCl since its diffusion coefficient is two times larger. For $MgCl_2$ and $Na_2SO_4$ the values of thickness and diffusion coefficient are quite close, so CP affects in a similar way these two salts and this effect is intermediate between $MgSO_4$ and NaCl. Table 2 also shows the mass-transfer coefficient calculated as the ratio of diffusion coefficient to the unstirred-layer thickness. According to Levich formula the effect of diffusion coefficient on the thickness is relatively weak (cubic root) so that some reduction in the thickness at smaller diffusion coefficients is largely overcompensated by the decrease in the diffusion coefficient itself.

Fig. 6 presents the rejection results in terms of reciprocal transmission, *f*, defined as

$$f = \frac{1}{1-R} \tag{21}$$

When the rejection is zero, the reciprocal transmission is 1. If the rejection is 1, the reciprocal transmission tends to infinity. Reciprocal transmission is a useful way of presenting results when the rejections are very high (for example, in the case of $Na_2SO_4$ where the rejection varies from 99.17% to 99.72%). In this situation the rejection dependence on the trans-membrane flux is practically not visible on the graphs, whereas for the reciprocal transmission it is very clear. In this work the trans-membrane flux will be expressed on (μm/s) units for convenience, since the results will be compared with other works where the fluxes were calculated in those units. Note here that the equivalence to ($L/m^2 \cdot h$) is: 1 μm/s = 3.6 $L/m^2 \cdot h$.

The results obtained in this work are comparable to previous studies performed with another test cell but using the same membrane and salts (feed concentration of 0.1 mol/L) at comparable trans-membrane volume fluxes [34]. Pages et al. observed intrinsic rejection of 60% for NaCl whereas this work obtained 75% (corresponding to f = 4.4). In the case of $MgCl_2$, the intrinsic rejection in the present work was 93% (f = 14), rather close to the value reported by Pages et al. around 95%. Finally, for $Na_2SO_4$ and $MgSO_4$ the intrinsic rejections were above 99% for both salt (f = 580 and f = 200 respectively) which is the same as obtained by Pages et al.

Expectedly, the effect of CP on the rejection is more pronounced at higher trans-membrane volume flows. At the largest flows the CP

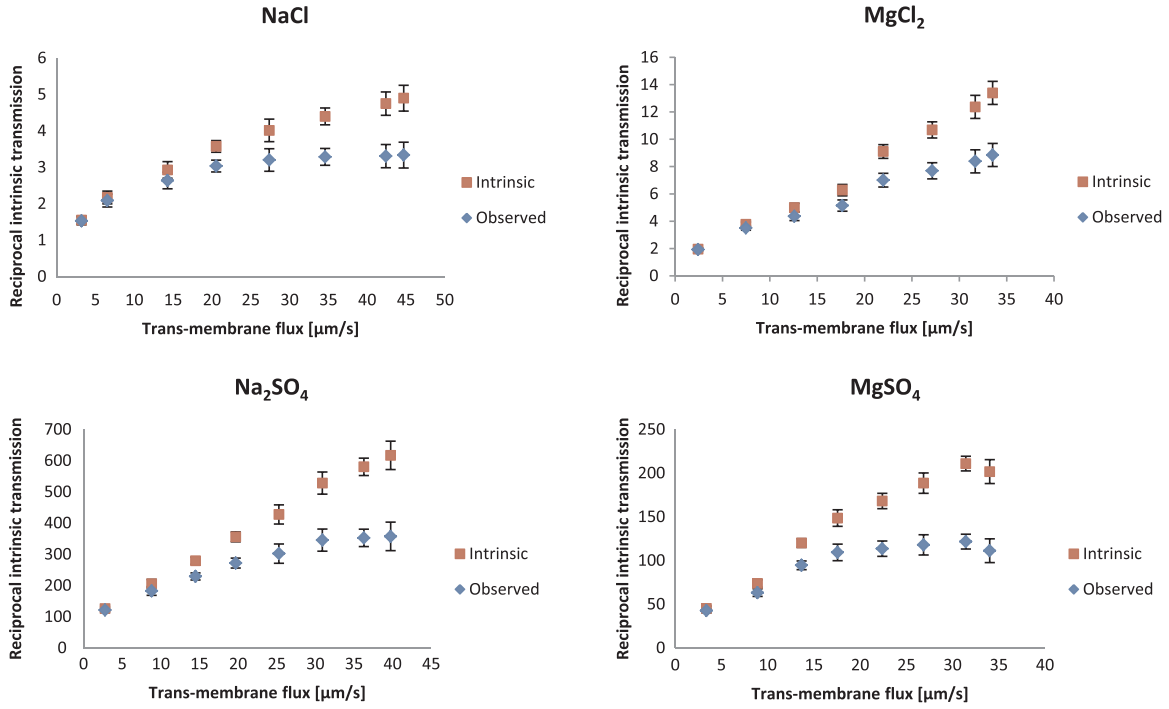


**Fig. 6.** Reciprocal transmission as a function of trans-membrane flux for several single salts.

correction (in terms of reciprocal transmission) is as large as about 2 times for the better rejected solutes ($Na_2SO_4$, $MgSO_4$) and about 50% for the moderately rejected salts (NaCl, $MgCl_2$).

### 4.4. Rejection of ions from electrolyte mixtures

In this section, the CP-correction procedure will be applied to multi-ion solutions. Each experiment used one dominant salt (NaCl, $MgCl_2$, $Na_2SO_4$ or $MgSO_4$) and trace salts ($NaNO_3$ and/or $NH_4Cl$).

Fig. 7 shows the reciprocal transmissions of NaCl (dominant salt) and $NH_4^+$ and $NO_3^-$ (traces). The intrinsic rejections were between 40% and 80% for $Na^+$, $Cl^-$ and $NH_4^+$ (f = 1.7–5.0) whereas $NO_3^-$ exhibited slightly negative rejections at low trans-membrane volume fluxes (−10% at 10 µm/s, corresponding to the reciprocal transmission of 0.91) while they turned positive (up to 50% (f = 2)) when the trans-membrane flux increased.

Reig et al. [35] studied the rejection of trace $NH_4^+$ and $NO_3^-$ from dominant-NaCl solutions depending on their feed concentration. Increasing NaCl concentration decreased its rejection as well as the rejections of the traces. The results of this study are in agreement with [35] taking into account that the feed concentration of the dominant salt was still lower than the minimum one studied in that paper (0.05 M). In [35] the observed rejection of dominant NaCl and $NH_4^+$ trace ranged from 15% to 70% while in the present work it was between 40% and 80% (f = 1.67–5), which is slightly higher probably due to the lower feed concentration. As for $NO_3^-$, Reig et al. reported observable rejections between 6% and 41% while in the present work observable rejections were from −13% to 31% (f = 0.88–1.37).

Negative rejections result from trans-membrane electric fields arising due to differences in the membrane permeabilities to cations and anions of dominant salt. These fields enhance or reduce the transport of ions through the membrane depending on the sign of their charge. In this case, $Na^+$ permeance is higher than $Cl^-$ so the arising electric field accelerates anions (like $NO_3^-$) and decelerates cations to keep electric current equal to zero. Negative rejections correspond to reciprocal transmissions smaller than one.

Initially the electromigration of $NO_3^-$ increases more rapidly than the trans-membrane volume flux and the rejection become more negative until it reaches a minimum (not observed in this study) and trans-membrane flux starts to increase more rapidly than the electromigration flux of $NO_3^-$ so the rejection becomes positive.

Similarly to the case of single salts, at low trans-membrane volume fluxes the difference between observed and intrinsic reciprocal transmissions is small since the CP is weak.

The next case study used $MgCl_2$ as the dominant salt and $Na^+$, $NH_4^+$ and $NO_3^-$ as the trace ions. Here an opposite situation is observed (Fig. 8). The membrane permeance to the divalent cation is lower than to the monovalent anion [36], so the trans-membrane electric field enhances the transport of cations. Consequently, traces of $Na^+$ and $NH_4^+$ are negatively rejected. In the case of $Na^+$ the intrinsic rejections were between −24% and −100% (f = 0.80-0.49) while for $NH_4^+$ they ranged from −30% to −175% (f = 0.77-0.36). In contrast, $NO_3^-$ rejections were positive, between 37–85% (f = 1.59–6.49), which is expectable given that the electric field retards the passage of this ion through the membrane.

Fig. 8 shows that there are pronounced negative rejections of $Na^+$ and $NH_4^+$ that decrease monotonically for all the trans-membrane fluxes measured. Besides, the CP-corrections for $Na^+$ and $NH_4^+$ are quite large. Due to the lower electrochemical mobility of $Mg^{2+}$ than $Cl^-$ in the unstirred layer, the electromigration flux has opposite directions within the membrane and unstirred layer which leads to considerable depletion of cations at the membrane surface. This is illustrated in Fig. 9 by the concentration profiles within the unstirred layer at each trans-membrane flux. The unstirred layer thickness is normalized so the value of 0 corresponds to the bulk solution (feed concentration) and the value of 1 to the membrane surface. Fig. 9 makes clear the difference between the feed concentration and the concentration at the membrane surface where the concentration is reduced by as much as a factor of 2 at the highest trans-membrane flux for both ions. Due to this, the magnitude of observed negative rejections turns out about two times smaller than that of intrinsic ones. Interestingly, the observed negative rejections pass through shallow minima and start becoming less negative while the intrinsic ones keep getting ever more negative within the studied range of trans membrane volume fluxes.

Another case study used dominant salts with a divalent anion ($Na_2SO_4$ and $MgSO_4$). In both cases the membrane permeance to $SO_4^{2-}$

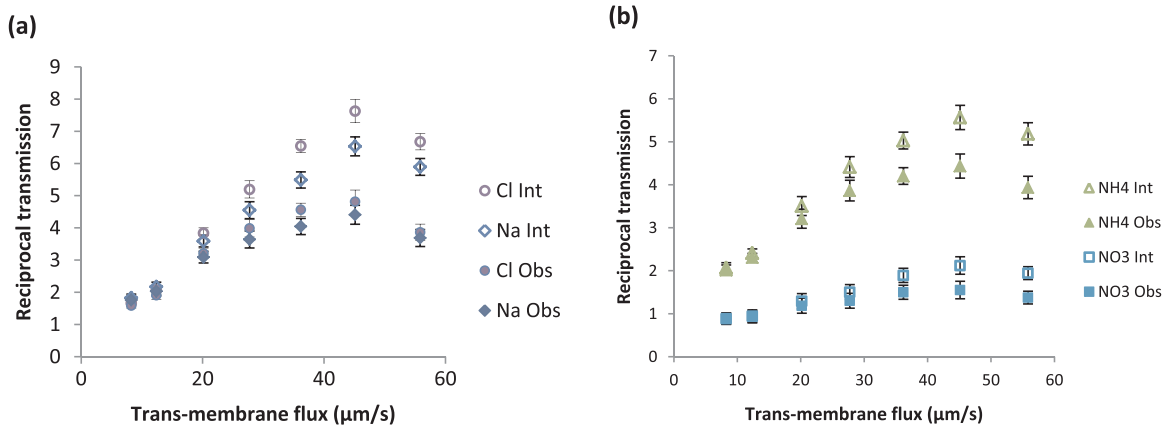


**Fig. 7.** Reciprocal transmission as a function of trans-membrane volume flux for: (a) dominant salt NaCl and (b) trace ions $NH_4^+$ and $NO_3^-$.

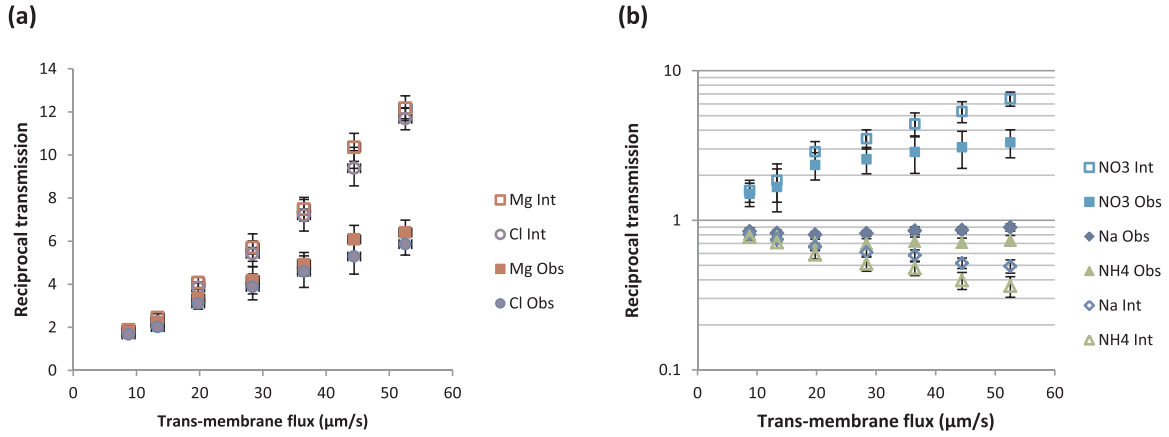


**Fig. 8.** Reciprocal transmission as a function of trans-membrane flux for: (a) dominant salt $MgCl_2$ and (b) trace ions $Na^+$, $NH_4^+$ and $NO_3^-$.

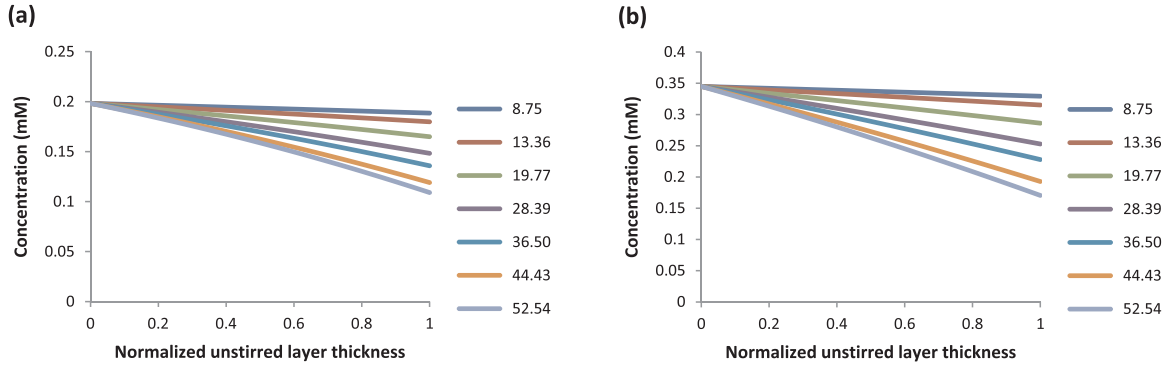


**Fig. 9.** Concentration profiles within the boundary layer for (a) $Na^+$ and (b) $NH_4^+$. Legend gives the trans-membrane flux (µm/s) for each profile.

is much lower than the permeance to the cation regardless of whether it is $Na^+$ or $Mg^{2+}$ [36]. Therefore, the transport of anions through the membrane is enhanced by the spontaneously-arising electric fields. Fig. 10 shows the reciprocal transmission for the dominant salt $Na_2SO_4$ and traces of $NH_4^+$, $Cl^-$ and $NO_3^-$. The dominant salt is highly rejected: $SO_4^{2-}$ rejections are above 99.7% (f = 356–812) and those of $Na^+$ are between 96% and 99% (f = 28–172).[1] $NH_4^+$ trace is quite well rejected, its intrinsic rejections were between 95.7% and 98.8% (f = 23–86). As for the trace anions, $NO_3^-$ was initially negatively rejected −131% (f = 0.43) and increased up to 63% (f = 2.76) whereas $Cl^-$ is positively rejected between 21% and 85% (f = 1.27–6.95).

In this case, the effect of CP on the negative rejections is somewhat weaker than in the previous case study (using $MgCl_2$ as the dominant salt). Although in the dominant salt the electrochemical mobility of cation ($Na^+$) is lower than that of anion ($SO_4^{2-}$) similarly to the previous case, here the negative rejections are experienced by anions (because the membrane permeability to $SO_4^{2-}$ is much lower than that to $Na^+$). Within the unstirred layer, their transport towards the membrane surface is enhanced by the spontaneously-arising electric fields (and not reduced as in the previous case). This makes the CP for anionic traces somewhat weaker.

Similar results were obtained using $MgSO_4$ as the dominant salt and

[1] Due to the very high rejection of $SO_4^{2-}$ the $Cl^-$ and $NO_3^-$ ions could not really be considered as genuine traces in this case. Accordingly, the reciprocal transmission of $Na^+$ could be essentially lower than that of $SO_4^{2-}$ because the trans-membrane passage of $Cl^-$ and $NO_3^-$ ions (especially enhanced in the case of $NO_3^-$ in agreement with its negative rejections) ensured zero electric current.

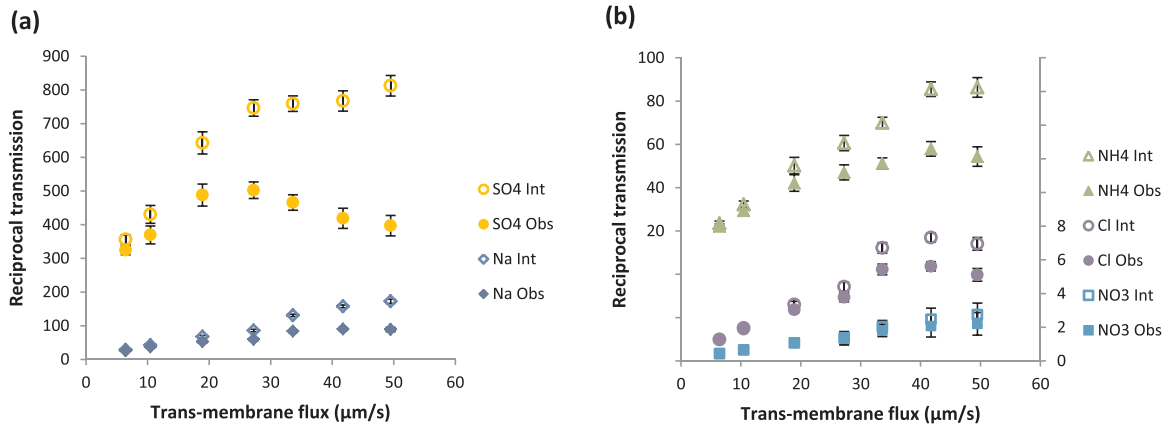


**Fig. 10.** Reciprocal transmission as a function of trans-membrane flux for: (a) dominant salt $Na_2SO_4$ and (b) trace ions $NH_4^+$, $Cl^-$ and $NO_3^-$.

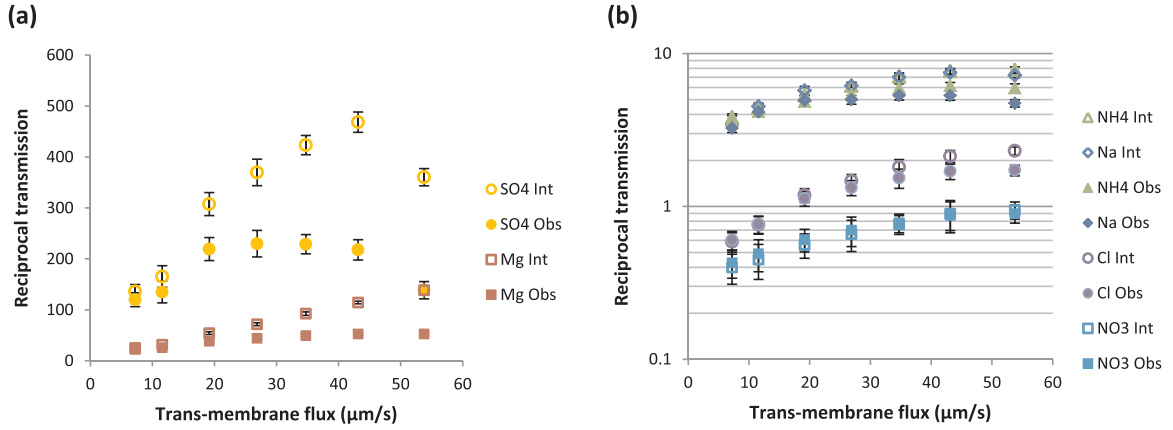


**Fig. 11.** Reciprocal transmission as a function of trans-membrane flux for: (a) dominant salt $MgSO_4$ and (b) trace ions $Na^+$ $NH_4^+$, $Cl^-$ and $NO_3^-$.

$Na^+$, $NH_4^+$, $Cl^-$ and $NO_3^-$ as the trace ions, as can be seen in Fig. 11. The dominant salt is highly rejected and $NH_4^+$ trace is well rejected, too: $Mg^{2+}$ rejection is between 96% and 99% (f = 25–138) and that of $SO_4^{2-}$ is above 99% (f = 136–360).[2] As for $NH_4^+$ and $Na^+$, they were also well rejected (74–87% or f = 3.8–7.8). In the case of the traces of anions, $Cl^-$ was negatively rejected, from −70% to 60% (f = 0.59–2.31), whereas $NO_3^-$ exhibited more pronounced negative rejections that did not turn to positive in the whole studied range of trans-membrane fluxes, between −151% and −5% (f = 0.40–0.95). These results are comparable to those presented by Pagès et al. [36], where one observed rejections around 96% for the dominant salt and 80% in the case of $NH_4^+$ and $Na^+$, whereas for $NO_3^-$ the rejections were between −50% and 40%.

## 5. Conclusions

In the membrane test cells reported previously there is inhomogeneous distribution of CP over the membrane surface. This makes difficult a quantitative decoupling of trans-membrane transfer from the external CP. Therefore, in membrane-testing devices it is desirable to reduce this inhomogeneity to a minimum to make possible quantitative interpretation of experimental data in terms of membrane properties.

A novel RDM design with equally-accessible membrane surface has been developed. Numerical simulations as well as experimental results demonstrate that the condition of having the same extent of CP over the whole membrane surface is satisfied in this set-up. Experiments using single salt and electrolyte mixtures have been performed in the new test cell and corrected for CP by using Levich equation (widely-used in electrochemistry) for the effective thickness of unstirred layer. The results obtained are semi-quantitatively similar to those obtained with the same NF membrane and feed solutions in other pressure-driven studies with a test cell GE SEPA™ CF II.

This novel membrane cell can be used for a systematic characterization of transport properties of NF/RO membranes. The obtained information can be used as input in the modelling of performance of practical membrane modules.

[2] Similarly to the previous case, the zero-current condition is fulfilled due to the negative rejections of “trace” anions.

## Acknowledgements

The authors gratefully acknowledge support from the project "Valorization of by-product from industrial effluents: integration of membrane technologies in the separation, concentration and purification steps" (Waste2Product, CTM2014-57302-R) funded by the Ministry of Science and Innovation (MINECO, Spain) and the Catalan government (project ref.2014SGR050).

## References

[1] C.P. Koutsou, A.J. Karabelas, Shear stresses and mass transfer at the base of a stirred filtration cell and corresponding conditions in narrow channels with spacers, J. Membr. Sci. 399–400 (2012) 60–72, http://dx.doi.org/10.1016/j.memsci.2012.01.029.

[2] V. Geraldes, V. Semião, M.N. de Pinho, Flow management in nanofiltration spiral wound modules with ladder-type spacers, J. Membr. Sci. 203 (2002) 87–102, http://dx.doi.org/10.1016/S0376-7388(01)00753-0.

[3] V. Geraldes, V. Semião, M.N. de Pinho, The effect of the ladder-type spacers configuration in NF spiral-wound modules on the concentration boundary layers disruption, Desalination 146 (2002) 187–194, http://dx.doi.org/10.1016/S0011-

9164(02)00467-8.
[4] V. Geraldes, V. Semiao, M. Norberta de Pinho, Concentration polarisation and flow structure within nanofiltration spiral-wound modules with ladder-type spacers, Comput. Struct. 82 (2004) 1561–1568, http://dx.doi.org/10.1016/j.compstruc.2004.03.052.
[5] L. Song, S. Ma, Numerical studies of the impact of spacer geometry on concentration polarization in spiral wound membrane modules, Ind. Eng. Chem. Res. 44 (2005) 7638–7645, http://dx.doi.org/10.1021/ie048795w.
[6] M. Amokrane, D. Sadaoui, M. Dudeck, C.P. Koutsou, New spacer designs for the performance improvement of the zigzag spacer configuration in spiral-wound membrane modules, Desalin. Water Treat. 3994 (2015) 1–9, http://dx.doi.org/10.1080/19443994.2015.1022003.
[7] M. Paipuri, S.H. Kim, O. Hassan, N. Hilal, K. Morgan, Numerical modelling of concentration polarisation and cake formation in membrane filtration processes, Desalination 365 (2015) 151–159, http://dx.doi.org/10.1016/j.desal.2015.02.022.
[8] J. Schwinge, D.E. Wiley, D.F. Fletcher, Simulation of the flow around spacer filaments between channel walls. 2. Mass-transfer enhancement, Ind. Eng. Chem. Res. 41 (2002) 4879–4888 〈http://www.scopus.com/inward/record.url?eid=2-s2.0-0037130790&partnerID=tZOtx3y1〉.
[9] T. Ishigami, H. Matsuyama, Numerical modeling of concentration polarization in spacer-filled channel with permeation across reverse osmosis membrane, Ind. Eng. Chem. Res. 54 (2015) 1665–1674, http://dx.doi.org/10.1021/ie5039665.
[10] M. Amokrane, D. Sadaoui, C.P. Koutsou, A.J. Karabelas, M. Dudeck, A study of flow field and concentration polarization evolution in membrane channels with two-dimensional spacers during water desalination, J. Membr. Sci. 477 (2015) 139–150, http://dx.doi.org/10.1016/j.memsci.2014.11.029.
[11] V. Geraldes, V. Semião, M. Norberta Pinho, Hydrodynamics and concentration polarization in NF/RO spiral-wound modules with ladder-type spacers, Desalination 157 (2003) 395–402, http://dx.doi.org/10.1016/S0011-9164(03)00422-3.
[12] J.M. Miranda, J.B.L.M. Campos, Mass transfer in the vicinity of a separation membrane - The applicability of the stagnant film theory, J. Membr. Sci. 202 (2002) 137–150, http://dx.doi.org/10.1016/S0376-7388(01)00747-5.
[13] M. Fernández de Labastida, E.E. Licon Bernal, A. Yaroshchuk, Implications of inhomogeneous distribution of concentration polarization for interpretation of pressure-driven membrane measurements, J. Membr. Sci. 520 (2016) 693–698, http://dx.doi.org/10.1016/j.memsci.2016.08.040.
[14] A.W. Mohammad, Y.H. Teow, W.L. Ang, Y.T. Chung, D.L. Oatley-Radcliffe, N. Hilal, Nanofiltration membranes review: recent advances and future prospects, Desalination 356 (2015) 226–254, http://dx.doi.org/10.1016/j.desal.2014.10.043.
[15] N. Hilal, N.A. Darwish, A.W. Mohammad, M.A. Arabi, A comprehensive review of nanofiltration membranes : treatment, pretreatment, modelling, and atomic force microscopy, Desalination 170 (2004) 281–308, http://dx.doi.org/10.1016/j.desal.2004.01.007.
[16] P. Feron, J.W. Van Heuven, J.J. Akkerhuis, R. Van Der Welle, Design and development of a membrane testcell with uniform mass transfer : application to characterisation of high flux gas separation membranes, J. Membr. Sci. 80 (1993) 157–164.
[17] M.Y. Jaffrin, Dynamic shear-enhanced membrane filtration : a review of rotating disks, rotating membranes and vibrating systems, J. Membr. Sci. 324 (2008) 7–25, http://dx.doi.org/10.1016/j.memsci.2008.06.050.
[18] R. Bouzerar, M.Y. Jaffrin, L. Ding, P. Paullier, Influence of geometry and angular velocity on performance of a rotating disk filter, AIChE J. 46 (2000) 257–265.
[19] R. Bouzerar, L. Ding, M.Y. Jaffrin, Local permeate flux – shear – pressure relationships in a rotating disk microfiltration module : implications for global performance, J. Membr. Sci. 170 (2000) 127–141.
[20] C. Torras, J. Pallares, R. Garcia-valls, M.Y. Jaffrin, Numerical simulation of the flow in a rotating disk filtration module, Desalination 235 (2009) 122–138, http://dx.doi.org/10.1016/j.desal.2008.02.006.
[21] A. Brou, L. Ding, P. Boulnois, M.Y. Jaffrin, Dynamic microfiltration of yeast suspensions using rotating disks equipped with vanes, J. Membr. Sci. 197 (2002) 269–282.
[22] M.Y. Jaffrin, L. Ding, O. Akoum, A. Brou, A hydrodynamic comparison between rotating disk and vibratory dynamic filtration systems, J. Membr. Sci. 242 (2004) 155–167, http://dx.doi.org/10.1016/j.memsci.2003.07.029.
[23] M. Frappart, O. Akoum, L.H. Ding, M.Y. Jaffrin, Treatment of dairy process waters modelled by diluted milk using dynamic nanofiltration with a rotating disk module, J. Membr. Sci. 282 (2006) 465–472, http://dx.doi.org/10.1016/j.memsci.2006.06.005.
[24] M. Frappart, M. Jaffrin, L.H. Ding, Reverse osmosis of diluted skim milk : comparison of results obtained from vibratory and rotating disk modules, Sep. Purif. Technol. 60 (2008) 321–329, http://dx.doi.org/10.1016/j.seppur.2007.09.007.
[25] R. Bouzerar, P. Paullier, M.Y. Jaffrin, Concentration of mineral suspensions and industrial effluents using a rotating disk dynamic filtration module, Desalination 158 (2003) 79–85.
[26] J. Luo, L. Ding, Y. Wan, P. Paullier, M.Y. Jaffrin, Application of NF-RDM (nanofiltration rotating disk membrane) module under extreme hydraulic conditions for the treatment of dairy wastewater, Chem. Eng. J. 163 (2010) 307–316, http://dx.doi.org/10.1016/j.cej.2010.08.007.
[27] J. Luo, L. Ding, Y. Wan, M.Y. Jaffrin, Flux decline control in nanofiltration of detergent wastewater by a shear-enhanced filtration system, Chem. Eng. J. 181–182 (2012) 397–406, http://dx.doi.org/10.1016/j.cej.2011.11.101.
[28] A.J. Bard, L.R. Faulkner, E. Swain, C. Robey, Electrochemical methods: fundamentals and Applications, n.d.
[29] M.T. Crespo, A review of electrodeposition methods for the preparation of alpha-radiation sources, Appl. Radiat. Isot. 70 (2012) 210–215, http://dx.doi.org/10.1016/j.apradiso.2011.09.010.
[30] S. Treimer, A. Tanga, D.C. Johnson, Consideration of the application of Koutecky-Levich plots in the diagnoses of charge-transfer mechanisms at rotated disk electrodes, Electroanalysis 14 (2002) 165–171.
[31] V.G. Levich, R.J. Seeger, Physicochemical Hydrodynamics, Am. J. Phys. 31 (1963), http://dx.doi.org/10.1119/1.1969158.
[32] P.M. Gresho, R.L. Sani, M.S. Engelman, Incompressible Flow and the Finite Element Method, Wiley, 2000.
[33] V. Geraldes, M.D. Afonso, Generalized mass-transfer correction factor for nanofiltration and reverse osmosis, AIChE J. 52 (2006) 3353–3362, http://dx.doi.org/10.1002/aic.10968.
[34] N. Pages, A. Yaroshchuk, O. Gibert, J. Luis, Rejection of trace ionic solutes in nano filtration : influence of aqueous phase composition, Chem. Eng. J. 104 (2013) 1107–1115, http://dx.doi.org/10.1016/j.ces.2013.09.042.
[35] M. Reig, E. Licon, O. Gibert, A. Yaroshchuk, J. Luis, Rejection of ammonium and nitrate from sodium chloride solutions by nanofiltration : effect of dominant-salt concentration on the trace-ion rejection, Chem. Eng. J. 303 (2016) 401–408, http://dx.doi.org/10.1016/j.cej.2016.06.025.
[36] N. Pagès, M. Reig, O. Gibert, J.L. Cortina, Trace ions rejection tunning in NF by selecting solution composition: ion permeances estimation, Chem. Eng. J. 308 (2017) 126–134, http://dx.doi.org/10.1016/j.cej.2016.09.037.

# CHAPTER 6

# Publication 3

*"Influence of membrane sealing in pressure-driven test cells on their performance"*

Journal of Membrane Science and Research 5 (2019) 240-243

Journal of Membrane Science & Research

journal homepage: www.msrjournal.com

Short Communication

# Influence of Membrane Sealing in Pressure-Driven Test Cells on Their Performance

Marc Fernández de Labastida [1,*], Andriy Yaroshchuk [2]

[1] *Department of Chemical Engineering and Barcelona Research Center in Multiscale Science and Engineering, Polytechnic University of Catalonia – BarcelonaTech, C/ Eduard Maristany 10-14 (Campus Diagonal-Besòs), 08930, Barcelona, Spain*
[2] *Department of Chemical Engineering, Polytechnic University of Catalonia – BarcelonaTech, av. Diagonal 647, 08028 Barcelona, Spain and ICREA, Passeig Lluís Companys 23, Barcelona, Spain*

## Article info

Received 2018-07-17
Revised 2018-10-19
Accepted 2018-10-20
Available online 2018-10-20

## Keywords

Concentration polarization
Cell design
Mass-transfer
Sealing
Pressure-driven

## Graphical abstract

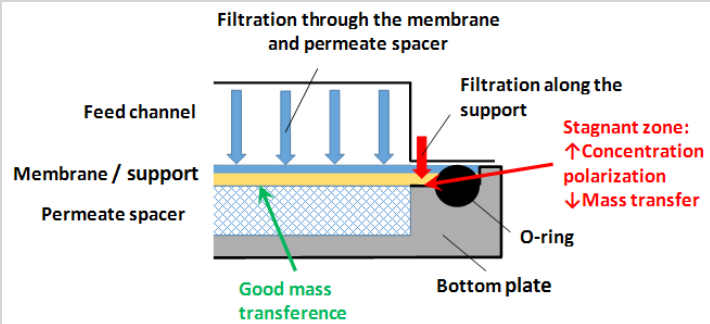


## Highlights

- Membrane sealing is a relevant factor as it may influence on test cell performance
- A peripheral part of the membrane is supported on the cell body due to sealing
- The effect of impermeable surface supporting a membrane was studied experimentally
- Membrane sealing create zones where mass-transfer conditions can be much worse
- Trans-membrane flux obtained are slightly affected by the membrane blocking

## Abstract

This communication demonstrates the relevance of membrane sealing in a test cell to its performance. Membranes need to be sealed, and therefore a more or less significant (depending on the test cell design) peripheral part of the membrane is supported directly by the cell body (instead of a permeate spacer). Although it may seem that there should be no filtration through the membrane when it is supported by an impermeable surface, this communication demonstrates that this is not generally true due to filtration along the membrane porous support. To confirm this, experiments were performed with a cross-flow test cell (GE SEPA™ CF II), blocking the membrane hydraulically from beneath in order to simulate the effect of having the membrane supported by an impermeable surface. The results show that the trans-membrane volume flux obtained in all cases is only slightly affected by the membrane blocking. In view of this, in the cell design, care should be taken to reduce such peripheral parts of the membrane to a minimum because it may be technically very difficult to have there the same conditions of concentration polarization as over the membrane part supported by the permeate spacer.



### 1. Introduction

Membrane characterization is important for the design of membrane processes since their performance and optimization depends on reliable information on the membrane properties.

In membrane modules, the membrane transport properties manifest themselves against the background of complicated flow-distribution and external-mass-transfer phenomena. Therefore, these properties (such as solute rejection and volume flux) are often studied in dedicated test cells, where attempts are made to reduce those complications to a minimum. Membrane test cells for pressure-driven measurements have various configurations [1–5]. However, irrespective of the details, in all cases the membrane must be sealed. Figure 1 shows the typical schematics of membrane sealing. The membrane is mechanically supported by a permeate spacer (or another porous material), but a strip at the membrane periphery is always put on an impermeable part of the test-cell body (red line in Figure 1b). This is due to the need to seal the membrane with an O-ring, which can be achieved only if it presses against a solid surface. Figure 1c also shows that mechanical fixation of the O-ring in a groove makes unavoidable the existence of a zone where the membrane's active surface is exposed to the feed solution but the hydrodynamic conditions are totally different from those in the principal feed channel. Moreover, the flow characteristics in this problematic zone may well be poorly reproducible because the height of the gap can be strongly dependent on the details of the test-cell assembly.

At first glance, it may appear that none of this matters because the membrane is supported by an impermeable surface, so there should be no filtration. The principal finding of this communication is that, actually, this is not generally true and there may be trans-membrane filtration within this zone due to lateral flows along the membrane support layers. Moreover, we will demonstrate experimentally that even for quite broad membrane strips of this kind the trans-membrane flux can be practically the same as for the part of the membrane supported by a permeate spacer. Understanding this is important for optimization of the design of membrane test cells.

* Corresponding author at: Phone: (+34) 934016997
E-mail address: marc.fdez.labastida@upc.edu (M. Fernández de Labastida)

DOI: 10.22079/JMSR.2018.90181.1204

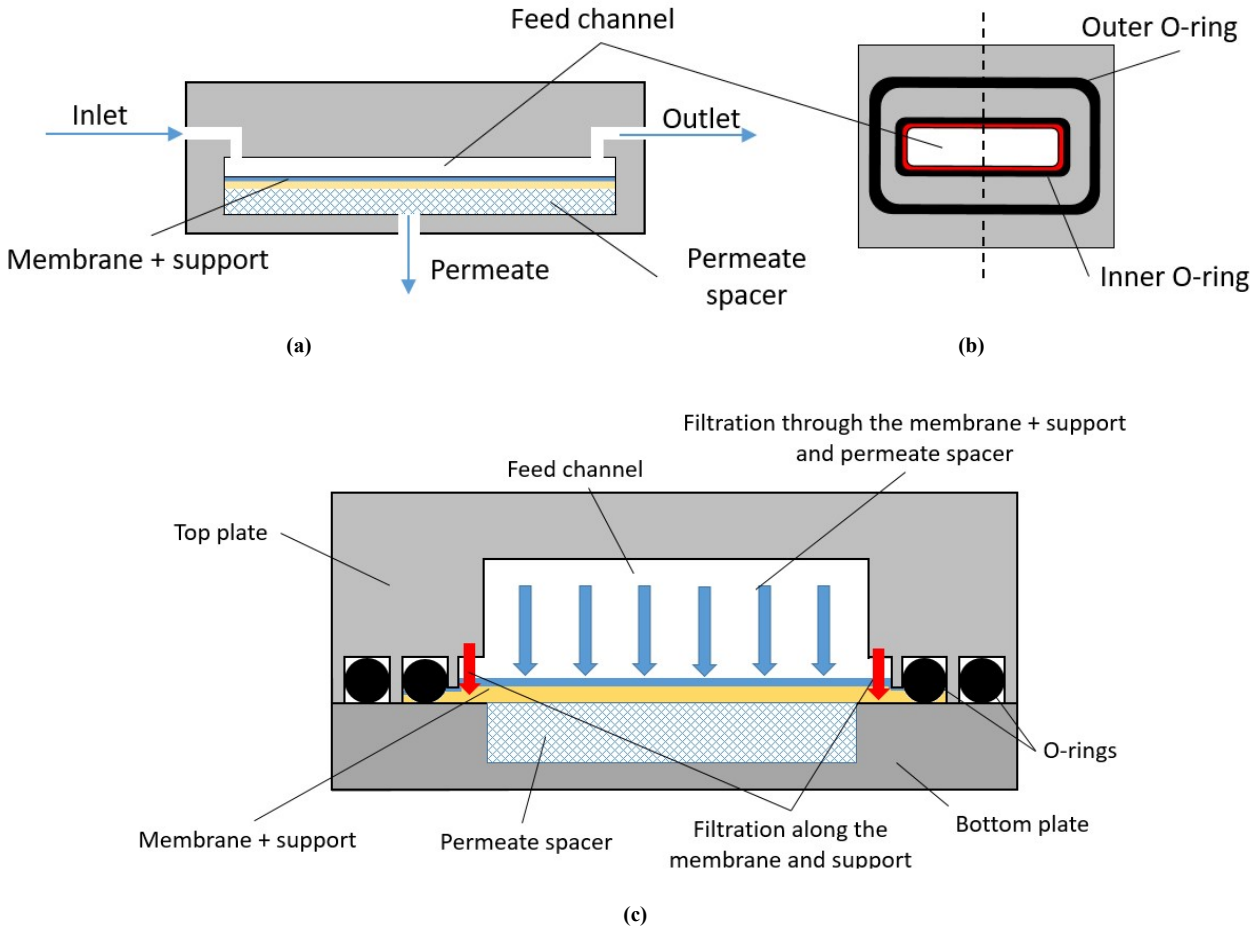


**Fig. 1.** Schematic diagram (not drawn to scale) of membrane sealing in a cell: a) process flow diagram; b) raised view of top plate of the cell; and c) cross-section of the cell. The dotted line in (b) indicates the cross section shown in (c).

## 2. Experimental

### *2.1. Materials*

All the experiments were performed with deionized water. Experimental data were obtained with polyamide thin-film composite NF membranes NF-270 and NF-90 supplied by Dow Chemical Company (USA). Table 1 shows the specifications of both membranes.

**Table 1**
Membrane specifications and operating limits.

| Parameter | NF270 / NF90 |
|---|---|
| Membrane type | Polyamide thin-film composite |
| Maximum operating temperature | 45 °C |
| Maximum operating pressure | 41 bar |
| Maximum feed flow rate | 1.4 $m^3/h$ |
| Maximum pressure drop | 1.0 bar |
| pH range, continuous operation | 2–11 |
| pH range, short-term cleaning (30 min) | 1–12 |
| Maximum feed silt density index | SDI 5 |
| Free chlorine tolerance | < 0.1 ppm |

### *2.2. Experimental set-up*

A flat-sheet cross-flow test cell (GE SEPA™ CF II) with an effective area of 0.014 $m^2$ was used to perform the experiments. The experimental set-up was described previously [6]. Feed solution was refrigerated in a tank (30 L) to keep the temperature constant at around 20 ± 1 °C throughout the experiments. The set-up ran in a continuous mode and both the permeate and the concentrate streams were recirculated to the feed tank to keep the composition of the feed solution constant. The set-up also includes a filter cartridge (pore size: 100 µm, Fisher Scientific) in the concentrate stream to avoid the presence of particles in the feed tank. The inlet and outlet pressures of the membrane test cell as well as the concentrate flow rate were monitored throughout the experiments. From the inlet and outlet pressure values, the average trans-membrane pressure (TMP) inside the membrane test cell was determined.

### *2.3. Operation procedure*

A new membrane was used for each experiment to guarantee the same initial conditions in all cases. Moreover, before starting each experiment, deionized water was pumped into the membrane test cell at 22 bar during 1.5 hours to ensure that the membrane hydraulic resistance remained constant throughout the measurements. Once it had been corroborated that the pure water flux was steady, the experiment started. Experiments were performed at a constant cross-flow rate and the TMP was increased from 2 to 12 bar. Permeate samples were collected at each TMP after the permeate flux reached a constant value.

To simulate the effect of a membrane supported by an impermeable surface, the membrane was blocked from beneath by using a plastic sheet made of low-density polyethylene (Vidrafoc) with an open strip along the

channel, equidistant from the walls (Figure 2). Several plastic sheets were used, leaving open strips of various widths in order to study the correlation between the trans-membrane flow and the unblocked area. Table 2 gives the unblocked surface area versus the strip width.

## 3. Results and discussion

Figure 3 shows the pressure dependences of trans-membrane flux calculated by using the whole membrane area of the test cell. These dependences are largely linear so they can be quantified by the slopes. Remarkably, those slopes are only slightly reduced despite the fact that the unblocked area is 5 to 20 times smaller than the area exposed on the membrane's active side. This shows that the parts of the membrane blocked from beneath by the plastic film are performing filtration almost unimpeded. The filtration along the membrane support layers is effective as long as the pressure drop in the lateral direction remains smaller than the TMP drop. The fact that in our measurements the flux was only slightly affected by the membrane-back blocking indicates that even with the relatively broad blocked strips used in this study the lateral pressure drop remained relatively small. It can be expected to be even smaller in a major part of test cells where such problematic zones usually make up a relatively small portion of the membrane surface. However, we should keep in mind that due to the much worse mass-transfer conditions in such zones, concentration polarization there can be very strong and the solute rejection virtually zero. This can considerably increase the (negative) impact of these zones on the measured rejection.

It can also be observed that in the case of NF90 membrane (Figure 3b), decreasing the uncovered area has a larger impact on the trans-membrane flux. This may be due to a lower lateral hydraulic permeability of the support layer of NF90 membrane as compared to NF270.

**Table 2**
Effective surface and area uncovered by the plastic sheet according to the strip width.

| Strip width (cm) | Unblocked area ($cm^2$) |
|---|---|
| 0.5 | 7 |
| 1 | 14 |
| 2 | 28 |
| No strips | 140 |

**Fig. 2.** Photograph of the plastic sheets used to block the membrane for each strip width: a) 2 cm, b) 1 cm, and c) 0.5 cm.

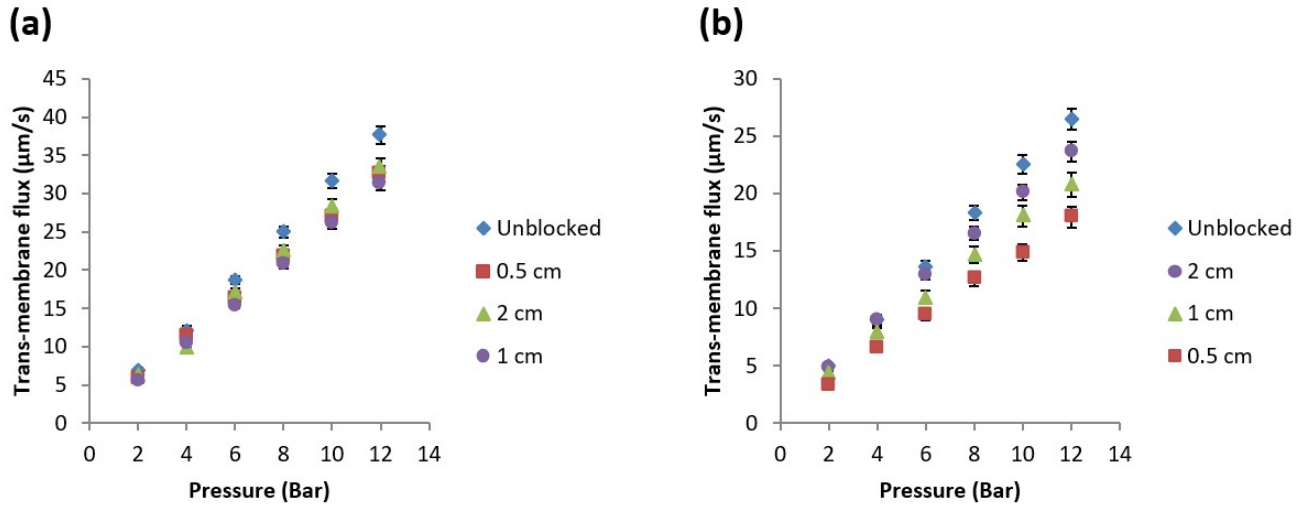


**Fig. 3.** Trans-membrane flux dependence on pressure for the unblocked membrane and the membrane covered by a plastic film for: a) NF270 and b) NF90. The legend gives the strip width.

## 4. Conclusions

Due to membrane-sealing requirements, in membrane test cells, there are always peripheral parts of the membrane supported by impermeable surfaces. This communication demonstrates that (somewhat counterintuitively) there is filtration through such parts of the membrane. This occurs due to the lateral volume transfer along the membrane support layers. Moreover, due to design constraints, it is very difficult to make the mass-transfer conditions over such parts of the membrane as good as in the feed channel. Actually, these conditions can even be expected to be much worse and poorly reproducible. Therefore, concentration polarization in such zones can be very strong, so they can make a disproportionally large contribution to the trans-membrane solute transfer, especially in the case of strongly rejected solutes. This can compromise the performance of test cells for pressure-driven membrane measurements and should be kept in mind while designing them.

## Acknowledgements

The authors gratefully acknowledge support from the project "Valorization of by-product from industrial effluents: integration of membrane technologies in the separation, concentration and purification steps" (Waste2Product, CTM2014-57302-R) funded by the Ministry of Science and Innovation (MINECO, Spain) and the Catalan government (project ref.2014SGR050).

## References

[1] C.F. Wan, T. Yang, G.G. Lipscomb, D.J. Stookey, T. Chung, Design and fabrication of hollow fiber membrane modules, J. Membr. Sci. 538 (2017) 96–107. doi:10.1016/j.memsci.2017.05.047.

[2] D. Attarde, M. Jain, K. Chaudhary, S.K. Gupta, Osmotically driven membrane processes by using a spiral wound module - Modeling , experimentation and numerical parameter estimation, Desalination 361 (2015) 81–94. doi:10.1016/j.desal.2015.01.025.

[3] M. Reig, N. Pagès, E. Licon, C. Valderrama, O. Gibert, A. Yaroshchuk, Evolution of electrolyte mixtures rejection behaviour using nanofiltration membranes under spiral wound and flat-sheet configurations, Desalin. Water Treat. 56 (2015) 3519-3529. doi:10.1080/19443994.2014.974215.

[4] G. Blandin, A.R.D. Verliefde, C.Y. Tang, A.E. Childress, P. Le-Clech, Validation of assisted forward osmosis ( AFO ) process : Impact of hydraulic pressure, J. Membr. Sci. 447 (2013) 1–11. doi:10.1016/j.memsci.2013.06.002.

[5] M.Y. Jaffrin, Dynamic shear-enhanced membrane filtration : A review of rotating disks , rotating membranes and vibrating systems, J. Membr. Sci. 324 (2008) 7–25. doi:10.1016/j.memsci.2008.06.050.

[6] M. Reig, E. Licon, O. Gibert, A. Yaroshchuk, J. L. Cortina, Rejection of ammonium and nitrate from sodium chloride solutions by nanofiltration : Effect of dominant-salt concentration on the trace-ion rejection, Chem. Eng. J. 303 (2016) 401–408. doi:10.1016/j.cej.2016.06.025.

# CHAPTER 7

# Publication 4

*"Transient membrane potential after concentration step: A new method for advanced characterization of ion-exchange membranes"*

Journal of Membrane Science 585 (2019) 271–281

Contents lists available at ScienceDirect

Journal of Membrane Science

journal homepage: www.elsevier.com/locate/memsci

# Transient membrane potential after concentration step: A new method for advanced characterization of ion-exchange membranes

Marc Fernández de Labastida[a,b,*], Andriy Yaroshchuk[c,d]

[a] Department of Chemical Engineering, Polytechnic University of Catalonia – BarcelonaTech, C/ Eduard Maristany 10-14 (Campus Diagonal-Besòs), 08930, Barcelona, Spain
[b] Barcelona Research Center in Multiscale Science and Engineering, C/ Eduard Maristany, 10-14 (Campus Diagonal-Besòs), 08930, Barcelona, Spain
[c] Department of Chemical Engineering, Polytechnic University of Catalonia – BarcelonaTech, av. Diagonal 647, 08028 Barcelona, Spain
[d] ICREA, Passeig Lluís Companys 23, Barcelona, Spain

ARTICLE INFO

*Keywords:*
Ion-exchange membrane
Transient membrane potential
Concentration step
Ion partitioning
Salt diffusion permeability

ABSTRACT

A better understanding of ion-transport mechanisms requires separate information on the equilibrium (partitioning) and kinetic (diffusivity) properties of the membranes with respect to ions. This work presents a novel non-stationary-diffusion method to determine salt diffusion and partitioning coefficients under (quasi)-linear conditions of relatively small concentration differences.

An ion-exchange membrane supported by a relatively thick coarse-porous support (glass frit) is placed in a two-compartment stirred cell. The salt concentration in one compartment is kept stationary during the measurement whereas in the other compartment, the initial solution is rapidly replaced by a solution of different concentration. As a result, there is a time-dependent electrical response due to a progressive redistribution of applied concentration difference between the membrane and the porous support and the different ion perm-selectivities of those media. A mathematical model is developed to interpret the data. The rate of signal relaxation is primarily controlled by the diffusion permeability of the membrane but is also affected by the salt partitioning. In addition, osmotic trans-membrane volume transfer has a significant impact on the relaxation process, so it needs to be taken into account. The osmotic permeability has been determined in separate measurements.

Systematic studies have been carried out at various NaCl concentrations with Nafion 120 and type 10 Fujifilm ion-exchange membranes. The results obtained for Nafion 120 are in agreement with the literature data. Well-established techniques have also been used to validate the novel approach. This allows for a relatively simple determination of salt permeability and partitioning coefficient in addition to the ion perm-selectivity, which is the only parameter available from the conventional measurements of stationary membrane potential.

## 1. Introduction

Ion-exchange membranes are central elements of electro-membrane processes [1–7]. For their optimization, it is important to have detailed information on the transport and equilibrium properties of ion-exchange membranes, in particular, separate information on the equilibrium (partitioning) and kinetic (diffusivity) properties of the membranes with respect to ions. The partition coefficient of an ion refers to its distribution between the membrane and the solution whereas the diffusivity coefficient is related to the ion mobility in the membrane [8].

Stationary techniques of membrane characterization such as membrane potential or DC electrical resistance provide only information on ionic permeabilities, which are products of partitioning and diffusion coefficients [9]. As the steady state permeability involves both properties, by knowing one of them the other can be calculated [10].

Equilibrium salt sorption can be measured via salt desorption using standard methods or advanced techniques such as attenuated total reflection Fourier transform infrared spectroscopy (ATR-FTIR) [11–14], Rutherford backscattering spectrometry (RBS) [15,16] or quartz crystal microbalance (QCM) sensors [17]. On the other hand, diffusivity may be measured using tracer-based techniques such as pulsed-field gradient nuclear magnetic resonance (PFG-NMR) [18,19]. Moreover, electrochemical impedance spectroscopy (EIS) has been used to determine

* Corresponding author. Department of Chemical Engineering, Polytechnic University of Catalonia – BarcelonaTech, C/ Eduard Maristany 10-14 (Campus Diagonal-Besòs), 08930, Barcelona, Spain.
*E-mail address:* marc.fdez.labastida@upc.edu (M. Fernández de Labastida).

https://doi.org/10.1016/j.memsci.2019.05.012
Received 20 November 2018; Received in revised form 27 April 2019; Accepted 4 May 2019
Available online 13 May 2019
0376-7388/ 

**List of symbols**

$a_0$ : activity of base solution
$a_i$ : activity at the interface membrane/porous support
$a_{step}$ : activity of step solution
$A$ : cross-sectional area of the frit
$C_0$ : concentration of base solution
$C_i$ : concentration at the interface membrane/porous support
$C_m$ : concentration at the membrane surface
$C_s$ : concentration in the porous support
$C_{step}$ : concentration of step solution
$c_X$ : fixed-charge concentration
$d_f$ : glass frit diameter of the porous part
$D_s^{(m)}$ : effective salt diffusion coefficient in the membrane without electrostatic correction
$D_m$ : salt diffusion coefficient in the membrane
$D_s$ : salt diffusion coefficient in the porous support
$D_s^{(eff)}$ : effective diffusion coefficient of salt in the frit (accounting for the porosity and tortuosity)
$D_+$ : diffusion coefficient of cation
$D_-$ : diffusion coefficient of anion
$F$ : Faraday constant
$H(\omega)$ : Fourier transform of unit-step function
$J_{salt}$ : salt molar flux
$J_v$ : osmotic flow
K : osmotic permeability
$L_m$ : thickness of the membrane
$L_s$ : thickness of the frit
$Pe$ : Péclet number
r : model parameter defined by Eq. (A3)
R : ideal gas constant
$t$ : time
$t_0$ : characteristic relaxation time defined by Eq. (A2)
$t_+^m$ : transport number of positive ions in the membrane
$t_+^b$ : transport number of positive ions in the frit
$T$ : absolute temperature
$T_m$ : salt transmission coefficient in membrane
x : longitudinal coordinate
$y$ : concentration scaled on fixed-charge concentration
$y_0$ : concentration of base solution scaled on fixed-charge concentration
$y_i$ : concentration at the interface scaled on fixed-charge concentration
$y_s$ : concentration of step solution scaled on fixed-charge concentration
$z_+$ : charge coefficient of cation
$z_-$ : charge coefficient of anion

*Greek letters*

$\alpha_m$ : chemical capacity of the membrane
$\alpha_s$ : chemical capacity of the frit
$\beta$ : model parameter defined by Eq. (A18)
$\delta(\omega)$ : delta function
$\theta$ : model parameter defined by Eq. (A19)
$\varphi$ : electrical potential
$\varphi_0$ : initial electrical potential difference
$\rho$: model parameter defined by Eq. (A4)
$\gamma$ : salt activity coefficient in the virtual solution
$\gamma_i$ : salt activity coefficient at the membrane/support interface
$\gamma_0$: salt activity coefficient at the initial concentration
$\gamma_{step}$ : salt activity coefficient of the non-equilibrium solution
$\nu$ : stoichiometric coefficient
$\Gamma_\pm$ : partition coefficient
$\lambda$ : parameter defined by Eq. (A14)
$\Delta\mu_S$ : relative salt chemical potential difference across the support
$\tau$ : dimensionless time scaled on the characteristic relaxation time defined by Eq. (A2)
$\chi$ : mechanical permeance
$\omega$ : dimensionless circular frequency

both partitioning and diffusivity coefficients in the case of electroactive solutes [20].

Non-stationary diffusion in principle allows for separate determination of those properties for a diffusing species from interpretation of a single time-resolved measurement [21]. However, the typical use of pure solvent in the receiving compartment (needed to reliably detect initially small concentration changes) [22] implies large trans-membrane salt-concentration differences and strongly non-linear diffusion that would complicate the interpretation in the case of ion-exchange membranes whose diffusion permeability is a strong function of salt concentration [23]. Non-stationary diffusion of radiotracer ions [8,24] can provide information on the ion diffusivity and partitioning from which the salt-related properties can be calculated. However, the use of radiotracers is possible only in certified laboratories. Besides, suitable radiotracers are available only for some ions.

A different approach based on time-resolved measurements consists in measuring the electrical response to a sudden change in the electrolyte concentration at one of the membrane sides [25–27]. Sørensen and Compañ developed a method to determine ion transport numbers within a surface layer of a membrane by measuring initial-time membrane potential. Once the membrane was equilibrated with an equilibrium solution, one of the membrane faces was exposed to a non-equilibrium solution and the membrane potential was measured immediately. Initially, the concentration gradient remained localized within a surface layer of the membrane. Therefore, the electrical response was controlled by the ion transport numbers within a narrow surface zone and could be estimated for each face of the membrane. The initial time method was used to evaluate the asymmetry between the two faces of a membrane and conclude if it was homogeneous or not.

Later, refs. [28,29] pointed out a problem related to the solution replacement technique (as implemented in Refs. [25–27]), which is the presence of an unstirred layer at the membrane surface that does not allow for a change in the electrolyte concentration directly at the membrane surface but only at the external surface of a boundary layer.

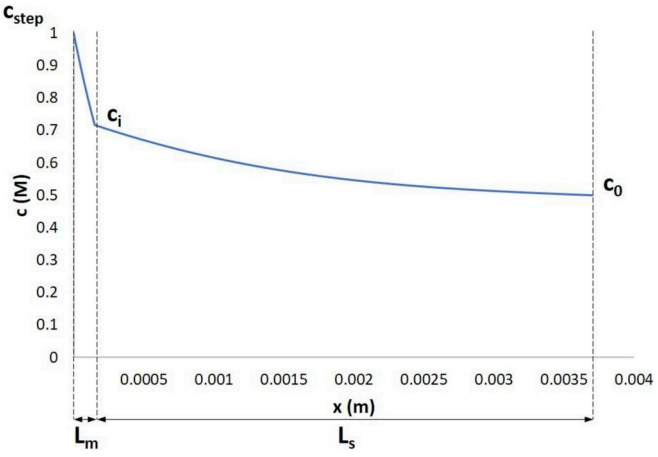


**Fig. 1.** Non-stationary salt-concentration profile in the system studied in this work.

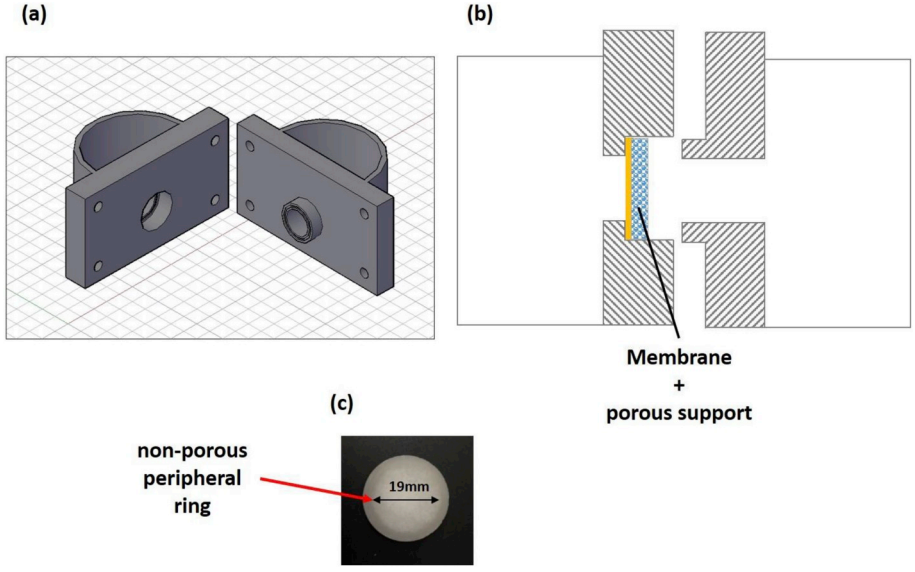


**Fig. 2.** a) Drawing of the cell, b) side view showing the assembly of the two half-cell with membrane and porous support and c) glass frit used as the porous support.

**Table 1**
Concentrations used in experiments.

| Membrane | Measurements performed | Lower concentration (M) | Higher concentration (M) |
|---|---|---|---|
| Nafion 120 | - Transient-membrane potential | 0.05 | 0.1 |
| | | 0.1 | 0.2 |
| | | 0.5 | 1 |
| | | 1 | 2 |
| Fujifilm Type 10 (CEM & AEM) | - Transient-membrane potential | 0.05 | 0.1 |
| | | 0.158 | 0.316 |
| | | 0.25 | 0.5 |
| | - Osmotic permeability | 0.5 | 1 |
| | | 0.75 | 1.5 |
| | - Membrane potential | 1 | 2 |
| | - Salt permeability | 0 | 0.05 |
| | | 0 | 0.1 |
| | | 0 | 0.158 |
| | | 0 | 0.316 |
| | | 0 | 0.25 |
| | | 0 | 0.5 |
| | | 0 | 0.75 |
| | | 0 | 1 |
| | | 0 | 1.5 |
| | | 0 | 2 |

**Table 2**
Properties of porous support.

| $\alpha_s$ | $D_s$ (m$^2$/s) | Pore size (μm) | $L_s$ (mm) |
|---|---|---|---|
| 0.34 ± 0.00 | $1.5{\cdot}10^{-10}$ | 10–16 | 3.65 ± 0.008 |

For nanofiltration membranes studied in Refs. [28,29] the characteristic relaxation time of the initial signal could be as short as a couple of milliseconds, so in the presence of an unstirred layer it was impossible to measure the initial membrane-potential values. Therefore, refs. [28,29] introduced an alternative approach to the rapid concentration change at the membrane surface (touching the membrane surface with a pendant drop).

However, in the case of ion-exchange membranes, the relaxation of initial signal takes tens of seconds since these membranes are relatively thick compared with the active layers of nanofiltration membranes. Therefore, the solution replacement can be implemented simply via evacuating an equilibrium solution and replacing it with a non-equilibrium one.

In this study, the electrical response to this is measured for a membrane supported by a relatively coarse-porous material. The different ion perm-selectivities of the membrane (thin and relatively dense) and porous support (thicker and much more porous than the membrane) make the response time-dependent due to the progressive redistribution of applied concentration difference between those two media. The porous support was characterized in separate measurements in terms of porosity and effective salt diffusivity needed for the interpretation of the results. Experimental data is fitted to a mathematical model that describes transient transport phenomena including osmosis, which has noticeable impact on the measurements (see **Supporting information** for detailed information).

First, the new procedure is applied to a membrane (Nafion 120) that has been previously extensively characterized by using well-established conventional techniques. The results will be compared with the literature to validate the new method. Further on, the method will be implemented for a range of NaCl concentrations to obtain information on concentration dependences of properties of a novel ion-exchange membrane (Type 10, Fujifilm NL). In this case, conventional techniques have been used in order to validate the new method because the corresponding results are not, yet, available in the literature for those membranes.

## 2. Theory

The present work considers a system consisting of a membrane and a porous support placed in a two-compartment cell. Initially, both compartments are filled with a base solution of concentration $c_0$; the membrane and the porous support are equilibrated with this solution. Suddenly, the solution facing the membrane is replaced by a solution of a different concentration, $c_{step}$.

Fig. 1 shows an example of non-stationary concentration profile occurring some time after a concentration step in a system formed by a membrane and a porous support as described. $L_m$, $L_s$ are the thicknesses of membrane and porous support respectively. $c_i$ is the salt concentration at the membrane/porous support interface.

The diffusion process occurs through a large chemical resistance (thin and relatively dense ion-exchange membrane) into a large chemical capacity (the porous support), which is much more porous and thicker than the membrane. In this way, there is a progressive redistribution of applied concentration difference between the membrane

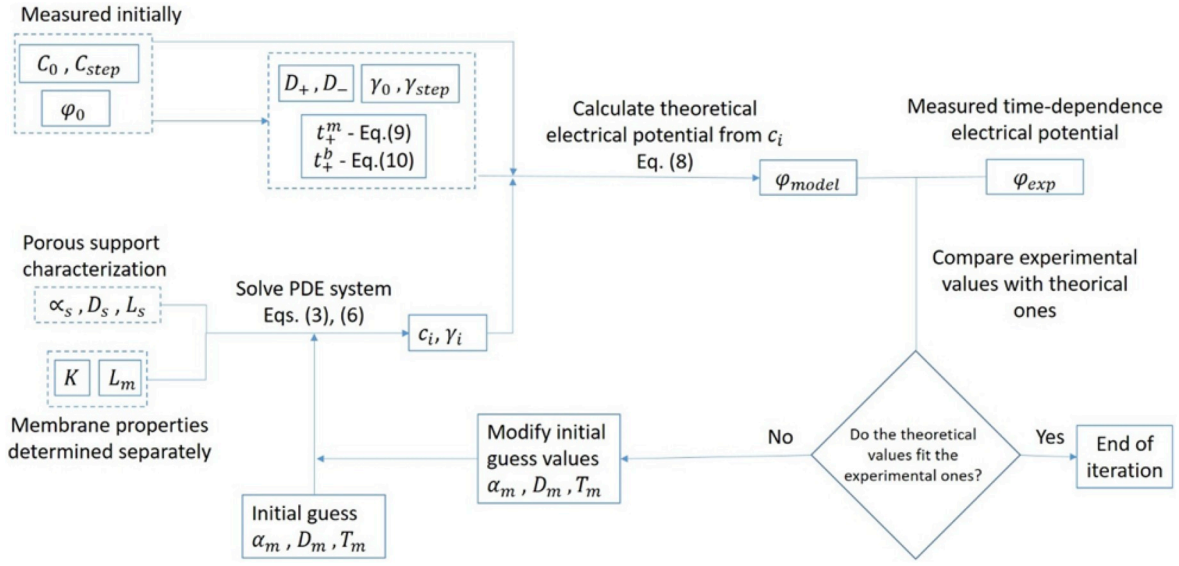


**Fig. 3.** Modelling procedure diagram to obtain model parameters $\alpha_m$, $D_m$, $T_m$ from the experimental data.

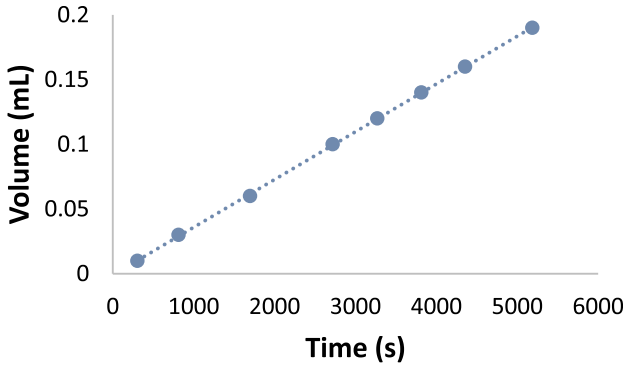


**Fig. 4.** Time dependence of closed half-cell volume in measurements of osmosis using CEM Type 10 Fujifilm. The solutions were 1 M and 2 M NaCl.

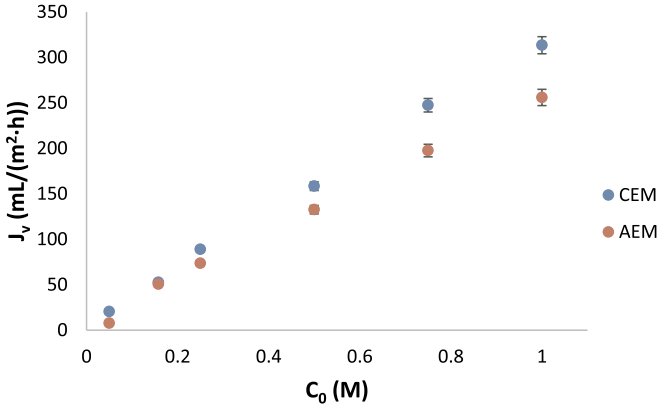


**Fig. 5.** Osmotic flux vs. lower concentration determined for Type 10 Fujifilm membranes CEM and AEM.

and the porous support. Due to the different ion perm-selectivities of those media this gives rise to a time-dependent electrical response. This is the fundamental reason why a porous support is needed, since it acts as additional diffusion resistance put on purpose to provoke a time-dependent electrical response. Having just a free-standing ion exchange membrane, the result would be a time-independent steady–state membrane potential.

Another important phenomenon occurring in the system is osmosis.

**Table 3**
Osmotic permeability of cation and anion exchange membrane Type 10 Fujifilm. $C_0$ is the lower concentration and the higher concentration is two times larger.

| $C_0$ (M) | $K \cdot 10^{-10}$ ($m^4$/(mol·s)) | |
|---|---|---|
| | CEM | AEM |
| 0.05 | 1.25 ± 0.59 | 0.47 ± 0.20 |
| 0.158 | 1.02 ± 0.11 | 0.98 ± 0.14 |
| 0.25 | 1.46 ± 0.16 | 1.21 ± 0.06 |
| 0.5 | 0.93 ± 0.04 | 0.77 ± 0.02 |
| 0.75 | 0.66 ± 0.02 | 0.53 ± 0.02 |
| 1 | 0.84 ± 0.0005 | 0.69 ± 0.02 |

Notably, the osmotic permeabilities do not show clear trends as functions of salt concentration. This is in disagreement with the standard Donnan model of ion-exchange membranes postulating that osmosis is controlled by the coion-exclusion phenomenon while the latter is a strong function of concentration. Below we will see that the same is true for the related salt-transmission coefficients.

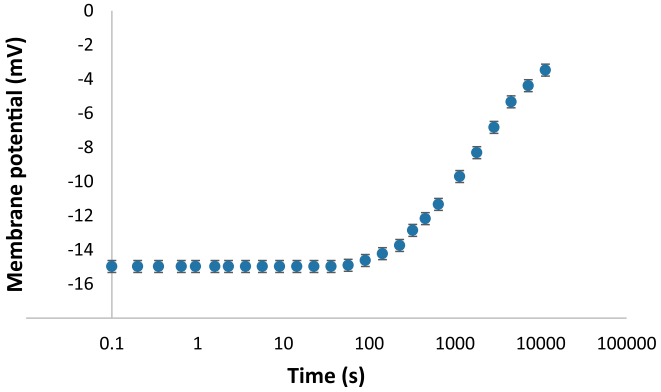


**Fig. 6.** Experimental time evolution of membrane potential for Nafion 120, $C_0 = 0.5M$ NaCl.

Some estimates concerning the influence of osmosis are presented in **Supporting information**. There is an osmotic flow, $J_v$, transporting water in the opposite direction to the salt transport:

$$J_v = -K \cdot (c_{step} - c_i) \quad (1)$$

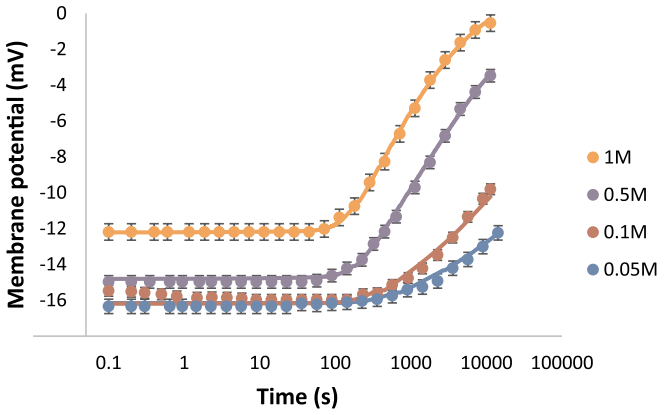


**Fig. 7.** Time evolution of trans-membrane potential for various base concentrations, $C_0$, for Nafion 120. $C_{step}$ is always two times higher than $C_0$. Symbols represent experimental data and solid lines are the theoretical fits.

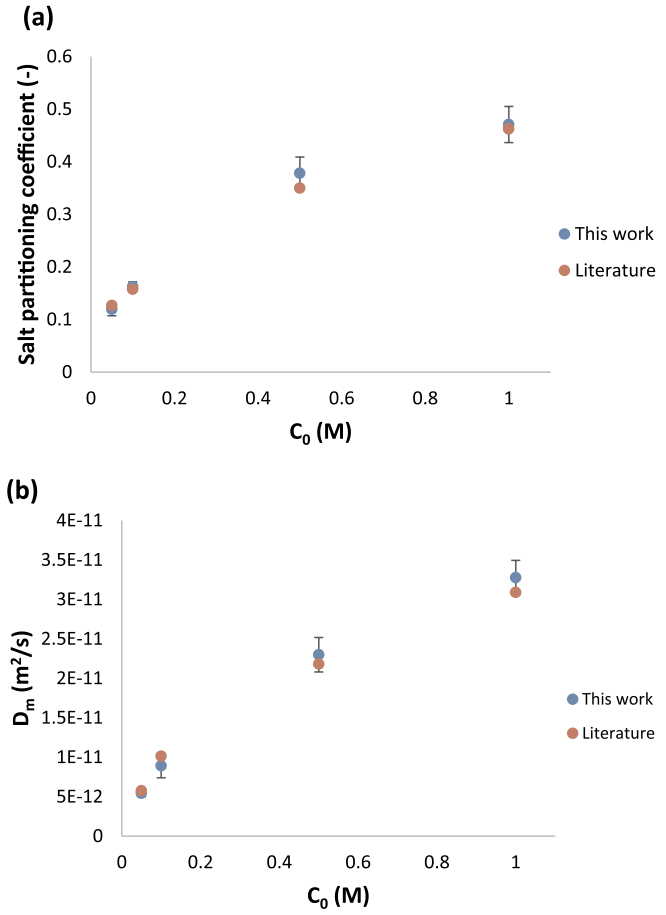


**Fig. 8.** (a) Partitioning and (b) effective salt diffusion coefficients obtained in this work for Nafion 120 membrane compared with the literature [37,38].

where $K$ is the osmotic permeability defined as:

$$K = \nu RT\chi(1 - T_m) \tag{2}$$

where $\nu$ is the stoichiometric coefficient, $R$ is the gas constant, $T$ is the absolute temperature, $T_m$ is the salt transmission coefficient (one minus salt reflection coefficient) and $\chi$ is the mechanical permeance.

Taking into account both transport phenomena, the salt mass balance in the membrane is described by:

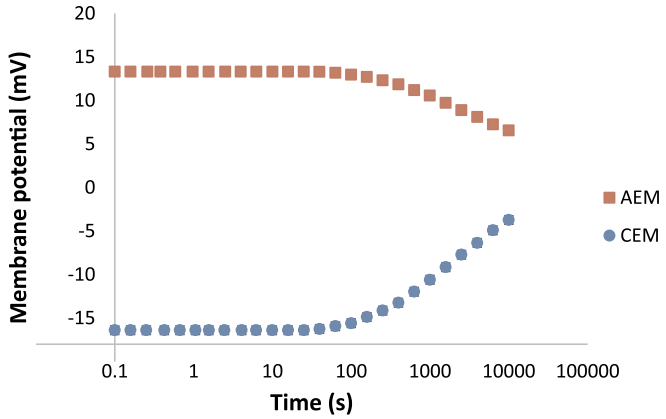


**Fig. 9.** Experimental time evolution of membrane potential for type 10 Fujifilm cation and anion exchange membranes for $C_0 = 0.5M$ NaCl.

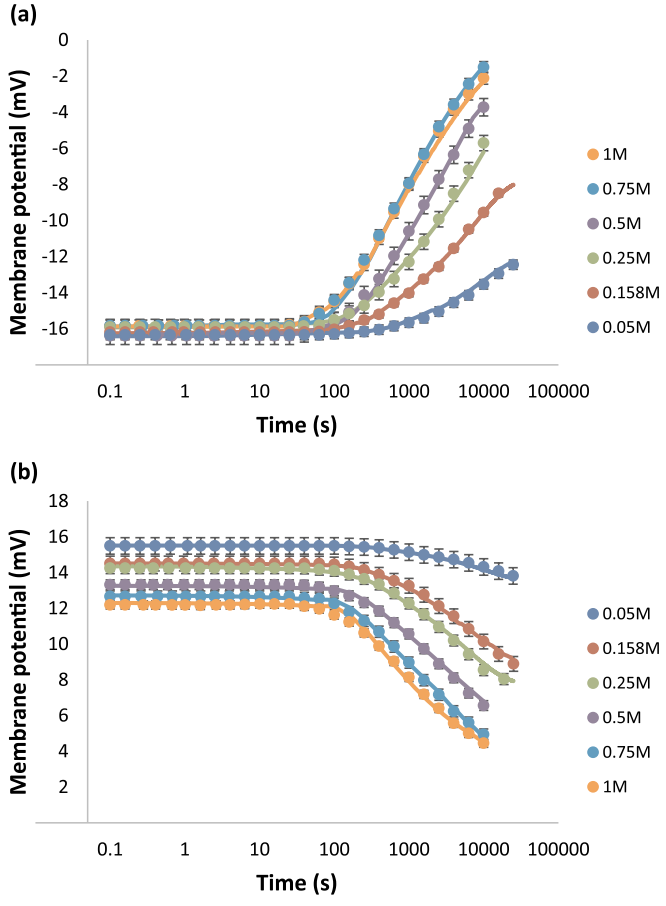


**Fig. 10.** Time evolution of trans-membrane potential for various base concentrations, $C_0$, for Type 10 Fujifilm membranes: a) CEM and b) AEM. $C_{step}$ is always two times higher than $C_0$. Symbols represent experimental data and solid lines are the theoretical fits.

$$\alpha_m \frac{\partial c_m}{\partial t} = \frac{\partial}{\partial x}\left[-D_m \cdot \left(1 + \frac{dln(\gamma)}{dln(c_m)}\right) \cdot \frac{\partial c_m}{\partial x} + J_v T_m c_m\right] \tag{3}$$

where $\alpha_m$ is the chemical capacity in the membrane, $c_m$ is the virtual salt concentration [30] in the membrane, $D_m$ is the effective salt diffusion coefficient in the membrane, $\gamma$ is the salt activity coefficient in the virtual solution, $x$ is the longitudinal coordinate ($0 < x < L_m$) and $T_m$ is the salt transmission coefficient. The concentration dependence of salt activity coefficient was taken from the literature [31].

**Table 4**
Counter-ion transport number in the membrane for cation and anion exchange membranes type 10 Fujifilm.

| $C_0$ (M) | $t^m_{counter-ion}$ | | | | | |
|---|---|---|---|---|---|---|
| | CEM | | | AEM | | |
| | Transient-membrane potential | Membrane potential | Relative difference (%) | Transient-membrane potential | Membrane potential | Relative difference (%) |
| 0.05 | 1.007 ± 0.007 | 0.993 ± 0.007 | 1.343 | 0.979 ± 0.003 | 0.982 ± 0.005 | 0.356 |
| 0.158 | 1.002 ± 0.003 | 1.002 ± 0.004 | 0.003 | 0.948 ± 0.008 | 0.951 ± 0.009 | 0.289 |
| 0.25 | 0.978 ± 0.011 | 1.001 ± 0.003 | 2.305 | 0.939 ± 0.009 | 0.931 ± 0.007 | 0.928 |
| 0.5 | 0.985 ± 0.005 | 0.987 ± 0.010 | 0.194 | 0.896 ± 0.004 | 0.893 ± 0.005 | 0.296 |
| 0.75 | 0.959 ± 0.004 | 0.986 ± 0.008 | 2.732 | 0.867 ± 0.006 | 0.874 ± 0.007 | 0.714 |
| 1 | 0.943 ± 0.007 | 0.974 ± 0.007 | 3.215 | 0.842 ± 0.004 | 0.847 ± 0.09 | 0.543 |

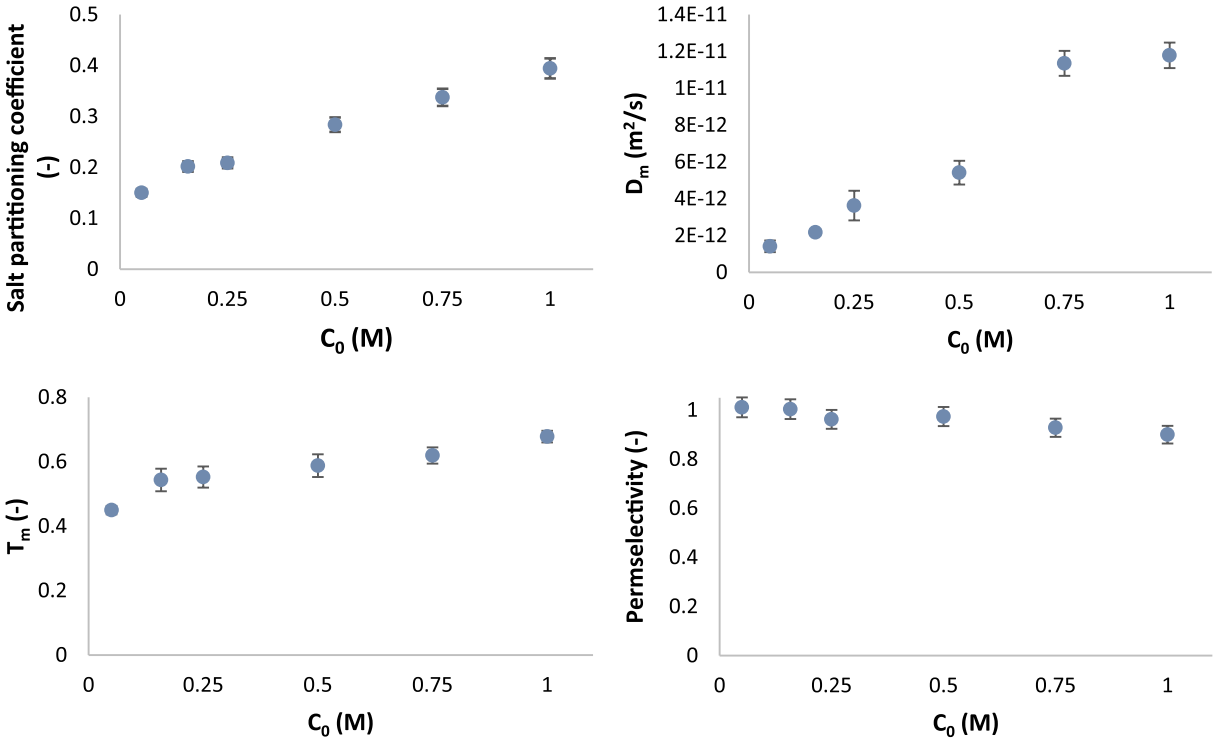


**Fig. 11.** Properties determined for Type 10 Fujifilm CEM.

The chemical capacity is a quantitative measure of how much salt has to be added to a unit of volume of a medium to change the salt chemical potential by a unit [32]. This property is related to the partition coefficient of either of the ions, $\Gamma_{\pm}$ as

$$\alpha_m = \Gamma_{\pm}\left(1 + \frac{dln\Gamma_{\pm}}{dlnc}\right) \tag{4}$$

It can be shown that due to the electroneutrality of membrane phase using either of ions gives the same result.

Eq. (3) has to be solved numerically with the following initial and boundary conditions:

$$c_m|_{x=0} = c_{step} \tag{5a}$$

$$c_m|_{x=L_m} = c_i \tag{5b}$$

For the salt transport in the porous support, a similar equation is used:

$$\alpha_s \frac{\partial c_s}{\partial t} = \frac{\partial}{\partial x}\left[-D_s \bullet \left(1 + \frac{dln(\gamma)}{dln(c_s)}\right) \bullet \frac{\partial c_s}{\partial x} + J_v c_s\right] \tag{6}$$

In this case $\alpha_s$ is the chemical capacity in the porous support (which is equal to the porosity), $c_s$ is the salt concentration in the porous support, $D_s$ is the salt diffusivity in the porous support, $x$ is the longitudinal coordinate $(L_m < x < (L_m + L_s))$ and the corresponding boundary conditions are:

$$c_s|_{x=L_m} = c_i \tag{7a}$$

$$c_s|_{x=(L_m+L_s)} = c_0 \tag{7b}$$

Eqs. (3) and (6) are a system of partial differential equations (PDE) that can be solved numerically and the evolution of electric potential difference, $\varphi$, is given by Ref. [33]:

$$\varphi = \frac{RT}{F}\left[(2t^m_+ - 1)ln\left(\frac{a_{step}}{a_i}\right) + (2t^b_+ - 1)ln\left(\frac{a_i}{a_0}\right)\right] \tag{8}$$

where R is the ideal gas constant, T is the absolute temperature, F is the Faraday constant, $a$ is the activity, $t^b_+$ is the transport number of cations in the porous support and $t^m_+$ is the transport number of cations in the membrane. The transport number of cations in the porous support is assumed to be equal to the transport number in the bulk electrolyte solution:

$$t^b_+ = \frac{z_+ \cdot D_+}{z_+ \cdot D_+ + z_- \cdot D_-} \tag{9}$$

Initially the whole concentration gradient is located on the

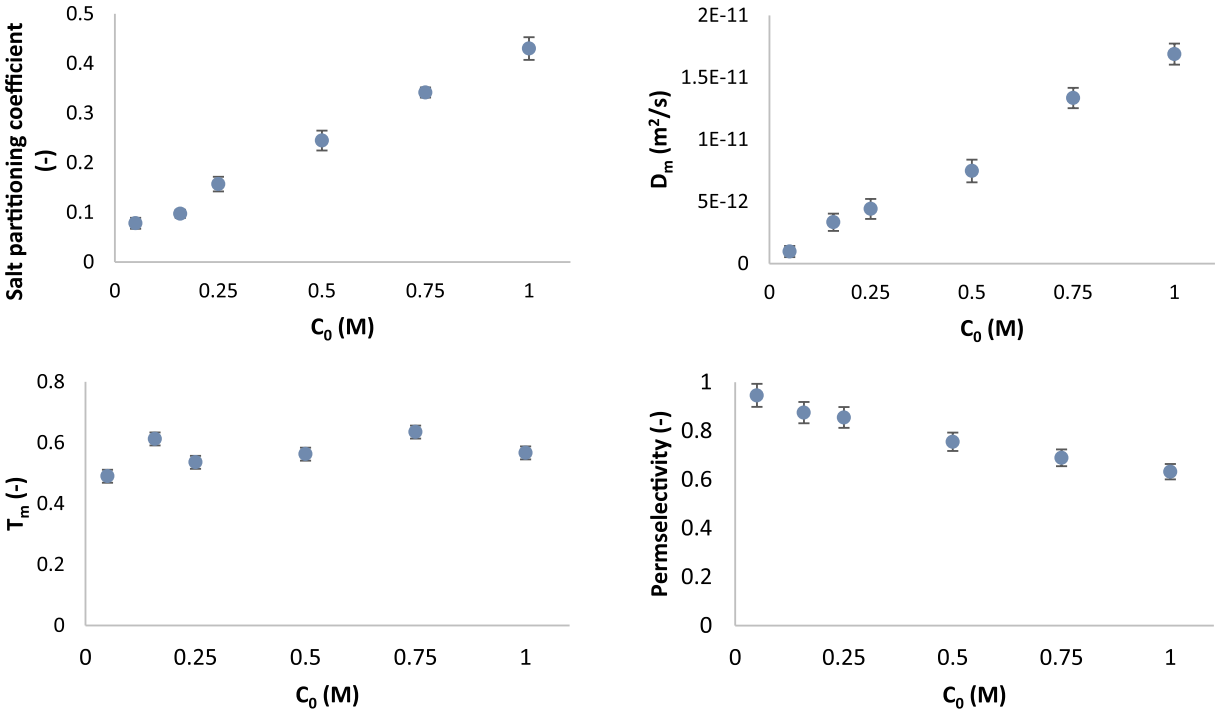


**Fig. 12.** Properties determined for Type 10 Fujifilm AEM.

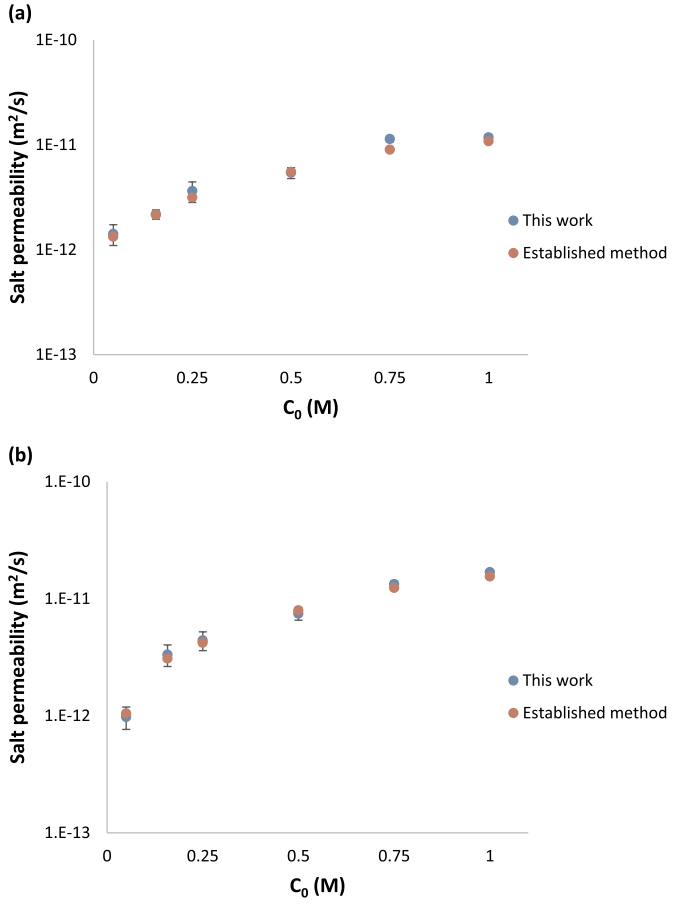


**Fig. 13.** Comparison of salt permeability estimated from the novel procedure presented in this work and the salt diffusion measurements in the case of Fujifilm Type 10 membranes: a) CEM and b) AEM.

membrane. Therefore, the transport number of positive ions in the membrane $t_+^m$, can be estimated from:

$$t_+^m = \frac{1}{2}\left[\frac{\frac{F\varphi_0}{RT}}{ln\left(\frac{a_{step}}{a_0}\right)} + 1\right] \quad (10)$$

where $\varphi_0$ is the initial value of electric-potential difference occurring just after the solution replacement.

The described model has been validated using several approaches (see **Supporting information**).

## 3. Experimental materials and methods

### 3.1. Materials

Experimental data have been obtained with two different ion-exchange membranes: Nafion 120 (DuPont) and Type 10 (the latter kindly provided by Fujifilm Manufacturing Europe BV (The Netherlands)). All the measurements were performed using NaCl solutions. Membranes were supported by porous glass frit discs of 25 mm in diameter having a non-porous peripheral edge (the porous part is 19 mm in diameter, see Fig. 2c), 3.65 mm of thickness and average pore size of 10–16 μm supplied by Duran Group (Germany). The chemical reagents were of analysis grade.

### 3.2. Experimental design

First, measurements of transient membrane potential after concentration step have been performed with Nafion 120 since it is a well-known membrane, so in the literature there are data available to compare with the results obtained by using the new procedure described in this work. Then, the same procedure has been applied to novel Fujifilm cation exchange membranes (CEM) and anion exchange membranes (AEM) of Type 10. In this case, we have also performed some measurements by using well-established techniques such as membrane potential and salt diffusion permeability to additionally validate our new approach. The osmotic permeability was measured as

well since it is a necessary input parameter of the model described in the previous section. All the measurements were performed at room temperature. Table 1 summarises the type of experiments and the concentrations on both sides of the membrane.

### 3.3. Measurements of transient-membrane potential after concentration step

Nafion 120 membranes were conditioned in boiling water for 30 min [34]. Membranes were equilibrated overnight with the solution of base concentration, $C_0$. Equilibrated sample was placed on top of the porous support in a two-compartment cell (Fig. 2a–b). Initially, both compartments (85 mL) are filled with the base solution and one of the measuring electrodes is located in each compartment. Electric potential difference was measured by Ag/AgCl reference electrodes with salt bridges filled with KCl 3 M (Metrohm, Switzerland) using a data acquisition card (NI USB-6001) and the software LabView (National Instruments, Austin). The asymmetry potential between the measuring electrode was measured separately and subtracted from the measured membrane-potential transients. The salt concentration on the porous support side (equilibrium compartment) is expected to be constant during the measurements. Once the measured electric potential difference between the two compartments stabilised, the solution in the compartment facing the membrane was replaced by the non-equilibrium solution of concentration $C_{step}$. The equilibrium solution was sucked out by a syringe, a process that takes typically around 10 s, whereas the new solution is just poured from a beaker. Measurements were performed for several base concentrations and the ratio $C_{step}$ to $C_0$ was 2 in all cases (see Table 1). The solution in the non-equilibrium compartment was stirred using a magnetic stirrer to keep the concentration at the membrane surface constant.

### 3.4. Measurements of osmotic permeability

Osmotic permeability was determined for the Type 10 Fujifilm membranes only. A membrane disk of 25 mm in diameter (4.91 $cm^2$ exposed area) was placed in a two-compartment stirred cell with a volume of 120 mL in each compartment. The compartment containing the more dilute solution was open while the other one was closed and equipped with a graduated pipette to measure changes in the volume as a function of time due to the osmotic flow. The membrane was equilibrated overnight with a solution having concentration between the dilute and higher-concentration solutions. Solutions were pre-heated moderately to remove dissolved air and avoid formation of bubbles during the measurement.

The slope of linear dependence of half-cell volume on time gives the osmotic flux, $J_v$. The osmotic permeability, $K$, was calculated as the ratio of osmotic flux and corrected concentration difference taking into account solution non-ideality by means of osmotic coefficient, $\phi$:

$$\boldsymbol{K = \frac{J_v}{C_2 \cdot \phi_2 - C_1 \cdot \phi_1}} \tag{11}$$

where $c$ is the salt concentration and the subscripts 1 and 2 denote the lower and higher concentration respectively.

The osmotic permeability was determined for the same concentration pairs $C_0 - C_{step}$ as used in the transient membrane potential measurements (see Table 1).

### 3.5. Glass frit characterization

For the interpretation of measurements of transient membrane potential, we need to know the porosity of and effective salt diffusion coefficient in the glass frit used as the porous support. They were determined in the following way.

First, the porosity was determined gravimetrically. A glass frit was immersed in distilled water, water from the surface was removed and the mass of the wet disc was recorded. Then, the disc was dried in an oven until the mass of the disc was stable. This procedure was repeated four times and the result is the average of the measurements. The porosity was calculated as:

$$\boldsymbol{porosity = \frac{(m_w - m_d)}{\frac{\pi}{4} \cdot d_f^2 \cdot \delta \cdot \rho_w}} \tag{12}$$

where $m_w$ and $m_d$ are the wet and dry masses respectively, $d_f$ is the diameter of the porous part, $\delta$ is the thickness and $\rho_w$ is water density.

The effective salt diffusion coefficient in the glass frit was estimated indirectly via measurements of AC electrical resistance. The measured resistance was compared to the electrical resistance of free solution of the same geometry calculated as

$$\boldsymbol{R_{electrolyte} = \frac{L_s}{\sigma \cdot A}} \tag{13}$$

where $A$ is the cross-sectional area of the porous part, $L_s$ is the frit thickness and $\sigma$ is the solution conductivity. It is assumed that due to the relatively large pore size (10–16 μm) the diffusivity-reduction factor is the same as the conductivity reduction.

A glass frit disc was sandwiched between two pieces of a stainless steel net (Dexmet corporation, USA) used as electrodes and the AC electrical resistance was measured with a sourcemeter (2400 Series SourceMeter, Keithley Instruments).

### 3.6. Modelling procedure

The procedure to fit the model described above to the experimental data is as follows.

1. Obtain the values of diffusion coefficient for each ion ($D_+$, $D_-$) and the activity coefficient ($\gamma_0$, $\gamma_{step}$)
2. Determine the transport numbers in the membrane ($t_+^m$) and in the bulk solution ($t_+^b$) using Eqs. 9 and 10 respectively
3. Solve numerically the PDE system formed by Eqs. (3) and (6). In this work, MATLAB and pdepe function to solve initial-boundary value problems for systems of parabolic and elliptic PDEs has been used. The concentration dependence of salt activity coefficient was taken from the literature [31]. The necessary values of $\alpha_s$, $D_s$, $L_s$ were determined from the porous-support characterization, $L_m$ was measured with a digital caliper and $K$ was obtained from the osmotic permeability measurements. The values of $\alpha_m$, $D_m$, $T_m$ are initially guessed to start the resolution
4. A time-dependence of $c_i$ is obtained from the previous step and the activity coefficient $\gamma_i$ is determined for each time. This concentration time-dependence is converted in membrane potential $\varphi_{model}$ using Eq. (8)
5. The function $\varphi_{model}$ is compared with the time-dependence potential obtained experimentally, $\varphi_{exp}$. The model parameters $\alpha_m$, $D_m$, $T_m$ are iteratively changed until the percentage difference between both values is below 1%.

### 3.7. Measurement of salt permeability and membrane potential

Salt permeability was measured by using methods previously reported in the literature [35]. A membrane disk of 38 mm in diameter (11.34 $cm^2$ exposed area) was placed in a two-compartment mechanically stirred cell with a volume of 220 mL in each compartment. One compartment was filled with salt solution of desired concentration (see Table 1) while the other one contained deionized water. A conductivity meter (GLP31, Crison) was used to track the changes in conductivity over time in the diluted compartment. Conductivity changes were converted to concentration changes by means of a calibration curve. Salt concentration time dependence was used to calculate salt permeability, $P_s$, taking into account osmosis as reported by Coronell at al [23].

Membrane potential was measured as described in Ref. [36]. A

membrane was placed in a two-compartment stirred cell where each compartment was filled with solutions of the same concentrations as used in the transient-membrane potential measurements (see Table 1). The electrical potential difference was measured by the same pair of reversible electrodes with salt bridges until it reached stationary state. From the stationary membrane potential, the counter-ion transport number in the membrane was estimated by using Eq. (10)

## 4. Results and discussion

### 4.1. Glass frit properties

Table 2 shows the properties of the glass frit. In the case of diffusion coefficient estimation in the glass frit, it was assumed that the modification in its electrical resistance compared to the free solution layer of the same geometry is the same as the increase in its diffusion resistivity. This assumption is quite realistic taking into account the relatively large pore size of the glass frit. The ratio between glass frit resistance to free solution resistance was 10.68 ± 0.26. Therefore, taking into account the salt diffusivity of NaCl in bulk solution ($1.62{\cdot}10^{-9}$ m$^2$/s) the effective diffusion coefficient in the glass frit was set at $1.5{\cdot}10^{-10}$ m$^2$/s.

### 4.2. Osmotic permeability determination

Fig. 4 shows a typical time evolution of volume transferred by osmosis.

The slope of volume vs. time dependence gives the osmotic flux, which has been determined for both anion and cation exchange membranes for a concentration range always using the same concentration pairs as in the measurements of transient membrane potential (see Table 1). Concentration in each compartment was determined after each measurement to corroborate that the salt concentration difference across the membrane did not change significantly over the experiments and the variation observed was always below 5%.

Fig. 5 shows the osmotic flux as a function of lower concentration. Expectedly, the higher is the concentration, the larger is the osmotic flux. It can also be seen that the osmosis is noticeably stronger in CEM than in AEM.

Table 3 presents the osmotic permeability calculated as the ratio between the measured osmotic flow and the concentration difference (corrected for the solution non-ideality). These values have been used in the model validation (see **Supporting information**) and will be used in the fitting of time dependences of transient membrane potential below.

### 4.3. Estimates of effective salt diffusion and partition coefficients

Fig. 6 shows a typical example of measurement of transient-membrane potential after concentration step with Nafion 120 membrane. All the presented results are averages of at least three measurements.

As can be seen from Fig. 6, when the solute concentration is suddenly changed at the membrane surface, an initial potential difference remains practically constant for a certain period of time. This is because in macroscopically homogeneous membranes transmembrane electric-potential difference is independent of shape of salt-concentration profile. Accordingly, the signal evolution begins only when the salt concentration at the interface starts to change. The diffusion occurs through a large chemical resistance, which is the thin and relatively dense ion-exchange membrane, into a large chemical capacity, namely the porous support, which is much more porous and thicker than the membrane. The salt chemical potential at the membrane/support interface remains practically constant until the chemical capacity of the adjacent part of the support is noticeably charged [29]. This explains why the initial period of constant signal is relatively long.

After that, the response becomes time-dependent because of progressive redistribution of applied concentration difference between the membrane and the porous support and the different ion perm-selectivities of those media. The pattern of signal relaxation is primarily controlled by the diffusion permeability of the membrane but is also affected by the salt partitioning coefficient. In addition, osmotic transmembrane volume transfer has a considerable impact on the relaxation process (see **Supporting information** for detailed information).

From the initially-constant signal one can determine the ionic perm-selectivity of the membrane according to the definition [36]:

$$permselectivity = \frac{t^m_{counter-ion} - t^b_{counter-ion}}{t^b_{co-ion}} \tag{14}$$

where $t$ is the transport number calculated from the initial membrane potential with Eq. (10). The superscripts $m$, $b$ refer to the membrane and bulk-solution phases. Measurements have been performed for Nafion 120 membranes at various values of base concentration $C_0$ and effective salt diffusion and partitioning coefficients have been determined by fitting the experimental data to the mathematical model as described above (see Fig. 3). The osmotic permeability was estimated from the osmotic flow data published by Narebska et al. [37]. The obtained results will be compared with the literature to validate the suggested procedure.

Fig. 7 shows the experimental data collected at several base solution concentration $C_0$. The ratio $C_{step}/C_0$ was kept at 2 in all the measurements (see Table 1). Each individual measurement was fitted separately and the averages of the obtained fitted parameters for each base concentration are presented as a result. Fig. 7 also presents the theoretical curves calculated for the average values of parameters in each case. It illustrates mostly excellent quality of the theoretical fits since the maximum deviation from the experimental data is 5%. It can also be seen that the initial membrane potential decreases (in absolute value) with concentration, which indicates that the electrochemical perm-selectivity decreases with concentration. This has been typically observed for ion-exchange membranes [28].

The average values of partitioning and effective salt diffusion coefficients obtained from the fitting are shown in Fig. 8 and compared with the data published in the literature [37,38]. In both cases the mean deviation is around 5%, so the results obtained by the presented method are in a very good agreement with the literature.

The same procedure was applied to two novel membranes, one cation- and another anion-exchange. Sample measurements for both Type 10 Fujifilm membranes are presented in Fig. 9. CEM Type 10 shows a behaviour quite similar to Nafion 120 whereas AEM Type 10 exhibits signals of opposite sign, which is due to the opposite (positive) sign of fixed charge.

The effect of variation of base concentration, $C_0$, has been studied in the concentration range between 0.05 M and 1 M NaCl keeping again $C_{step}$ always two times higher than the base solution concentration $C_0$ (see Table 1). The results are presented in Fig. 10. Along with the experimental data, Fig. 10 shows the theoretical fits obtained for each curve, whose deviations from experimental data are below 10% in all cases. The characteristic relaxation time decreases when the base concentration increases. A shorter relaxation time implies higher diffusion permeability, so this should increase with the salt concentration.

Fig. 10 also shows that the initial membrane potential decreases (in absolute value) with concentration but this dependence is relatively weak in the case of CEM, whereas for AEM it is stronger. This decrease has also been observed in the measurements with Nafion 120, which is due to the decrease in electrochemical perm-selectivity with concentration observed in ion-exchange membranes as explained above. This is reflected in the counter-ion transport numbers presented in Table 4, which also shows the counter-ion transport number determined by the stationary-membrane-potential method. The results obtained in both cases are quite similar.

The values of partitioning, effective salt diffusion and transmission

coefficients and perm-selectivity obtained from the fitting are shown in Fig. 11 and in Fig. 12 as functions of base concentration. In both cases there are increasing trends in the partitioning and effective salt diffusion coefficients with the base concentration, which is in agreement with the mechanism of Donnan exclusion of co-ions from ion-exchange materials. The same can be said about the decreasing trend of perm-selectivity. It is also seen that the perm-selectivity for CEM is higher than in the case of AEM. A part of this could be an artefact due to the junction potential in reference electrodes as discussed by Kingsbury et al. [39].

As for the transmission coefficient, in the case of CEM it seems to be slightly increasing with the concentration whereas for AEM it remains roughly constant. The osmotic permeability determined experimentally is the product of two parameters: mechanical permeance and salt transmission coefficient (see Eq. (3)). The lack of pronounced dependence of transmission coefficient on salt concentration is in disagreement with the classical Donnan-exclusion model. However, a qualitatively similar behaviour was also observed with Nafion 120 cation-exchange membrane [40]. Besides, the relaxation pattern is primarily controlled by the diffusion permeability whereas the sensitivity to the salt transmission coefficient is essentially weaker. As a result, the determinations of perm-selectivity and salt diffusion permeability are quite robust while the transmission coefficient is estimated less reliably, although it does not affect much the determination of the other parameters. This may explain the larger scattering of its concentration dependences.

Finally, the time-dependence of salt concentration in the receiving compartment obtained from the salt-diffusion measurements will be used to calculate the salt permeability (**see supporting information**). As mentioned above, salt permeability is the product of diffusion and partition coefficients. Considering that in transient-membrane potential after concentration step we obtain an effective salt diffusion coefficient $D_m$ that includes partitioning coefficient, the results obtained from the two different measurements can be compared.

At this point it is necessary to remind that the concentration difference between the solutions on both sides of the membrane in the salt-diffusion experiments was different from the case of transient-membrane potential after concentration step. Therefore, both results cannot be compared directly. However, the additivity principle [34].

$$J_S(C_i \rightarrow C_j) = \sum_{i=1}^{j-1} J_S(C_i \rightarrow C_{i+1}) \tag{17}$$

can be used to calculate the salt fluxes corresponding to the concentration gradients in transient-membrane potential after concentration step from the salt-diffusion measurements.

Fig. 13 shows the salt permeability estimated by both methods for Fujifilm Type 10 CEM and AEM. The difference in both cases are below 10% so the procedure presented in this work is in agreement with results of independent measurements carried out with a well-known technique.

## 5. Conclusions

Ion-exchange membranes are central elements of electro-membrane processes. For their optimization, it is important to have detailed information on the transport and equilibrium properties of ion-exchange membranes, in particular, separate information on the partitioning and diffusivity properties of the membrane with respect to ions.

To obtain this information, a novel approach of non-stationary diffusion (tracked via transient membrane potential) under conditions of relatively small concentration differences has been developed. It allows for a relatively simple determination of effective salt diffusion and partitioning coefficients in addition to the ion perm-selectivity, which is the only parameter provided by conventional stationary measurements of membrane potential.

Osmosis was included in the mathematical model developed to interpret the results. This model has been validated via comparison with (quasi)analytical solutions available in limiting cases. Osmotic permeability was determined in separate experiments.

Systematic studies have been carried out at various NaCl concentrations for two different types of membrane. The new method was validated via comparison with the literature and also with measurements by well-established techniques, so it can be used for systematic characterization of ion-exchange membranes.

## Acknowledgements

This work has been performed within the scope of RED-Heat-to-Power project (Conversion of Low Grade Heat to Power through closed loop Reverse Electro- Dialysis) - Horizon 2020 Programme, Grant Agreement n. 640667.

## Appendix A. Supplementary data

Supplementary data to this article can be found online at https://doi.org/10.1016/j.memsci.2019.05.012.

## References

[1] T. Luo, S. Abdu, M. Wessling, Selectivity of Ion Exchange Membranes: A Review, (2018), https://doi.org/10.1016/j.memsci.2018.03.051.
[2] M. Micari, M. Bevacqua, A. Cipollina, A. Tamburini, W. Van Baak, T. Putts, G. Micale, E ff ect of di ff erent aqueous solutions of pure salts and salt mixtures in reverse electrodialysis systems for closed-loop applications, J. Membr. Sci. 551 (2018) 315–325, https://doi.org/10.1016/j.memsci.2018.01.036.
[3] A. Tamburini, M. Tedesco, A. Cipollina, G. Micale, M. Ciofalo, M. Papapetrou, W. Van Baak, A. Piacentino, Reverse electrodialysis heat engine for sustainable power production, Appl. Energy 206 (2017) 1334–1353, https://doi.org/10.1016/j.apenergy.2017.10.008.
[4] M. Reig, X. Vecino, C. Valderrama, O. Gibert, J.L. Cortina, Separation and Puri fi cation Technology Application of selectrodialysis for the removal of as from metallurgical process waters : recovery of Cu and Zn, Separ. Purif. Technol. 195 (2018) 404–412, https://doi.org/10.1016/j.seppur.2017.12.040.
[5] M. Reig, S. Casas, C. Valderrama, O. Gibert, J.L. Cortina, Integration of monopolar and bipolar electrodialysis for valorization of seawater reverse osmosis desalination brines : production of strong acid and base, DES 398 (2016) 87–97, https://doi.org/10.1016/j.desal.2016.07.024.
[6] T. Rijnaarts, N.T. Shenkute, A. Wood, W.M. De Vos, K. Nijmeijer, Divalent cation removal by donnan dialysis for improved reverse electrodialysis (2018), https://doi.org/10.1021/acssuschemeng.8b00879.
[7] C. Agarwal, R.W. Cattrall, S.D. Kolev, Donnan dialysis based separation of gold ( III ) from electronic waste solutions using an anion exchange pore- fi lled membrane, J. Membr. Sci. 514 (2016) 210–216, https://doi.org/10.1016/j.memsci.2016.04.033.
[8] A.N. Naik, C. Agarwal, S. Chaudhury, A. Goswami, Non-stationary radiotracer method for diffusion coefficients of Cs , Ba , Eu tracers in Nafion-117 membrane, 6395 (2016), https://doi.org/10.1080/01496395.2016.1256324.
[9] R. Bernstein, Y. Kaufman, V. Freger, Membrane characterization, Encycl. Membr. Sci. Technol. (2013) 41, https://doi.org/10.1002/elan.
[10] G.M. Geise, B.D. Freeman, D.R. Paul, Sodium chloride diffusion in sulfonated polymers for membrane applications, J. Membr. Sci. 427 (2013) 186–196, https://doi.org/10.1016/j.memsci.2012.09.029.
[11] V. Freger, A. Ben-David, Use of attenuated total reflection infrared spectroscopy for analysis of partitioning of solutes between thin films and solution, Anal. Chem. 77 (2005) 6019–6025, https://doi.org/10.1021/ac050689w.
[12] A. Ben-David, Y. Oren, V. Freger, Thermodynamic factors in partitioning and rejection of organic compounds by polyamide composite membranes, Environ. Sci. Technol. 40 (2006) 7023–7028, https://doi.org/10.1021/es0609912.
[13] A. Ben-David, S. Bason, J. Jopp, Y. Oren, V. Freger, Partitioning of organic solutes between water and polyamide layer of RO and NF membranes: correlation to rejection, J. Membr. Sci. 281 (2006) 480–490, https://doi.org/10.1016/j.memsci.2006.04.017.
[14] A. Ghoufi, E. Dražević, A. Szymczyk, Interactions of organics within hydrated selective layer of reverse osmosis desalination membrane: a combined experimental and computational study, Environ. Sci. Technol. 51 (2017) 2714–2719, https://doi.org/10.1021/acs.est.6b05153.
[15] X. Zhang, D.G. Cahill, O. Coronell, B.J. Mariñas, Partitioning of salt ions in FT30 reverse osmosis membranes, Appl. Phys. Lett. 91 (2007), https://doi.org/10.1063/1.2802562.
[16] B. Mi, B.J. Mariñas, D.G. Cahill, RBS characterization of arsenic(III) partitioning from aqueous phase into the active layers of thin-film composite NF/RO membranes, Environ. Sci. Technol. 41 (2007) 3290–3295, https://doi.org/10.1021/es062292v.
[17] J. Wang, R.S. Kingsbury, L.A. Perry, O. Coronell, Partitioning of alkali metal salts

and boric acid from aqueous phase into the polyamide active layers of reverse osmosis membranes, Environ. Sci. Technol. 51 (2017) 2295–2303, https://doi.org/10.1021/acs.est.6b04323.
[18] I. Nicotera, C. Simari, L.G. Boutsika, L. Coppola, K. Spyrou, A. Enotiadis, NMR investigation on nanocomposite membranes based on organosilica layered materials bearing different functional groups for PEMFCs, Int. J. Hydrogen Energy 42 (2017) 27940–27949, https://doi.org/10.1016/j.ijhydene.2017.05.014.
[19] R. Mueller, V. Hariharan, C. Zhang, R. Lively, S. Vasenkov, Relationship between mixed and pure gas self-diffusion for ethane and ethene in ZIF-8/6FDA-DAM mixed-matrix membrane by pulsed field gradient NMR, J. Membr. Sci. 499 (2016) 12–19, https://doi.org/10.1016/j.memsci.2015.10.036.
[20] E. Drazevic, S. Bason, K. Kosutic, V. Freger, Enhanced partitioning and transport of phenolic micropollutants within polyamide composite membranes, Environ. Sci. Technol. 46 (2012) 3377–3383, https://doi.org/10.1021/es204188j.
[21] J. Kamcev, D.R. Paul, G.S. Manning, B.D. Freeman, Accounting for frame of reference and thermodynamic non-idealities when calculating salt diffusion coefficients in ion exchange membranes, J. Membr. Sci. 537 (2017) 396–406, https://doi.org/10.1016/j.memsci.2017.05.034.
[22] A. Cañas, M.J. Ariza, J. Benavente, Characterization of active and porous sublayers of a composite reverse osmosis membrane by impedance spectroscopy , streaming and membrane potentials, salt diffusion and X-ray photoelectron spectroscopy measurements 183 (2001) 135–146.
[23] R.S. Kingsbury, S. Zhu, S. Flotron, O. Coronell, Microstructure determines water and salt permeation in commercial ion-exchange membranes, ACS Appl. Mater. Interfaces 10 (2018) 39745–39756, https://doi.org/10.1021/acsami.8b14494.
[24] A. Goswami, A. Acharya, A.K. Pandey, Membrane (2001) 9196–9201, https://doi.org/10.1021/jp010529y.
[25] V. Compan, M.L. Lopez, T.S. Soerensen, J. Garrido, Transport numbers in the surface layers of asymmetric membranes from initial time measurements, J. Phys. Chem. 98 (1994) 9013–9021, https://doi.org/10.1021/j100087a033.
[26] V. Compañ, T.S. Sorensen, S.R. Rivera, Comparison of initial time and stationary state measurements of the emf of concentration cells using phenolsulfonic acid membrane separators (1995) 12553–12558.
[27] V. Compañ, T.S. Sorensen, A. Andrio, D. Abajo, Transport numbers from initial time and stationary state measurements of EMF in non-ionic polysulphonic membranes, 8 (1997) 7–10.
[28] A. Yaroshchuk, Y. Boiko, A. Makovetskiy, Electrochemical perm-selectivity of active layers and diffusion permeability of supports of an asymmetric and a composite NF membrane studied by concentration-step method, Desalination 245 (2009) 374–387, https://doi.org/10.1016/j.desal.2009.02.001.
[29] A.E. Yaroshchuk, A.L. Makovetskiy, Y.P. Boiko, E.W. Galinker, Non-steady-state membrane potential: theory and measurements by a novel technique to determine the ion transport numbers in active layers of nanofiltration membranes, J. Membr. Sci. 172 (2000) 203–221.
[30] A. Yaroshchuk, X. Martínez-Lladó, L. Llenas, M. Rovira, J. de Pablo, Solution-diffusion-film model for the description of pressure-driven trans-membrane transfer of electrolyte mixtures: one dominant salt and trace ions, J. Membr. Sci. 368 (2011) 192–201, https://doi.org/10.1016/j.memsci.2010.11.037.
[31] W.J. Hamer, Y.-C. Wu, Osmotic coefficients and mean activity coefficients of uni-univalent electrolytes in water at 25 °C, J. Phys. Chem. Ref. Data 1 (1972) 1047–1100.
[32] A. Yaroshchuk, O. Zhukova, M. Ulbricht, V. Ribitsch, Electrochemical and other transport properties of nanoporous track-etched membranes studied by the current switch-off technique (2005) 6872–6882, https://doi.org/10.1021/la050499g.
[33] A.E. Yaroshchuk, V. Ribitsch, The uses of non-steady-state membrane characterisation techniques for the study of transport properties of active layers of nanofiltration membranes : theory with experimental examples, Chem. Eng. J. 80 (2000) 203–214.
[34] A. Narebska, S. Koter, W. Kujawski, Irreversible thermodynamics of transport across charged membranes. Part I - macroscopic resistance coefficients for a system with Nafion 120 membrane, J. Membr. Sci. 25 (1985) 153–170.
[35] J. Kamcev, E.S. Jang, N. Yan, D.R. Paul, B.D. Freeman, Effect of ambient carbon dioxide on salt permeability and sorption measurements in ion-exchange membranes, J. Membr. Sci. 479 (2015) 55–66, https://doi.org/10.1016/j.memsci.2014.12.031.
[36] G.M. Geise, H.J. Cassady, D.R. Paul, E. Logan, M.A. Hickner, Specific ion effects on membrane potential and the permselectivity of ion exchange membranes, Phys. Chem. Chem. Phys. 16 (2014) 21673–21681, https://doi.org/10.1039/C4CP03076A.
[37] A. Narębska, S. Koter, W. Kujawski, Ions and water transport across charged nafion membranes. Irreversible thermodynamics approach, Desalination 51 (1984) 3–17, https://doi.org/10.1111/j.1467-9353.2006.00281.x.
[38] E.H. Cwirko, R.G. Carbonell, Ionic equilibria in ion-exchange membranes: a comparison of pore model predictions with experimental results, 67 (1992) 211–226, https://doi.org/10.1016/0376-7388(92)80026-g.
[39] R.S. Kingsbury, S. Flotron, S. Zhu, D.F. Call, O. Coronell, Junction potentials bias measurements of ion exchange membrane permselectivity, Environ. Sci. Technol. 52 (2018) 4929–4936, https://doi.org/10.1021/acs.est.7b05317.
[40] W. Kujawski, A. Narebska, Transport of electrolytes across charged membranes. Part IV. Frictional interactions of the neutral and alkaline permeants and the permeability/reflection phenomena* 56 (1991), pp. 99–112.

## *Further reading*

[41] A.E. Yaroshchuk, Negative rejection of ions in pressure-driven membrane processes, Adv. Colloid Interface Sci. 139 (2008) 150–173, https://doi.org/10.1016/j.cis.2008.01.004.

# CHAPTER 8

# Results

# 8. Results

The most relevant results of each chapter are discussed below.

## 8.1 Key findings in concentration polarization inhomogeneity

A review of CFD studies simulating the flow and CP in narrow rectangular channels show inhomogeneous CP distribution over the membrane surface. However, this fact has been disregarded in the previous studies and simulation results are frequently reported in terms of Sherwood number (or mass-transfer coefficient) averaged over the membrane surface.

The consequences of neglecting the inhomogeneity of CP can be illustrated postulating a probability distribution-function of unstirred-layer thickness and using a locally 1D description of CP. This simple approach allows determining an effective unstirred-layer thickness that would correspond to the average permeate concentration assuming that there is no distribution of extent of CP.

The obtained effective thickness of unstirred-layer is function of solute rejection, Péclet number and probability-distribution function. For illustration purposes, the results were obtained using a specific probability-distribution function (log-normal distribution), although it was also seen that the conclusions are valid for a broader range of distribution functions.

According to this analysis, averaging local unstirred-layer thickness is correct in the limiting case of weak CP ($Pe \to 0$). However, averaging local Sherwood number (inversely proportional to the unstirred-layer thickness) is incorrect even in this limiting case.

The averaging of Sherwood number underestimated the average impact of even weak inhomogeneous CP amplifying the contribution of zones with the weakest CP. In the particular case of log-normal distribution function, it was found that the averaging of Sherwood number underestimates the extent of weak CP by a factor of almost 3.

At finite Péclet numbers, even the arithmetic averaging is incorrect. This analysis shows that at moderate to strong CP, the effective unstirred-layer thickness depends strongly on the solute intrinsic rejection, trans-membrane volume flux and solute diffusion coefficient. Disregarding the CP inhomogeneity over the membrane surface under-estimates the CP of strongly positively-rejected solutes and over-estimates the CP for the negatively-rejected ones. This is explained by the fact that the poorly-stirred zones, where the unstirred-layer

thickness is larger than the average value of unstirred-layer thickness, contribute disproportionally to the trans-membrane flux of solute depending on the sign of the rejection. In the case of strongly-rejected solutes, the over-proportionally accumulation of solutes within poorly-stirred zones increase the average concentration at the membrane surface. Similarly, the concentration of negatively-rejected solutes is reduced and tends to zero within poorly-stirred zones, so it makes under-proportional contribution to the trans-membrane flux of such solutes. The differences in the effective thicknesses of unstirred-layer between the highest positive and the negative rejections were as large as four to six times for the broader distribution function.

This approach was also tested with a CFD-generated probability-density function of local Sherwood number and the obtained results are qualitatively similar to the ones obtained for the broader log-normal distribution. Some even more pronounced deviations were obtained in the case of CFD-generated distribution since it is still broader than the log-normal distribution function used previously.

This study shows that irrespective of the specific form of probability distribution function (if sufficiently broad), using a single value of unstirred-layer thickness (or mass- transfer coefficient) does not reflect the considerable dependence of overall CP on the intrinsic solute rejection, diffusion coefficient and trans-membrane flux. This is especially problematic in the case of several solutes with very different intrinsic rejections as for example in the NF of multi-ionic solutions, where simultaneous positive and negative rejections typically occur.

It is desirable to reduce the inhomogeneity of CP to a minimum in test-cell devices since this inhomogeneity is difficult to take into account in the interpretation of experimental data to obtain reliable information on the membrane transport properties.

## 8.2 Key findings in rotating disk-like membrane

A novel design of test cell with equally-accessible membrane surface has been developed based on the rotating disk electrode combined with the possibility of applying trans-membrane hydrostatic pressure differences of up to 20 bar. Implementing the classical configuration of infinite rotating disk into a pressure-driven test cell implies some deviations from the ideal case geometry due to the sealing at the edge of the membrane. CFD simulation allow quantifying the impact of deviations from the ideal geometry in the distribution of unstirred-layer thickness of the test cell designed.

Results showed that the effective thickness remains practically constant up to the vicinity of the sealing ring where it increases. This is logical since the geometry and flow pattern deviates considerably in this point due to the existence of a peripheral ring used to seal the membrane. The numerical results are close to the theoretical predictions obtained by using Levich formula. The deviations are around 4% as a maximum, which may be related to different definitions of effective unstirred-layer thickness in this study and the theoretical analysis by Levich.

The simulations became unstable at higher rotation speeds. The largest velocity gradients occur close to the external periphery of the rotating body whereas they remain limited near to the central part of the membrane. This seems to indicate that instabilities occur primarily in the regions located far away from the membrane surface, not affecting directly the equal-accessibility.

In view of the CFD simulations results, membrane filtration close to the sealed membrane edge need to be excluded to avoid the impact of deviations in this zone on the permeate composition. To that end, a narrow external plastic ring was placed at the peripheral membrane part. Then, the system was also validated experimentally by measuring the observed rejection dependence on rotation speed for a single salt (0.01M $MgCl_2$). Then, the observed rejection can be corrected for CP by means of Levich formula used to estimate the unstirred-layer thickness. Observed rejection increased with rotation speed whereas intrinsic rejection remained practically constant which demonstrates that the designed test cell is equally-accessible.

Test cell performance was tested in a number of experiments using singles salts and electrolyte mixtures as feed solutions and correcting for CP by using Levich formula for the

effective thickness of unstirred-layer. The results obtained are comparable to previous studies carried out with a test cell GE SEPA™ CF II at similar trans-membrane volume fluxes.

Besides, SDEM model was used to fit experimental intrinsic rejections as a function of trans-membrane flux and to determine membrane permeance to dominant salt and trace ions in each case. For $NH_4^+$ as trace ion, the permeance was only possible to determine for dominant $MgSO_4$, whereas in the other cases ion rejection became insensitive to model parameters so in those cases the ion permeance could only be estimated by the order of magnitude. The same occurred for $Na^+$ traces with dominant $MgCl_2$. The results were compared with the literature and their consistency and relation with NF separation mechanisms was discussed. The obtained sequence in membrane permeance to dominant salt were qualitatively in agreement with the results published in the literature. The differences in membrane permeances of cations and anions of the dominant salt give rise to the spontaneously arising electric fields that strongly influence the rejection of trace ions. Due to the action of those fields, ion rejections were not directly correlated with the ion permeances in some cases.

Finally, the ion rejection of binary mixtures of NaCl and $MgCl_2$ was also studied. In this case, the intrinsic rejections were fitted using an analytical solution to the equation of solution-diffusion-electromigration transport of ions for a system of three ions of different charges. Ionic permeances were determined for different compositions. It was observed that increasing $MgCl_2$ molar fraction increased strongly the permeance to $Na^+$ whereas it decreased for $Mg^{2+}$. $Cl^-$ permeance also increased with the addition of $MgCl_2$ until it reached a constant value.

## 8.3 Key findings in transient membrane potential after concentration step

A novel approach of non-stationary diffusion measurements under conditions of relatively small concentration differences allows a relatively simple determination of effective salt diffusion and partitioning coefficients in addition to the ion perm-selectivity, which is the only parameter obtained in conventional stationary measurements of membrane potential.

The potential difference after the concentration step remains constant for a relatively long period. This is because in macroscopically homogeneous membranes transmembrane electric-potential difference is independent of shape of salt-concentration profile. Accordingly, the time-dependent signal evolution begins only when the salt concentration at the membrane/support interface starts to change. The salt chemical potential at the

membrane/support interface remain practically constant until the chemical capacity of the adjacent part of the support is noticeably charged. The initial period of constant signal is relatively long because the diffusion occurs through a large chemical resistance (thin and relatively dense ion-exchange membrane) into a large chemical capacity (porous and thick support). Ionic perm-selectivity can be estimated from the initial potential difference.

After the initial period, there is a progressive redistribution of applied concentration difference between the membrane and the porous support due to the difference in the ion perm-selectivities, so the potential difference becomes time-dependent. The signal relaxation is primarily controlled by the diffusion permeability of the membrane but is also affected by the salt partitioning coefficient. Moreover, it was found that osmotic trans-membrane volume transfer has a considerable impact on the relaxation process. Therefore, osmosis was determined in separate measurements and it was included in the mathematical description. The developed model allowed fit the experimental time-dependent membrane potential and determining the salt diffusion coefficient, partition coefficient, salt transmission coefficient and perm-selectivity.

The novel approach presented was validated in two different ways. First, some measurements were performed for a well-known membrane (Nafion 120) and the obtained results were compared with the literature. Then, the same procedure was used with two novel membranes (Type 10 Fujifilm CEM/AEM) and the results were compared with the ones obtained by such a well-established technique as the classical salt-diffusion measurements based on time-dependence of salt concentration in the receiving compartment. Additionally, perm-selectivity was also determined alternatively by the stationary membrane potential method for Type Fujifilm membranes.

In all the cases, the results obtained by means of transient membrane potential after concentration step were in good agreement with either the literature or the alternative established technique since the maximum deviations were below 10%.

The effect of variation of base concentration was studied in the concentration range between 0.05M and 1M NaCl keeping always the concentration of step solution always two times higher than the base solution concentration.

There were increasing trends in both partitioning and effective salt diffusion coefficients with the base concentration, whereas the opposite trend was observed for perm-selectivity. This

is in agreement with the mechanism of Donnan exclusion of co-ions from ion-exchange materials.

The decrease in electrochemical perm-selectivity with concentration is reflected in the decrease of initial membrane potential (in absolute value) with concentration. Moreover, the increase in diffusion permeability with concentration due to the weaker Donnan exclusion of coions manifest itself in the decrease of the characteristic relaxation time with concentration.

Transmission coefficient did not show a pronounced dependence on salt concentration (it only presented a slightly increasing in the case of cation-exchange membranes whereas remained roughly constant for anion-exchange membranes). This is in disagreement with the Donnan-exclusion model, although a qualitatively similar behavior was also observed in the literature with Nafion 120. Moreover, the sensitivity of relaxation pattern to salt transmission coefficient is weak since it is primarily controlled by diffusion permeability. Therefore, the determination of salt transmission coefficient is less reliable than diffusion permeability and perm-selectivity.

Besides, this approach was also applied to non-conventional electrolyte solutions such as LiCl and KOAc. Different trends were obtained depending on the nature of fixed charge of the membrane. For CEM, the order observed in partition and diffusion coefficients was: LiCl<NaCl<KOAc. As for perm-selectivity, the results obtained for LiCl and NaCl were very similar whereas the values obtained for KOAc were considerably lower. The opposite trends were obtained with AEM. In the case of perm-selectivity, greater differences among the different electrolyte solutions were obtained compared to the case of CEM.

Finally, the effect of temperature was studied using NaC as electrolyte solution. Logically, increasing the temperature increased the effective salt diffusion coefficient. For the salt partition coefficient, there were not observed clear trends whereas perm-selectivity decreased with temperature, although the effect was especially pronounced for CEM.

## 8.4 Key findings in influence of membrane sealing in pressure-driven processes

In pressure-driven membrane test cells, there is a peripheral part at the edge of the membrane that is supported directly by impermeable cell body (instead of a permeate spacer) due to the need of membrane sealing.

To study the effect of having the membrane supported by an impermeable surface, several experiments were performed with a cross-flow test cell (GE SEPA™ CF II) where the membrane was hydraulically blocked from beneath by using different size plastic sheets. Trans-membrane flux of pure water was only slightly reduced despite of the fact that membrane area exposed was decreased between 5 to 20 times. Therefore, these results confirmed that there is trans-membrane filtration through membrane along the membrane support even if the membrane is supported by an impermeable surface.

Mass-transfer in such zones is expected to be much worse and poorly reproducible, so CP in such zones can make a disproportionally larger contribution to the trans-membrane solute transfer, compromising dramatically the test cell performance.

# CHAPTER 9

# Conclusions

# 9. Conclusions

Membrane characterization is essential in membrane research and development since a better understanding of the membrane structure, chemistry, morphology or transport mechanisms allows improving new membrane preparation and processes optimization.

Optimization of membrane performance depends on a large number of parameters that need to be accurately determined, so there is a wide variety of characterization techniques. Moreover, there is a continuous improving and expansion of methods for membrane characterization motivated by the constant growth of membrane technologies.

This thesis is focused on two specific issues of membrane separation processes. In pressure-driven membrane processes, a review of the literature shows that one of the most problematic factors that need to be controlled is CP. On the other hand, it is seen that optimization of electro-membrane processes based on ion-exchange membranes requires detailed information on the transport and equilibrium properties of ion exchange membranes. In particular, separate information on the partitioning and diffusivity properties of the membrane with respect to ions.

The principal conclusion of this thesis are:

1. It was showed that there is a considerable distribution of extent of CP over the membrane surface especially in spacer-filled channels, usually disregarded in the studies found in the literature. The consequences of disregarding this fact were qualitatively illustrated by postulating a probability distribution of unstirred-layer thickness over the membrane surface and using a locally 1D description of CP. In view of the complexity of Inhomogeneous CP on the interpretation of experimental data, it is desirable to reduce this inhomogeneity to a minimum in the membrane test-cell.

2. A novel RDM design with equally-accessible membrane surface was developed. It was proven that the condition of having the same extent of CP over the whole membrane surface is satisfied in the developed set-up via numerical simulations and experimental results. The new cell utility was demonstrated performing experiments using single salts and electrolyte mixtures and the obtained results were corrected for CP by using Levich equation (widely-used in electrochemistry) to estimate the effective thickness of unstirred layer. Moreover, SDEM was used to fit ion rejection dependence on trans-

membrane flux and the ionic permeances were determined. The obtained results are semi-quantitatively similar to those obtained with the same NF membrane and feed solutions in other pressure-driven studies using a commercial test cell (GE SEPA™ CF II).

The novel membrane cell can be used for a systematic characterization of transport properties of NF/RO membranes and the obtained information can be used as input in the modelling of performance of practical membrane modules.

3. A novel approach to studies of non-stationary diffusion (tracked via transient membrane potential) under conditions of relatively small concentration differences was developed. A mathematical model was developed to interpret the time-dependent electric-potential signal measured experimentally. It allows for a relatively simple determination of effective salt diffusion and partitioning coefficients in addition to the ion perm-selectivity, which is the only parameter provided by conventional stationary measurements of membrane potential. It was observed that osmotic trans-membrane volume transfer has a considerable impact on the measured signal relaxation, so osmotic permeability was measured in separate experiments and osmosis was included in the mathematical model. This model was validated via comparison with (quasi)analytical solutions available in limiting cases. Moreover, the new approach was validated via comparison with the literature for a well-known membrane and also by using well-established techniques in the case of two novel membranes. The developed approach can be used for systematic characterization of ion-exchange membranes.

The new procedures developed in this thesis can be used for systematic characterization of transport properties of NF/RO and ion-exchange membranes and the obtained information may be useful as input in the modelling of membrane performance.

# ANNEX 1

# Publication 5

*"Nanofiltration of multi-ion solutions: quantitative control of concentration polarization and interpretation by solution-diffusion-electro-migration model"*

# Nanofiltration of multi-ion solutions: quantitative control of concentration polarization and interpretation by solution-diffusion-electro-migration model

Marc Fernández de Labastida[1,2], Andriy Yaroshchuk[3,4]

[1]Department of Chemical Engineering, Polytechnic University of Catalonia – BarcelonaTech, C/ Eduard Maristany 10-14 (Campus Diagonal-Besòs), 08930, Barcelona, Spain

[2]Barcelona Research Center on Multiscale Science and Engineering, C/ Eduard Maristany, 10-14 (Campus Diagonal-Besòs), 08930, Barcelona, Spain

[3]Department of Chemical Engineering, Polytechnic University of Catalonia – BarcelonaTech, av. Diagonal 647, 08028 Barcelona, Spain

[4]ICREA, Passeig Lluís Companys 23, Barcelona, Spain

## Abstract

For effective use of advanced engineering models of nanofiltration quality of experimental input is crucial especially in electrolyte mixtures where simultaneous rejections of various ions may be very different. In particular, this concerns quantitative control of concentration polarization (CP). This work used a novel design of test cell with equally-accessible membrane surface (rotating disk-like membrane) so the CP extent was the same over the whole membrane surface. This condition, that is not satisfied in conventional membrane test cell, made possible correcting for CP easily even in multi-ion systems.

Ion rejections were studied experimentally for several dominant salts (NaCl, $MgCl_2$, $Na_2SO_4$ and $MgSO_4$) and trace ions ($Na^+$, $NH_4^+$, $Cl^-$ and $NO_3^-$) using NF270 membrane. The solution-diffusion-electro-migration model was used to obtain ion membrane permeance from the experimental data. Experimental data could be well fitted by the model except in the case of $NH_4^+$. Correlations between the ion permeances and type of dominant salt are discussed in the context of established mechanisms of NF such as Donnan and dielectric exclusion. The obtained information contributes to systematic transport characterization of NF membranes and can be ultimately useful for the CFD modelling of performance of membrane modules in various applications.

*Keywords:* concentration polarization, ion rejection, unstirred-layer thickness, ionic permeance, solution-diffusion-electromigration model

# 1. Introduction

A considerable effort has been devoted to NF modelling and several approaches can be found in the literature [1–7]. Nonetheless, the complexity of transport mechanisms of nanofiltration (NF) makes difficult development of predictive models, especially in the case of multi-electrolyte solutions containing both mono and divalent ions.

In general, there are two kinds of transport models of NF: mechanistic models and irreversible thermodynamics descriptions [1]. The former usually use the concept of nanoporous materials in which ion exclusion (steric, electric and dielectric) and hindered diffusion and convection occur [2,6]. These models are based on macroscopic approaches probably applicable for the description of ultrafiltration but questionable if applied to sub-nanopores. Besides, they rely on chemical and physical characterization of the membranes that is challenging.

On the other hand, irreversible thermodynamics uses only phenomenological coefficients to describe ion fluxes in terms of gradients of ion electrochemical potentials and trans-membrane volume flow. This treatment combined with some assumptions leads to simplified models such as Spiegler-Kedem [4,7], extended Spiegler-Kedem [8], solution-diffusion [9] or solution-diffusion-electromigration [10].

Due to the complexity of mechanistic modelling, advanced engineering models based on irreversible thermodynamics seem to remain the approach of choice for practical NF modelling [1]. Even though they do not assume any (microscopic) physical ion exclusion mechanism, they should take into account principal macroscopic physico-chemical phenomena using a limited number of fitting parameters obtainable from a well-defined set of experiments. Thus for instance, solution-diffusion-electromigration model (SDEM) of NF accounts for the ion transport due to trans-membrane electric fields that spontaneously arise owing to different membrane permeances to cations and anions [10]. This approach has been extensively tested [11–15] and demonstrated to reproduce several observed experimental trends using a limited number of adjustable parameters.

Including convection to the SDEM ion transport mechanisms would extend the applicability scope of this engineering model. However, this would also double the number of adjustable parameters since the transmission coefficients would be added to the ionic permeances for each ion. Unambiguous determination of this increased number of model parameters relies on the accuracy of experimental data. An important factor to control is concentration polarization (CP) in membrane test cells.

In a major part of membrane test cells for pressure-driven processes the extent of CP is inhomogeneous. Disregarding this fact can lead to considerable underestimation or overestimation of impact of CP depending on the sign of solute rejection [16]. Therefore, CP inhomogeneity can have a considerable impact on the determination of membrane transport properties from experimental data especially in the case of very different simultaneous rejections in multi-ion solutions. Meanwhile, in the previous studies using SDEM the thickness of unstirred layer was used as a single adjustable parameter for the description of rejection of all the solutes (dominant salts as well as trace ions).

To address this issue, a novel design of rotating disk-like membrane test cell with equally-accessible surface of a flat-sheet membrane has been developed [17]. Numerical simulations and experimental validation demonstrated the same extent of CP over the whole membrane surface. Once this condition is satisfied, it is easy to decouple the external mass transfer problem from that of transmembrane transport. This is highly desirable considering the complexity of transport phenomena in NF since coupled models involve too many adjustable parameters and uncertainties. The set-up was used previously for the CP-correction of observable ion rejections obtained in NF with a commercial NF membrane. However, the intrinsic ion rejections were previously not interpreted by using a model.

In this work, such an interpretation is carried out by using the SDEM model. As a result, ion permeances are determined from the experimental data obtained with the RDM cell by using a commercial NF270 membrane and various feed solutions consisting of a dominant salt and trace ions. The effect of kind of dominant salt on ion permeance is investigated and discussed.

# 2. Experimental materials and methods

## *2.1 Materials*

All experimental data was obtained with polyamide thin-film composite NF membrane NF-270 (Dow Chemical Company, USA). Membranes were mechanically supported by sintered stainless steel disc of 25mm in diameter and average pore size of 40 μm (GKN Sintered Metals, Germany). The chemical reagents used to prepare feed aqueous solutions in the experiments were of analysis grade.

## *2.2 Experimental set-up and operation procedure*

The experimental setup and procedures were described in [17].

## *2.3 Experimental design*

**Table 1** shows the feed concentration of salts in each experiment. Experimental measurements were repeated to check reproducibility.

**Table 1**

**Concentration experimental design**

| Experiment | Dominant salt | Trace salt | Feed concentration (mol/L) | |
|---|---|---|---|---|
| | | | Dominant salt | Trace salt |
| 1 | NaCl | $NH_4Cl + NaNO_3$ | 0.01 | $2 \cdot 10^{-4}$ |
| 2 | $MgCl_2$ | | | |
| 3 | $Na_2SO_4$ | | | |
| 4 | $MgSO_4$ | | | |

# 3. Theory

## *3.1 Solution-diffusion-electromigration model*

The SDEM is an advanced engineering model based on a (reduced) irreversible thermodynamics approach that describes ion rejections as a function of trans-membrane flux using membrane permeances to the ions of the dominant and trace salts as model parameters.

For the description of concentration polarization, we use the model of unstirred layer. In the particular case of RDM cell, this model has been demonstrated to be quantitatively applicable [17] (in contrast to any other cell configuration) while the thickness of the CP layer can be estimated by using Levich equation [18]:

$$\delta \approx 1.61 \cdot \left(\frac{D}{\nu}\right)^{1/3} \cdot \sqrt{\frac{\nu}{2\pi \cdot \left(\frac{N}{60}\right)}} \text{ (m)} \quad (1)$$

where

$\nu$ : kinematic viscosity ($m^2/s$)

$D$ : solute diffusion coefficient ($m^2/s$)

$N$ : rotation speed (rpm)

The observed rejections measured experimentally can be corrected for CP as described in [17] by solving the following system of first-order ordinary differential equations:

$$\frac{dc_i}{d\xi} = \left(c_i - c_{ip}\right) \cdot Pe_i - Z_i c_i \cdot \frac{\sum_j^n Z_j \cdot (c_j - c_{jp}) \cdot Pe_j}{\sum_j^n Z_j^2 c_j} \quad (2)$$

where

$$Pe_{i,j} \equiv \frac{J_v \cdot \delta}{D_i} \quad (3)$$

$\xi$ is the coordinate normalized by the unstirred layer thickness, $D_i$ is the ionic diffusion coefficient, $Z_i$ is the charge of each ion, $c_i$ is ionic concentration, $J_v$ is the trans-membrane flow flux and $c_{ip}$ are the permeate concentrations. Eq. (2) gives as a result the

concentrations of all the ions at the membrane surface, $c_{im}$, which allows to calculate intrinsic rejections as:

$$R_s^{int} = 1 - \frac{C_{ip}}{C_{im}} \quad (4)$$

This approach automatically accounts for the coupling between the ion flows within the unstirred layers via spontaneously-arising electric fields. This procedure is valid provided that (as in this test cell) the membrane surface is equally accessible so the permeate concentrations are the same over the whole membrane area. If this is not the case, the permeate composition is a result of mixing permeates of different composition depending on the local extent of CP.

The intrinsic rejections estimated for each ion allow obtaining the necessary model parameters to calculate ionic permeances by means of SDEM. First, the intrinsic rejection of dominant salt is fitted to obtain the membrane permeance to the dominant salt, Ps:

$$R_s^{int} = \frac{\frac{J_v}{P_s}}{1+\frac{J_v}{P_s}} \quad (5)$$

Then, intrinsic reciprocal transmissions of trace ions, $f_t$, are fitted to Eq. (6) as functions of reciprocal intrinsic transmission of dominant salt, $f_s$:

$$f_t = (f_s)^b + K \cdot \left(\frac{f_s-(f_s)^b}{1-b}\right) \quad (6)$$

where

$$f_s = \frac{1}{1-R_s^{int}} \quad (7)$$

$$f_t = \frac{1}{1-R_t^{int}} \quad (8)$$

Finally, permeances to ions of dominant salt ($P_{\pm}$) and permeances to trace ions ($P_t$ ) can be estimated as:

$$P_{\pm} = \frac{P_s}{1-\left(\frac{z_+}{z_-}\right)\cdot b} \quad (9)$$

$$P_t = \frac{P_s}{K} \quad (10)$$

# 4. Results and discussion

## *4.1 Rejection of ions from electrolyte mixtures*

This section discusses the membrane permeances to ions estimated from a set of experiments using several single dominant salts (NaCl, $MgCl_2$, $Na_2SO_4$ or $MgSO_4$) and trace salts ($NaNO_3$ and/or $NH_4Cl$). The intrinsic rejections calculated via the CP correction from the results obtained in a previous work [17] are fitted to the SDEM model to determine membrane permeances to dominant salts and ion permeances in each case. The results are compared with the literature and their consistency and relation with NF separation mechanisms are discussed.

**Table 2** presents the membrane permeances to dominant salt and the permeance obtained for each ion from the fitting of experimental data to the SDEM model. It can be seen a notable difference between the experiments where $SO_4^{2-}$ was the dominant anion with respect to the cases where $Cl^-$ was the dominant anion. $SO_4^{2-}$ is a highly rejected ion, so for $Na_2SO_4$ and $MgSO_4$ the membrane permeance to dominant salt is an order of magnitude lower than for the experiments with dominant NaCl and $MgCl_2$ that are moderate rejected salts.

**Table 2**

**Membrane permeance to dominant salt and membrane permeance to each ion depending on dominant salt**

| Dominant salt | Ps (µm/s) | Ion permeance (µm/s) | | | | | |
|---|---|---|---|---|---|---|---|
| | | $Na^+$ | $Mg^{2+}$ | $NH_4^+$ | $Cl^-$ | $NO_3^-$ | $SO_4^{2-}$ |
| NaCl | 7.5 | 20-113 | - | >60 | 3.9 | 13.8 | - |
| $MgCl_2$ | 6.1 | >250 | 3.7 | >700 | 9.3 | 16.9 | - |
| $Na_2SO_4$ | 0.16 | >0.8 | - | >100 | 3.4 | 9.8 | 0.06 |
| $MgSO_4$ | 0.23 | 79.4 | 0.9 | 80 | 15.7 | 41.9 | 0.13 |

**Fig. 1** shows the reciprocal intrinsic transmissions of the dominant salt NaCl and $NH_4^+$ and $NO_3^-$ as trace ions. The symbols represent experimental data whereas the lines correspond to the SDEM fits. The experimental data for the dominant salt are in a relatively good agreement with the model (predicting linear dependence) with exception of the highest trans-membrane flux (55 µm/s). Similar situation is observed for the traces, although in the case of $NH_4^+$ the deviations start at a lower trans-membrane flux (35 µm/s) and are more pronounced than in the case of dominant salt. Actually, modelling for $NH_4^+$ became insensitive to the value of ionic permeance as this increased, so it was not possible to estimate an exact value in this case.

**(a)**

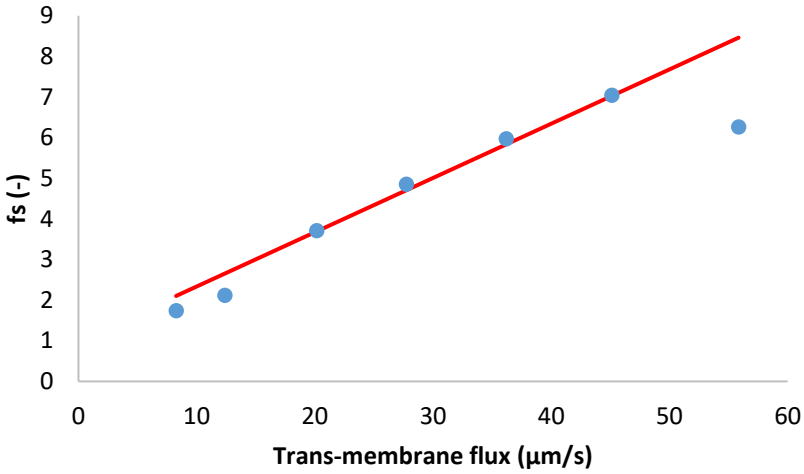


**(b)**

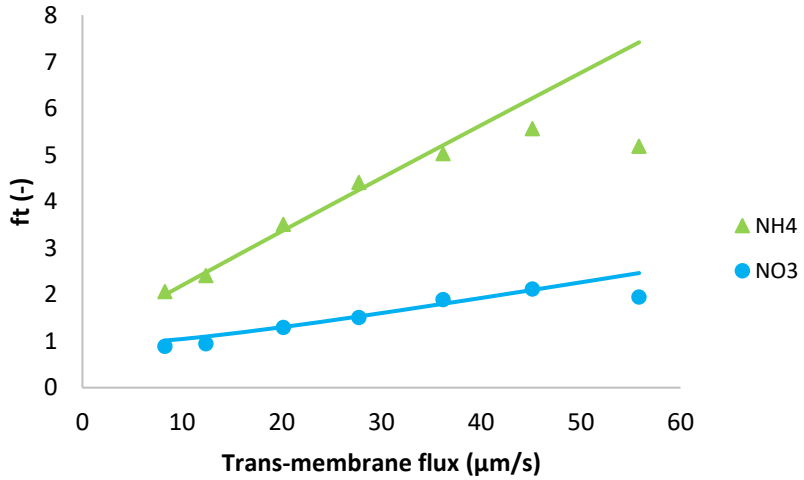


**Fig. 1** Reciprocal intrinsic transmissions as functions of trans-membrane volume flux for: (a) dominant salt NaCl and (b) trace ions $NH_4^+$ and $NO_3^-$

Both dominant salt and $NH_4^+$ trace were well-rejected as can be seen in **Fig. 1,** their rejections being between 40% and 80% (f=1.7-5.0). $NO_3^-$ trace experienced negative intrinsic rejections at low trans-membrane fluxes (-10%, corresponding to reciprocal intrinsic transmissions smaller than 1), that became positive (up to 50% (f=2)) as trans-membrane flux increased. Negative rejections are due to spontaneously arising trans-membrane electric fields induced owing to different membrane permeances to cations and anions of the dominant salt. These fields accelerate or decelerate the transport of ions through the membrane depending on the sign of their charge to keep the electric current equal to zero. In the case of dominant NaCl solution, the membrane is less permeable to $Cl^-$ than to $Na^+$ (see **Table 2**), which is expectable given that NF270 is negatively charged. The resulting electric field enhances the transport of $NO_3^-$ so slightly negative rejections occur at low trans-membrane fluxes due to the fact that the permeance to $NO_3^-$ is noticeably higher than that to $Cl^-$. Finally, $NO_3^-$ rejections turn positive when the electromigration $NO_3^-$ flux tends to saturation while the permeate gets ever more diluted due to the linear increase in the trans-membrane volume.

Reig et al. [15] studied the effect of dominant NaCl feed concentration on the removal of $NH_4^+$ and $NO_3^-$ traces. The authors observed that increasing dominant salt concentration decreased the rejection of dominant salt and trace ions. In agreement with this, the membrane permeance to dominant salt determined in the present study (at a lower concentration) is lower than the value reported by Reig et al.

In the next case study, the dominant salt was $MgCl_2$ and $Na^+$, $NH_4^+$ and $NO_3^-$ were the trace ions. **Fig. 2** shows the model fit of the experimental data. Similarly to the previous case, for the dominant salt there are some deviations between the experimental data and the modelling curves. However, the quality of linear fit is quite good.

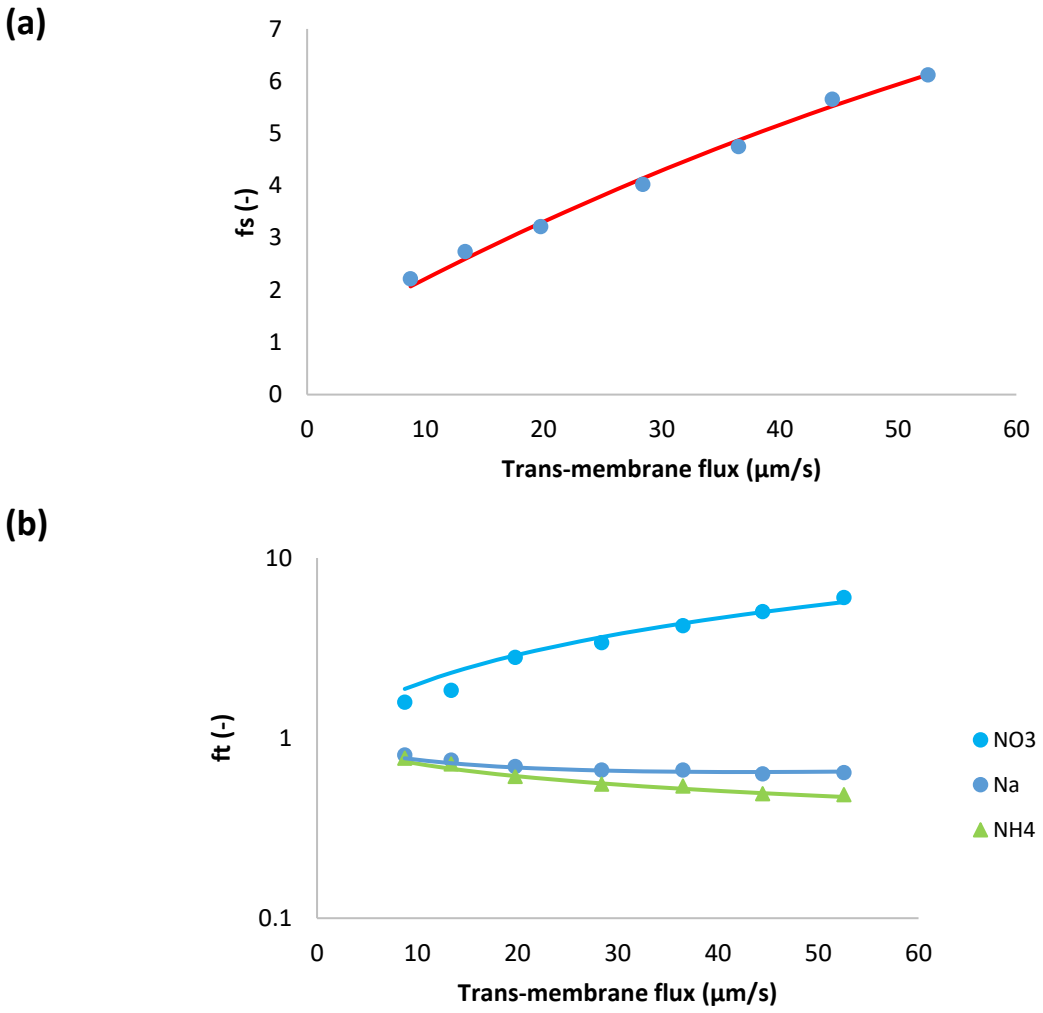


**Fig. 2** Reciprocal transmission as a function of trans-membrane flux for: (a) dominant salt $MgCl_2$ and (b) trace ions $Na^+$ ,$NH_4^+$ and $NO_3^-$

In this case, the presence of a divalent cation leads to the opposite situation compared with the previous case. The membrane permeance to $Mg^{+2}$ is lower than to $Cl^-$ (see **Table 2**), so the spontaneously arising electric field accelerates the transport of cations. As a result, $Na^+$ and $NH_4^+$ were negatively rejected whereas $NO_3^-$ rejection was positive as can be seen in **Fig. 2**.

$MgCl_2$ dominant salt rejections (between 45% and 90% (f=2.22-11.92)) are higher than those of NaCl, which is expectable considering that dielectric exclusion is stronger in electrolytes with double-charge ions. Accordingly, the membrane permeance to $MgCl_2$ is lower than to NaCl (**Table 2**). Due to the better rejection of $MgCl_2$ (the larger difference in the permeances between $Mg^{2+}$ and $Cl^-$, and much higher ion permeances for both trace

cations) in this case the cationic traces experience quite pronounced negative rejections: $Na^+$ intrinsic rejections were between -24% and -100% (f=0.80-0.49) and for $NH_4^+$ they ranged from -30% to -175% (f=0.77-0.36). Similarly to the previous case, for both $NH_4^+$ and $Na^+$ the fitted ion rejections were rather insensitive to the assumed values of ion permeances so these could only be determined by the order of magnitude. Nonetheless, they are clearly by an order of magnitude larger than in the case of dominant NaCl. This may be due to a much stronger exclusion of $Mg^{2+}$ ions from the membrane phase than that of $Cl^-$. As demonstrated in [19] such preferential exclusion of cations gives rise to the appearance of an inter-phase electrostatic-potential difference that can enhance the partitioning of other cations (including monovalent) into the membrane phase and can considerably increase the membrane permeance to them.

On the other hand, $NO_3^-$ was much better rejected than in the presence of NaCl as the dominant salt (intrinsic rejections were between 37%-85% (f=1.59-6.49)), which is expectable given that the electric field retards the passage of this ion through the membrane in dominant $MgCl_2$.

Pagès et al. [14] studied $MgCl_2$ as a dominant salt and a number of trace ions using a higher feed solution concentration (0.1M) than the one used in this work. The authors reported a membrane permeance to dominant salt around 2 μm/s, which is lower than the one estimated in this work at a lower feed solution concentration. Unlike the case of dominant NaCl, this trend is in disagreement with the simple Donnan rejection mechanism but has already been reported in other studies for $MgCl_2$ [20] as well as for $CaCl_2$ [3]. A possible explanation for this as a result of combination of impact of unequal ion exclusion from the membrane and its negative surface charge has been put forward in [21].

The last two cases ($Na_2SO_4$ and $MgSO_4$) have in common the divalent anion $SO_4^{2-}$. The membrane permeance to this ion is much lower than the permeance to either of the dominant cations (see **Table 2**). Therefore, in both cases the transport of trace anions is enhanced by the spontaneously-arising electric fields whereas that of trace cations is retarded. In these cases, trace ions could not be considered genuine traces due to the very high rejections of $SO_4^{2-}$. Accordingly, the reciprocal transmission of the more permeable ion (such as $Na^+$ in $Na_2SO_4$) could be essentially lower than that for $SO_4^{2-}$ because the trans-membrane passage of anion traces partially contributed to the fulfilment of zero electric current condition.

**Fig. 3** shows the reciprocal transmission of the dominant $Na_2SO_4$ and traces of $NH_4^+$, $Cl^-$ and $NO_3$. The dominant salt and $NH_4^+$ trace are highly rejected: $SO_4^{2-}$ rejections are above 99.7% (f=356-812) and for $Na^+$ and $NH_4^+$, the intrinsic rejections are between 96% and 99% (f=28-172). Notably, in situations of a very strong asymmetric in the permeances to the dominant cation and anions (like in the case of $Na_2SO_4$), the determination of permeance of the more permeable ion (such as $Na^+$ in $Na_2SO_4$) becomes very imprecise since its variation does not influence the salt permeance. Accordingly, the value of $Na^+$ permeance in this case is just illustrative. The situation with $NH_4^+$ is similar.

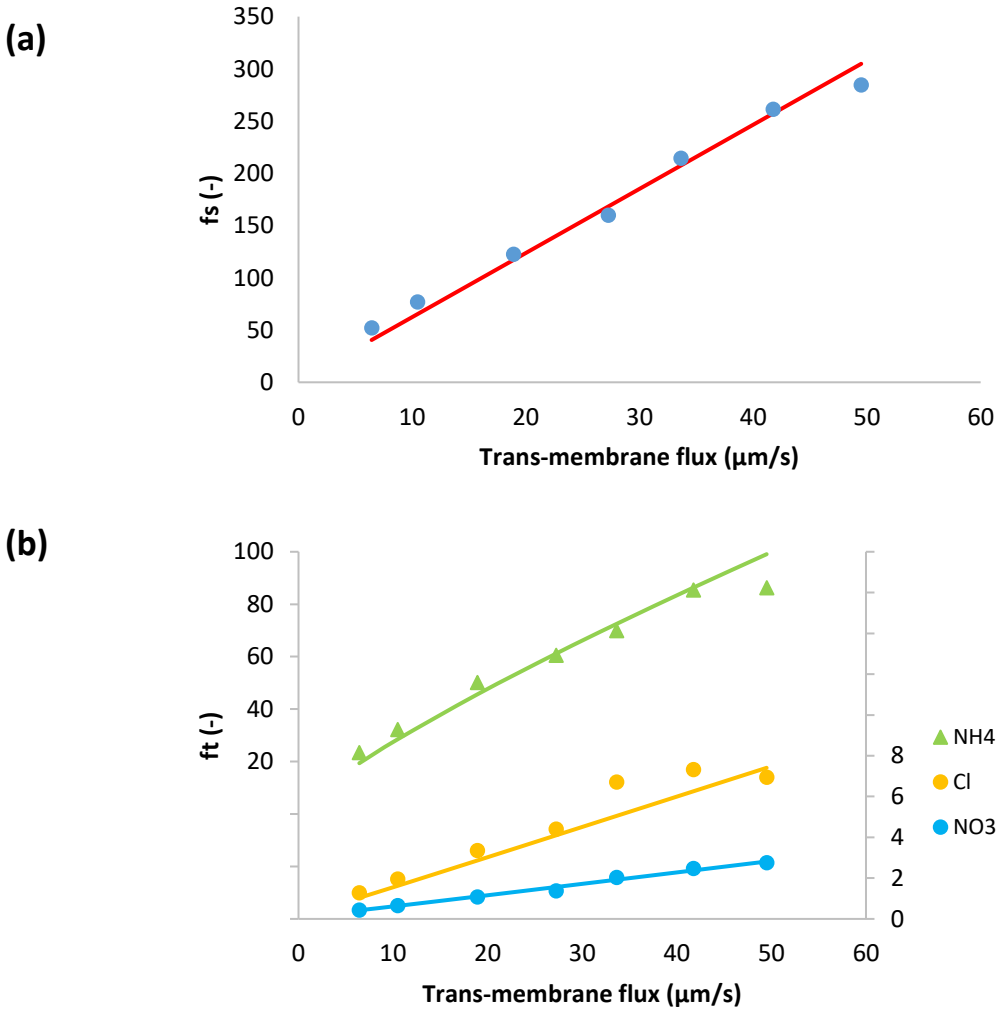


**Fig. 3** Reciprocal transmission as a function of trans-membrane flux for: (a) dominant salt $Na_2SO_4$ and (b) trace ions $NH_4^+$, $Cl^-$ and $NO_3^-$

As for the trace anions, $NO_3^-$ presented initially pronounced negative rejections (-131% or f=0.43) that turned to positive reaching a maximum value of 63% (f=2.76) while $Cl^-$ was positively rejected in all the trans-membrane flux range studied (between 21% and 85% or f=1.27-6.95).

Such behavior of trace $NO_3^-$ is primarily explained by the very high rejection of dominant salt (and very strong asymmetry in the permeances to the dominant cations and anions). Due to these factors, the spontaneously-arising electric fields are very strong already at quite low trans-membrane volume flows (hence, initially pronounced negative rejections). At the same time, these fields tend to saturation already at still relatively low fluxes, which gives rise to the rapid change to the positive rejections of trace $NO_3^-$. Comparison of behavior of traces of $NO_3^-$ and $Cl^-$ in this case shows that occurrence of negative rejections also requires the trace anion to have a certain minimum permeance, which is largely surpassed by $NO_3^-$ but not reached by $Cl^-$ (hence, the lack of negative rejections for it).

The last case studied is $MgSO_4$ as dominant salt with $Na^+$, $NH_4^+$, $Cl^-$ and $NO_3^-$ as trace ions (**Fig. 4**). The dominant salt was highly rejected as in the previous case and the trace cations were well rejected, too: $Mg^{2+}$ rejection is between 96% and 99% (f=25-138), $SO_4^{2-}$ is above 99% (f=136-360) and $Na^+$, $NH_4^+$ traces rejections ranged between 74% to 87% (f=3.8-7.8). Concerning the trace anions, both of them exhibited negative rejections: $Cl^-$ was negatively rejected at low trans-membrane flux (-70%) and increased up to 60% (f=0.59-2.31) while for $NO_3^-$ rejections were negative in all the range of trans-membrane fluxes studied (between -151% and -5% (f=0.40-0.95)). To fit these more pronounced negative rejections by the model we had to assume noticeably higher ion permeances for the trace single-charge anions than in the case of dominant $Na_2SO_4$. Remarkably, the ratio of permeances to $NO_3^-$ and $Cl^-$ for all the studied cases was roughly around 3.

**(a)**

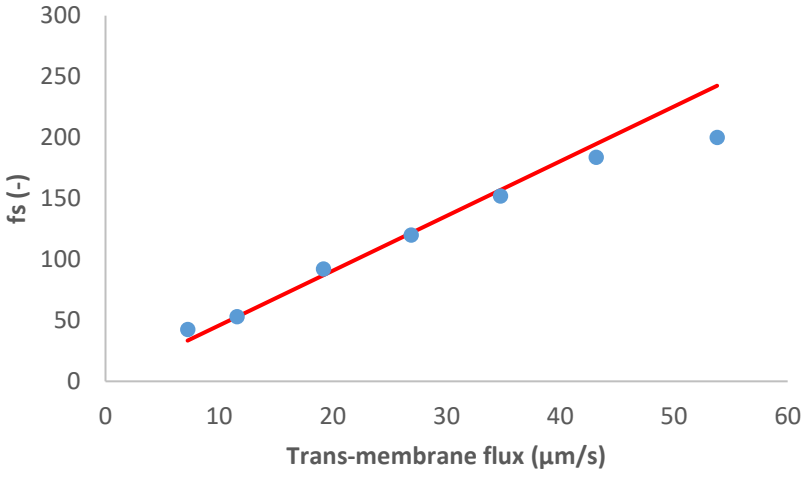


**(b)**

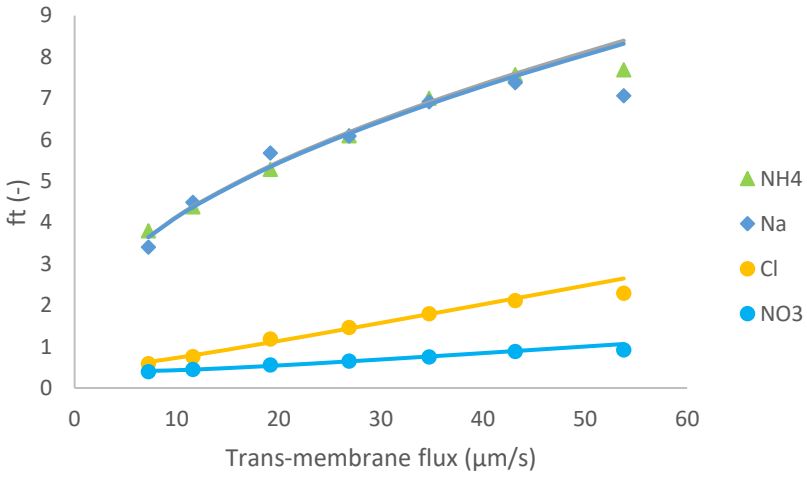


**Fig. 4** Reciprocal transmission as a function of trans-membrane flux for: (a) dominant salt $MgSO_4$ and (b) trace ions $Na^+$, $NH_4^+$, $Cl^-$ and $NO_3^-$

The obtained sequence of membrane permeances to dominant salt is in qualitative agreement with the published results for negatively charged membranes [14,22]. It can be explained by a combination of Donnan and dielectric exclusion of ions. Donnan exclusion is due to the interactions of ions with fixed electric charges. Dielectric exclusion is caused by interactions betweeen charged solutes and bound charges induced by them at pore surfaces due to different dielectric constants of membrane matrix and liquid inside pores [23]. Donnan exclusion is stronger for double-charge coions (ions whose charge sign coincide with that of fixed charges) while dielectric exclusion is much stronger for double-charge ions irrespective of sign of their charge. This explains the much lower membrane

permeance to $Na_2SO_4$ than to NaCl. Dielectric exclusion alone would give rise to a still stronger exclusion of $MgSO_4$ than of $Na_2SO_4$. However, the double-charged $Mg^{2+}$ may well strongly bind to the negative surface charge thus reducing its magnitude and that of the Donnan exclusion. Likely for that reason, the membrane permeance to $MgSO_4$ was somewhat higher than to $Na_2SO_4$.

$Na^+$ and $Cl^-$ were studied both as dominant and trace ions. In the cases where $Na^+$ was part of a dominant salt (NaCl, $Na_2SO_4$) lower values of permeances were obtained. The lowest permeance to $Na^+$ corresponds to $Na_2SO_4$, which is expectable given that it is strongly affected by dielectric exclusion in this case. Indeed, the interphase potential attracting $SO_4^{2-}$ ions to the membrane phase (to make their concentration stoichiometric to that of $Na^+$) simultaneously expulses positively-charged $Na^+$ [19]. In the case of dominant $MgCl_2$, the situation is opposite, namely, the interphase potential (arising due to the different extents of dielectric exclusion for $Mg^{2+}$ and $Cl^-$) attracts cations to the membrane phase in this case making the permeance to sodium ions high. Finally, in the case of $MgSO_4$ the extent of dielectric exclusion for both dominant ions is roughly the same so the additional trace $Na^+$ attraction to the membrane phase does not occur and the permeance to it is lower, accordingly.

Regarding $Cl^-$, the highest permeance was obtained for it when added as a trace to dominant $MgSO_4$. This could be explained by the presence of a divalent cation, which reduced the Donnan exclusion of anions (see above). Qualitatively the same could explain the relatively large permeance to $Cl^-$ as a part of dominant $MgCl_2$. The $Cl^-$ permeances are surprisingly close in the cases of dominant NaCl and $Na_2SO_4$. Given the very different patterns of interaction of dominant anions with the membrane in these two cases, this seems to be rather a result of accidental compensation of counteracting trends characteristic of Donnan and dielectric exclusion.

$NH_4^+$ and $NO_3^-$ were trace ions in all the experiments. For the $NH_4^+$ traces, the fitted permeances in most cases were so high that the rejections became insensitive to the permeance to this ion. Accordingly, only lower limits for the permeances could be determined. Just for the dominant $MgSO_4$ the fitting procedure allowed to estimate a specific value for the $NH_4^+$ permeance. Even though the permeances could not be determined accurately, the results seem to indicate that the highest permeance occurred in $MgCl_2$, which could have the same mechanisms as in the case of traces of $Na^+$ (see above).

In the case of dominant $Na_2SO_4$, the asymmetry of dielectric exclusion of dominant cations and anions was in favor of the latter. Accordingly, the interphase potential repulsed cations (including traces of $NH_4^+$) from the membrane phase, hence the lower permeance. Overall, the permeances to $NH_4^+$ seem to be noticeably larger than those to $Na^+$, which is rather difficult to explain by simple mechanisms given, for example, the very close hydrated radii of those two ions in aqueous solutions. Apparently, some more subtle phenomena related to different details of interaction of these two ions with water and membrane matrix are in play.

The dependence of permeances to $NO_3^-$ on the kind of dominant salt roughly followed that observed for $Cl^-$ but the nitrate permeances on average were around 3 times larger. Again, this is rather difficult to explain by simple mechanisms given the very close hydrated radii of those two ions in aqueous solutions. Like in the case of $NH_4^+$ vs. $Na^+$, subtler mechanisms seem to be in play.

## 5. Conclusions

Modelling NF processes is a difficult task due to the complexity of transport phenomena. Inhomogeneous distribution of CP over the membrane surface complicates the task additionally. Therefore, unambiguous determination of model parameters from experimental data requires quantitative control of CP.

The effect of valence type of dominant salt on the rejection of single-charge trace cations and anions was studied using the RDM cell with equally accessible membrane surface developed previously. In this way, the CP extent was the same over the whole membrane surface.

SDEM allowed fitting experimental data and determining membrane permeances to ions except for trace $NH_4^+$. In that case, the ion rejection became insensitive to the exact values so the permeance could only be estimated in one of the studied cases (dominant $MgSO_4$).

The results obtained in terms of membrane permeances to the dominant salts are in qualitative agreement with those obtained in other studies with the same NF membrane and feed solutions by using the GE SEPA™ CF II test cell.

It was confirmed once again that the differences between the membrane permeances to the dominant salt ions give rise to spontaneously arising electric fields that strongly influence the trace ion rejections. Due to the action of those fields, ion rejections are not directly correlated with the ion permeance in most cases. At the same time, they can be quantitatively related to them by using the SDEM model.

## List of symbols

$b$: parameter in Eq. (5)

$c_i$ : ionic concentration

$c_m$ : surface membrane concentration

$c_{ip}$ : ionic permeate concentration

$D$ : diffusion coefficient of the salt

$D_i$ : ionic diffusion coefficient

$f_s$: intrinsic reciprocal transmission of dominant salt

$f_t$: intrinsic reciprocal transmission of trace ions

$J_V$ : trans-membrane flux

$K$: parameter in Eq. (5)

$N$ : rotation speed (rpm)

$P_{\pm}$: ionic permeances to single ions of dominant salts

$P_s$: permeance to the dominant salt

$P_t$: permeance to trace ions

$Pe_i$ : ionic Péclet number

$R_s^{int}$ : intrinsic rejection of the dominant salt

$R_t^{int}$ : intrinsic rejection of the trace ion

$Z_i$: charge of ion

*Greek letters*

$\delta$ : thickness of concentration polarization layer

$\xi$: coordinate normalized by the local unstirred layer thickness

ν : kinematic viscosity

## Acknowledgements

The authors gratefully acknowledge support from the project Waste2Product (CTM2014-57302-R) and by the R2MIT (CTM2017-85346-R) funded by the Spanish Ministry of Economy and Competitiveness (MINECO) and the Catalan Government (2017-SGR-312).

## References

[1] A. Yaroshchuk, M.L. Bruening, E. Zholkovskiy, Modelling nanofiltration of electrolyte solutions, Adv. Colloid Interface Sci. 268 (2019) 39–63. doi:10.1016/j.cis.2019.03.004.

[2] P. Ortiz-albo, R. Ibañez, A. Urtiaga, I. Ortiz, Phenomenological prediction of desalination brines nanofiltration through the indirect determination of zeta potential, Sep. Purif. Technol. (2018). doi:10.1016/j.seppur.2018.08.066.

[3] N. Fridman-bishop, K.A. Tankus, V. Freger, Permeation mechanism and interplay between ions in nano fi ltration, J. Memb. Sci. 548 (2018) 449–458. doi:10.1016/j.memsci.2017.11.050.

[4] S.S. Wadekar, R.D. Vidic, Insights into the rejection of barium and strontium by nanofiltration membrane from experimental and modeling analysis, J. Memb. Sci. 564 (2018) 742–752. doi:10.1016/j.memsci.2018.07.060.

[5] A.W. Mohammad, Y.H. Teow, W.L. Ang, Y.T. Chung, D.L. Oatley-Radcliffe, N. Hilal, Nanofiltration membranes review: Recent advances and future prospects, Desalination. 356 (2015) 226–254. doi:10.1016/j.desal.2014.10.043.

[6] K. Thibault, H. Zhu, A. Szymczyk, G. Li, The averaged potential gradient approach to model the rejection of electrolyte solutions using nanofiltration: Model development and assessment for highly concentrated feed solutions, Sep. Purif. Technol. 153 (2015) 126–137. doi:10.1016/j.seppur.2015.08.041.

[7] S. Anisah, M. Kanezashi, H. Nagasawa, T. Tsuru, Hydrothermal stability and permeation properties of TiO2-ZrO2 (5/5) nanofiltration membranes at high temperatures, Sep. Purif. Technol. 212 (2019) 1001–1002. doi:10.1016/j.seppur.2018.12.006.

[8] A.L. Ahmad, M.F. Chong, S. Bhatia, Mathematical modeling and simulation of the multiple solutes system for nanofiltration process, J. Memb. Sci. 253 (2005) 103–115. doi:10.1016/j.memsci.2005.01.005.

[9] A. Yaroshchuk, X. Martínez-Lladó, L. Llenas, M. Rovira, J. de Pablo, Solution-diffusion-film model for the description of pressure-driven trans-membrane transfer of electrolyte mixtures: One dominant salt and trace ions, J. Memb. Sci. 368 (2011) 192–201. doi:10.1016/j.memsci.2010.11.037.

[10] A. Yaroshchuk, M.L. Bruening, E. E. Licon Bernal, Solution-Diffusion–Electro-Migration model and its uses for analysis of nano fi ltration , pressure-retarded osmosis and forward osmosis in multi-ionic solutions, J. Memb. Sci. 447 (2013) 463–476. doi:10.1016/j.memsci.2013.07.047.

[11] J. Lopez, M. Reig, O. Gibert, C. Valderrama, J.L. Cortina, Evaluation of NF membranes as treatment technology of acid mine drainage: metals and sulfate removal, Desalination. 440 (2018) 122–134. doi:10.1016/j.desal.2018.03.030.

[12] J. López, M. Reig, A. Yaroshchuk, E. Licon, O. Gibert, J.L. Cortina, Experimental and theoretical study of nanofiltration of weak electrolytes: SO42–/HSO4–/H+ system, J. Memb. Sci. 550 (2018) 389–398. doi:10.1016/j.memsci.2018.01.002.

[13] A. Yaroshchuk, M.L. Bruening, An analytical solution of the solution-diffusion-electromigration equations reproduces trends in ion rejections during nanofiltration of mixed electrolytes, J. Memb. Sci. 523 (2017) 361–372. doi:10.1016/j.memsci.2016.09.046.

[14] N. Pagès, M. Reig, O. Gibert, J.L. Cortina, Trace ions rejection tunning in NF by selecting solution composition: Ion permeances estimation, Chem. Eng. J. 308 (2017) 126–134. doi:10.1016/j.cej.2016.09.037.

[15] M. Reig, E. Licon, O. Gibert, A. Yaroshchuk, J.L. Cortina, Rejection of ammonium and nitrate from sodium chloride solutions by nanofiltration: Effect of dominant-salt concentration on the trace-ion rejection, Chem. Eng. J. 303 (2016) 401–408. doi:10.1016/j.cej.2016.06.025.

[16] M. Fernández de Labastida, E.E. Licon Bernal, A. Yaroshchuk, Implications of inhomogeneous distribution of concentration polarization for interpretation of pressure-driven membrane measurements, J. Memb. Sci. 520 (2016) 693–698. doi:10.1016/j.memsci.2016.08.040.

[17] M. Fernández de Labastida, E.E. Licón Bernal, M. Bondarenko, A. Yaroshchuk, Rotating disk-like membrane cell for pressure-driven measurements with equally-accessible membrane surface: Numerical simulation and experimental validation, J. Memb. Sci. 550 (2018) 492–501. doi:10.1016/j.memsci.2017.10.057.

[18] V.G. Levich, R.J. Seeger, Physicochemical Hydrodynamics, Am. J. Phys. 31 (1963). doi:10.1119/1.1969158.

[19] A.E. Yaroshchuk, Non-steric mechanism of nanofiltration: Superposition of donnan and dielectric exclusion, Sep. Purif. Technol. 22–23 (2001) 143–158. doi:10.1016/S1383-5866(00)00159-3.

[20] G.M. Geise, D.R. Paul, B.D. Freeman, Fundamental water and salt transport properties of polymeric materials, Prog. Polym. Sci. 39 (2014) 1–42. doi:10.1016/j.progpolymsci.2013.07.001.

[21] A. Yaroshchuk, Y. Zhu, M. Bondarenko, M.L. Bruening, Deviations from Electroneutrality in Membrane Barrier Layers: A Possible Mechanism Underlying High Salt Rejections, Langmuir. 32 (2016) 2644–2658. doi:10.1021/acs.langmuir.5b04588.

[22] J.V. Nicolini, C.P. Borges, H.C. Ferraz, Selective rejection of ions and correlation with surface properties of nanofiltration membranes, Sep. Purif. Technol. 171 (2016) 238–247. doi:10.1016/j.seppur.2016.07.042.

[23] A.E. Yaroshchuk, Dielectric exclusion of ions from membranes, Adv. Colloid Interface Sci. 85 (2000) 193–230. doi:10.1016/S0001-8686(99)00021-4.

# ANNEX 2

# Publication 6

*"Interaction between $Na^+$ and $Mg^{2+}$ in electrolyte mixtures during nanofiltration with equally-accessible surface"*

# Interaction between $Na^+$ and $Mg^{2+}$ in electrolyte mixtures during nanofiltration with equally-accessible surface

Marc Fernández de Labastida[1,2], Andriy Yaroshchuk[3,4]

[1]Department of Chemical Engineering, Polytechnic University of Catalonia – BarcelonaTech, C/ Eduard Maristany 10-14 (Campus Diagonal-Besòs), 08930, Barcelona, Spain

[2]Barcelona Research Center in Multiscale Science and Engineering, C/ Eduard Maristany, 10-14 (Campus Diagonal-Besòs), 08930, Barcelona, Spain

[3]Department of Chemical Engineering, Polytechnic University of Catalonia – BarcelonaTech, av. Diagonal 647, 08028 Barcelona, Spain

[4]ICREA, Passeig Lluís Companys 23, Barcelona, Spain

## Abstract

The complexity of transport mechanisms occurring in nanofiltration membranes difficult the development of predictive modelling of ion rejection, especially in multi-ion solutions. In this work, the ion rejection of electrolyte mixtures of NaCl and $MgCl_2$ of different compositions is studied using a commercial NF270 membrane. A novel design of rotating disk-like membrane with equally accessible surface previously developed was used to perform the experiments. Due to the equal accessibility, concentration polarization can be easily corrected even for multi-ion systems. The obtained intrinsic rejections are fitted using an analytical solution to the equations governing the solution-diffusion-electromigration transport of the ions of binary salt mixtures with a common ion. In this way, the ionic permeances were determined from experimental data as a function of feed composition. It was observed that increasing $MgCl_2$ molar fraction increased strongly the permeance to $Na^+$ whereas it decreased for $Mg^{2+}$. $Cl^-$ permeance also increased with the addition of $MgCl_2$ until it reached a constant value. Advanced engineering models with a limited number of thermodynamic coefficients determined experimentally proved to be an effectively alternative to mechanistic models in NF description.

*Keywords:* concentration polarization, ion rejection, electrolyte mixture, ionic permeance, solution-diffusion-electromigration model

# 1. Introduction

Nanofiltration (NF) is an effective, commercial membrane separation process in between ultrafiltration and reverse osmosis widely used for water and wastewater treatment, pharmaceutical, biotechnology or food engineering [1]. NF most relevant characteristics are its ability to reject selectively divalent ions and organic molecules, higher permeate fluxes and low operating pressures compared with reverse osmosis. On the other hand, performance of NF membranes depends strongly on solution composition, thus ion rejection in electrolyte mixtures may turn out very different from the rejection in single-salt solutions. Due to the complexity of transport phenomena occurring in NF processes, establishing predictive modelling of ion rejection is difficult, especially in multi-ion solutions.

Numerous studies can be found in the literature addressing NF modelling through different approaches [1–7]. All of them can be classified into two kind of transport models: mechanistic models and irreversible thermodynamics description [2]. Mechanistic models commonly use the extended Nernst-Planck equation, treating NF membranes as nanoporous materials that present hindered transport of ions coupled with steric, electric and dielectric exclusion. These models may contribute to a better understanding of the ion-transport mechanism in NF since they include membrane characteristics into the physical description of phenomena. However, accurate knowledge on the physical structure and electrochemical properties of NF membranes are challenging to obtain due to the complex multi-layer structure of NF membranes. Therefore, the application of these models under realistic conditions is questionable due to the lack of accuracy on the prediction.

Conversely, irreversible thermodynamics description give rise to advanced engineering models that use only phenomenological coefficients to describe ion flux as a function of gradient of ion electrochemical potentials and trans-membrane volume flows. This treatment combined with some assumptions lead to simpler models such as Spiegler-Kedem [5,7], solution-diffusion [8] or solution-diffusion-electromigration [9]. These models proved to fit successfully experimental data and allow describing observed trends without specify any physico-chemical ion exclusion mechanism. For instance, solution-diffusion-electromigration model (SDEM) describes ion transport accounting for spontaneously arising trans-membrane electric fields in NF due to different permeances to cations and anions using ionic permeances as phenomenological coefficients obtained from a well-defined set of experiments. This

approach has been widely used [10–13] and explains several observed experimental trends using a limited number of adjustable parameters.

However, determining membrane permeances to individual ions may be difficult, even within the scope of solution-diffusion with constant ion permeances except for some specific cases. Yaroshchuk et al. developed a quasi-analytical protocol for the case of electrolyte mixtures consisting in a dominant salt and any number of traces that allows estimating ionic permeabilities [8,14]. Fridman et al. assumed a high constant value of permeability in the case of seawater as a feed solution, where the membrane permeability to monovalent ions is much higher than for the divalent ion [15].

In general, modelling require solving a system of ordinary differential equations with one degree of freedom, which involve an uncertainty iterative procedure where different combinations of fitting parameters may exist. Yaroshchuk and Bruening developed an analytical solution to the equations governing the solution-diffusion-electromigration transport of the ions from two salts that contain a common ion [16]. This analytical solution was used to calculate trends of ion fluxes, concentrations and electric fields. The authors also explored modelling of literature data for a solution containing NaCl and $CaCl_2$ with the developed analytical solution, although they did not estimate separate permeances for $Na^+$ and $Cl^-$.

A number of studies devoted to electrolyte mixtures demonstrated the complexity of the membrane separation phenomena [8,15,17–22], showing that the membrane permeance to salt and ions can vary significantly depending on the feed composition or how the increase in the molar fraction of a divalent ion may affect strongly the rejection of a monovalent ion, frequently reporting trends that are not predicted by the standard ion exclusion mechanisms. Recently, Fridman et al. used a phenomenological approach to investigate systematically NF separation of mixtures NaCl and $CaCl_2$ at different pH values [23]. The authors pointed out that the conventional ion exclusion mechanism using a mean-field approach are not sufficient.

An important factor usually disregarded is the distribution of concentration polarization (CP) over the membrane surface in the existing test cells [24]. This fact complicates the interpretation of experimental data, especially in NF of electrolyte mixtures when very different ion rejections occur simultaneously. To overcome this difficulty, a new test-cell design with a rotating disk-like membrane was developed to achieve a homogeneous distribution of CP, which allows easy corrections even in multi-ion solutions [25].

This work presents a systematic study of ion rejection dependence on feed composition for an electrolyte mixture composed of NaCl and $MgCl_2$ using a commercial NF270 membrane. Experiments were performed with a rotating disk-like membrane test cell with equally-accessible membrane surface previously developed and the observed rejections were corrected for CP. Moreover, the calculated intrinsic rejection data were modelled using an analytical solution to the equations governing the solution-diffusion-electromigration transport of the ions of binary salt mixtures with a common ion. In this way, the ion permeances were determined for each experiment, and thus their dependence on feed solution composition.

# 2. Experimental materials and methods

## *2.1 Materials*

Experiments were performed with polyamide thin-film composite NF membrane NF-270 (Dow Chemical Company, EE.UU.). Membranes were mechanically supported by sintered stainless steel disc of 25mm in diameter and average pore size of 40 µm (GKN Sintered Metals, Germany). The chemical reagents used to prepare feed aqueous solutions in the experiments were of analysis grade.

## *2.2 Experimental set-up and operation procedure*

A RDM test cell **(Fig. 1)** used to carry out the membrane filtration experiments was described previously in [25]. The flat disc membrane employed is 25mm in diameter although the effective area of filtration is reduced to 2.84 $cm^2$ ( equivalent to 19mm in diameter) since in this test cell the membrane filtration in the peripheral membrane zone need to be excluded (see details in [25]). The rotation speed was set to 1000 rpm with a variable frequency drive control in all the experiments and a digital tachometer was used to control it. Feed solution (10L) was set at a constant temperature of 20ºC ± 1ºC and pumped into the RDM cell running through a filter cartridge (100µm). After that, concentrated steam was recirculated working in a continuous mode with constant feed composition.

A new piece of membrane was used in each experiment to guarantee the same initial condition in all the measurements. The membranes were soaked in ultrapure water overnight. Before starting an experiment, the membrane was compacted to reach a steady state on the membrane hydraulic resistance avoiding any change during the experiment. First, compaction

was done with deionized water at the maximum pressure (15bar) for 1h. The water permeability was calculated during the compaction to verify that in the end it reaches a steady value. Then, the same procedure was applied thereafter with the feed solution.

Experiments were performed at a constant pump flow rate of 1.5 L/min. The trans-membrane pressure was increased from 2 to 14 bar and permeate samples were collected at each point once a steady state was reached, which was controlled measuring permeate conductivity. Feed samples were also collected initially and at the end of the experiment to check that the feed composition was constant over the experiment.

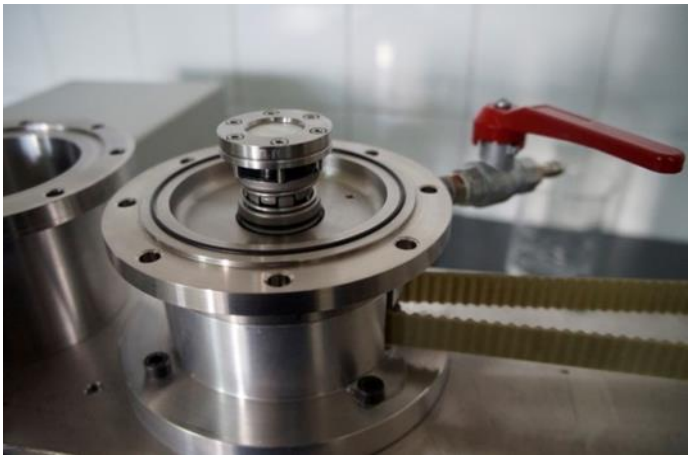

**Fig. 1** Photo of RDM cell used

## *2.3 Analytical techniques*

The conductivity was measured by a conductivity meter (GLP31, Crison) to have a rough estimate of ion rejection. Afterwards, the samples were analyzed by ionic chromatography (DIONEX ICS-1000 / ICS-1100) using two different columns, IONPAC® CS16 and IONPAC® AS23 (Dionex), to analyze cations and anions respectively.

## *2.4 Experimental design*

**Table 1** shows the feed concentration of salts in each experiment. Experimental measurements were done in duplicate to check reproducibility.

**Table 1**

**Concentration experimental design**

| Experiment | $\chi MgCl_2$ | Feed concentration (mmol/L) | | |
|---|---|---|---|---|
| | | $Na^+$ | $Mg^{2+}$ | $Cl^-$ |
| 1 | 0.1 | 21.43 | 2.38 | 26.19 |
| 2 | 0.25 | 16.67 | 5.56 | 27.79 |
| 3 | 0.375 | 13.16 | 7.89 | 28.94 |
| 4 | 0.5 | 10 | 10 | 30 |
| 5 | 0.625 | 7.14 | 11.9 | 30.94 |
| 6 | 0.75 | 4.55 | 13.64 | 31.83 |
| 7 | 0.9 | 1.72 | 15.52 | 32.76 |

# 3. Theory

## *3.1 Correction for CP in multi-ion solutions*

In this work, the use of a rotating disk-like membrane test cell guarantee that the membrane surface is equally accessible and the permeate concentration are the same over the whole membrane area. Therefore, the experimentally observed rejection can be corrected for CP within the scope of Nernst model as described in [25].

First, the thickness of CP layer is estimated using the Levich formula [26]:

$$\delta \approx 1.61 \cdot \left(\frac{D}{\nu}\right)^{1/3} \cdot \sqrt{\frac{\nu}{2\pi \cdot \left(\frac{N}{60}\right)}} \text{ (m)} \quad (1)$$

where

$\nu$ : kinematic viscosity ($m^2/s$)

$D$ : solute diffusion coefficient ($m^2/s$)

$N$ : rotation speed (rpm)

Once the thickness of CP is known, the concentration of all the ions at the membrane surface, $c_{im}$, is obtained by solving the following system of first-order ordinary differential equations:

$$\frac{dc_i}{d\xi} = \left(c_i - c_{pi}\right) \cdot Pe_i - Z_i c_i \cdot \frac{\sum_j^n Z_j \cdot \left(c_j - c_{pj}\right) \cdot Pe_j}{\sum_j^n Z_j^2 c_j} \quad (2)$$

where

$$Pe_{i,j} \equiv \frac{J_v \cdot \delta}{D_i} \quad (3)$$

$\xi$ is the coordinate normalized by the local unstirred layer thickness, $D_i$ is the ionic diffusion coefficient, $Z_i$ is the charge of each ion, $c_i$ is ionic concentration, $J_v$ is the trans-membrane flow flux and $c_{ip}$ are the permeate concentrations. Then, intrinsic rejections is calculated as:

$$R_s^{int} = 1 - \frac{C_{pi}}{C_{im}} \quad (4)$$

This approach automatically account for the coupling between the ion flows within the unstirred layers via spontaneously-arising electric fields. This procedure is only valid if the CP is homogeneously distributed over the membrane surface. If this condition is not satisfied, the permeate composition is a result of mixing of permeates of different composition depending on the local extent of CP.

### *3.2 Solution-diffusion-electromigration model*

The SDEM describes ion rejections as a function of trans-membrane flux using membrane permeance to the ions as phenomenological parameters. The analytical solution developed in [16] for three ions enables the calculation of ion rejection from ion permeance. This analytical solution may be used inversely to estimate ionic permeances from the intrinsic rejections obtained from experimental measurements after correction for CP.

The analytical solution uses the relative double ionic strength, $u$, defined as:

$$u = \frac{Z_1^2 \cdot c_1 + Z_2^2 \cdot c_2 + Z_3^2 \cdot c_3}{c_1 + c_2 + c_3} \quad (5)$$

The subscripts refer to the specific ion, $Z$ is the ion charge and $c$ is the ion concentration.

An initial value for the permeance of each ion, $P_i$, is guessed and some parameters are estimated:

$$\Pi = Z_1 \cdot Z_2 \cdot Z_3 \quad (6)$$

$$\beta_{ij} = \frac{Z_1^i \cdot (Z_2^j - Z_3^j)}{P_1} - \frac{Z_2^i \cdot \left(Z_1^j - Z_3^j\right)}{P_2} + \frac{Z_3^i \cdot (Z_1^j - Z_2^j)}{P_3} \quad (7)$$

Then, the values of relative double strength are calculated in the feed solution, $u_0$, and in the permeate solution, $u_p$, according to Eq. (5). Additionally, $F_p$ and $F_m$ are estimated as:

$$F_p = \frac{\sqrt{\left(\Pi \cdot \beta_{02} + \beta_{12} \cdot u_p\right)^2 - 4 \cdot \Pi \cdot \left(\Pi \cdot \beta_{01} + \beta_{11} \cdot u_p\right) \cdot \left(\Pi \cdot \beta_{-11} + \beta_{01} \cdot u_p\right)} - \left(\Pi \cdot \beta_{02} + \beta_{12} \cdot u_p\right)}{2 \cdot \left(\Pi \cdot \beta_{-11} + \beta_{01} \cdot u_p\right)} \quad (8)$$

$$F_m = \frac{\sqrt{\left(\Pi \cdot \beta_{02} + \beta_{12} \cdot u_p\right)^2 - 4 \cdot \Pi \cdot \left(\Pi \cdot \beta_{01} + \beta_{11} \cdot u_p\right) \cdot \left(\Pi \cdot \beta_{-11} + \beta_{01} \cdot u_p\right)} + \left(\Pi \cdot \beta_{02} + \beta_{12} \cdot u_p\right)}{2 \cdot \left(\Pi \cdot \beta_{-11} + \beta_{01} \cdot u_p\right)} \quad (9)$$

After that, the sum of the concentration of all ions in the permeate solution, $C_p$, can be calculated as:

$$C_p = C_0 \cdot \left[\frac{F_m+u_0}{F_m+u_p}\right]^{\frac{F_m}{F_p+F_m}} \cdot \left[\frac{F_p-u_0}{F_p-u_p}\right]^{\frac{F_p}{F_p+F_m}} \quad (10)$$

Finally, concentration of the specific ions in the permeate, $c_{pi}$, and trans-membrane volume flow, $J_v$, are obtained as:

$$c_{p1} = C_p \cdot \frac{u_p+Z_2 \cdot Z_3}{(Z_1-Z_2)\cdot(Z_1-Z_3)} \quad (11a)$$

$$c_{p2} = C_p \cdot \frac{u_p+Z_1 \cdot Z_3}{(Z_2-Z_1)\cdot(Z_2-Z_3)} \quad (11b)$$

$$c_{p3} = C_p \cdot \frac{u_p+Z_1 \cdot Z_2}{(Z_3-Z_1)\cdot(Z_3-Z_2)} \quad (11c)$$

$$J_v = \left(\frac{C_0}{C_p}-1\right) \cdot \frac{(Z_1-Z_2)\cdot(Z_2-Z_3)\cdot(Z_1-Z_3)}{\Pi\cdot\beta_{-11}+\beta_{01}\cdot u_p} \quad (12)$$

Ion permeances are found iteratively to match the trans-membrane volume fluxes and permeate concentration measured experimentally with the values calculated with the model.

# 4. Results and discussion

## *4.1 Ion rejection in the three-ion system*

In this section, the dependence of ion rejection on trans-membrane flux is studied for NaCl-$MgCl_2$ mixtures of different compositions **(see Table 1)**. The intrinsic rejections calculated via CP correction are fitted to the analytical solution of the SDEM model to determine the ionic permeances. Ion rejection results are presented as reciprocal transmission, $f$:

$$f = \frac{1}{1-R} \tag{13}$$

Representing the rejection results in terms of reciprocal transmissions is useful when the ion rejection barely changes with the trans-membrane volume flux. In this case, reciprocal transmission dependence on trans-membrane flux may be clearer than ion rejection.

**Fig. 2** shows the reciprocal intrinsic transmission dependence on trans-membrane flux in the limiting cases of single salts for both NaCl and $MgCl_2$ at 0.1M feed concentration [25]. There is a significant difference in the rejection between both salts: the maximum intrinsic rejection for NaCl was 75% (corresponding to f=4.4) whereas it is up to 93% (f=14) in the case of $MgCl_2$. This is explained by dielectric exclusion since it stems from the interactions between charged solutes in the equilibrium bulk solution and bound charges induced at the membrane interface due to dielectric polarization [27]. Thus, the higher charge density of $Mg^{2+}$ compared to $Na^{+}$ makes dielectric exclusion stronger for $MgCl_2$ and its rejection higher than NaCl rejection.

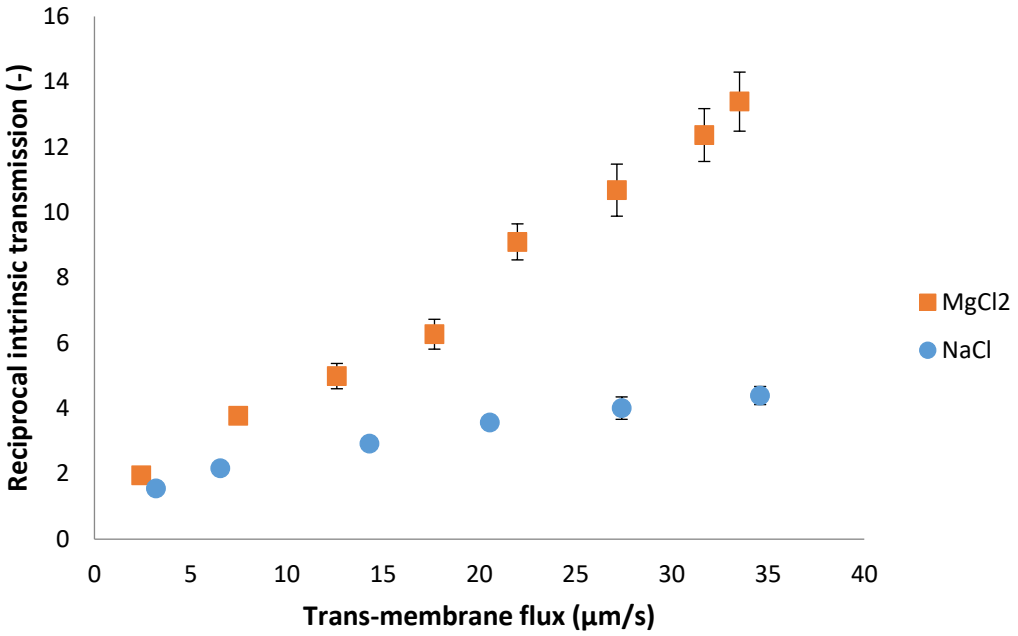


**Fig. 2** Reciprocal intrinsic transmission as a function of trans-membrane flux for NaCl and $MgCl_2$ as single salts

The rejections of cation and anion in the single salt are equal whereas in a three-ion system there are some differences due to the trans-membrane electric fields arising during the transport, so the behaviour of ion rejection is strongly influenced by those electric fields [28]. **Fig. 3** presents the reciprocal intrinsic transmission for each ion in three particular cases: dominant NaCl ($\chi_{MgCl_2} = 0.1$), equally molar mixture ($\chi_{MgCl_2} = 0.5$) and dominant $MgCl_2$ ($\chi_{MgCl_2} = 0.9$). The figure also shows the intrinsic reciprocal transmission of pure salt for comparison. In the case of dominant NaCl **(Fig. 3a)**, the intrinsic rejections for $Na^+$ and $Cl^-$ were between 15% and 80% (f=1.16-5), which are similar to the NaCl rejection as a single salt. In contrast, $Mg^{2+}$ rejection ranged from 40% to 96% (f=1.68-26.54), which is higher than its rejection as $MgCl_2$ single salt. In this situation, the spontaneously arising electric field is controlled by the difference in the membrane permeance between $Na^+$ and $Cl^-$. Since the membrane permeance to $Na^+$ is higher than to $Cl^-$ and the molar fraction of $MgCl_2$ is relatively low, the spontaneously arising electric field decelerates $Mg^{2+}$, increasing considerably its rejection.

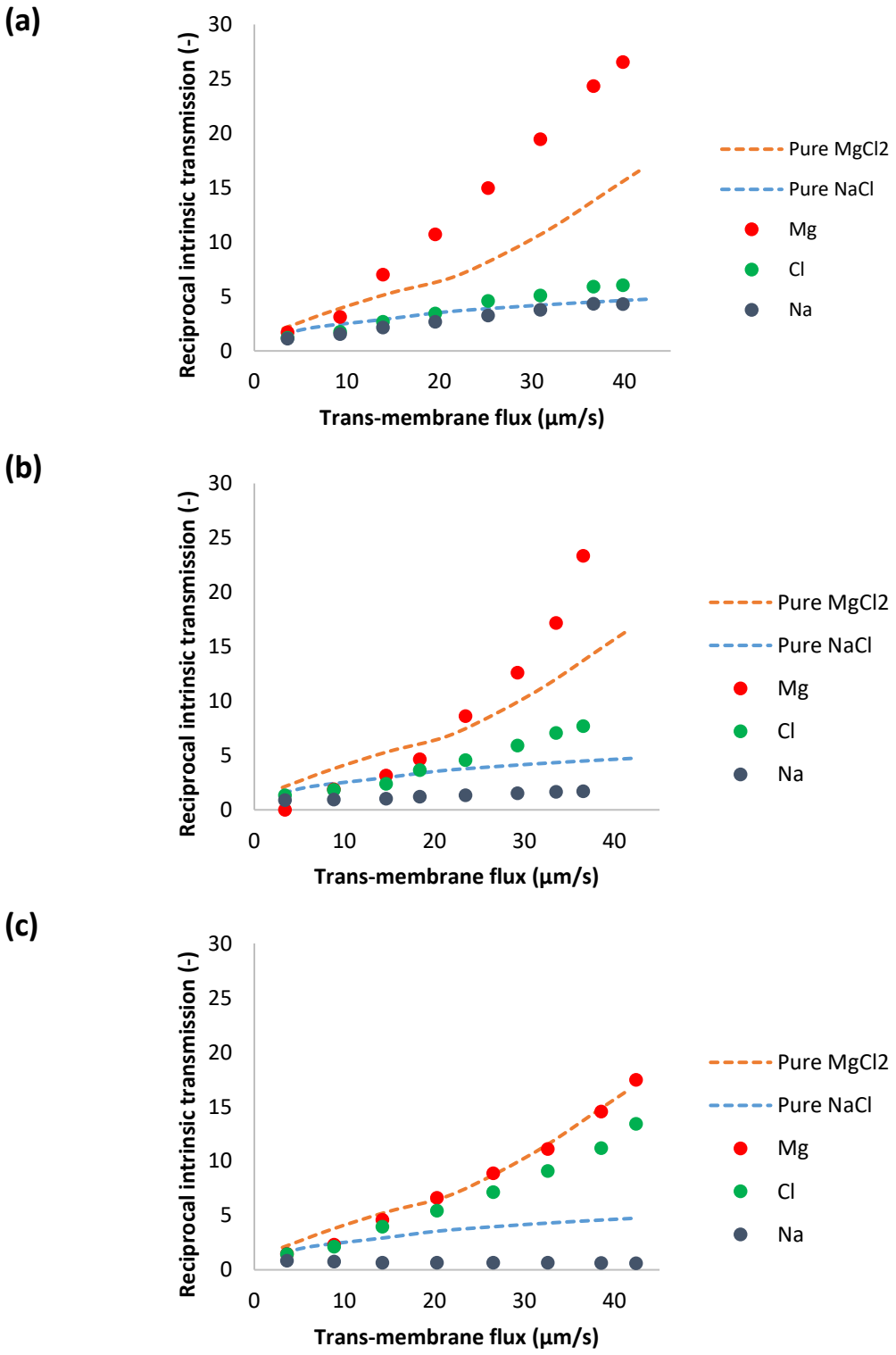


**Fig. 3** Reciprocal intrinsic transmission as a function of trans-membrane flux for three different feed compositions of $MgCl_2$ molar fraction: (a) 0.1, (b) 0.5 and (c) 0.9

As long as $MgCl_2$ feed molar fraction increases, the arising electric field decreases and eventually there is a change in its direction once $MgCl_2$ becomes dominant and the spontaneously arising electric field is controlled by the difference between the membrane permeance to $Mg^{2+}$ and $Cl^-$. In this case, the electric field enhances the transport of cations and retards anions to keep zero electric current since the membrane permeance to $Mg^{2+}$ is lower than to $Cl^-$. Therefore, increasing $MgCl_2$ feed molar fraction decreases the rejection of $Na^+$ and $Mg^{2+}$ whereas the rejection of $Cl^-$ increases as can be seen in **Fig. 3b**. Actually, $Na^+$ rejections were even negative at low trans-membrane volume fluxes (-12%, f=0.89) and turned positive (up to 41.62% (f=1.71)) when the trans-membrane volume flux increased. Initially the electromigration of $Na^+$ increases more rapidly than the trans-membrane volume flux and the rejection decreases until it reaches a minimum (frequently not observed) and the rejections eventually become positive when the trans-membrane volume flux increases more rapidly than the electromigration flux [25,28].

Due to the better rejection of $MgCl_2$ (the larger differences in the permeances between $Mg^{2+}$ and $Cl^-$), $Na^+$ negative rejections are so pronounced that they even decreased monotonically for all the trans-membrane fluxes measured (from -20% (f=0.83) to -64% (f=0.61)) when the feed molar fraction of $MgCl_2$ was high compared to NaCl **(see Fig. 3c)**. Similarly to the previous case, increasing the feed molar fraction of $MgCl_2$ increased the rejection of $Cl^-$ and decreased the rejection of $Mg^{2+}$: $Cl^-$ intrinsic rejections were between 30% and 93% (f=1.44-11.18) whereas for $Mg^{2+}$, they varied from 32% to 94% (f=1.47-14.55). Besides, both rejections are similar and closer to the rejection of $MgCl_2$ as a single salt.

**Fig. 4** shows the reciprocal transmission of each ion for several feed compositions. Moreover, it also presents the theoretical fits obtained by means of the analytical solution of SDEM model for the three ions mixture. These results illustrate the strong dependence of ion rejection on feed composition. As can be seen in **Fig. 4a**, increasing the fraction of $Mg^{2+}$ reduces $Na^+$ rejection to the point of reaching negative rejections at low trans-membrane volume fluxes starting at a feed molar fraction of $MgCl_2$ of 0.375. As the fraction of $Mg^{2+}$ increases, negative rejections became more pronounced as explained above. This is consistent with NF data reported in the literature showing high negative rejection of trace monovalent ions [12,13,26,30].

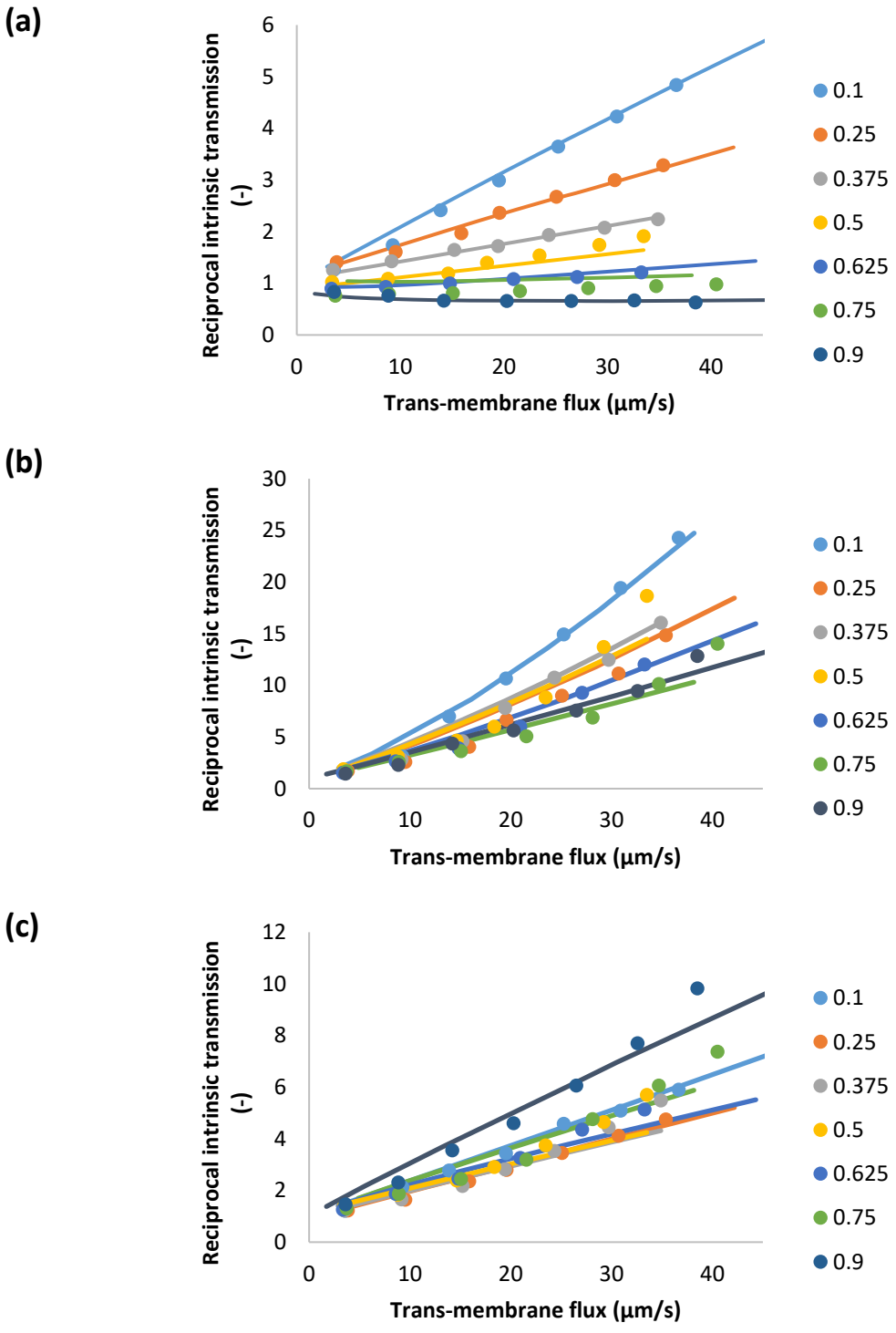


**Fig. 4** Reciprocal intrinsic transmission as a function of trans-membrane flux for: (a) $Na^{+}$, (b) $Mg^{2+}$ and (c) $Cl^{-}$. The legend gives the feed molar fraction of $MgCl_2$. Symbols represent experimental data and solid lines are the theoretical fits.

As for $Mg^{2+}$ and $Cl^-$, there are also differences in ion rejection with feed composition although there are not as pronounced as in the case of $Na^+$ **(see Figs. 4b-4c)**. $Cl^-$ rejection increased from 16%-83% (f = 1.19-6.15) to 30%-92% (f = 1.44-14.17) when the molar fraction of $MgCl_2$ increases since it has to match the rejections of either of the two cations in the two limiting cases of single salts. On the contrary, $Mg^{2+}$ rejection decreased slightly, from 40%-96% (f = 1.69-26.93) to 31%-94% (f = 1.47-19.41), with increasing feed molar fraction of $MgCl_2$.

## *4.2 The effect of ion composition on ion permeances*

The ion permeances as a function of $MgCl_2$ molar fraction are shown in **Fig. 5**. Previous studies reported that in the limiting case of NaCl as dominant salt and $Mg^{2+}$ as trace ion, membrane permeance to $Na^+$ was higher than to $Cl^-$ and $Mg^{2+}$ was the least permeable [29]. The same order of membrane permeances was reported in the opposite situation (dominant $MgCl_2$ and $Na^+$ as trace ion): membrane permeance to $Na^+$ was still larger whereas $Mg^{2+}$ exhibit lower permeance compared with the value as trace ion. $Cl^-$ was part of the dominant ion in both cases and its membrane permeance was barely higher in NaCl dominant salt.

The results presented in this work fall in between this two limiting cases and are qualitatively in agreement with the results reported in the literature. $Na^+$ is the most permeable ion: its permeance was 30.43 μm/s at the lowest $MgCl_2$ molar fraction studied and it increased up to 294.47 μm/s with the increasing feed molar fraction of $MgCl_2$. As discussed above, a monovalent ion such as $Na^+$ is strongly affected by arising spontaneously electric field in the presence of a divalent cation [26,29]. On the other hand, $Mg^{2+}$ turn out to be the least permeable ion whereas $Cl^-$ permeance remained between the values of $Na^+$ and $Mg^{2+}$. The fact that membrane permeance to $Cl^-$ is lower than to $Na^+$ is expected taking into account the negative charge of NF270. Due to electrical repulsion, $Cl^-$ is rejected stronger than $Na^+$ and its membrane permeance is lower. As for $Mg^{2+}$, it is additionally affected by dielectric exclusion that is stronger for divalent ion. Actually, the difference among $Mg^{2+}$ permeance and the others expands as $MgCl_2$ molar fraction increases since $Mg^{2+}$ permeance decreases from 5.17 μm/s to 3.5 μm/s. Bason et al. suggested ion pairing-like binding of divalent cation to fixed charge membrane that may lead to saturation of ion adsorption [30]. If the concentration at the membrane surface remains constant (due to ion uptake saturation), the increase in the feed concentration would decrease the partition coefficient, decreasing the permeances as a result. The binding of $Mg^{2+}$ to membrane fixed charge may also explain the behaviour observed for $Cl^-$: its membrane permeance increased noticeably until the feed molar fraction

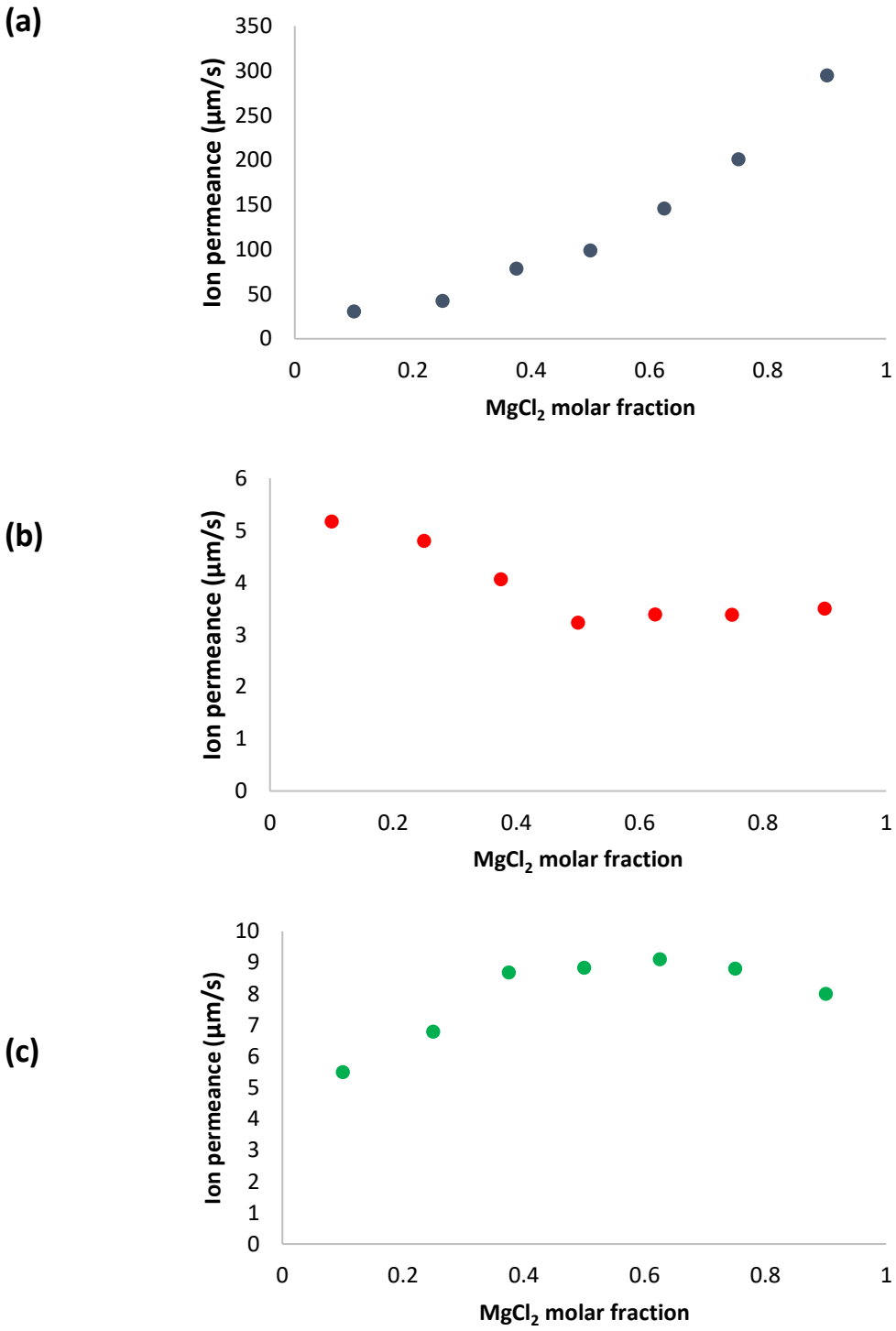


**Fig. 5** Ion permeance for each ion as a function of feed molar fraction of $MgCl_2$

of $MgCl_2$ reached a value of 0.375. From this point forward the permeance to $Cl^-$ became approximately constant around 8.68 μm/s. Strong binding of divalent ions compared with monovalent ions reduces fixed charge concentration, thus the membrane effectively behaves as an uncharged polymer [31]. Therefore, the increase in $Mg^{2+}$ concentration decreases the exclusion of $Cl^-$ via neutralization of membrane fixed charge, increasing its membrane permeance. Eventually, the membrane permeance to $Cl^-$ remains constant once the ion adsorption saturation was reached.

Some of the obtained results are in disagreement with the standard Donnan exclusion mechanism. This fact manifests the complexity of the rejection mechanism in NF: it is not limited to a combination of steric hindrance and Donnan exclusion, but also other mechanism such as dielectric exclusion. Moreover, taking into account the interactions among these mechanisms is challenging. The presence of fixed charge in the membrane due to ion adsorption or functional groups ionization weakens (reduce) dielectric exclusion whereas the dielectric exclusion strengthen the Donnan exclusion [27].

Experimental data reported in previous studies already supported this fact [8,15,17,20,22,23,32]. For instance, Reig et al. found that in NaCl solutions the membrane permeance to $Na^+$ increased with increasing feed concentration with negatively charged membranes whereas the opposite trend is expected according to Donnan exclusion mechanism [17]. Similarly, other studies showed that the rejection of salts with double-charge cations became higher when its concentration increased [8,20,22,32].

Recently, Freger et al. studied NF separation of binary mixtures of NaCl and $CaCl_2$ at different pH values for two fixed values of total chloride concentration [23]. The authors concluded that Steric-Donnan-Dielectric mechanism of ion exclusion is not suitable to describe ion permeation in NF and suggested that it is mainly controlled by the solvation (Born) energy of the ions. The results in this study are qualitatively in agreement with [23] taking into account that the divalent cation in that paper was $Ca^{2+}$ instead of $Mg^{2+}$. In [23] the membrane permeance to divalent cation decreased with increasing concentration of double-charge salt and a strong influence of divalent cation on monovalent cation permeance was also observed. As for the common ion $Cl^-$, the authors determined its permeance assuming that it does not change with composition. In the present study, this value was fitted without any restriction and the obtained results showed that this assumption seems to be valid for the most part of

the molar fraction range studied except for the mixtures of low feed molar concentration of $MgCl_2$.

## 5. Conclusions

The actual rejection mechanism of NF is complex and makes difficult the development of models for performance prediction, especially in multi-ion mixtures containing simultaneously mono and divalent ions. This work studied the ion transport through a NF membrane for ternary electrolyte mixtures (NaCl-$MgCl_2$) of different compositions.

Experimental data was obtained using a RDM cell with equally-accessible membrane surface, which allows a quantitative control of the extent of CP. In this way, corrections for CP can easily be made even in electrolyte mixtures.

An analytical solution to the differential equations of SDEM model developed for three ions was used to fit the experimental data and the ion permeances were determined for each feed composition. It was found a strong dependence of $Na^+$ permeance on feed composition and a decrease in the case of $Mg^{2+}$. $Cl^-$ permeance rise initially with the addition of $Mg^{2+}$ but turn out to be constant for the most composition range investigated.

The model allowed the fitting of experimental data and reproduced effectively experimental trends typical for NF ternary ion mixtures of different compositions. Conversely, the models based on Donnan-Steric exclusion/Hindrance require the determination of membrane properties that are challenging to obtain and predict trends that have never been observed experimentally. Therefore, advanced engineering models may be more convenient than mechanistic models for NF description for the foreseeable future.

# List of symbols

$c_i$ : concentration of ion $i$

$c_{im}$ : concentration of ion $i$ at the membrane surface

$c_{pi}$: concentration of ion $i$ in the permeate solution

$C_0$: sum of the concentration of all ions in the feed solution

$C_p$: sum of the concentration of all ions in the permeate solution

$D$ : diffusion coefficient of the salt

$D_i$ : ionic diffusion coefficient

$f$: reciprocal transmission

$F_p$: function defined in Eq. (8)

$F_m$: function defined in Eq. (9)

$J_V$ : trans-membrane volume flux

$N$ : rotation speed (rpm)

$P_i$: membrane permeance to ion $i$

$Pe_i$ : ionic Péclet number

$R_i$: membrane rejection of ion $i$

$R_s^{int}$ : intrinsic rejection of the salt

$u$: relative double ionic strength

$u_0$: relative double ionic strength in the feed solution

$u_p$: relative double ionic strength in the permeate solution

$Z_i$: charge of ion $i$

*Greek letters*

$\beta_{ij}$: constant defined in Eq. (7)

$\delta$ : thickness of concentration polarization layer

$\xi$: coordinate normalized by the local unstirred layer thickness

$\Pi$: product of the charges of the three ions

ν : kinematic viscosity

$\chi$: feed molar fraction of $MgCl_2$

## Acknowledgements

The authors gratefully acknowledge support from the project Waste2Product (CTM2014-57302-R) and by the R2MIT (CTM2017-85346-R) funded by the Spanish Ministry of Economy and Competitiveness (MINECO) and the Catalan Government (2017-SGR-312).

## References

[1] A.W. Mohammad, Y.H. Teow, W.L. Ang, Y.T. Chung, D.L. Oatley-Radcliffe, N. Hilal, Nanofiltration membranes review: Recent advances and future prospects, Desalination. 356 (2015) 226–254. doi:10.1016/j.desal.2014.10.043.

[2] A. Yaroshchuk, M.L. Bruening, E. Zholkovskiy, Modelling nanofiltration of electrolyte solutions, Adv. Colloid Interface Sci. 268 (2019) 39–63. doi:10.1016/j.cis.2019.03.004.

[3] P. Ortiz-albo, R. Ibañez, A. Urtiaga, I. Ortiz, Phenomenological prediction of desalination brines nanofiltration through the indirect determination of zeta potential, Sep. Purif. Technol. (2018). doi:10.1016/j.seppur.2018.08.066.

[4] N. Fridman-bishop, K.A. Tankus, V. Freger, Permeation mechanism and interplay between ions in nanofiltration, J. Memb. Sci. 548 (2018) 449–458. doi:10.1016/j.memsci.2017.11.050.

[5] S.S. Wadekar, R.D. Vidic, Insights into the rejection of barium and strontium by nanofiltration membrane from experimental and modeling analysis, J. Memb. Sci. 564 (2018) 742–752. doi:10.1016/j.memsci.2018.07.060.

[6] K. Thibault, H. Zhu, A. Szymczyk, G. Li, The averaged potential gradient approach to model the rejection of electrolyte solutions using nanofiltration: Model development and assessment for highly concentrated feed solutions, Sep. Purif. Technol. 153 (2015) 126–137. doi:10.1016/j.seppur.2015.08.041.

[7] S. Anisah, M. Kanezashi, H. Nagasawa, T. Tsuru, Hydrothermal stability and permeation properties of TiO2-ZrO2 (5/5) nanofiltration membranes at high temperatures, Sep. Purif. Technol. 212 (2019) 1001–1002. doi:10.1016/j.seppur.2018.12.006.

[8] A. Yaroshchuk, X. Martínez-Lladó, L. Llenas, M. Rovira, J. de Pablo, Solution-diffusion-film model for the description of pressure-driven trans-membrane transfer of electrolyte mixtures: One dominant salt and trace ions, J. Memb. Sci. 368 (2011) 192–201. doi:10.1016/j.memsci.2010.11.037.

[9] A. Yaroshchuk, M.L. Bruening, E. E. Licon Bernal, Solution-Diffusion – Electro-Migration model and its uses for analysis of nanofiltration , pressure-retarded osmosis and forward osmosis in multi-ionic solutions, J. Memb. Sci. 447 (2013) 463–476. doi:10.1016/j.memsci.2013.07.047.

[10] J. Lopez, M. Reig, O. Gibert, C. Valderrama, J.L. Cortina, Evaluation of NF membranes as treatment technology of acid mine drainage: metals and sulfate removal, Desalination. 440 (2018) 122–134. doi:10.1016/j.desal.2018.03.030.

[11] J. López, M. Reig, A. Yaroshchuk, E. Licon, O. Gibert, J.L. Cortina, Experimental and theoretical study of nanofiltration of weak electrolytes: $SO_4^{2-}/HSO_4^{-}/H^{+}$ system, J. Memb. Sci. 550 (2018) 389–398. doi:10.1016/j.memsci.2018.01.002.

[12] N. Pagès, M. Reig, O. Gibert, J.L. Cortina, Trace ions rejection tunning in NF by selecting solution composition: Ion permeances estimation, Chem. Eng. J. 308 (2017) 126–134. doi:10.1016/j.cej.2016.09.037.

[13] M. Reig, E. Licon, O. Gibert, A. Yaroshchuk, J.L. Cortina, Rejection of ammonium and nitrate from sodium chloride solutions by nanofiltration: Effect of dominant-salt concentration on the trace-ion rejection, Chem. Eng. J. 303 (2016) 401–408. doi:10.1016/j.cej.2016.06.025.

[14] N. Pages, A. Yaroshchuk, O. Gibert, J. Luis, Rejection of trace ionic solutes in nano fi ltration : In fl uence of aqueous phase composition, 104 (2013) 1107–1115. doi:10.1016/j.ces.2013.09.042.

[15] N. Fridman-Bishop, O. Nir, O. Lahav, V. Freger, Predicting the Rejection of Major Seawater Ions by Spiral-Wound Nanofiltration Membranes, Environ. Sci. Technol. 49 (2015) 8631–8638. doi:10.1021/acs.est.5b00336.

[16] A. Yaroshchuk, M.L. Bruening, An analytical solution of the solution-diffusion-electromigration equations reproduces trends in ion rejections during nanofiltration of mixed electrolytes, J. Memb. Sci. 523 (2017) 361–372. doi:10.1016/j.memsci.2016.09.046.

[17] M. Reig, E. Licon, O. Gibert, A. Yaroshchuk, J.L. Cortina, Rejection of ammonium and nitrate from sodium chloride solutions by nanofiltration: Effect of dominant-salt concentration on the trace-ion rejection, Chem. Eng. J. 303 (2016) 401–408. doi:10.1016/j.cej.2016.06.025.

[18] S. Déon, A. Escoda, P. Fievet, P. Dutournié, P. Bourseau, How to use a multi-ionic transport model to fully predict rejection of mineral salts by nanofiltration membranes, Chem. Eng. J. 189–190 (2012) 24–31. doi:10.1016/j.cej.2012.02.014.

[19] A. Escoda, S. Déon, P. Fievet, Assessment of dielectric contribution in the modeling of multi-ionic transport through nanofiltration membranes, J. Memb. Sci. 378 (2011) 214–223. doi:10.1016/j.memsci.2011.05.004.

[20] S. Bason, V. Freger, Phenomenological analysis of transport of mono- and divalent ions in nanofiltration, J. Memb. Sci. 360 (2010) 389–396. doi:10.1016/j.memsci.2010.05.037.

[21] S. Déon, P. Dutournié, L. Limousy, P. Bourseau, Transport of salt mixtures through nanofiltration membranes: Numerical identification of electric and dielectric contributions, Sep. Purif. Technol. 69 (2009) 225–233. doi:10.1016/j.seppur.2009.07.022.

[22] C. Mazzoni, S. Bandini, On nanofiltration Desal-5 DK performances with calcium chloride-water solutions, Sep. Purif. Technol. 52 (2006) 232–240. doi:10.1016/j.seppur.2006.04.004.

[23] N. Fridman-bishop, K.A. Tankus, V. Freger, Permeation mechanism and interplay between ions in nanofiltration, J. Memb. Sci. 548 (2018) 449–458. doi:10.1016/j.memsci.2017.11.050.

[24] M. Fernández de Labastida, E.E. Licon Bernal, A. Yaroshchuk, Implications of inhomogeneous distribution of concentration polarization for interpretation of pressure-driven membrane measurements, J. Memb. Sci. 520 (2016) 693–698. doi:10.1016/j.memsci.2016.08.040.

[25] M. Fernández de Labastida, E.E. Licón, M. Bondarenko, A. Yaroshchuk, Rotating disk-like membrane cell for pressure-driven measurements with equally-accessible membrane surface: Numerical simulation and experimental validation, J. Memb. Sci. 550 (2018) 492–501. doi:10.1016/j.memsci.2017.10.057.

[26] V.G. Levich, R.J. Seeger, Physicochemical Hydrodynamics, Am. J. Phys. 31 (1963). doi:10.1119/1.1969158.

[27] A.E. Yaroshchuk, Dielectric exclusion of ions from membranes, Adv. Colloid Interface Sci. 85 (2000) 193–230. doi:10.1016/S0001-8686(99)00021-4.

[28] A. Yaroshchuk, M.L. Bruening, An analytical solution of the solution-diffusion-electromigration equations reproduces trends in ion rejections during nanofiltration of mixed electrolytes, J. Memb. Sci. 523 (2017) 361–372. doi:10.1016/j.memsci.2016.09.046.

[29] N. Pages, A. Yaroshchuk, O. Gibert, J.L. Cortina, Rejection of trace ionic solutes in nanofiltration: Influence of aqueous phase composition, Chem. Eng. Sci. 104 (2013) 1107–1115. doi:10.1016/j.ces.2013.09.042.

[30] S. Bason, V. Freger, Phenomenological analysis of transport of mono- and divalent ions in nanofiltration, J. Memb. Sci. 360 (2010) 389–396. doi:10.1016/j.memsci.2010.05.037.

[31] G.M. Geise, D.R. Paul, B.D. Freeman, Fundamental water and salt transport properties of polymeric materials, Prog. Polym. Sci. 39 (2014) 1–42. doi:10.1016/j.progpolymsci.2013.07.001.

[32] D.X. Wang, L. Wu, Z.D. Liao, X.L. Wang, Y. Tomi, M. Ando, T. Shintani, Modeling the separation performance of nanofiltration membranes for the mixed salts solution with $Mg^{2+}$ and $Ca^{2+}$, J. Memb. Sci. 284 (2006) 384–392. doi:10.1016/j.memsci.2006.08.004.

# ANNEX 3

## Publication 7

*"Perm-selectivity, ion partition and effective diffusion coefficient determination for different electrolytes by transient membrane potential after concentration step method"*

# Perm-selectivity, ion partition and effective diffusion coefficient determination for different electrolytes by transient membrane potential after concentration step method

Marc Fernández de Labastida[1,2], Andriy Yaroshchuk[3,4]

[1]Department of Chemical Engineering, Polytechnic University of Catalonia – BarcelonaTech, C/ Eduard Maristany 10-14 (Campus Diagonal-Besòs), 08930, Barcelona, Spain

[2]Barcelona Research Center in Multiscale Science and Engineering, C/ Eduard Maristany, 10-14 (Campus Diagonal-Besòs), 08930, Barcelona, Spain

[3]Department of Chemical Engineering, Polytechnic University of Catalonia – BarcelonaTech, av. Diagonal 647, 08028 Barcelona, Spain

[4]ICREA, Passeig Lluís Companys 23, Barcelona, Spain

## Abstract

Ion partitioning and diffusivity are fundamental properties to understand ion transport through ion-exchange membranes and optimize electro-membrane processes. Time-resolved measurements of membrane potential have proven useful to provide this kind of information.

In the transient membrane potential after concentration step, an ion-exchange membrane is supported by a relatively thick coarse-porous support (glass frit). After applying a concentration jump to the membrane surface, the different ion perm-selectivities of the membrane and porous support make an electrical response time-dependent due to the progressive redistribution of applied concentration difference between both media. The measured signal can be fitted to a model to determine salt permeability and partitioning coefficient in addition to the ion perm-selectivity, which is the only parameter available from the conventional measurements of stationary membrane potential. In addition, the model also considers osmotic trans-membrane volume transfer.

This approach was used to study ion partitioning, effective diffusion coefficient and perm-selectivity for different electrolytes (NaCl, LiCl and KOAc) with type 10 Fujifilm ion-exchange membranes. In addition, those properties were also determined at different temperatures in the case of NaCl.

*Keywords:* ion-exchange membrane; transient membrane potential; concentration step; ion partitioning; salt diffusion permeability

# 1. Introduction

Ion-exchange membranes are used in a wide range of well-established electro-membrane processes such as electrodialysis, diffusion dialysis and electrolysis [1–8]. The continuous research and development gives rise to emerging applications related to environmentally friendly ("clean") energy processes such as capacitive deionization [9], polymer electrolyte membrane fuel cells [10], redox flow batteries [11], reverse electrodialysis cells [12] or water electrolysis [13].

Ion-exchange membranes are dense polymeric membranes with electrical fixed-charged groups in the polymer matrix. Their properties are controlled primarily by the amount of fixed charge in the membrane (ion exchange capacity), nature of the charged groups and their distribution in the membrane and the amount of water molecules adsorbed in the membrane. The principal properties that should be considered depend strongly on the application, but one of the most important is the permselectivity, which describes the key feature of ion-exchange membranes: its ability to allow the passage of oppositely charged groups (counter-ions) while restricting similarly charged ions (co-ions). An ideal ion-exchange membrane should exclude completely co-ions and the permselectivity would be equal to one. However, there is some transport of co-ions and water through the membrane, which affects its performance and ultimately the efficiency of the electro-membrane processes (decreasing purity in separation processes or reducing efficiency in energy-conversion applications). Therefore, a better understanding of ion-transport mechanisms is crucial to improve the ion-exchange membrane performance.

Transport across ion-exchange membranes occurs principally under concentration or electric potential difference as a driving force by means of several transport mechanisms (convection, diffusion and electromigration) acting simultaneously. The contribution of each transport mechanism depends on the relative difference between the concentration difference and the magnitude of applied electric field. The most applied approach in the literature to address ion transport through ion-exchange membranes is based on the extended Nernst-Planck equation, which describes ionic flux as a sum of three terms to reflect the contribution of each transport mechanism. In this way, only one diffusion coefficient per ionic specie is needed,

and Nernst Planck equation can easily be coupled with other equations to describe hydrodynamics and boundary conditions. Therefore, it has been widely applied as basis for quantitative treatment [1]. However, some restrictions (isothermal systems, homogeneous media, and multicomponent systems) reduce the application of this equation. Alternatively, one can use Stefan-Maxwell frictional treatment which is more general and suitable in the diffusion of multi-components systems [1].

A different more fundamental approach is based on the principles of irreversible thermodynamics which describe membrane phenomena by coupling driving forces with resultant permeation fluxes of species through the membrane using phenomenological equations derived from dissipation function without postulating any mechanistic model of membrane transport [14]. Irreversible thermodynamics consider interactions among different ions and solvent whereas the Nernst-Planck equation assumes that cations and anions independently migrate in the solution and membrane matrix. Therefore, irreversible thermodynamics is more realistic and rigorous.

There are six independent transport parameters that allow to model fluxes of electrolyte ions, and solvent through ion exchange membranes according to the irreversible thermodynamics equations [15]. However, a complete characterization of membrane transport properties in terms of irreversible thermodynamics is a laborious process since phenomenological coefficients must be obtained from independent experiments. Therefore, correct selection of simplified models (and corresponding reduced set of experimental measurements) is an important issue.

In addition to perm-selectivity, separate information on partition and diffusion coefficients allow a better understanding of ion transport across ion-exchange membranes. The partition coefficient of an ion refers to its distribution between the membrane and the solution (equilibrium) whereas the diffusivity coefficient is related to the ion mobility in the membrane (kinetic) [16]. Very recently, a novel technique based on non-stationary diffusion was developed to determine salt permeability, partition coefficient and perm-selectivity [17]. The electrical response is measured for a membrane supported by a relatively coarse-porous material. The different ion perm-selectivities between both media make the response time-dependent due to the progressive redistribution of applied concentration difference. A mathematical model was presented to interpret the experimental data and the results

showed a good agreement. This novel approach was validated experimentally by comparison of literature data and by means of well-established techniques.

Novel technologies of energy production using Reverse Electrodialysis use non-conventional salt solutions to improve the efficiency of this processes [18,19]. In this work, the ion transport across Fujifilm cation exchange membranes (CEM) and anion exchange membranes (AEM) of Type 10 was investigated for different electrolytes (NaCl, LiCl and KOAc) at room temperature. Moreover, measurements were also performed at 50ºC and 75ºC for NaCl to study the effect of temperature.

## 2. Theory

The system studied consist of an ion-exchange membrane and a porous support placed in a two-compartment cell that initially are equilibrated with a base solution of concentration $c_0$. The membrane is exposed to a non-equilibrium solution of concentration $c_{step}$ and a progressive redistribution of applied concentration between both compartment occurs as explained in detail in [17]. The evolution of electric potential difference is given by:

$$\varphi = \frac{RT}{F}\left[(2t_+^m - 1)ln\left(\frac{a_{step}}{a_i}\right) + (2t_+^b - 1)ln\left(\frac{a_i}{a_0}\right)\right] \quad (1)$$

where R is the ideal gas constant, T is the absolute temperature, F is the Faraday constant, *a* is the activity, $t_+^b$ is the transport number of cations in the porous support and $t_+^m$ is the transport number of cations in the membrane. The subscripts 0, step and I refer to the base solution, the non-equilibrium solution and the interface membrane/porous support respectively. The transport number of cations in the porous support and in the membrane can be estimated as:

$$t_+^b = \frac{z_+ \cdot D_+}{z_+ \cdot D_+ + z_- \cdot D_-} \quad (2)$$

$$t_+^m = \frac{1}{2}\left[\frac{\frac{F\varphi_0}{RT}}{ln\left(\frac{a_{step}}{a_0}\right)} + 1\right] \quad (3)$$

where $\varphi_0$ is the initial value of electric-potential difference occurring just after the solution replacement, $z_+$, $z_-$ are the charge coefficient of cation and anion, $D_+$, $D_-$ are the diffusion coefficient of cation and anion.

The concentration at the membrane/porous support interface can be estimated solving numerically the following system of partial differential equations:

$$\alpha_m \frac{\partial c_m}{\partial t} = \frac{\partial}{\partial \mathrm{x}}\left[-D_m \cdot \left(1 + \frac{dln(\gamma)}{dln(c_m)}\right) \cdot \frac{\partial c_m}{\partial x} + J_v T_m c_m\right] \quad (4)$$

$$\alpha_s \frac{\partial c_s}{\partial t} = \frac{\partial}{\partial \mathrm{x}}\left[-D_s \cdot \left(1 + \frac{dln(\gamma)}{dln(c_s)}\right) \cdot \frac{\partial c_s}{\partial x} + J_v c_s\right] \quad (5)$$

where $\alpha_m$, $\alpha_s$ are the chemical capacity in the membrane and in the porous support respectively, $c_m$ is the virtual salt concentration in the membrane [20], $D_m$ is the effective salt diffusion coefficient in the membrane, $D_s$ is the salt diffusivity in the porous support, $\gamma$ is the salt activity coefficient in the virtual solution, $x$ is the longitudinal coordinate across the membrane or the porous support, $T_m$ is the salt transmission coefficient and $J_v$ is the osmotic flow that transport water in the opposite direction to the salt transport:

$$J_v = -K * (c_{step} - c_i) \quad (6)$$

where $K$ is the osmotic permeability.

The initial and boundary conditions to solve the system of partial differential equations are:

$$c_m|_{x=0} = c_{step} \quad (7a)$$

$$c_m|_{x=L_m} = c_i \quad (7b)$$

$$c_s|_{x=L_m} = c_i \quad (7c)$$

$$c_s|_{x=(L_m+L_s)} = c_0 \quad (7d)$$

The chemical capacity is related to the partition coefficient of either of the ions, $\Gamma_\pm$ as:

$$\alpha_m = \Gamma_\pm\left(1 + \frac{dln\Gamma_\pm}{dlnc}\right) \quad (8)$$

It can be shown that due to the electroneutrality of membrane phase using either of ions gives the same result.

# 3. Experimental materials and methods

## *3.1 Materials*

Experiments were carried out using cation CEM and AEM Type 10 kindly provided by Fujifilm Manufacturing Europe BV (The Netherlands). Membranes were supported by porous glass frit discs of 25mm in diameter having a non-porous peripheral edge (the porous part is 19mm in diameter, see **Fig. 1c**), 3.65mm of thickness and average pore size of 10-16µm supplied by Duran Group (Germany). The chemical reagents were of analysis grade.

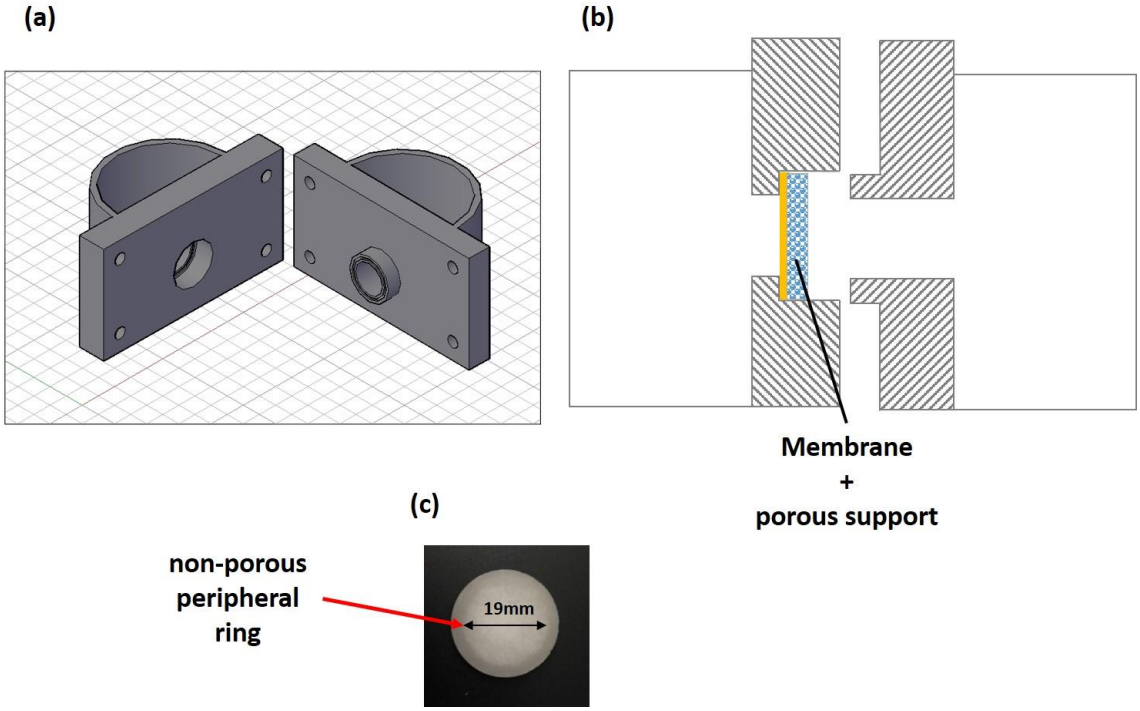


**Fig. 1** a) Drawing of the cell, b) side view showing the assembly of the two half-cell with membrane and porous support and c) glass frit used as the porous support

## 3.2 Measurements of transient-membrane potential after concentration step

Membranes were equilibrated overnight with the solution of base concentration, $C_0$. Each equilibrated membrane was placed along with the porous support in a two-compartment cell as shown in **Figs. 1a-1b**. The capacity of each compartment is 85 mL. The electric potential difference between both compartments is measured with a pair of Ag/AgCl reference electrodes with salt bridges filled with KCl 3M (Metrohm, Switzerland) using a data acquisition card (NI USB-6001) and the software LabView (National Instruments, Austin) to obtain the time-dependent signal. Initially, the two compartments are filled with the base solution and the electric potential difference is measured until a stationary value is reached. In this way, the asymmetry potential between the measuring electrodes is determined and afterwards, it is subtracted from the measured transient membrane potential. Once the asymmetry potential is constant, the solution in the compartment facing the membrane was replaced by the non-equilibrium solution of concentration $C_{step}$. The solution in the non-equilibrium compartment was stirred using a magnetic stirrer to keep the concentration at the membrane surface constant. The temperature of solutions was regulated with a thermostat ministat 230 (Huber, Germany)

## 3.3 Measurements of osmotic permeability

The osmotic permeability was determined for the same concentration pairs $C_0 - C_{step}$ as used in the transient membrane potential measurements. Membrane were equilibrated overnight with a solution having an intermediate concentration between $C_0$ and $C_{step}$.

A membrane disk of 25 mm in diameter (4.91 $cm^2$ exposed area) was placed in a two-compartment cell with a volume of 120 mL in each compartment. Solutions were pre-heated moderately to remove dissolved air and avoid formation of bubbles during the measurement. The temperature of solutions was regulated with a thermostat ministat 230 (Huber, Germany)**.**The osmotic flow was determined measuring the changes in volume as a function of time using an attached graduated pipette.

The osmotic permeability, $K$, was calculated as the ratio of osmotic flux and corrected concentration difference taking into account solution non-ideality by means of osmotic coefficient, $\phi$:

$$K = \frac{J_v}{C_2 \cdot \phi_2 - C_1 \cdot \phi_1} \quad (9)$$

where $c$ is the salt concentration and the subscripts 1 and 2 denote the lower and higher concentration respectively.

### *Glass frit properties*

The properties of the glass frit used as porous support were determined in [17] and are summarized in **Table 1**.

**Table 1**

**Properties of porous support**

| $\alpha_s$ | $D_s$ (m²/s) | Pore size (µm) | $L_s$ (mm) |
|---|---|---|---|
| 0.34 ± 0.00 | $1.5 \cdot 10^{-10}$ | 10-16 | 3.65 ± 0.008 |

## 4. Results and discussion

### *4.1 Osmotic permeability determination*

The osmotic permeability was determined for both anion and cation exchange membranes for each electrolyte at room temperature. Concentration in each compartment was determined after each measurement to corroborate that the salt concentration difference across the membrane did not change significantly over the experiments and the variation observed was always below 5%.

**Fig. 2** shows the osmotic flux as a function of base concentration $C_0$ for each electrolyte at room temperature. As expected, the osmotic flux increases with increasing concentration. Osmotic flux is higher in CEM than in AEM, which was previously observed in the case of NaCl [17]. Moreover, it can be seen that difference among electrolytes are remarkably stronger in the case of CEM.

**(a)**

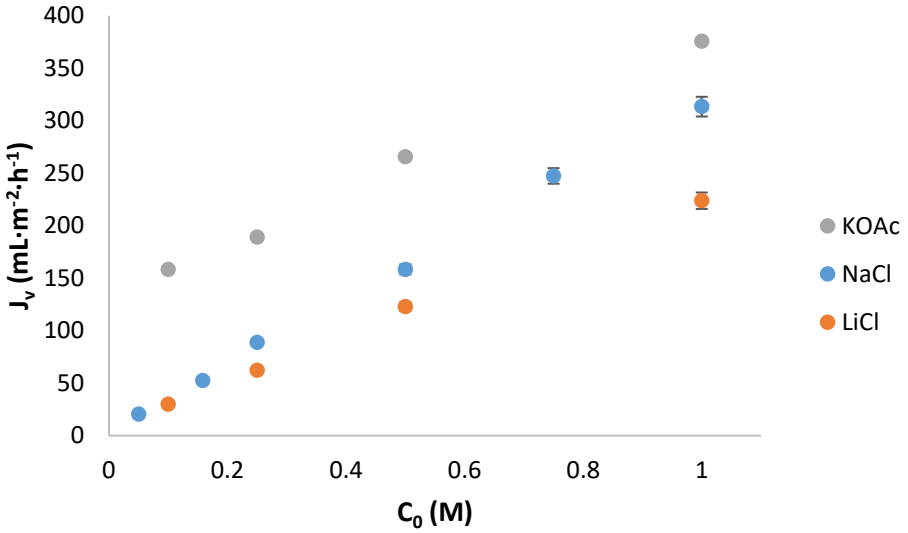


**(b)**

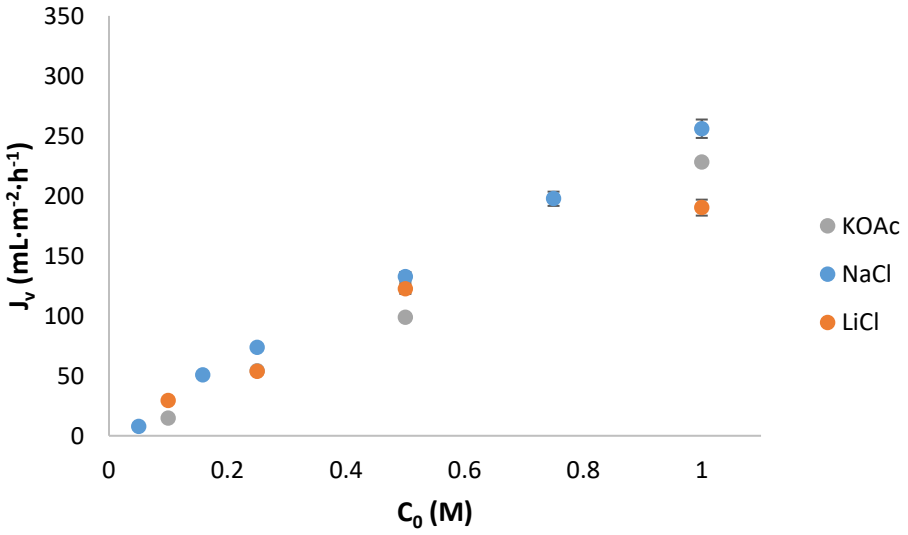


**Fig. 2** Osmotic flux vs. lower concentration determined for each electrolyte with Type 10 Fujifilm membranes: a) CEM and b) AEM

Moreover, the effect of temperature on osmotic flux can be seen in **Fig. 3** for the case of NaCl. The increase in the temperature increased the osmotic flux up to 6 times.

**(a)**

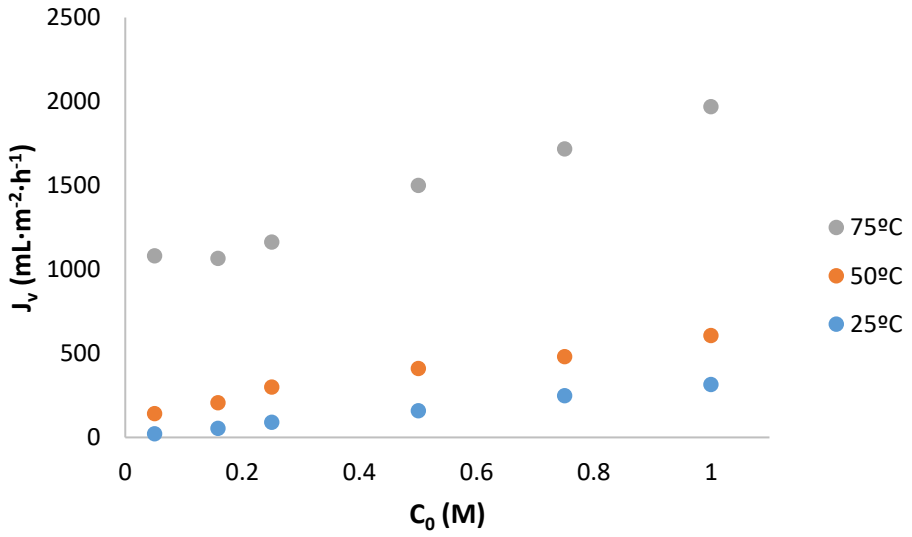


**(b)**

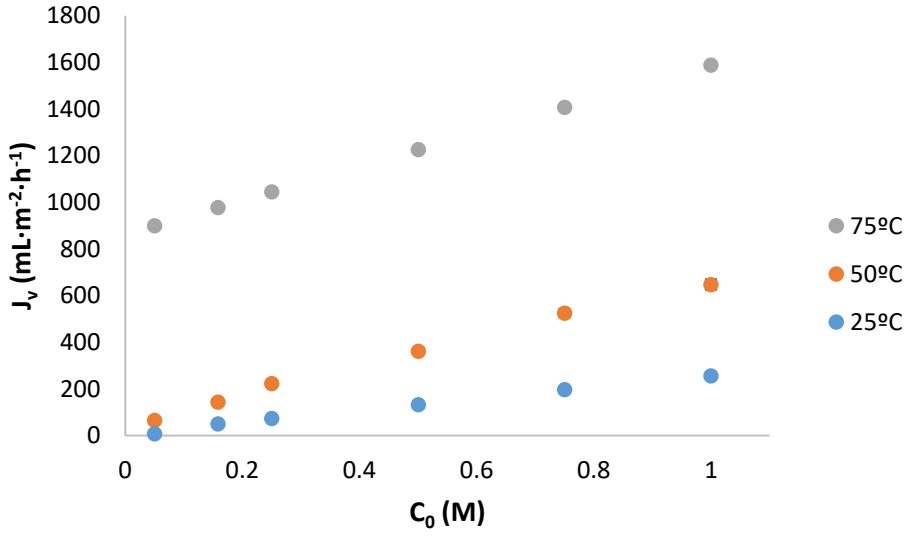


**Fig. 3** Osmotic flux vs. lower concentration determined for NaCl at different temperatures using Type 10 Fujifilm membranes: a) CEM and b) AEM

The estimated osmotic permeability are presented in **Table 2** (NaCl) and **Table 3** (LiCl and KOAc). These values are used afterward in the fitting of time dependences of transient membrane potential.

**Table 2**

**Osmotic permeability of cation and anion exchange membrane Type 10 Fujifilm for NaCl depending on the temperature. $C_0$ is the lower concentration and the higher concentration is two times larger.**

| $C_0$ (M) | $K \cdot 10^{-10}$ ($m^4/(mol \cdot s)$) | | | | | |
|---|---|---|---|---|---|---|
| | 25ºC | | 50ºC | | 75ºC | |
| | CEM | AEM | CEM | AEM | CEM | AEM |
| 0.05 | 1.25± 0.59 | 0.47±0.20 | 8.46±0.34 | 3.97±0.04 | 65.57±3.28 | 54.64±1.09 |
| 0.158 | 1.02±0.11 | 0.98±0.14 | 3.95±0.20 | 2.77±0.06 | 20.61±0.21 | 18.94±0.95 |
| 0.25 | 1.46±0.16 | 1.21±0.06 | 3.61±0.04 | 2.69±0.13 | 14.12±0.42 | 12.70±0.13 |
| 0.5 | 0.93±0.04 | 0.77±0.02 | 2.39±0.05 | 2.10±0.04 | 8.82±0.26 | 7.21±0.07 |
| 0.75 | 0.66±0.02 | 0.53±0.02 | 1.81±0.05 | 1.98±0.06 | 6.54±0.20 | 5.36±0.21 |
| 1 | 0.84±0.0005 | 0.69±0.02 | 1.67±0.08 | 1.79±0.04 | 5.48±0.11 | 4.42±0.18 |

**Table 3**

**Osmotic permeability of cation and anion exchange membrane Type 10 Fujifilm for LiCl and KOAc at room temperature. $C_0$ is the lower concentration and the higher concentration is two times larger.**

| $C_0$ (M) | $K \cdot 10^{-10}$ ($m^4$/(mol·s)) | | | |
|---|---|---|---|---|
| | LiCl | | KOAc | |
| | CEM | AEM | CEM | AEM |
| 0.1 | 0.90±0.04 | 0.89±0.09 | 4.62±0.18 | 0.43±0.08 |
| 0.25 | 0.73±0.08 | 0.63±0.07 | 2.11±0.11 | 0.60±0.05 |
| 0.5 | 0.66±0.02 | 0.66±0.04 | 1.37±0.002 | 0.51±0.03 |
| 1 | 0.51±0.006 | 0.43±0.01 | 0.97±0.01 | 0.51±0.03 |

Notably, the osmotic permeabilities do not show clear trends as functions of salt concentration of NaCl. This is in disagreement with the standard Donnan model of ion-exchange membranes postulating that osmosis is controlled by the coion-exclusion phenomenon while the latter is a strong function of concentration.

## 4.2 Estimation of effective salt diffusion and partition coefficients for different electrolytes

This section explores the dependence of salt partitioning, salt diffusion coefficient and perm-selectivity on concentration using three different electrolytes (NaCl, LiCl and KOAc) at room temperature. Measurements have been performed for Fujifilm Type 10 membranes at various values of base concentration $C_0$ and effective salt diffusion and partitioning coefficients have been determined by fitting the experimental data to the mathematical model as described in [17].

**Fig. 4** shows a typical measurement of transient-membrane potential after concentration step. All the presented results are averages of at least three measurements.

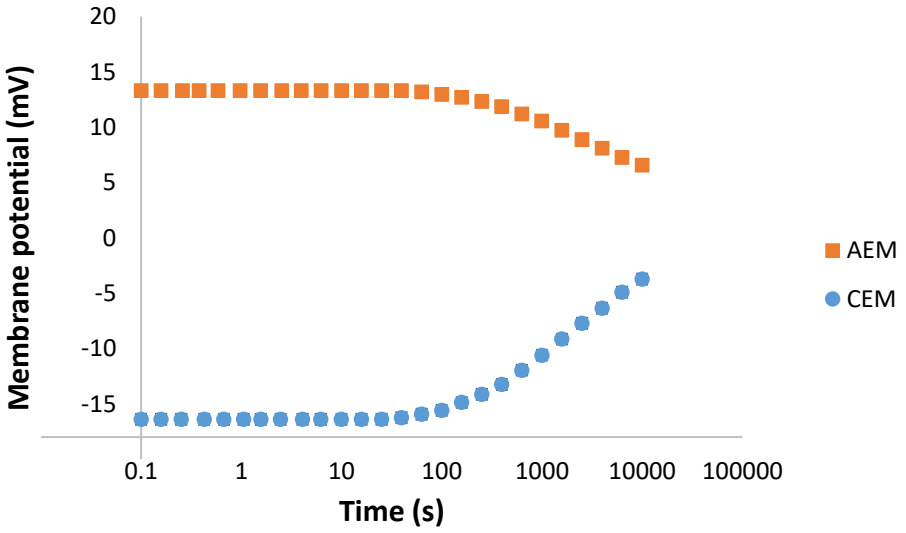


**Fig. 4** Experimental time evolution of membrane potential for type 10 Fujifilm cation and anion exchange membranes for $\boldsymbol{C_0 = 0.5M}$ NaCl

The diffusion occurs through a large chemical resistance (the thin and relatively dense ion-exchange membrane) into a large chemical capacity (the porous support, which is much more porous and thicker than the membrane). Due to the different ion-permselectivities between those media and the progressive redistribution of applied concentration difference between them, there is a time-dependent trans-membrane potential difference. However, the signal remains initially constant for a certain period since it is independent of shape of salt concentration profile in macroscopically homogeneous media. Within the initial time span, the salt chemical potential at the membrane/support interface remains practically constant

until the chemical capacity of the adjacent part of the support is noticeably charged [21]. Then, the salt concentration at the interface start to change and the signal evolution begins.

The relaxation pattern is primarily controlled by the diffusion permeability of the membrane but also affected by the salt partitioning coefficient and the osmotic trans-membrane volume transfer. On the other hand, it was found that the relaxation process is less sensitive to the salt transmission coefficient [17].

As can be seen in **Fig. 4**, the sign of the initial trans-membrane potential depends on the type of ion exchange membrane (CEM or AEM) due to the opposite sign of fixed charge. The transport number in the membrane can be estimated from the initial membrane potential and afterwards determine the perm-selectivity as:

$$permselectivity = \frac{t^m_{counter-ion} - t^b_{counter-ion}}{t^b_{co-ion}} \quad (10)$$

The superscripts *m*, *b* refer to the membrane and bulk-solution phases.

**Figs. 5-7** shows the experimental time-dependence of membrane potential obtained at different base solution concentration $C_0$ for NaCl, LiCl and KOAc respectively. The ratio $C_{step}/C_0$ was kept at 2 in all the measurements (see **Table 1**). Each individual measurement was fitted separately and the averages of the obtained fitted parameters are used to calculate the theoretical curve that are also presented in **Figs. 5-7**. The deviation between experimental data and the models are below 10% in all cases.

It can be seen in all the cases that the characteristic relaxation time decreases when the base concentration increases. A shorter relaxation time implies a higher diffusion permeability, which is logical due to the weaker Donnan exclusion of co-ions at higher concentrations. **Fig. 5** also shows that the initial membrane potential decreases (in absolute value) with concentration in the case of NaCl. This dependence is clearly seen for AEM whereas for CEM is relatively weak. This indicates that the electrochemical perm-selectivity decreases with concentration, which has been typically observed in ion-exchange membranes [22]. However, the trend of initial membrane potential observed for NaCl is different for the other studied electrolytes. As can be seen for LiCl in **Fig. 6**, the initial membrane potential decreases with concentration for AEM (as in the case of NaCl) whereas it increases (in absolute value) for CEM.

**(a)**

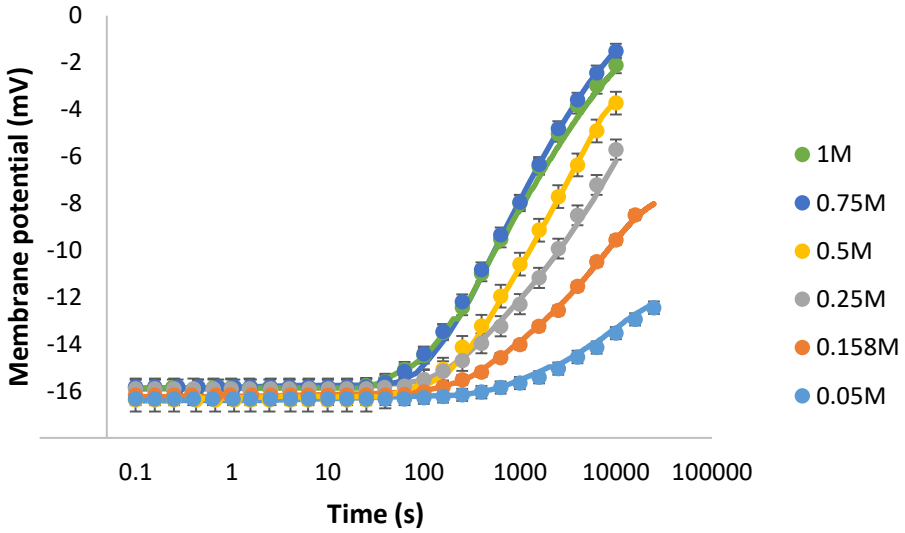


**(b)**

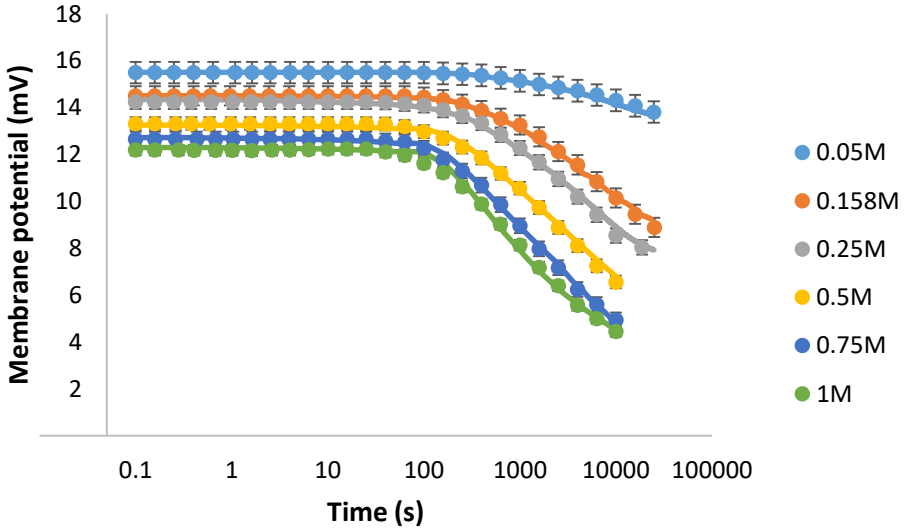


**Fig. 5** Time evolution of trans-membrane potential for various base concentrations, $C_0$, of NaCl for Type 10 Fujifilm membranes: a) CEM and b) AEM. $\boldsymbol{C_{step}}$ is always two times higher than $\boldsymbol{C_0}$. Symbols represent experimental data and solid lines are the theoretical fits

**(a)**

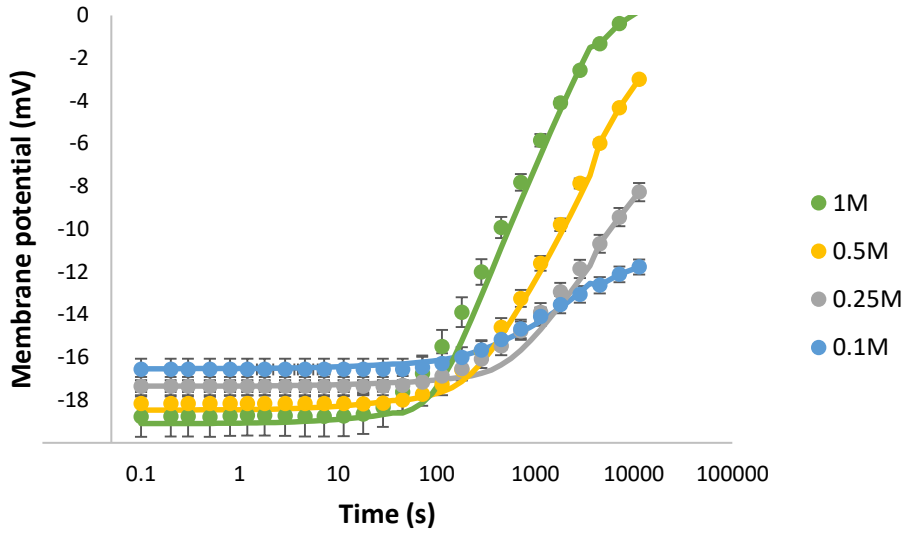


**(b)**

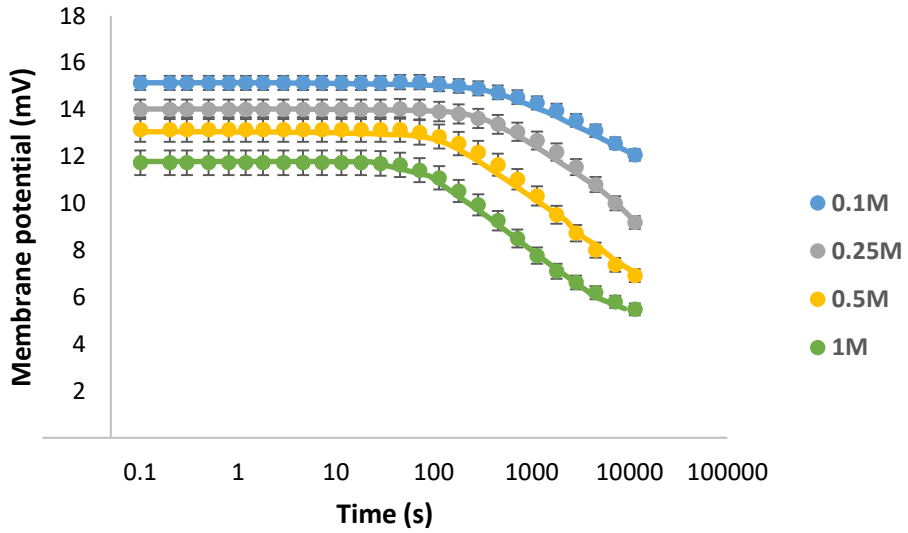


**Fig. 6** Time evolution of trans-membrane potential for various base concentrations, $C_0$, of LiCl for Type 10 Fujifilm membranes: a) CEM and b) AEM. $\boldsymbol{C_{step}}$ is always two times higher than $\boldsymbol{C_0}$. Symbols represent experimental data and solid lines are the theoretical fits

**(a)**

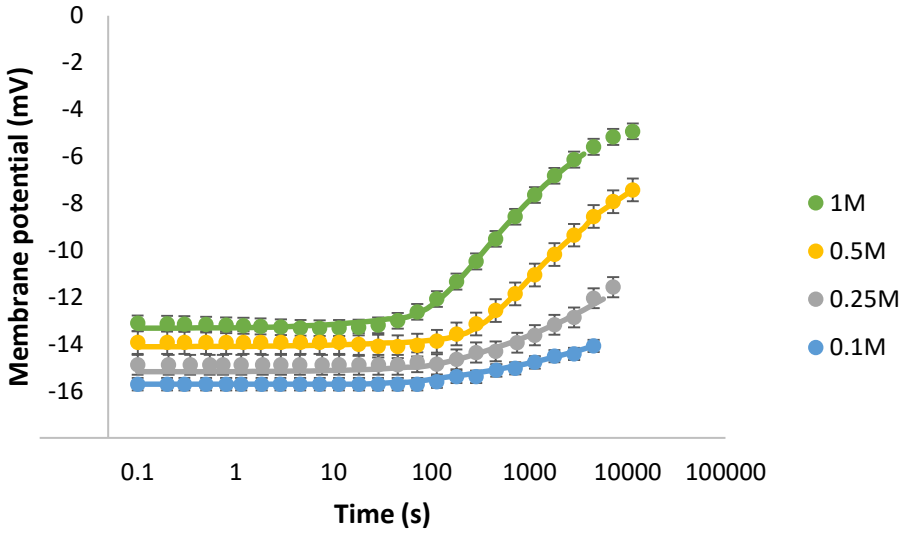


**(b)**

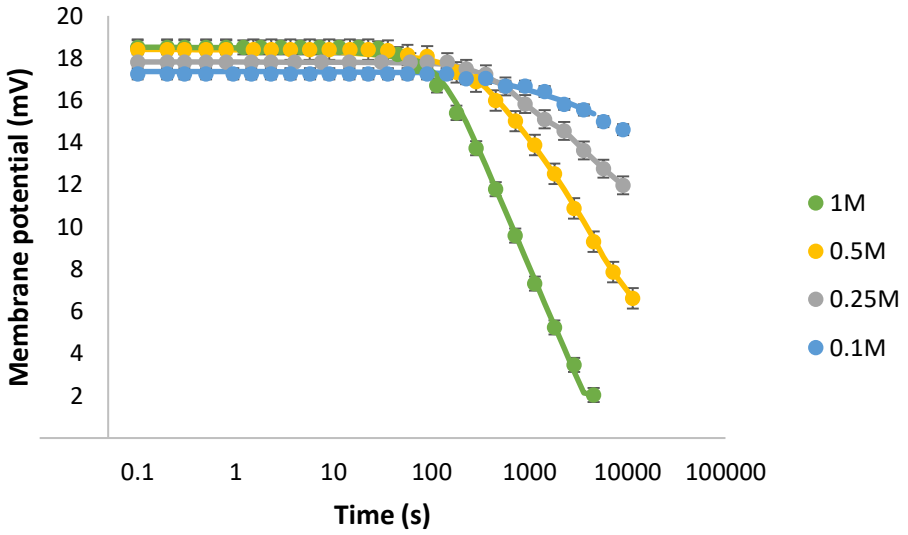


**Fig. 7** Time evolution of trans-membrane potential for various base concentrations, $C_0$, of KOAc for Type 10 Fujifilm membranes: a) CEM and b) AEM. $\boldsymbol{C_{step}}$ is always two times higher than $\boldsymbol{C_0}$. Symbols represent experimental data and solid lines are the theoretical fits

On the other hand, in the case of KOAc is observed the opposite situation (see **Fig. 7**): the initial membrane potential decreases (in absolute value) for CEM but increases with AEM. In any case, the perm-selectivity always decreases with concentration (as will be seen below) but the initial membrane potential for LiCl and KOAc does not follow the trend observed for NaCl due to differences in the dependence of salt activity coefficient on concentration.

The values of partitioning, effective salt diffusion coefficient and perm-selectivity obtained from the fitting are shown in **Fig. 8** and in **Fig. 9** as functions of base concentration for each electrolyte. In both cases, there are increasing trends in the partitioning and effective salt diffusion coefficients with the base concentration, which is in agreement with the mechanism of Donnan exclusion of co-ions from ion-exchange materials. The same can be said about the decreasing trend of perm-selectivity.

Ion sorption depends mainly on the nature of the charged groups in the membrane matrix. Counter-ion concentration in ion exchange membranes equilibrated with an electrolyte solution is much greater than co-ion concentration due to Donnan exclusion that prevents co-ions transport through the membrane. In this study, in the case of CEM counter-ions are $Li^+$, $Na^+$ and $K^+$ whereas co-ions are $Cl^-$ and $CH_3COO^-$.

As can be seen in **Fig. 8**, salt partition coefficient and effective diffusion coefficient followed the order: LiCl < NaCl < KOAc. These results are in agreement with the literature data reported with Nafion membranes, which are also cation exchange membranes. Those studies revelled that $Li^+$ had the lowest partitioning coefficient compared to other alkali metals [23] and also the lowest ion mobility [24]. Moreover, it was found that diffusion permeability with LiCl was lower than with NaCl whereas in the case of KCl was noticeably higher than both of them [25]. This fact is also consistent with the results of the present study, where effective diffusion coefficient with NaCl was only 1.4 times higher than with LiCl (at the highest base concentration) but the difference respect KOAc increased up to 3.55 times. The perm-selectivity followed the opposite order: perm-selectivity values for LiCl and NaCl were between 1 and 0.9 (slightly higher in the case of LiCl), while on the contrary the perm-selectivity obtained for KOAc was notably lower (0.87-0.47). Ionic interactions between counter-ions or co-ions with fixed-charge in the membrane influences the perm-selectivity [26–28]. In this case, LiCl and NaCl have in common the same co-ion, so the results can be interpreted as counter-ion effect on perm-selectivity. A counter-ion with a higher charge density binds stronger to the fixed charge groups in the membrane, which may result in the

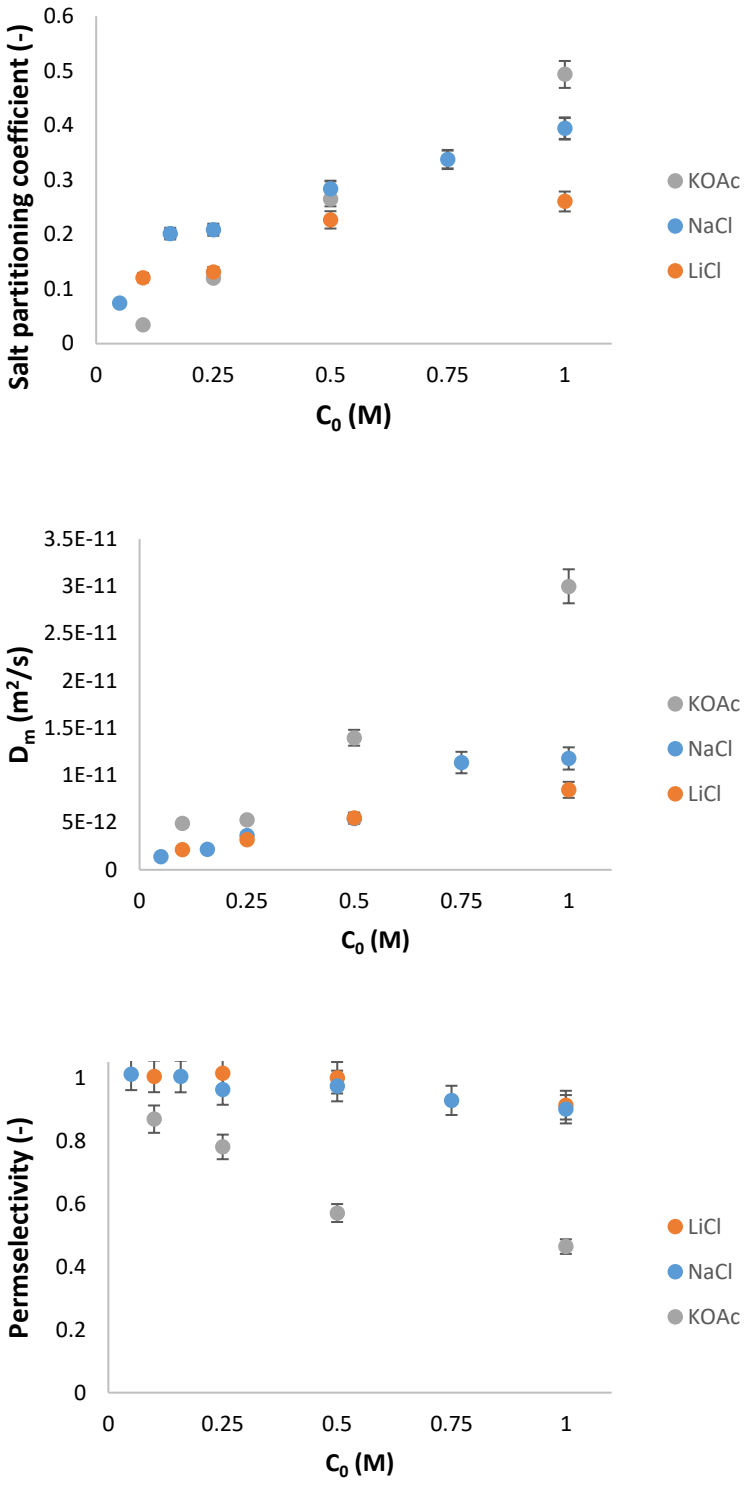


**Fig. 8** Properties determined for Type 10 Fujifilm CEM with different electrolytes at room temperature

screening of fixed charge concentration (counter-ion condensation). Therefore, the ion-exchange membrane behaves more like an uncharged polymer and the exclusion of co-ions decreases as a result. According to this, since LiCl has the lowest charge density, it turns out to be the most perm-selectivity.

As for the results with AEM, opposite trends were obtained for the properties with respect to electrolyte **(see Fig. 9)**. In these measurements, $Cl^-$ and $CH_3COO^-$ are the counter-ions and $Li^+$, $Na^+$ and $K^+$ are the co-ions. The salt partitioning coefficient for the electrolytes that have $Cl^-$ as counter-ion turn out to have the highest partition and salt effective diffusion coefficients. This is due to the fact that $Cl^-$ is more mobile than acetate and also more likely to interact with the fixed charge of AEM [26,29]. Moreover, Cl- is also more mobile than acetate.However, the differences between electrolytes were not as pronounced as in the previous case (the maximum difference between LiCl and KOAc for the effective diffusion coefficient was only 1.45).

On the other hand, KOAc present the highest perm-selectivity. As for NaCl and LiCl, as long as they have a common counter-ion, this two experiments can be used to see the effect of the co-ion on perm-selectivity (similar to the previous case where it was seen the effect of counter-ions for a common co-ion). NaCl perm-selectivity changes from 0.95 to 0.63 whereas the values for LiCl are still lower (between 0.87 and 0.35).

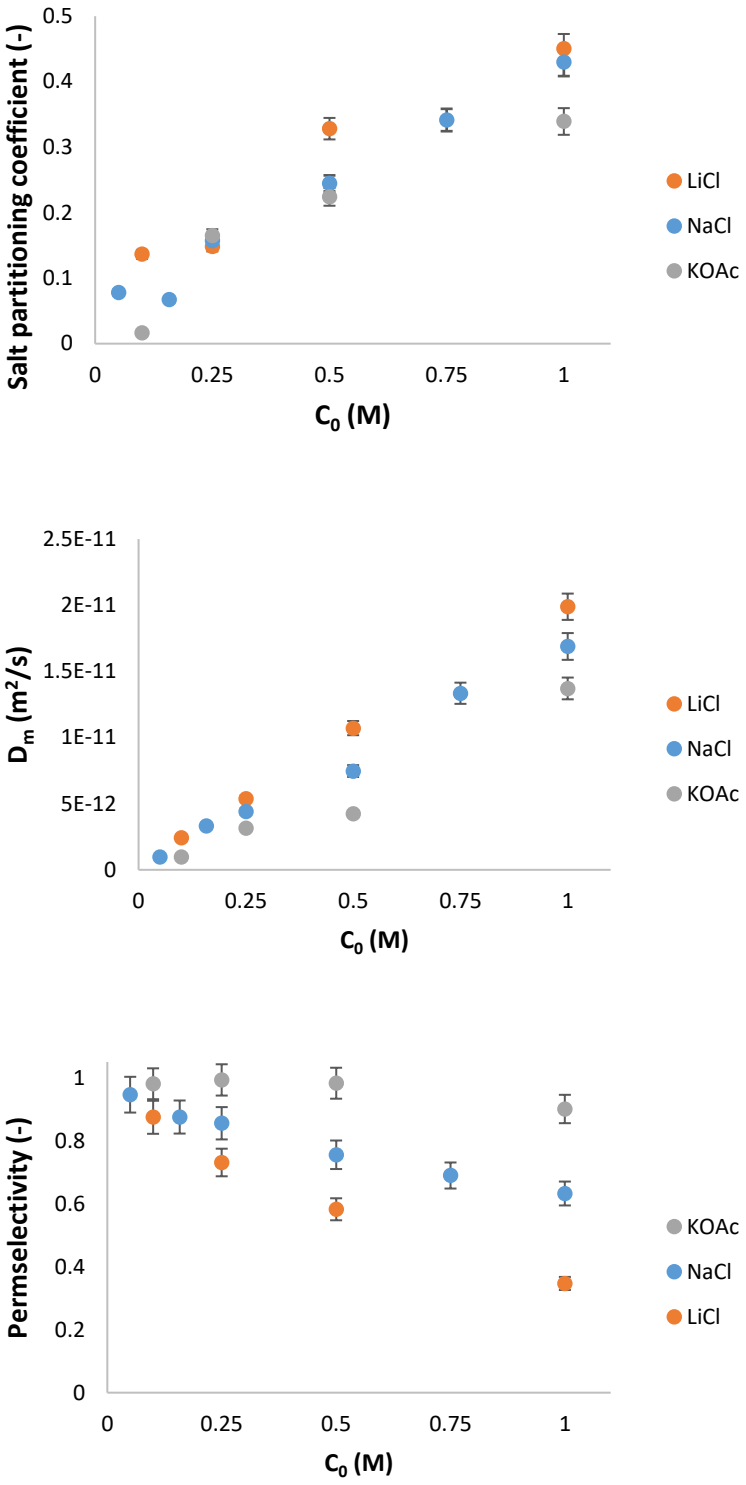


**Fig. 9** Properties determined for Type 10 Fujifilm AEM with different electrolytes at room temperature

### *4.3 Estimation of effective salt diffusion and partition coefficients: effect of the temperature*

The effect of temperature on salt partitioning, salt diffusion coefficient and perm-selectivity dependences on concentration is studied in the case of NaCl. Measurements have been performed for Fujifilm Type 10 membranes at 50ºC and 75ºC (**see. Figs. 10-11**).

**(a)**

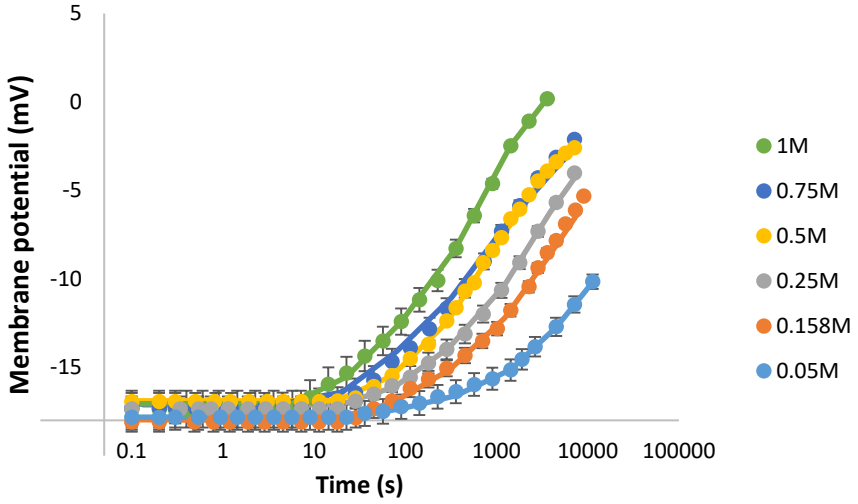


**(b)**

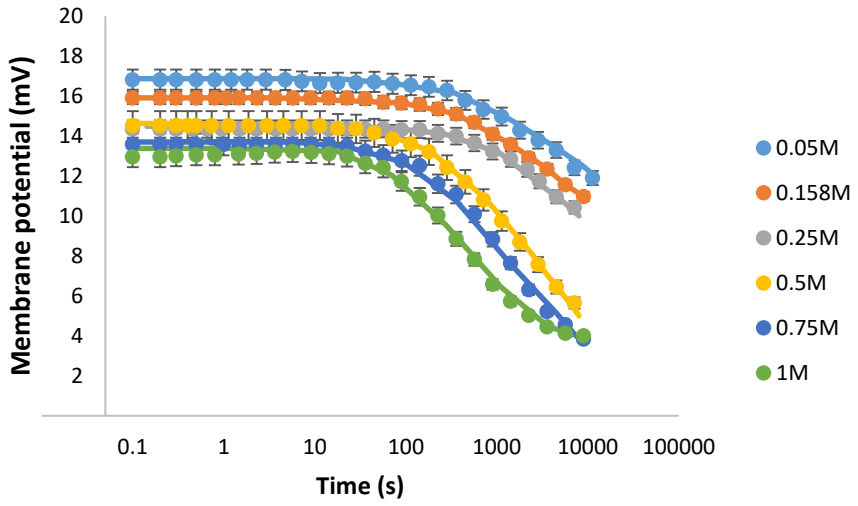


**Fig. 10** Time evolution of trans-membrane potential for various base concentrations, $C_0$, of NaCl at T = 50ºC with Fujifilm Type 10 membranes: a) CEM and b) AEM. $\boldsymbol{C_{step}}$ is always two times higher than $\boldsymbol{C_0}$. Symbols represent experimental data and solid lines are the theoretical fits

**(a)**

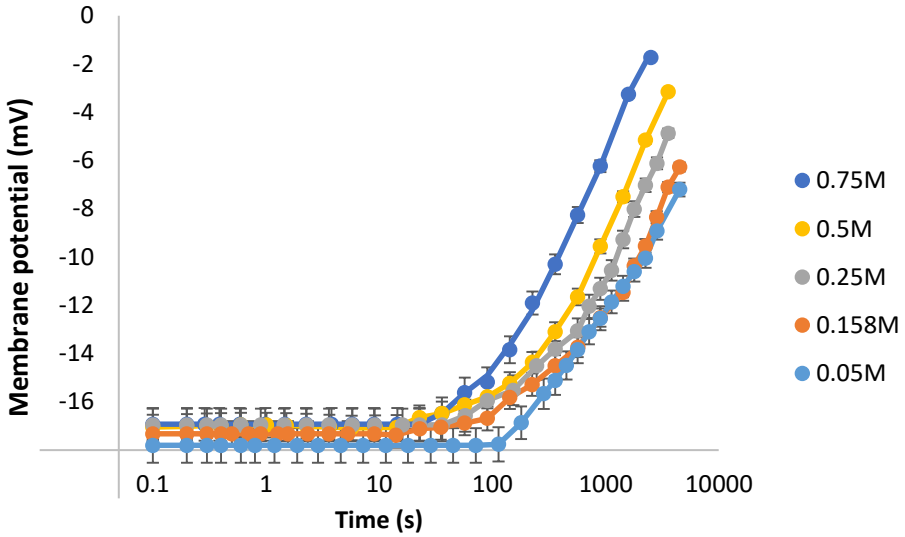


**(b)**

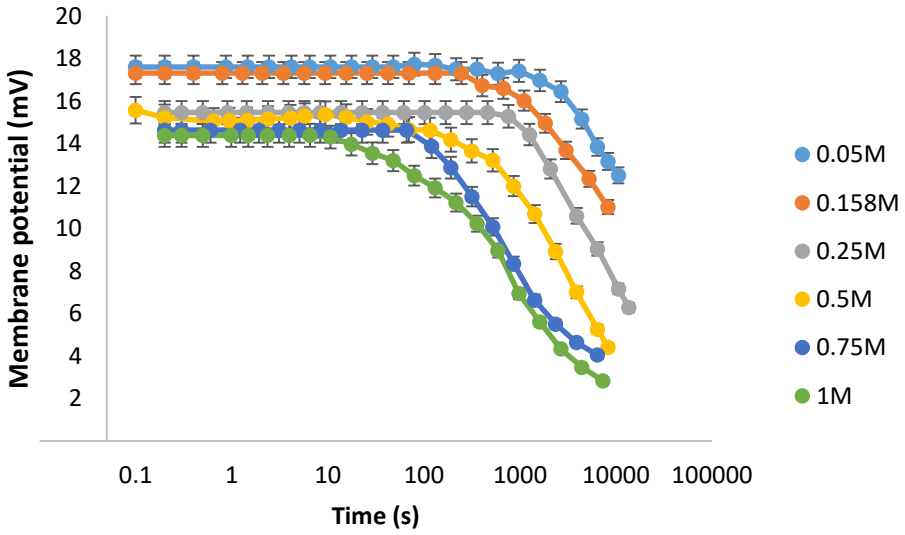


**Fig. 11** Time evolution of trans-membrane potential for various base concentrations, $C_0$, of NaCl at T = 75ºC using Fujifilm Type 10 membranes: a) CEM and b) AEM. $\boldsymbol{C_{step}}$ is always two times higher than $\boldsymbol{C_0}$. Symbols represent experimental data and solid lines are the theoretical fits

The fundamental difference observed in the measured transient trans-membrane potential for both membranes is the decreasing in relaxation time with temperature, as expected.

**Fig. 12** and **Fig. 13** present the dependences of partitioning, effective salt diffusion coefficient and perm-selectivity on base concentration at different temperatures for both membranes. In both cases, there is an increase in effective salt diffusion coefficient with temperature, as reflected by the decreasing in relaxation time in the measured transient membrane potential. In respect to ion partition and perm-selectivity, there are not clear trends with temperature. In the case of CEM, it seems that increasing temperature decreases ion partitioning and perm-selectivity. A decrease in ion sorption has been observed with Nafion membranes [30]. This fact was explained by the increase of fixed charge concentration at higher concentrations. According to the Donnan theory, this effect prevents sorption of electrolyte in the membrane. Therefore, at high concentration of the base solution and at elevated temperature, the partition coefficient should increase only slightly or even it may decrease.

On the other hand, in AEM the ion partitioning increased with temperature whereas the values of perm-selectivity barely changed.

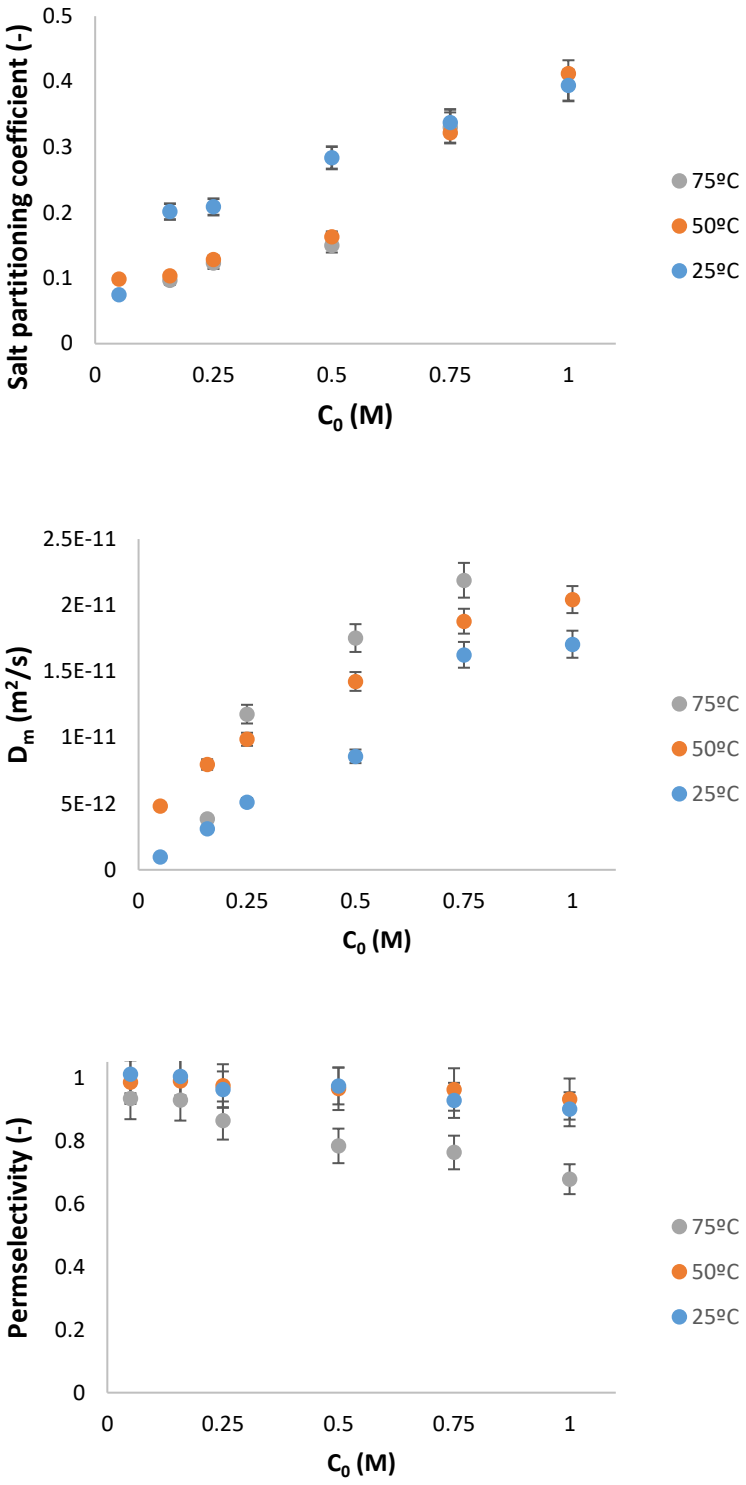


**Fig. 12** Properties determined for Type 10 Fujifilm CEM with NaCl at different temperatures

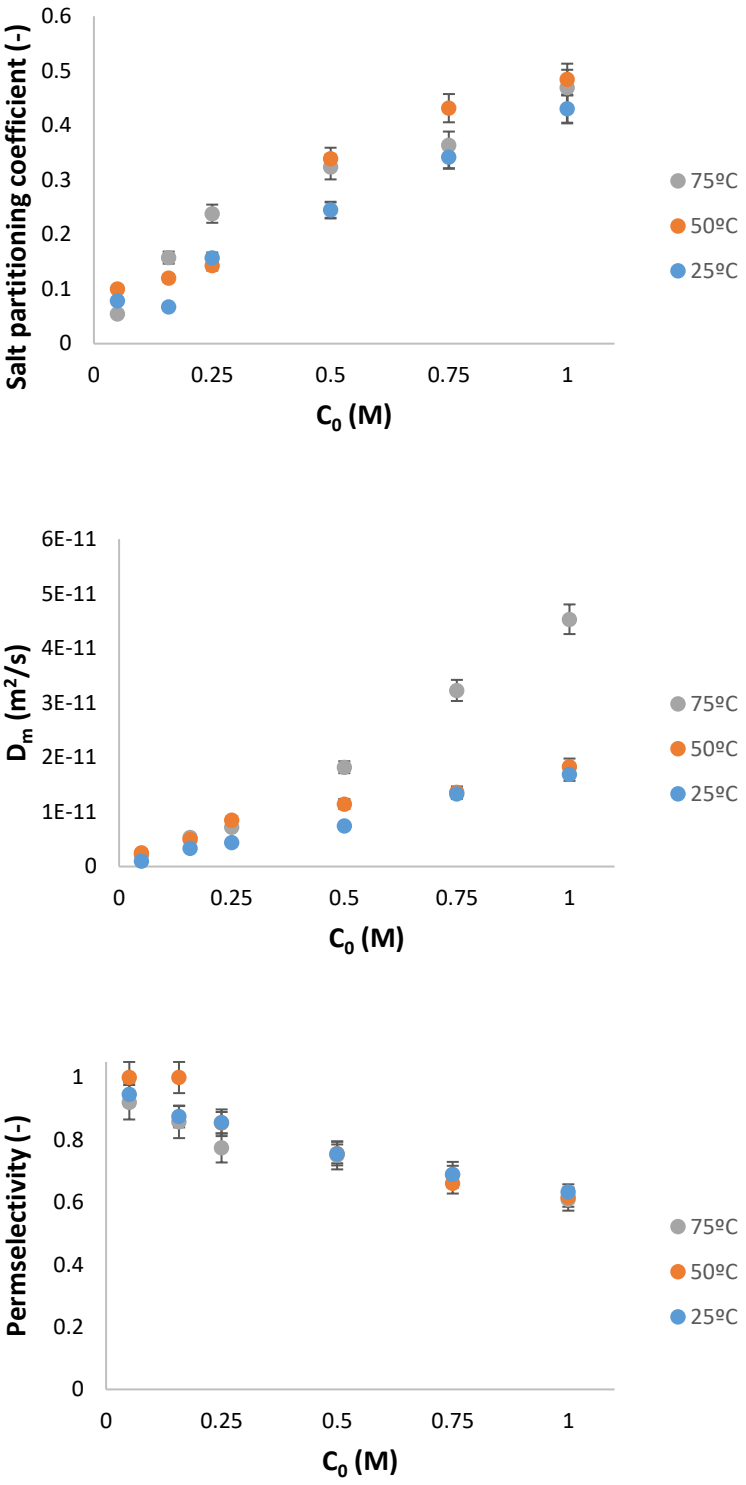


**Fig. 13** Properties determined for Type 10 Fujifilm AEM with NaCl at different temperatures

# 5. Conclusions

For some applications of ion-exchange membranes ion partitioning and mobility are key parameters for ion transport description through the membrane. These properties are strongly influenced by specific interactions between electrolyte solutions and fixed charge in the membrane matrix.

Transient membrane potential after concentration provide information on perm-selectivity, partitioning and diffusivity properties for different electrolytes (NaCl, LiCl and KOAc). It were obtained different trends depending on the type of membrane (CEM or AEM) due to the different nature of fixed charge concentration. For CEM, the order observed in partition and diffusion coefficient were: LiCl < NaCl < KOAc. As for the perm-selectivity, LiCl presented the highest perm-selectivity whereas KOAc values were considerably lower. In the case of AEM, the lowest partition and diffusion coefficient were obtained for KOAc and the highest for LiCl. The perm-selectivity was higher for KOAc and the lowest for LiCl in this case.

Moreover, it was shown the effect of temperature on those properties in the case of NaCl as electrolyte solution. Logically, increasing the temperature increased the effective salt diffusion coefficient whereas for the partition coefficient there were not observed clear trends. The perm-selectivity decreased with temperature in the case of CEM whereas the changes were less pronounced with AEM.

Separate measurements of osmotic flow showed that osmosis is stronger for LiCl and KOAc than previously observed for NaCl (especially in the case of KOAc).

# List of symbols

$a_0$: activity of base solution

$a_i$: activity at the interface membrane/porous support

$a_{step}$: activity of step solution

$C_0$: concentration of base solution

$C_i$: concentration at the interface membrane/porous support

$C_m$: concentration at the membrane surface

$C_s$: concentration in the porous support

$C_{step}$: concentration of step solution

$d_f$: glass frit diameter of the porous part

$D_s^{(m)}$: effective salt diffusion coefficient in the membrane without electrostatic correction

$D_m$: salt diffusion coefficient in the membrane

$D_s$: salt diffusion coefficient in the porous support

$D_+$: diffusion coefficient of cation

$D_-$: diffusion coefficient of anion

$F$: Faraday constant

$J_v$ : osmotic flow

K: osmotic permeability

$L_m$: thickness of the membrane

$L_s$: thickness of the frit

R: ideal gas constant

$t$: time

$t_0$: characteristic relaxation time defined by Eq. (A2)

$t_+^b$: transport number of positive ions in the frit

*T*: absolute temperature

$T_m$: salt transmission coefficient in membrane

x : longitudinal coordinate

$z_+$: charge coefficient of cation

$z_-$: charge coefficient of anion

*Greek letters*

$\alpha_m$: chemical capacity of the membrane

$\alpha_s$: chemical capacity of the frit

$\varphi$: electrical potential

$\varphi_0$: initial electrical potential difference

$\gamma$: salt activity coefficient in the virtual solution

$\gamma_i$: salt activity coefficient at the membrane/support interface

$\gamma_0$: salt activity coefficient at the initial concentration

$\gamma_{step}$: salt activity coefficient of the non-equilibrium solution

$\nu$: stoichiometric coefficient

$\Gamma_{\pm}$: partition coefficient

## Acknowledgements

This work has been performed within the scope of RED-Heat-to-Power project (Conversion of Low Grade Heat to Power through closed loop Reverse Electro- Dialysis) - Horizon 2020 Programme, Grant Agreement n. 640667.

## References

[1] T. Luo, S. Abdu, M. Wessling, Selectivity of Ion Exchange Membranes: A Review, (2018). doi:10.1016/j.memsci.2018.03.051.

[2] M. Micari, M. Bevacqua, A. Cipollina, A. Tamburini, W. Van Baak, T. Putts, G. Micale, E ff ect of di ff erent aqueous solutions of pure salts and salt mixtures in reverse electrodialysis systems for closed-loop applications, J. Memb. Sci. 551 (2018) 315–325. doi:10.1016/j.memsci.2018.01.036.

[3] A. Tamburini, M. Tedesco, A. Cipollina, G. Micale, M. Ciofalo, M. Papapetrou, W. Van

Baak, A. Piacentino, Reverse electrodialysis heat engine for sustainable power production, Appl. Energy. 206 (2017) 1334–1353. doi:10.1016/j.apenergy.2017.10.008.

[4] M. Reig, X. Vecino, C. Valderrama, O. Gibert, J.L. Cortina, Application of selectrodialysis for the removal of As from metallurgical process waters: Recovery of Cu and Zn, Sep. Purif. Technol. 195 (2018) 404–412. doi:10.1016/j.seppur.2017.12.040.

[5] M. Reig, S. Casas, C. Valderrama, O. Gibert, J.L.L. Cortina, Integration of monopolar and bipolar electrodialysis for valorization of seawater reverse osmosis desalination brines: Production of strong acid and base, Desalination. 398 (2016) 87–97. doi:10.1016/j.desal.2016.07.024.

[6] T. Rijnaarts, N.T. Shenkute, A. Wood, W.M. De Vos, K. Nijmeijer, Divalent Cation Removal by Donnan Dialysis for Improved Reverse Electrodialysis, (2018). doi:10.1021/acssuschemeng.8b00879.

[7] C. Agarwal, R.W. Cattrall, S.D. Kolev, Donnan dialysis based separation of gold ( III ) from electronic waste solutions using an anion exchange pore- fi lled membrane, J. Memb. Sci. 514 (2016) 210–216. doi:10.1016/j.memsci.2016.04.033.

[8] J. Ran, L. Wu, Y. He, Z. Yang, Y. Wang, C. Jiang, L. Ge, E. Bakangura, T. Xu, Ion exchange membranes: New developments and applications, J. Memb. Sci. 522 (2017) 267–291. doi:10.1016/j.memsci.2016.09.033.

[9] W. Shi, X. Liu, C. Ye, X. Cao, C. Gao, J. Shen, Efficient lithium extraction by membrane capacitive deionization incorporated with monovalent selective cation exchange membrane, Sep. Purif. Technol. 210 (2019) 885–890. doi:10.1016/j.seppur.2018.09.006.

[10] D. Saebea, C. Chaiburi, S. Authayanun, Model based evaluation of alkaline anion exchange membrane fuel cells with water management, Chem. Eng. J. 374 (2019) 721–729. doi:10.1016/j.cej.2019.05.200.

[11] T. Wang, S.J. Moon, D.S. Hwang, H. Park, J. Lee, S. Kim, Y.M. Lee, S. Kim, Selective ion transport for a vanadium redox flow battery (VRFB) in nano-crack regulated proton exchange membranes, J. Memb. Sci. 583 (2019) 16–22. doi:10.1016/j.memsci.2019.04.017.

[12] S. Mehdizadeh, M. Yasukawa, M. Kuno, Y. Kawabata, M. Higa, Evaluation of energy harvesting from discharged solutions in a salt production plant by reverse electrodialysis (RED), Desalination. 467 (2019) 95–102. doi:10.1016/j.desal.2019.04.007.

[13] D.D. Tham, D. Kim, C2 and N3 substituted imidazolium functionalized poly(arylene ether ketone) anion exchange membrane for water electrolysis with improved chemical stability, J. Memb. Sci. 581 (2019) 139–149. doi:10.1016/j.memsci.2019.03.060.

[14] Y. Tanaka, Ion exchange membranes : fundamentals and applications: Second edition, Elsevier Inc., Amsterdam, 2015.

[15] B. Auclair, V. Nikonenko, C. Larchet, M. Métayer, L. Dammak, Correlation between transport parameters of ion-exchange membranes, 195 (2002) 89–102.

[16] A.N. Naik, C. Agarwal, S. Chaudhury, A. Goswami, Non-stationary radiotracer method for diffusion coefficients of Cs , Ba , Eu tracers in Nafion-117 membrane, 6395 (2016). doi:10.1080/01496395.2016.1256324.

[17] M. Fernández de Labastida, A. Yaroshchuk, Transient membrane potential after concentration step: A new method for advanced characterization of ion-exchange membranes, J. Memb. Sci. 585 (2019) 271–281. doi:10.1016/j.memsci.2019.05.012.

[18] F. Giacalone, C. Olkis, G. Santori, A. Cipollina, S. Brandani, G. Micale, Novel solutions for closed-loop reverse electrodialysis: Thermodynamic characterisation and perspective analysis, Energy. 166 (2019) 674–689. doi:10.1016/j.energy.2018.10.049.

[19] B. Ortega-Delgado, F. Giacalone, A. Cipollina, M. Papapetrou, G. Kosmadakis, A. Tamburini, G. Micale, Boosting the performance of a Reverse Electrodialysis – Multi-Effect Distillation Heat Engine by novel solutions and operating conditions, Appl. Energy. 253 (2019). doi:10.1016/j.apenergy.2019.113489.

[20] A. Yaroshchuk, X. Martínez-Lladó, L. Llenas, M. Rovira, J. de Pablo, Solution-diffusion-film model for the description of pressure-driven trans-membrane transfer of electrolyte mixtures: One dominant salt and trace ions, J. Memb. Sci. 368 (2011) 192–201. doi:10.1016/j.memsci.2010.11.037.

[21] A.E. Yaroshchuk, A.L. Makovetskiy, Y.P. Boiko, E.W. Galinker, Non-steady-state membrane potential: Theory and measurements by a novel technique to determine the ion transport numbers in active layers of nanofiltration membranes, J. Memb. Sci. 172 (2000) 203–221.

[22] A. Yaroshchuk, Y. Boiko, A. Makovetskiy, Electrochemical perm-selectivity of active layers and diffusion permeability of supports of an asymmetric and a composite NF membrane studied by concentration-step method, Desalination. 245 (2009) 374–387. doi:10.1016/j.desal.2009.02.001.

[23] L. Yang, C. Tang, M. Ahmad, A. Yaroshchuk, M.L. Bruening, High Selectivities among Monovalent Cations in Dialysis through Cation-Exchange Membranes Coated with Polyelectrolyte Multilayers, ACS Appl. Mater. Interfaces. 10 (2018) 44134–44143. doi:10.1021/acsami.8b16434.

[24] T. Okada, H. Satou, M. Okuno, M. Yuasa, Ion and water transport characteristics of perfluorosulfonated ionomer membranes with H+ and alkali metal cations, J. Phys. Chem. B. 106 (2002) 1267–1273. doi:10.1021/jp013195l.

[25] I.A. Stenina, P. Sistat, A.I. Rebrov, G. Pourcelly, A.B. Yaroslavtsev, Ion mobility in Nafion-117 membranes, Desalination. 170 (2004) 49–57. doi:10.1016/j.desal.2004.02.092.

[26] A. Münchinger, K.D. Kreuer, Selective ion transport through hydrated cation and anion exchange membranes I. The effect of specific interactions, J. Memb. Sci. 592 (2019). doi:10.1016/j.memsci.2019.117372.

[27] H.J. Cassady, E.C. Cimino, M. Kumar, M.A. Hickner, Specific ion effects on the permselectivity of sulfonated poly(ether sulfone) cation exchange membranes, J. Memb. Sci. 508 (2016) 146–152. doi:10.1016/j.memsci.2016.02.048.

[28] G.M. Geise, H.J. Cassady, D.R. Paul, E. Logan, M.A. Hickner, Specific ion effects on membrane potential and the permselectivity of ion exchange membranes, Phys. Chem. Chem. Phys. 16 (2014) 21673–21681. doi:10.1039/C4CP03076A.

[29] P. Ray, V.K. Shahi, T. V. Pathak, G. Ramachandraiah, Transport phenomenon as a function of counter and co-ions in solution: Chronopotentiometric behavior of anion exchange membrane in different aqueous electrolyte solutions, J. Memb. Sci. 160 (1999) 243–254. doi:10.1016/S0376-7388(99)00088-5.

[30] A. Narębska, R. Wódzki, K. Erdmann, Properties of perfluorosulfonic acid membranes in concentrated sodium chloride and sodium hydroxide solutions, Die Angew. Makromol. Chemie. 111 (1983) 85–95. doi:10.1002/apmc.1983.051110107.